Modelling the depth-dependent permeability barrier of the skin

Mark Daniël Antal van Logtestijn

PhD Thesis

Department of Bioengineering,
Imperial College London

Supervisor: Dr. Reiko J. Tanaka

July 2017

Submitted in fulfilment of the requirements for the degree of Doctor of Philosophy and the Diploma of Imperial College London

Abstract

In the upper layers of our skin, the stratum corneum and the tight junctions in the stratum granulosum form permeability barriers which prevent dehydration and protect against external pathogens. The onset and deterioration of skin diseases, such as atopic dermatitis, are often caused or accompanied by barrier defects due to dysregulation of barrier homeostasis. As the cells constantly move up through the epidermis, several depth-dependent processes control the maintenance of the tight junction barrier during turnover, and induce the building, maintenance and degradation of the stratum corneum barrier. An understanding of these depth-dependent processes is required to study barrier homeostasis in physiological and pathological conditions. Adopting a modelling approach to integrate and compare available experimental data, a compartmental model of the stratum corneum is developed to characterise and visualise the resistance to water diffusion along its depth. The resulting resistance profiles, obtained from non-invasive *in vivo* confocal Raman spectroscopy and trans-epidermal water loss data, demonstrate a depth-dependent permeability barrier in the stratum corneum. Combined with models of barrier components and regulation of desquamation, the resistance profiles form a framework for studying stratum corneum barrier homeostasis. The selective permeability of the single-layered tight junction barrier is important in conserving specific environments on both sides of the barrier, which induce keratinocyte differentiation. In order to maintain its barrier function, the tight junctions have to be replaced continually while keratinocytes transition the barrier. Our 3D model of the stratum granulosum simulates the proposed mechanisms of barrier transition, and identifies how the temporal coordination of the transition ensures a constant barrier function. This thesis demonstrates how depth-dependent processes contribute to the regulation of both epidermal barriers in a continuously self-renewing tissue.

Declaration of Originality

I declare that this thesis is my own work. Any work of others has been acknowledged and referenced.

Mark van Logtestijn
Department of Bioengineering
Imperial College London

Copyright Declaration

'The copyright of this thesis rests with the author and is made available under a Creative Commons Attribution Non-Commericial No Derivitives licence. Researchers are free to copy, distribute or transmit the thesis on the condition that they attribute it, that they do not use it for commercial purposes and that they do not alter, transform or build upon it. For any reuse or redistribution, researchers must make clear to others the license terms of this work.'

Acknowledgements

First and foremost, I would like to express my gratitude to my supervisor Dr Reiko J. Tanaka, for all the support and encouragement during this research project. She has been the most dedicated and engaged supervisor a PhD student could wish for.

I am grateful for the collaboration with Dr Georgios N. Stamatas, for all his discussion and always being available to support me with his knowledge of skin biology and suggestions for interesting research directions.

I would like to thank all the current and past Tanaka group members, in particular Elisa, Panayiotis, Sang, Alejandro, Neville, Scott, Neville, and Luke, who have made my time at Imperial scientifically challenging, exciting and fun.

I would like to thank the following people for their collaboration: Dr Peter J. Caspers, Dr Sanja Kezic, Dr Douglas R. Hoffman, Dr David W. Koenig, Dr Masahiro Ono, Dr Mariko Yokouchi, Dr Toru Atsugi, Dr Mayumi Kajimura, Dr Makoto Suematsu, Dr Mikio Furuse, Dr Masayuki Amagai, Dr Akiharu Kubo; and Dr Elise Boireau-Adamezyk for kindly providing me with the Raman data.

I would like to thank Beverley for proofreading this thesis.

This research project was funded by a studentship from Johnson&Johnson. I would like to thank Johnson&Johnson and Georgios Stamatas for the financial support; this project would not have been possible without it.

Last but not least, I am forever indebted to my parents Henk and Hanneke and my siblings Merijn and Arlaine for their unconditional support, and for always bringing joy to my life.

Contents

Abstract i

Declaration of Originality ii

Copyright Declaration iii

Acknowledgements iv

Table of Contents ix

List of Figures xiii

List of Tables xiv

1 Introduction 1

1.1 Heterogeneity in the skin barrier 2

1.2 Better understanding of epidermal barrier homeostasis requires modelling of depth-dependent processes 4

1.3 Aims 6

1.4 Publications 7

1.5 Outline 8

2 The skin's depth-dependent permeability barrier **10**

2.1 Structure and function of the epidermis 11

2.1.1 The stratum corneum 11

2.1.2 The stratum granulosum and the tight junction barrier 15

2.1.3 Atopic dermatitis 17

2.2 Non-invasive *in vivo* experimental techniques for experimental dermatology 18

2.3 Modelling the skin's permeability barrier 21

2.4 Conclusion 23

3 Characterising depth-dependent water permeability barrier in the SC using resistance profiles **25**

3.1 Introduction 25

3.2 Resistance to water diffusion in the stratum corneum is depth-dependent 27

3.2.1 Introduction 27

3.2.2 Results and Discussion 29

3.2.3 Conclusions 38

3.2.4 Methods 40

3.3 Discussion 42

3.3.1 Discussion on results of application and future direction 42

3.3.2 Results on depth-dependency of SC barrier in relation to existing literature 45

3.3.3 Application and visualisation of resistance profiles 51

4 Resistance profiles: application and analysis **53**

4.1 Water resistance profile as a marker of skin barrier damage in atopic dermatitis patients . . . 55

4.2 Correlation between SC thickness, TEWL and water concentration . . . 60

4.3 Depth profiles of lipids and NMF partially explain the resistance profiles 64

4.3.1 Least squares regression . . . 65

4.3.2 Depth profiles of the contribution of SC components to resistance 67

4.4 Discussion . . . 69

5 Depth-dependent regulation of stratum corneum homeostasis **72**

5.1 Introduction . . . 72

5.2 Modelling depth-dependency of components . . . 75

5.2.1 Natural moisturising factor . . . 75

5.2.2 Water and relative humidity . . . 81

5.2.3 Corneodesmosomes . . . 82

5.2.4 Lipids . . . 83

5.3 Desquamation: pH-dependent KLK activity model . . . 85

5.3.1 Model . . . 87

5.3.2 Results and validation . . . 93

5.4 Integration into SC barrier homeostasis model . . . 97

5.4.1 Model . . . 98

5.4.2 Results . . . 100

5.5 Discussion . . . 102

6 Extension into the stratum granulosum: tight junction barrier homeostasis 104

6.1 Introduction . . . 104

6.2 Methods . . . 110

6.2.1 3D f-TKD cell model and geometry . . . 110

6.2.2 Obtaining geometrical parameters from experimental data . . . 113

6.2.3 3D model of the stratum granulosum . . . 115

6.2.4 Simulation . . . 117

6.2.5 Calculation of TJ barrier turnover indices . . . 119

6.2.6 Experimental data . . . 120

6.3 Results . . . 121

6.3.1 Temporal coordination of SG2 cell transition maintains TJ barrier homeostasis . . . 121

6.3.2 Identifying the parameters of the temporal coordination of barrier transition . . . 123

6.3.3 Minimal experimental data required to predict temporal coordination parameters and transition dynamics . . . 127

6.3.4 Biological significance of the waiting time . . . 130

6.4 Discussion . . . 134

6.4.1 Epidermal homeostasis . . . 135

6.4.2 Interplay between TJ and SC barriers . . . 138

7 Concluding remarks 142

A Supplementary information 146

A.1 Overview of TEWL and water concentration profile data . . . 146

A.2 Overview of SC barrier homeostasis model variables and nominal parameter set 149

A.3 Choice of waiting time distribution 151

A.4 Optimisation 153

A.5 Robustness of optimal waiting time distribution to cost function weights 154

B Copyright permission **155**

Bibliography **157**

List of Figures

2.1 The stratum corneum and tight junction barriers in the upper layers of the epidermis 12

2.2 The stratum corneum 14

3.1 Depth-dependent SC resistance to water diffusion 31

3.2 Comparison of permeability barrier for different types of skin 33

3.3 Resistance profiles before and 30 minutes after topical application of different oils 35

3.4 Results of *in silico* absorption-desorption experiment with topically applied water 37

3.5 Model for studying contribution of NMF to barrier function 44

3.6 *In silico* simulation of tape stripping experiments with depth-dependent permeability barrier. 47

3.7 Similarities between experimental and data and simulation of tape stripping using depth-dependent profiles 48

3.8 Tape stripping data reveals a depth-dependent resistance profile 50

4.1 Resistance profiles for non-lesional skin from AD patients and for healthy skin following chemical and mechanical insults 57

4.2 Quantification of damage and recovery of barrier function from insults on healthy skin and its comparison to AD non-lesional skin 59

4.3 Least squares regression results, including thickness 68

4.4 Least squares regression results, with normalised profiles 70

5.1 Overview of relation between submodels 74

5.2 Filaggin processing forms natural moisturising factor along the depth of the SC 76

5.3 Simulation of filaggrin and NMF depth profiles 78

5.4 Simulation of filaggrin and NMF profiles with reduced initial fillagrin and fillagrin degradation rate 80

5.5 KLK is activated and inhibited along depth of SC 88

5.6 Inhibition of KLK by LEKTI through pH-dependent association and dissociation 89

5.7 Schematic overview of qualitative gradients of concentrations and rates 92

5.8 Simulation of LEKTI, KLK and the LEKTI-KLK complex profiles 93

5.9 Degradation activity $D^{KLK}(pH)$ for increasing pH at top of SC from 5 to 7 95

5.10 Comparison of KLK activity to experimental data. 96

5.11 Comparison of barrier component degradation to experimental data. . . 97

5.12 Simulation of changes in relative humidity 100

5.13 Simulation of the effect of increased surface pH 101

6.1 Overview of transition phases and tight junctions 107

6.2 f-TKD geometry 110

6.3 TKD decomposition in three layers 111

6.4 Decomposition of f-TKD 112

6.5 Experimental image (left) and simulation (right). A star * denotes a cell in transition 113

6.6 Derivation of angle θ . . . 114

6.7 3D model of SG2 and underlying layers . . . 116

6.8 Example simulation result . . . 119

6.9 Movie shows simulation of TJ barrier transition over time . . . 122

6.10 Proposed temporal coordination of the SG2 cell turnover cycle . . . 123

6.11 Side view of fitted linear plane and data points . . . 128

6.12 Interdependence of simulation indices . . . 129

6.13 Cycle time and waiting time distribution can be predicted from static experimental measurement sof r_{trans} and r_{nb} . . . 130

6.14 Waiting time affects cycle time and could function as a buffer to maintain the tight junction barrier function during increased proliferation . . . 131

6.15 Changes in waiting and transition time distinctly alter experimentally measurable indices . . . 133

6.16 Schematic overview of stratum corneum homeostasis model and tight junction barrier extension . . . 139

6.17 Proposed model for interplay between stratum corneum and tight junction barriers through calcium . . . 141

A.1 Water concentration profiles before and after application of four different oils. . . . 147

A.2 Water concentration profiles for AD patients . . . 147

A.3 TEWL data before and after abrasion and the application of SLS. . . . 148

A.4 Water concentration profiles before and after abrasion and the application of SLS . . . 148

A.5 The normal distribution can match experimental data, and can approximate other distributions . . . 152

A.6 Optimisation using a priori simulation results for different normal waiting time distributions with a range of mean and standard deviation values 153

A.7 Robustness of optimal waiting time distribution to cost function weights 154

B.1 Elsevier copyright permission confirmation 156

List of Tables

4.1 Correlation between TEWL, thickness, and surface water concentration for different skin sites 61

4.2 Correlation between TEWL, thickness, and surface water concentration for all skin sites combined 63

5.1 Nominal parameters used for simulation of NMF model. 79

5.2 Affinity constants for different pH levels 90

5.3 KLK activity for different pH levels 91

5.4 Desquamation model simulation parameters 94

6.1 TKD geometry obtained from experimental data and geometric equations 115

6.2 Nominal parameters used in simulation 124

6.3 Experimentally obtained parameters for transition dynamics. 126

A.1 TEWL data for infants, adults and skin sites 146

A.2 TEWL data before and after the application of four different oils 146

A.3 Overview of variables in the SC barrier homeostasis model 149

A.4 Nominal simulation parameter values for the SC barrier homeostasis model 150

B.1 Permission to republish third party copyrighted work 155

Abbreviations

AD	Atopic dermatitis
bTJ	Bicellular tight junction
CD	Corneodesmosomes
CRS	Confocal Raman Spectroscopy
EDU	Epidermal differentiation unit
EPU	Epidermal proliferation unit
FLG	Filaggrin
f-TKD	Flattened tetrakaidecahedron
KLK	Kallikrein (a family of serine proteases)
LC	Langerhans cell
LSR	Least squares regression
LEKTI	Lympho-epithelial Kazal-type-related inhibitor
NMF	Natural moisturising factor
NS	Netherton syndrome
ODE	Ordinary differential equation
PK/PD	Pharmacokinetic/pharmacodynamic
PC	Progenitor cell
PDE	Partial differential equation
RH	Relative humidity
SC	Stratum Corneum
SG	Stratum granulosum
SLS	Sodium Lauryl Sulphate
TER	Trans-epithelial electrical resistance

TEWL Trans-epidermal water loss

TKD Tetrakaidecahedron

TJ Tight junction

tTJ Tricellular tight junction

ZO Zonula occludens

Chapter 1

Introduction

The outermost layers of our skin, the epidermis, is an epithelial tissue that covers the body. Even though our skin is not our largest organ by weight or functional surface area [1, 2], despite it often being credited as such in dermatology or skin biology publications, it is the main interface of our body with the external environment. In this function, it possesses remarkable barrier qualities that protect us from external pathogens, and prevents uncontrolled loss of water from the body.

We often regard our skin as mainly important to our appearance, but we do not regularly think about the amazing protective barrier and immune functions. It is incredible to realise that, when touching your skin, a layer of just 10–20 µm is responsible for its main protective barrier function and prevents dehydration; for instance, mice without a stratum corneum or with a defective tight junction barrier die from dehydration at birth [3, 4, 5].

The epidermis has two main permeability barriers residing in its uppermost layers: the stratum corneum (SC) barrier and tight junction (TJ) barrier in the stratum granuloum (SG), just below the SC. The main function of the SC and TJ barriers is to provide a permeability barrier, both inside-out and outside-in. The SC prevents dehydration by limiting the outflow of water, and protects the body from penetrating pathogens [6]. Our skin should be impermeable enough to prevent water loss and influx of external penetrants, yet allow a small amount of water to be lost through the skin in order for the outer layers to maintain flexibility, and provide water to enzyme reactions. Al-

though the SC is often referred to as a dead layer of cells, as the corneocytes lose their nucleus, these active enzyme reactions are vital for maintaining barrier homeostasis [7].
The TJ barrier in the SG has recently been shown to be an important second permeability barrier in the epidermis. It has selective permeability to calcium and various other ions, thereby regulating the distinct milieus in the SC and the underlying viable epidermis. These are important for keratinocyte differentiation and the formation of the SC [8, 9].

Both barriers interact with each other, mainly through calcium which reaches peak concentrations in the SC/SG interface [10, 9, 8, 11]. While high calcium concentrations trigger the formation of tight junctions, they also play a vital role in regulating cornification [6].
Besides its barrier functions, the epidermis also serves as a front line of immune responses through dendritic Langerhans cells [12].

Many skin diseases are barrier-related; either they are initiated by a leaky barrier or their pathogenesis leads to alteration of expression of barrier components or dysregulation of barrier homeostasis [13, 14, 15]. Skin diseases such as atopic dermatitis (AD) can have a strong impact on people's lives, and have a high and increasing prevalence [16]. For instance, up to 20% of the population in western countries develop AD in their life [17]. Patients can suffer from pain, itch, discomfort, insecurity and/or stress. In the case of AD it can be the first stage in the development of asthma and other atopic diseases later in life [18, 19].

1.1 Heterogeneity in the skin barrier

Human skin is a heterogeneous tissue. There is high variation in the barrier function of skin: both interpersonal variation with race and age and differences between anatomic sites [20]. Compared to adults skin, infant skin (< 12 months) is structurally and compositionally different yet functional. For example, infants have higher transepidermal water loss (TEWL, a marker of barrier function), more water content yet

lower NMF, and higher pH (newborns) [21, 22]. Perhaps the clearest difference in skin barrier function and structure is between anatomic sites. Different skin sites vary in SC thickness, barrier function as measured by TEWL, and structure [23, 24, 25]. Local and interpersonal differences reflect the variety of requirements of skin structure and function. These differences indicate variability in barrier components, processes and regulation to achieve desired functionality.

Not only does the skin differ significantly with race, age and anatomic site, its composition changes with depth too. In the epidermis, four different layers contribute to the orderly differentiation of keratinocytes to ultimately form the SC. Newly produced cells at the basal layer of the epidermis move up through the different layers, each with its own micro environment and function in differentiation, until the cells are shed off at the skin's surface. After keratinocytes have been pushed up from the proliferating basal layer to the top of the stratum granuloum, through various functional layers, cornification of keratinocytes takes place to form corneocytes. In the stratum corneum, cellular envelopes and intercellular lipid bilayers are formed, contributing to the permeability barrier, with corneodesmosomes strongly linking cells together [26]. Towards the top of the SC, cells are shed off in a process called desquamation. This heterogeneity in depth is necessary for the continuous self-renewal of the epidermis, while maintaining its barrier function.

As completely different environments exist on both sides of the SC barrier (inside the body and outside), various gradients are formed inside the SC. Most notably, there is a steep water gradient from a high water concentration inside the epidermis to a low water concentration at the surface of the SC [27, 28]. Also, gradients of pH [29] and natural moisturising factor [30, 31] have been observed. Altogether, this leads to a spatially heterogeneous tissue, and a depth-dependent SC barrier. For instance, Kubo *at al.* have shown different permeabilities to small metal ions within the SC [32].

Similar to the SC, the TJ barrier junction is subject to continuous renewal, and faces challenges to maintain barrier homeostasis under these conditions. The difference is that the SC is a stratified epithelium consisting of multiple layers, while the TJ barrier is one simple continuous layer covering the intercellular spaces [33, 34]. To maintain

the TJ barrier while cells transition, the TJs have to be translocated without breaking their continuous cover. The mechanisms and signalling of transition mechanisms should act at the right location and depth.

For such a heterogeneous tissue, depth-dependent processes and regulation are important to maintain specific functions along the depth of the epidermis, which help sustain barrier function in a continuously self-renewing tissue. Consequently, further research should aim at advancing our understanding of the role of depth-dependent processes regulating the permeability barrier. This knowledge can contribute towards the understanding and treatment of skin diseases, many of which are barrier-related, and the optimisation of transdermal drug delivery.

1.2 Better understanding of epidermal barrier homeostasis requires modelling of depth-dependent processes

Despite the indubitable importance of depth-dependent processes in the regulation epidermal barrier homeostasis, integrated experimental or modelling approaches to study these are limited. A myriad of experimental and clinical data, which describes the structure and function of individual barrier components and the state of the barrier in pathological or physiological conditions, is available. However, these data are often obtained from isolated experiments, where a single or small number of components or barrier properties are considered, while the interaction between many components and processes on various temporal spatial scales determines the functioning of a tissue. The scale and complexity of the regulation of epidermal barrier homeostasis is impossible to capture in single experiments. Instead, mathematical models and frameworks that integrate various experimental data can be adopted to study these complex interactions. Complementing experimental data with mathematical models enables analysis of large sets of data, and simulation and prediction of different biological scenarios and conditions.

The application of mathematical modelling is widespread in dermatology, mainly in

the area of permeation and pharmacokinetic modelling. Modelling approaches that aim for mechanistic or system understanding of barrier homeostasis are less common. However, systems biology applications within the field of dermatology, or 'systems dermatology', is emerging [35, 36]. An example of such an approach is the development of a model for studying atopic dermatitis. Tanaka *et al.* propose a model of AD that incorporates barrier homeostasis, inflammation and their interplay, demonstrating the role of feedback in the regulation of kallikrein activity [37]. Extension of this model to include two time-scales at both the cellular and tissue level by Domínguez-Hüttinger *et al.* reveals the effect of risk factors on the onset of AD through the interaction between barrier defects and inflammation [38]. The model is then further developed by incorporating a double switch mechanism that explains how Th2 sensitisation can be triggered by environmental stressors [39]. This example shows how the continual development and refinement of models can successfully advance our understanding of underlying regulatory mechanisms in health and disease.

Quantitative understanding of the permeability of the skin is increasingly important in a number of ways. As the barrier limits transdermal drug delivery, mathematical modelling is used to enhance our understanding of permeation and absorption of topically applied transdermal drugs, cosmetics, skin treatment, and for toxicity testing [40, 41, 42].
Nowadays, pharmacokinetic modelling is an integral part of the design and review of new drugs and cosmetic products by informing and directing experiments and clinical trials, for example by predicting dosage. Additionally, accurate mathematical models can be used as replacement for animal models.

Non-invasive experimental techniques such as confocal Raman spectroscopy (CRS) [43] provide a unique opportunity to study the epidermis *in vivo*, which could provide additional data on SC barrier structure, components, interactions and their depth-dependency. For example, the depth-dependent levels of water concentration and changes in the structure and organisation of lipids in the SC can be measured by CRS [28].

In this thesis, we take a modelling approach to combine and integrate such experimen-

tal data in order to increase our understanding of the depth-dependent permeability barrier in the SC. Furthermore, we propose models for studying the regulation of barrier homeostasis of both the SC and the TJ barrier.

1.3 Aims

The main overarching aim of this thesis is to gain a better understanding of the depth-dependency of the skin's permeability barrier and the role of depth-dependent processes in regulating barrier homeostasis while continuously self-renewing. The depth-dependency is crucial in maintaining both barriers during turnover. As the cells constantly move up through the epidermis, several depth-dependent processes control the building, maintenance and degradation of the SC barrier. Therefore, we want to investigate how the permeability barrier changes along the depth of the SC, and which components and mechanisms regulate these changes. In the SG, the TJs have to be replaced continually due to the cells translocating across the barrier. The mechanisms responsible for the orderly TJ barrier transition require temporal and spatial coordinated along the depth of the SG. We want to study how this coordination in time and place ensures barrier that the TJ barrier is maintained, at the same place in depth, while TJs between the transitioning cells are replaced. We plan to achieve this by using mathematical modelling in combination with experimental data. The models will be simple and only capturing the essential components and interactions, and lead to further insight by integrating available measurement data.

In particular, the objectives to achieve the aim are:

To characterise the depth-dependency of the SC permeability barrier. In order to understand the depth-dependency of the barrier, we first need to characterise the barrier along the depth of the SC. Therefore, we develop a compartmental model of the resistance to water diffusion within the SC that can be applied directly to available experimental data.

To study the role of depth-dependency in SC barrier regulation and homeostasis. For

this objective, sub-models describing the depth-dependent profiles of the main barrier components will be constructed, as well as a model of the depth-dependent regulation of desquamation. Using such models, we can simulate the interaction between the barrier components and how their depth-dependency contributes to regulating barrier homeostasis.

To model the TJ barrier transition. We create a 3D geometrical model of the maintenance of the TJ barrier function while keratinocytes translocate from the basal to the apical side of the barrier. Simulation results can be compared and fitted to experimentally data to obtain transition dynamics and propose a temporal coordination mechanisms.

Together, addressing these objectives will lead to a better understanding of the depth-dependency of the skin's permeability barrier and the role of depth-dependent processes in regulating both TJ and SC barrier homeostasis in a constantly renewing tissue.

1.4 Publications

The following peer-reviewed journal publications are (partially) reproduced in this thesis:

- **M.D.A. van Logtestijn**, E. Domínguez-Hüttinger, G.N. Stamatas, R.J. Tanaka. Resistance to water diffusion in the stratum corneum is depth-dependent. *PLoS ONE* 10(2): e0117292. February 11, 2015. DOI: 10.1371/journal.pone.0117292. *Reproduced in chapter 3.*

- **M.D.A. van Logtestijn**, P.J. Caspers, S. Kezic, D.R. Hoffman, D.W. Koenig, M. Ono, G.N. Stamatas, and R.J. Tanaka. Water resistance profile as a marker of skin barrier damage in atopic dermatitis patients. *Journal of Dermatological Science*, pages 126-128, volume 81, issue 2, February, 2016. DOI: 10.1016/j.jdermsci.2015.10.017. *Reproduced in chapter 4.*

- M. Yokouchi, T. Atsugi, **M.D.A. van Logtestijn**, R.J. Tanaka, M. Kajimura, M. Suematsu, M. Furuse, M. Amagai, A. Kubo. Epidermal cell turnover across tight junctions based on Kelvins tetrakaidecahedron cell shape. *eLife* 2016;5:e19593. DOI: 10.7554/eLife.19593.
  Chapter 6 is a continuation of this work. Two figures are reproduced in chapter 6, and part of the published code is used.

The following manuscripts are currently in preparation:

- Mathematical modelling of stratum corneum barrier homeostasis. *In preparation; results from chapter 4.*
- Mathematical modelling of epidermal cell turnover suggests tight junction barrier transition timings and mechanisms. *In preparation; results from chapter 5.*

1.5 Outline

This thesis is organised in the following way. First, the two epidermal permeability barriers are introduced in chapter 2 to provide background information on the structure and function of SC and TJ barriers and their depth-dependency. As the skin disease atopic dermatitis is discussed in various parts of this thesis, an overview of AD pathogenesis and its relation to the skin barrier is included as well. In a brief review of the modelling literature, we highlight past approaches to epidermal homeostasis and permeability modelling.

In chapter 3 the *SC compartment model* is proposed to characterise the depth-dependency of resistance to water diffusion in the SC. Different sets of data are analysed using the resistance profiles to compare the permeability barrier between skin sites, infants versus adults, after application of oils, and for dynamic simulation of absorption-desorption experiments. The SC compartment model is applied to additional experimental data in chapter 4, where we obtain the depth-dependent barrier profiles from AD patients and healthy subjects during recovery after mechanical and chemical barrier damage. To study how depth-dependency in the SC plays a role in regulation

of barrier homeostasis, simple mathematical models describing the depth-dependent profiles of barrier components and the regulation of desquamation are proposed in chapter 5. These submodels are combined to form the *SC barrier homeostasis model* which provides a framework for studying SC barrier homeostasis.

In chapter 6, the research on depth-dependent barrier function is extended to the SG and its TJ barrier. Modelling of the 3D geometry of keratinocytes and the SG is used to simulate the transition of cells through the TJ barrier.

The thesis ends with a summary of the results and concluding remarks in chapter 7.

Chapter 2

The skin's depth-dependent permeability barrier

This chapter provides an introduction to the biology of the two main skin barriers: the stratum corneum and the tight junction barrier in the stratum granulosum. We present an overview of the existing body of research on the skin's permeability barrier, which focusses on the structure and composition of the SC and TJ barriers, their permeability to a variety of substances, and depth-dependent processes and their importance to barrier homeostasis. In skin diseases such as atopic dermatitis, the skin's permeabilty barrier can be disrupted, causing further damage. Since AD is the main skin disease that will be discussed in this thesis, the underlying mechanisms of atopic dermatitis and its relation to barrier function are elaborated in section 2.1.3. The experimental techniques that are commonly used in experimental dermatology and clinical settings are presented in section 2.2. These techniques include the measurement of barrier function by trans-epidermal water loss (TEWL), and techniques that enable measurement along the depth of the SC to construct depth profiles of SC components or properties, such as confocal Raman spectroscopy (CRS) and tape stripping. The (published) experimental data presented in this thesis were obtained by CRS and TEWL measurements. The chapter ends with a review of the current state of modelling the skin's permeability barrier and its depth-dependency.

2.1 Structure and function of the epidermis

Human skin is generally divided into two layers, the epidermis and the dermis, separated by a basement membrane. The epidermis is a stratified epithelial tissue which can further be divided into four distinct layers, each with their own structure and function: the basal layer (stratum basale), spinous layer (stratum spinosum), granular layer (stratum granulosum) and cornified layer (stratum corneum) (figure 2.1). The self-renewing epidermis continually replaces its cells, a process that spans 25–56 days for the viable epidermis [44, 45, 46] and around two weeks 14 days for the stratum corneum [47, 48]. In the basal layer, proliferating basal cells create new keratinocytes that will eventually replace the desquamated apoptotic corneocytes at the top of the stratum corneum. The keratinocytes then transition through all layers, each of which includes several elements that contribute to the keratinocytes' differentiation, until the cells reach the SG/SC interface. There, the process of cornification takes place, in which the keratinocytes lose their nucleus and form their specific structure to effectively function as a protective barrier.

2.1.1 The stratum corneum

The skin has a remarkable ability to protect the body against outflow of water and other substances, and against inflow of external pathogens. The stratum corneum is only roughly 10–20 µm in thickness, depending on skin site [49]. Its barrier function is largely dependent on the structure and form of the SC, a classic example of 'function follows form'. The SC structure can be represented by a 'bricks and mortar' model, first coined by Peter Elias in 1983 [50], based on the separation of corneocytes (bricks) and intercellular lipid bilayers (mortar). The flattened corneocytes are about 1 µm thick, and are stacked in a staggered way, creating a tortuous extracellular pathway (figure 2.2) [51, 52]. Lipid bilayers are responsible for blocking the extracellular route of diffusion, and are therefore considered to be a main contributor to barrier resistance. These lipids are released by lamellar bodies in the SC/SG interface, after which they are processed and organised into lipid bilayers [53]. This intercellular lipid matrix

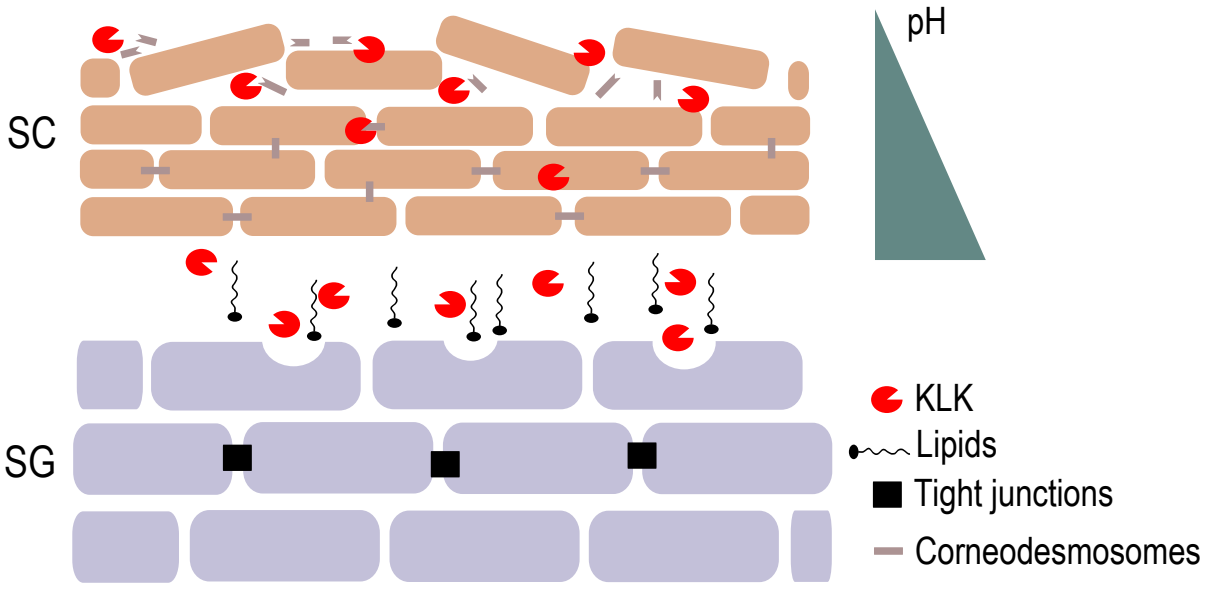


Figure 2.1: **The stratum corneum and tight junction barriers in the upper layers of the epidermis.** The tight junction barrier is formed by a single layer of tight junctions that connect neighbouring cells in the stratum granolusum. Lipids and proteases are released to the extracellular space in the SC/SG interface. These lipids form intercellular lipid bilayers which obstructs the permeation of substrances through the SC. A pH gradient regulates desquamation: the degradation of corneodesmosomes by KLKs leading to the shedding of corneocytes.

contains free fatty acids, ceramides and cholesterol in approximately equimolar ratios [54]. Given that a sufficient amount of lipids is present, it is the ratio of the different lipids groups and their spatial organisation and conformation that determines their effectiveness in creating resistance to diffusion [55, 54]. Two lipid packings are found in the SC: hexagonal and orthorhombic, with the latter packing providing a more effective barrier [55].

While the lipids cover the extracellular pathway between the corneocytes, the corneocytes themselves also undergo a major transformation to limit transcellular permeation and provide SC integrity and cohesion. During cornification or keratinisation (the process of terminal differentiation of keratinocytes), elastic fibrous proteins known as keratins, expressed in the viable epidermis, are processed to form filaments [56]. These keratin filaments are aggregated into bundles by flaggrin, which helps

form the flat shape of the corneocytes in the SC [57]. The cornified cell envelope is then assembled through crosslinking the keratin filaments to various proteins and lipids by transglutaminases [58, 26]. Furthermore, the desmosomes linking cells in deeper layers are strengthened to form corneodesmosomes by crosslinking specific proteins [59].

An important state of the stratum corneum is its hydration [60]. Hydration or water content is vital for appearance and physical skin characteristics such as plasticity and tensile strength. Water is also necessary for the functioning of hydrolytic enzymes that control maturation and desquamation [61, 62, 63]. One of the main contributors to SC hydration is a group of intracellular hygroscopic compounds called natural moisturising factor (NMF). Some of its most abundant components include free amino acids, pyrrolidone carboxylic acid, sugars, lactate, urea, salts and ions (full composition of NMF has been published elsewhere, e.g. [61]). NMF is mostly a breakdown products from proteins such as filaggrin [64, 65]. They retain water inside the corneocytes by providing sites for hydrogen-binding of water. The level of water binding, or water mobility, is a continuous scale: from 'bound' water molecules with direct hydrogen bonds to NMF components; to 'intermediately mobile' water with hydrogen bonds to bound water molecules; to 'mobile' water which can diffuse more freely [66, 67, 68]. The distribution of water mobility changes with depth [66, 67]. Despite the importance of hydration, its exact relation to barrier function remains unclear. For example, dry skin (e.g. because of a lack of NMF) does not necessarily affect TEWL ([69] and references therein).

Stratum corneum homeostasis

SC homeostasis is considered here to be the maintenance of a healthy SC structure and thickness, providing a well functioning permeability barrier. It is achieved by the careful balancing of tightly controlled cornification and desquamation processes. The first part of barrier homeostasis we consider is the process of cornification and its regulation (in particular the temporal regulation, its spatial regulation is discussed further in chapter 6). Cornification takes place at the SG/SC interface, where its main processes include the release of lamellar bodies which contain the extracellular lipids and

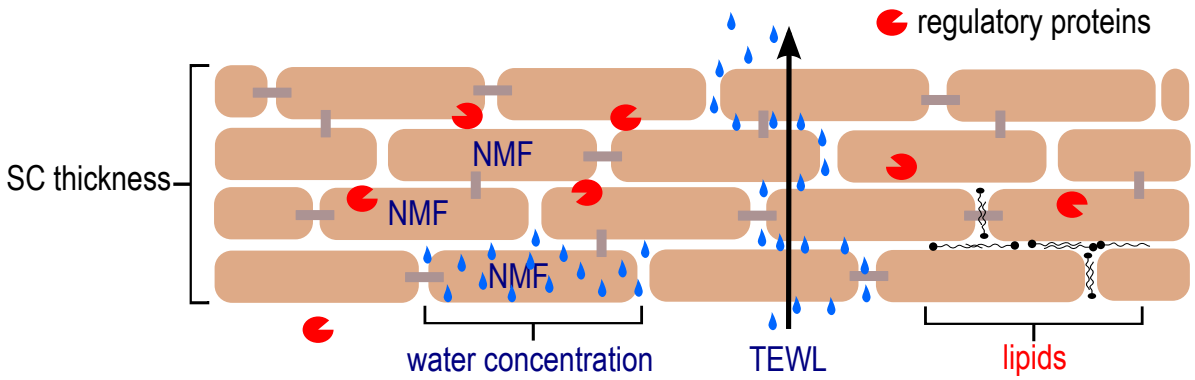


Figure 2.2: **The stratum corneum.** The permeability barrier of the stratum corneum is formed by the lipid bilayers blocking the extracellular pathway. The barrier function is measured by trans-epidermal water loss (TEWL). Water, bound to natural moisturising factor inside the corneocytes, provides hydration to the skin, and is necessary for enzyme reactions including regulatory proteases such as KLKs.

essential proteins, and the terminal differentiation of keratinocytes into corneocytes [70]. Different mechanisms are known to induce or inhibit the rate of cornification, which are most apparent after barrier damage. For instance, after barrier disruption by tape stripping or application of acetone, the main recovery mechanism is an alteration in cornification processes [71, 72, 73]. Both positive and negative feedbacks with different rates and timing ensure a controlled reacting balancing a quick improvement of barrier function and replacement of the SC in the longer term [72, 73, 74, 75]. The epidermal calcium gradient regulates differentiation and cornification processes, with TEWL as a signal of barrier function. This gradient can be established and maintained by the SC barrier [74]. When the barrier is disrupted, TEWL will increase. With this increased water flux, the calcium ion concentrations will change [76, 74, 77]: Specifically, the calcium concentration peak at the SG/SC interface will decrease [78, 79]. A decrease in calcium levels will lead to an immediate release of pre-formed lamellar bodies, thus initiating barrier repair [80, 74]. If TEWL is lowered by occlusion after barrier damage, recovery is delayed [80, 74].

Cornification needs to be balanced by matching rates of desquamation to maintain a steady state SC thickness. Desquamation is the shedding of cells from the top of the skin. To prepare for desquamation, corneodesmosomes are degraded by proteases,

which causes the layers of the skin to become increasingly detached until the corneocytes are shed off [81]. For proper skin functioning, it is essential that desquamation only takes places at the top of the SC. Therefore, both the rate of desquamation and the location of protease activity and corneodesmosome breakdown must be tightly regulated. The most-studied serine proteases which are considered largely responsible for the degradation of corneodesmosomes are the stratum corneum tryptic enzyme (KLK5) and the stratum corneum chymotryptic enzyme (KLK7) [82, 83]. These are released to the extracellular space by lammellar bodies in their inactive pro-forms (pro-KLK5 and pro-KLK7) before they are activated into KLK5 and KLK7 respectively [84, 85]. The active forms are then inhibited by a lympho-epithelial kazal-type-related inhibitor (LEKTI), such that they are unable to break down corneodesmosomes [86]. Only towards the top of the SC is this inhibition reversed, allowing active KLK to degrade corneodesmosomes to conduce desquamation. The effect of the absence of LEKTI can be observed in patients with Netherton syndrome (NS), where LEKTI deficiency is cause by a loss-of-function mutation in the *SPINK5* gene (serine protease inhibitor of kazal type 5) which encodes LEKTI [87]. The skin of NS patients is dehydrated and inflamed, stunted growth, which can be attributed to a lack of KLK inhibition [88].

Desquamation and its regulation will be discussed in more detail in chapter 5, where the depth-dependent interaction between desquamatory proteases and their inhibition regulated by pH will be modelled.

2.1.2 The stratum granulosum and the tight junction barrier

Only in the last twenty years, when the focus of research interests shifted towards the barrier function of the TJs in the epidermis, has the concept of TJs as a permeability barrier been explored. Over these last two decades, it has become increasingly clear that besides the SC as the main permeability barrier on the interface between our body and the outside, the TJ barrier also plays a major role as a selective permeability barrier by limiting transport and separating the viable epidermis from the SC [89, 90, 91]. It functions as a regulatory and signalling mechanism, affecting other layers of the

epidermis and their homeostatic processes [34]. TJs have since attracted great research interest, both in its constituent proteins and function.

Tight junctions are cell-cell junctions which form a barrier in the SG [92, 93]. They consist of a complex structure with a number of transmembrane proteins, including zona occuldens, occludin, claudins and junctional adhesion molecules [94, 95, 96, 97]. In the 1970s, Claude [98, 99] found that the structure of zonula occludens contributed to barrier function in simple epithelia, and discovered that the tight junction strands exponentially increase the transepithelial resistance (TER), a measure of the strength of the permeability barrier. Although there was plenty of evidence of TJs in simple epithelia, evidence of the TJ barrier in the statified epithelium of the epidermis was scarce until the beginning of this century. Studies in animal models have suggested the importance of TJ for control of skin permeability: Furuse *et al.* reported that mice lacking claudin-1 die from dehydration [3]; Schluter *et al.* found that cells of the uppermost granular layer are connected by a continuous TJ barrier that contributes to the paracellular distribution of water, solutes, and particles [100]. The intercellular TJ complexes limit the diffusion of water and solutes from SG to SC through the intercellular spaces, and thereby control permeability of the paracellular pathway [101]. The horizontal layer of TJs seals all intercellular, creating an inside-outside barrier which separates the epidermis into an apical and a basal compartment to maintain their respectively unique micro-environments [102].

Besides its barrier function, the TJ also plays a role in the immune response through langerhans cells (LC) [103]. Langerhans cells (epidermis-specific dendritic cells) are the only immune cells present in the SC [12]. Once the LCs are activated, their tips are extended through TJ barrier to just below the SC [104, 105]. The TJs form a new structure around the extended LC tips to maintain barrier function. However, tight junctions proteins and barrier are negatively affected by cytokines [106].

Tight junction defects have been found in a number of pathologic skin conditions [107, 91, 34]. For example, in the cases of atopic dermatitis [108, 109, 110, 111] and psoriasis [112], TJ protein expression is altered and the TJ barrier is damaged. TJs are also thought to play a role in regulation of aged skin [113].

As the tight junction barrier is involved in epidermal homeostasis and terminal differentiation, it is susceptible to playing a role in tumorigenesis [114, 115]. TJ proteins are either up or down regulated in cancer, and it is likely that TJ barrier disruption either accompanies tumorgenesis or initiates disturbance of homeostasis [116, 117, 118, 119, 120].

The mechanisms of maintaining a functional TJ barrier during continuous turnover as well as the role of the TJ barrier in epidermal homeostasis will be further investigated and discussed in chapter 6.

2.1.3 Atopic dermatitis

In this thesis, we focus on the skin disease atopic dermatitis (AD). AD is a common chronic inflammatory skin disease with high and increasing incidence [121, 17, 16]. Its main symptons are pruritis, xerosis and erythema, and is further characterised by a combination of defects in innate immunity response and a defective SC barrier [121, 122, 14]. Even in non-lesional skin sites, the permeability barrier is affected [123]. Additionally, tight junction defects have been observed in AD, indicating that, besides the SC barrier, the tight junction barrier in the SG is affected as well [109, 124].
Initially, AD was considered mainly an immunologic disease. Recently, however, the importance of the aberrant barrier has been recognised, and a discussion started about the question where the altered immune system leads to (inside-outside), and whether the defect barrier predates a dysregulated immune system (outside-inside). Several observations support either the inside-outside hypothesis, the outside-inside hypothesis, or both (see for example Elias *et al.* and references therein [125]). This suggest the immune systems and skin barrier mutually affect each other, leading to the current outside-inside-outside hypothesis: Abnormalities in barrier structure and function lead to more penetration of pathogens and in turn increase immune reaction and inflammation, which further deteriorates the barrier [126, 125, 15, 127]. Moreover, high IgE levels caused by the sustained inflammation leads to pruritus, and the provoked scratching further increases barrier defects [121, 128].
Exact causes of the initial barrier defects that could lead to the onset of AD are un-

known, although several risk factors have been identified [38]. The highest risk factor for developing AD is a filaggrin loss-of-function mutation [129]; 14-56% of all European AD patients have this mutation [130]. However, 40% of people with a filaggrin mutation never develop AD [131].
Common treatment of AD includes a combination of both barrier-improving emollients and anti-inflammatory topical corticosteroids [132].

The outside-inside-outside view of AD pathogenesis emphasises the relevance of skin barrier in diseases. Children, who have an underdeveloped SC barrier, are more likely to develop AD. AD can be the first step in the atopic march: the development of other allergic diseases like asthma and rhinitis [133, 134]. Treatment of neonates with moisturisers and emollients, which improve the permeability barrier, prevents the developement of AD [135, 136] and the subsequent atopic march [137].

In this thesis, we explicitly study AD in chapters 4 and 5. In chapter 4, we obtain data from AD patients to compare their barrier function to healthy patients and. In chapter 5, the SC barrier homeostasis model is perturbed to replicate AD conditions and the consequent misregulation. Moreover, the relevance and implications of our findings on barrier function to AD are discussed throughout this thesis.

2.2 Non-invasive *in vivo* experimental techniques for experimental dermatology

One of the advantages of studying the epidermis is its accessibility, which enables the studying of tissue *in vivo*. Over the years, a number of *in vivo* experimental measurement techniques have been developed, with trans-epidermal water loss (TEWL) measurements being the most frequently used technique. TEWL is a common indicator of SC barrier function, and currently the main experimental and clinical way to characterise barrier function. The SC is the main barrier to water loss, and the water lost per unit of time and skin surface determines the functioning of the barrier, with lower TEWL values representing a better barrier. TEWL is measured using either open

chamber or closed chamber technologies. They both use the humidity gradient of water vapour caused by the loss of water from the skin and temperature measurements to derive TEWL [138]. TEWL is sensitive to a range of physiological and environmental factors, such as changes in relative humidity and temperature, age, circadian rhythm, season, ethnicity, and skin site [139, 20].

While TEWL is the main available indicator, some researchers have suggested that TEWL measurements alone are not sufficient to describe skin barrier function in several cases. For example, Chilcott *et al.* investigated the permeability of *in vitro* pig skin to titrated water, and concluded that *in vitro*, basal TEWL rates do not correlate with skin barrier function measured *in vitro* using titrated water [140]. According to Lu *et al.*, baseline TEWL is not enough to quantify the intrinsic barrier function, as cosmetic dry skin has the same TEWL as normal skin, but higher thickness and lower barrier quality (as measured by the change in TEWL after tape stripping) [141].

In this thesis, we combine TEWL with confocal Raman spectroscopy (CRS) measurements. CRS is a microscopy technique in which a laser is focused at a certain depth in the skin, and the scattered light is collected. The wavelength shift of the reflected light results from changes in the energy states of the molecules. From these obtained Raman spectra, wavelength shift bands can be linked to skin components such as water, lipids and NMF, and its band intensities correspond to relative amounts of those molecules [43, 27, 28]. Spectra can be obtained from two regions. The fingerprint region (400-1800 cm^{-1}) contains information on keratin, lipids and NMF components, whereas the high wavernumber region (2600-3800 cm^{-1}) is used to obtain water/protein and lipid/protein ratios, and has further information on the molecular-bound states of water [66]. Raman profiles of water concentration clearly confirmed the existence of a water concentration gradient in the SC, as well as profiles of NMF and lipids [142, 143, 28, 144, 145].

Besides obtaining depth profiles of SC components, there are various further applications of CRS, some of which will be applied in this thesis. CRS water profiles can be used to calculate (functional) SC thickness [146, 147, 148, 149]. While there is a water concentration gradient in the SC, there is a constant water concentration in the SG and the rest of epidermis. Therefore, the water concentration plateaus at the SC/SG inter-

face. The depth of intersection of the SC gradient and the (flat) gradient below is taken as the SC thickness. This point also corresponds to an the start of an increase in CRS obtained NMF profiles, as filaggrin is only broken down to NMF at the bottom of the SC [150, 151]. In this thesis, SC thickness is calculated in the same way [148].
Other applications include rapid determination of filaggrin genotypes based on Raman NMF levels, which is useful for AD patients [152]. Filaggrin mutations lead to lower NMF and correlate with AD severity [153], and children with the least filaggrin and NMF are more likely to develop AD [154]. Also, Raman can be used to obtain (time-course) profiles of compounds into the SC in order to study penetration of drugs through the SC as well as penetration enhancers for transdermal drug delivery [155, 156, 151, 157, 158].

The advantage of CRS is that it is truly non-invasive, whereas other depth-profiling techniques usually depend on more invasive methods such as tape stripping or taking biopsies. Tape stripping is the removal of layers of corneocytes using adhesive strips. It is used for two main purposes. Tape stripping induces barrier damage by removing layers of cells, and the state of barrier after the damage and its recovery can subsequently be measured, for example using TEWL, pH or hydration measurements [159, 160, 161]. Furthermore, the strips contain the removed contents of the SC at the measurement depth, which can be analysed to obtain depth profiles of SC components [162, 163, 164]. The thickness removed by a tape strip changes with SC integrity, skin site, applied pressure and duration [165, 166, 167, 168]. As it is important to quantify the thickness removed for the constructing depth profiles, it is often more accurately derived from the amount of protein removed by the tape strip, assuming the amount of protein is constant across the SC [169, 170]. While tape stripping is only minimally invasive, it still disrupts the SC, inducing water loss and immune reactions, thereby initiating barrier repair mechanisms.

2.3 Modelling the skin's permeability barrier

Mathematical modelling of the skin has been commonplace for the last decades. Here, an overview is provided of the modelling approach that have been applied to various aspects of skin research, with a special focus on modelling of the permeability barrier and models that include spatial effects and depth-dependency.

The stratum corneum functions as the permeability barrier of the skin and, unsurprisingly, a large body of skin-focused modelling research focuses on this permeability barrier function. As diffusion of substances through the SC is passive, the starting point for most of this research is Fick's laws of diffusion [171]. Arguably the most important 'model' in understanding SC permeability is the 'bricks and mortar' model, which separates SC permeation into a transcellular (corneocytes or bricks) and an extracellular pathway (lipids bilayers or mortar). The question of which of the two is the main pathway through which water and other molecules permeate has been a topic of discussion [172, 173, 174]. Finite element methods [175, 176, 177, 178] and PDE diffusion models [174, 179, 180, 181, 182] have used the 2D geometry of the bricks and mortar model to study permeation of various molecules and chemicals through both pathways. Using a (flattened) tetrakaidecahedron to approximate the geometry of keratinocytes and corneocytes [183], geometric models can accurately represent the SC structure in 3D to further refine permeation modelling [184, 185, 186].

Compartment models are often used in pharmacokinetic/pharmacodynamic (PK/PD) modelling, where the SC is represented by one compartment with a single diffusion coefficient [187, 188]. In this thesis, the model of the SC consists of several compartments, each with a different coefficient to incorporate spatial differences within the SC. Other modelling that incorporates the heterogeneity of the SC includes Hansen *et al.* [189] who examined the role of corneocytes in skin transport using two-compartment models of the SC, and Anissimov and Roberts [190] who studied the effects of variable diffusion coefficients in the SC on absorption kinetics.

Quantitative mathematical models that describe the permeation of substances such as drugs through the epidermis have various applications, including the prediction of

dermal absorption and transdermal drug delivery [188, 41, 40, 191, 42]. Several such mathematical models aim at predicting skin permeability by considering experimentally determined structural parameters of the permeants (for overview see [192]). For example, the Potts and Guy model uses the molecular weight and the octanol-water partition coefficient of the permeating molecules to obtain a general prediction of the permeability of compounds through skin [193].

Where the permeation of molecules and chemicals *into* the skin is of pharmacological importance, the outflow of water measured by TEWL is often used as a marker for skin barrier function. The widespread use to TEWL, and ease of using a non-invasive measurement technique led to the availability of large amounts of experimental and clinical TEWL data. This makes TEWL ideal for modelling, and we find several models that rely on TEWL data, for example Hadgraft and Lane who propose a simple geometric model of the extracellular pathway length which directly relates to TEWL, and provides a possible explanation for differences in TEWL between skin sites [194]. Fitting of curves to profiles of TEWL measured after sequantial tape stripping can determine SC thickness and the (constant) diffusion coefficient of water [160, 195].
TEWL is also used in modelling of water sorption experiments, for example by predicting and fitting of TEWL curves after occlusion [196, 197]. Water sorption models are useful for determining SC water content and permeability of *ex vivo* skin [198, 199]. Recently, Li *et al.* have presented a PDE model of water transport in the SC which simulates the effects of water content (hydration) on diffusion of water and swelling of the SC [200, 201].

In addition to the mainly ODE and PDE-based modelling of the SC discussed above, a variety of model types and approaches have been applied to study other epidermal properties and epidermal homeostasis. Agent-based models, where the interaction between cells and their differentiation are described by pre-set rules, can be employed to simulate epidermal homeostasis [202, 203, 204, 205, 206, 207] and psoriasis [208, 209], and to analyse stem cell proliferation and clone dynamics [210, 211, 212]. For example, the agent-based epidermal model (excluding the SC) of Grabe *et al.* simulates epidermal homeostasis, and accurately predicts tissue dynamics and the establishment of the

epidermal calcium gradient [213].
Clonal lineage models have been fitted to experimental clone data to infer stem cell proliferation and epidermal homeostasis dynamics [214, 215, 210, 216, 217]. Furthermore, systems biology models have been used to study immune interactions in the skin [218], as well as the interplay between barrier function and immune system [38].

Modelling approaches that explicitly considering the TJ barrier have been sparse. To my knowledge, tight junctions are only included in the attempts of Adams *et al.* to model the regulation of the epidermal calcium gradient, where tight junctions provide resistance against the movement of calcium through the SG TJ barrier [219, 220, 221].

2.4 Conclusion

This chapter provided a broad introduction on the SC and TJ barriers, the technology used to obtain the experimental data in this thesis, and an overview of skin permeability barrier modelling literature.

While some parts are discussed in more detail in the following chapters, this chapter has defined the scope of the research presented in this thesis. Besides its barrier function, the epidermis also provides the first line of the immune system. In this thesis, we do not consider immune system reactions and their effects on the barriers, while acknowledging the importance of its interplay with epidermal barrier homeostasis, especially in diseases such as AD.

As is clear from the literature presented above, there is a wealth of biological knowledge on the structure and function of both epidermal barriers. However, many pieces of biological understanding are isolated, and it is not often possible to connect or test multiple interactions experimentally. Modelling can play a role in studying barrier homeostasis and its regulation which is a result of the interaction of multiple components. Despite the importance of depth-dependent processes in regulating and maintaining both the SC and TJ barriers despite continuous turnover, modelling efforts remain limited. Although there are a number of studies focusing on epidermal homeostasis, the role of TJ and SC barriers are not considered. Specifically, to date there are

no known models that aim to describe the depth-dependency of the SC barrier and its regulation. Developing such a model will be the focus of the next chapters.

Chapter 3

Characterising depth-dependent water permeability barrier in the SC using resistance profiles

3.1 Introduction

The stratum corneum is a heterogeneous tissue, with distinct processes and composition at different depths. Despite being a layer of anucleated cells, it has to perform a variety of functions while continuously renewing. Its permeability barrier function, limiting the outflow of water and protecting the body against external pathogens, can be seen as the 'raison d'être' of the stratum corneum [222].

This chapter aims to characterise the permeability barrier in more detail, focusing on the depth-dependency of the barrier. From the moment cornification takes place at the SG/SC interface, cornceocytes move up and a series of processes along the depth of the SC form, maintain and break down the permeability barrier. These processes are tightly controlled in a tissue where active regulation through expression is impossible. This highlights the importance of understanding how differences along the depth determine the SC barrier function and its regulation.

With recent advances in experimental techniques such as confocal Raman spectroscopy

(CRS), a very accessible tissue such as the SC can be studied across its depth, non-invasively and *in vivo*. Naturally, this provides a number of advantages over invasive or *in vitro* experiments. *In vitro* experiments only study a specific part of the entire system in artificial conditions, omitting essential information about interactions between and signals. Even minimally invasive techniques such as tape stripping disrupt skin barrier homeostasis and lead to (immune) reactions which alter structure and function. Widely available non-invasive experimental techniques like TEWL and CRS create a unique opportunity to study the state of the stratum corneum and its barrier function *in vivo*, both clinically and experimentally. Modelling provides a way to combine that data to gain additional insight.

In this chapter, a compartment model of resistance to water diffusion is developed, with compartments representing different depths in the SC. The model combines experimental TEWL and Raman data to describe the barrier function along the depth. Applying compartmental models to the skin is far from new, especially in pharmacokinetics (see chapter 2 for an overview). The novelty of the model presented here is that the SC is composed of several compartments to represent varying barrier function along the depth of the SC, as well as its design to directly incorporate experimental Raman and TEWL data. Whereas most previous models of SC permeability use a single compartment for the SC and assume a constant diffusion coefficient, our results show a depth-dependent profile of the resistance to water diffusion in the SC. In the discussion section of this chapter we will consider the differences between our results and previous findings in detail.

Characterising the permeability barrier along SC depth in human subjects, across a variety of skin sites and conditions, contributes to understanding how the barrier is formed, maintained and broken down through depth-dependent processes. Nowadays, plenty of clinical and experimental data is available. Our model provides a simple tool to incorporate experimental data into a new index that can intuitively be used to compare barrier function. Furthermore, the resistance profiles can serve as a framework for further investigation into how the permeability is formed by the components, and regulated to maintain a functional skin barrier while continuously renewing the

SC (chapter 5).

The next section describes the development and application of a model to describe the permeability barrier of the SC in a depth-dependent manner. The subsequent discussion focuses on various aspects of the presented resistance profile model including its usage and applicability, and the results in relation to the existing body of literature regarding the depth-dependency of the stratum corneum permeability barrier.

3.2 Resistance to water diffusion in the stratum corneum is depth-dependent

This section is reproduced from the paper *'Resistance to Water Diffusion in the Stratum Corneum Is Depth-Dependent'* [223] published by Van Logtestijn *et al.*[1] in *PLOS ONE*[2] in 2015 under a Creative Commons Attribution (CC BY) license.

3.2.1 Introduction

The main function of the stratum corneum (SC) is to provide a permeability barrier that limits the inflow of external potential irritants, while at the same time controlling the outflow of water from the body to prevent dehydration and retain water [222]. Appropriate hydration in the SC is vital not only for helping to plasticize keratin fibers and provide flexibility to the skin, but also for realization and regulation of all the biochemical processes occurring in the SC by its constituent components [224]. These processes, in turn, contribute to forming, maintaining, and degrading the permeability barrier and to ensuring an appropriate level of SC hydration.

[1]Mark D. A. van Logtestijn[a], Elisa Domínguez-Hüttinger[a], Georgios N. Stamatas[b], Reiko J. Tanaka[a]. [a] Department of Bioengineering, Imperial College London, UK. [b] Johnson & Johnson Santé Beauté France, Issy-les-Moulineaux, France

[2]Published: *PLoS ONE* 10(2): e0117292, February 11, 2015. DOI: 10.1371/journal.pone.0117292

Extensive research has revealed the contribution of many SC components to the permeability barrier. Corneocytes, the main components of the SC, are held together by corneodesmosomes to form tight cellular junctions to provide structural integrity to the SC [59]. They are surrounded by a lipid matrix, where lipid bilayers limit the movement of water and other substances through the SC [225]. Corneocytes contain keratin filaments, filaggrin, and natural moisturising factors (NMFs) that bind water to provide hydration [62]. Each corneocyte is surrounded by an insoluble cornified envelope created by cross-linking of membrane proteins and lipids [58]. Given that all these SC components build up the permeability barrier via different processes that occur dynamically along the depth of the SC, from their formation at the bottom of the SC to their desquamation at the outermost layers, the functioning and structure of the permeability barrier naturally change in a depth-dependent manner.

The permeability barrier is typically assessed through measuring transepidermal water loss (TEWL) [139, 20], which gives a single value that does not, by itself, provide information about the depth-dependency of the permeability barrier. The depth-dependency of the permeability barrier has been previously investigated by measuring TEWL after removal of the SC layers by tape stripping [160, 195, 141]. Tape stripping has been also used for depth profiling of several SC components [163]. However, with recent advances in confocal Raman spectroscopy, we are now able to evaluate the depth-dependency of the water permeability barrier using non-invasive *in vivo* measurement data. Accordingly, this paper aims to propose a novel method to combine these non-invasive *in vivo* measurement data and derive the depth-dependent resistance of the SC to water diffusion, using a mathematical model.

While previous pharmacokinetic models of the SC for studying transepidermal drug delivery and absorption mostly assume that the SC is a single compartment with a fixed diffusion coefficient [188, 40], this paper proposes a mathematical model of SC water permeability barrier by assuming that the SC consists of multiple compartments. Each of those compartments is located sequentially at a different depth, and can have a different diffusion coefficient. These novel assumptions enable us to explicitly address and investigate the depth-dependency of the SC permeability barrier.

Note that the possibility of representing the SC by multiple compartments has been previously suggested [226, 227] but with the assumption of a constant diffusion coefficient for all the compartments, which does not allow for evaluation of varied permeability along the depth of the SC.

To demonstrate that the proposed mathematical model can effectively evaluate the depth-dependency of the water permeability barrier, we apply the model to previously published experimental data on TEWL and water concentration measured non-invasively at different depths in the SC by confocal Raman spectroscopy. The original studies for these data sets compared the skin of infants and adults [22], different skin sites [228], and the skin before and after application of oils [229]. For each of these data sets, we derive the resistance profiles, which characterise the depth-dependency of the permeability barrier. Quantitative characterisation of the obtained resistance profiles enable us to investigate underlying mechanisms for formation, maintenance, and degradation of the permeability barrier, and their comparison between different skin types can reveal the mechanisms responsible for differences in SC morphology and physiology. Furthermore, our mathematical model allows us to conduct *in silico* experiments to predict the spatial-temporal dynamics of water diffusion in the SC, which is difficult to obtain through conventional experiments. Combining the available TEWL and water concentration data using a mathematical model complements experiments in gaining quantitative understanding of intricate biological mechanisms.

3.2.2 Results and Discussion

The SC compartment model

To study the depth-dependency of the SC water permeability barrier, we develop a mathematical model of the SC consisting of multiple compartments, which we refer to as the *SC compartment model* in this paper. The model incorporates Fick's first law of diffusion [230] at each compartment at different depths in the SC (Figure 3.1a). The application of Fick's first law determines the relationship between TEWL and the water concentration, measured non-invasively at the top and bottom of the i-th compartment

($i = 1, 2, \ldots n$) of the SC, by

$$\text{TEWL} = D_i K_i \frac{\Delta W_i}{\Delta x_i} = \frac{W_i - W_{i-1}}{R_i}, \tag{3.1}$$

where D_i, K_i, Δx_i, and R_i are the diffusion coefficient, partition coefficient of water between the SC and the ambient air, thickness, and resistance of the i-th compartment, respectively. The $\Delta W_i = W_i - W_{i-1}$ is the difference in water concentration at the top and bottom of the i-th compartment, with W_i being the water concentration in steady-state measured at the bottom of the i-th compartment. The W_0 is the water concentration on top of the outermost compartment, which is in direct contact with the environment, and W_n is the water concentration in the top layer of the viable epidermis. The TEWL for each compartment is the same as TEWL measured conventionally at the top of the SC [231], since the water flux in steady state is equal to the rate of TEWL throughout the SC. The water concentration [% mass ratio water/protein] at sequential depths can be measured by confocal Raman spectroscopy [27].

Depth-dependent resistance to water diffusion characterizes permeability barrier

Using the SC compartment model (3.1), we derive the *resistance* of each compartment to water diffusion by $R_i = \frac{W_i - W_{i-1}}{\text{TEWL}}$, which characterizes how difficult it is for the water to diffuse through the i-th compartment. The resistance R_i is also described with both the diffusion coefficient and the partition coefficient as $\frac{\Delta x_i}{D_i K_i}$ from (3.1), suggesting that both water permeability (diffusion) and binding of water to NMFs (partition) are contributing to the resistance. Plotting the calculated resistances of all the compartments against their respective depth, and interpolating them, provides the *resistance profile* (Figure 3.1b). We use the depth normalized by the SC thickness to facilitate the comparison between the resistance profiles of skin with different thickness.

With regard to the depth-dependency of the permeability barrier, it has been suggested that the SC consists of three distinct regions (bottom, middle, and top) with different "metal-ion barrier properties" [32], with the middle region being the main barrier against diffusion of metal-ions such as potassium and chromium (VI). Despite the difference between metal-ion and water diffusion, we similarly define bottom, middle,

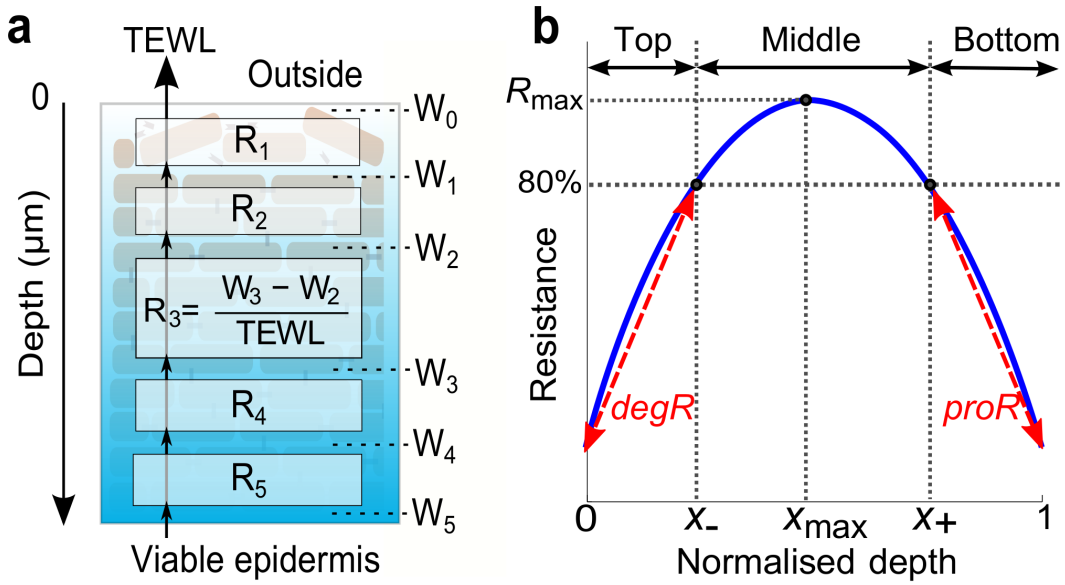


Figure 3.1: Depth-dependent SC resistance to water diffusion. (**a**) Schematic representation of the SC compartment model (5 compartments). Resistance R_i ($i = 1, 2, \ldots, 5$) of i-th compartment is determined from TEWL and water concentration W_{i-1} and W_i at the top and bottom of the compartment. (**b**) Typical resistance profile describing SC depth-dependent resistance. Depth is normalized by SC thickness. $R_{\max}$, $degR$, $proR$ are functional indices and X_-, X_+ and $X_{\max}$ are structural indices for resistance profiles.

and top regions in a typical resistance profile (Figure 3.1b), such that each of the regions corresponds to the formation, maintenance, and degradation of the permeability barrier, respectively. The middle region is the area where the resistance is maintained above 80% of the maximum value ($R_{\max}$ attained at depth $X_{\max}$) throughout. The threshold value of 80% is chosen arbitrarily to capture the distinct region in the middle of the SC, where the profile is relatively flat compared to the other regions and resistance is maintained, as shown in the resistance profile for adults (Figure 3.2b). The bottom region comprises the bottom of the SC (normalized depth=1) to depth $X+$, at which the resistance increases to 80% of $R_{\max}$. This increase in resistance in the bottom region can be attributed to the processing of various components that constitute the barrier. For example, lipids released from lamellar bodies at the SC/stratum granulosum (SG) interface are processed and self-organized to form the intercellular lipid matrix; the organisation of lipids changes with depth [55]; cross-linking of ker-

atin, membrane proteins, and lipids create an insoluble cornified envelope; tightening of corneodesmosome junctions further strengthens the structure of the SC as a barrier from the SG upwards [232, 233]; corneodesmosome concentration and protease activity also change with depth [234]. The production rate of resistance is defined by $proR = \frac{0.8R_{\max} - R(1)}{1 - X+}$, where $R(1)$ is the resistance at the SC/SG interface. Finally, the top region is where the resistance decreases from 80% of $R_{\max}$ at depth X- towards the outermost layer (depth=0). This decrease in resistance is due to active kallikreins (desquamatory serine proteases) degrading corneodesmosomes and the resulting removal of corneocytes and lipids [81]. The degradation rate of resistance is defined by $degR = \frac{0.8R_{\max} - R(0)}{X-}$, where $R(0)$ is the resistance at the outermost compartment.

The resistance profiles are quantitatively characterized by $R_{\max}$, *proR*, and *degR*, all of which indicate the functioning of the SC as a water permeability barrier and are referred to as functional indices. The term $R_{\max}$ indicates the overall strength of the barrier resistance, higher *proR* values imply more efficient mechanisms of barrier construction, and *degR* indicates the efficiency of desquamation processes to degrade the barrier towards the uppermost layer. The spatial characteristics of the resistance profiles can be quantified by $X_{\max}$, X-, and X+, which we refer to as structural indices. The term $X_{\max}$ specifies where the resistance peaks in the SC, higher X+ values indicate that the barrier is formed within a smaller region of depth, and higher X- values suggest that the barrier degradation starts deeper in the SC. Both functional and structural indices enable us to quantitatively compare the resistance profiles obtained for different skin types and help us to study the contributions of constituent barrier components to formation, maintenance and degradation of the permeability barrier, as discussed below.

Age- and site-dependent differences in permeability barrier captured using resistance profiles

To exemplify how the resistance profiles provide insights in the underlying mechanisms related to the depth-dependent permeability barrier, we first apply the SC compartment model to previously published data on water concentration profiles (Fig-

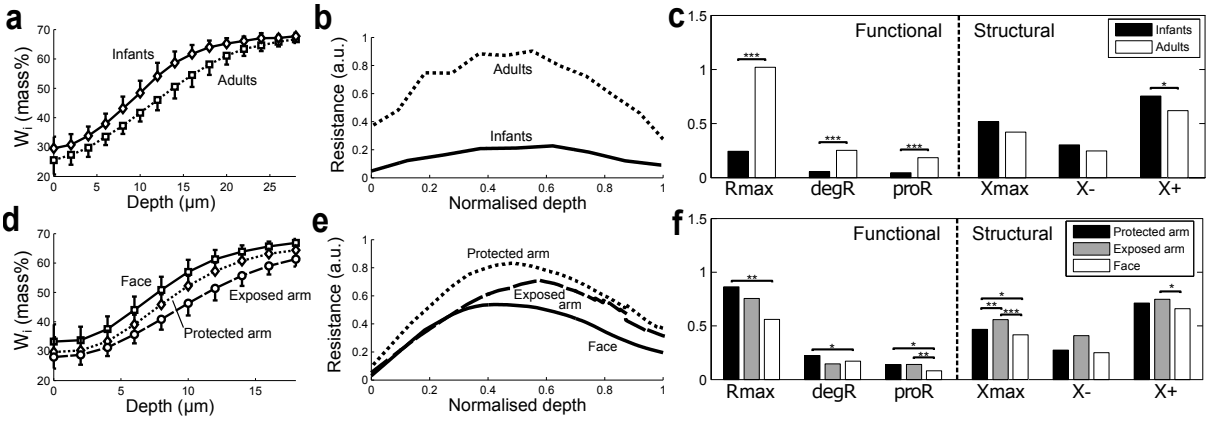


Figure 3.2: **Comparison of permeability barrier for different types of skin.** (**a, d**) Water concentration profiles (means +/− SD), (**b, e**) resistance profiles (means), and (**c, f**) quantitative indices for resistance profiles (means, with significance * $p<0.05$, ** $p<0.01$, *** $p<0.001$) for (**a-c**) volar forearm of 12 infants (3-12 months) and 12 adults (14-73 years) and (**d-f**) face (cheek), exposed arm (dorsal forearm), and protected (upper inner) arm of 20 adults (18-70 years).

ure 3.2a) and TEWL [22] (Appendix A.1) to derive the resistance profiles for adults and infants of 3-12 months old (details in Methods). Infant skin undergoes a maturation process during the early years of life, starting as early as 3 months old [22, 235], when the morphology and physiology of the SC barrier fully develops [236]. The immaturity of the SC barrier for infants of this age (3-12 months old) is conventionally documented by higher TEWL values compared to adult skin [22, 235], although TEWL for babies immediately after birth is reported to be almost the same as that for adults [237]. The resistance profiles for adults and infants (Figure 3.2b) further reveal the depth-dependent function and structure of the SC as a water permeability barrier. The resistance profile for infants clearly shows a much lower resistance than for adults throughout the thickness of the SC. This lower resistance in infants is reflected in significantly lower values for all the functional indices ($R_{\max}$, *proR*, and *degR*, Figure 3.2c), indicating a less efficient barrier function compared to adult skin. In particular, a lower *proR* for infants could be attributed to their higher keratinocyte turnover rates due to increased proliferation [238]. This means that cells move up quicker and have shorter resident times in the epidermis, resulting in less mature differentiation and

cornification and thus a less efficient formation of the barrier. Interestingly, however, the differences observed in structural indices ($X_{\max}$, X- and X+) are not as significant, suggesting that the processes related to formation, maintenance and degradation of the permeability barrier are activated at similar relative depths in the SC.

We also derived and compared the resistance profiles for different skin sites on adults using previously published data on water concentration profiles (Figure 3.2d) and TEWL [228] (Appendix A.1). It is well known that the face has a thinner SC [147] and higher TEWL values [139] than the arms, and they are conventionally used as an indication of a weaker permeability barrier for the face. The weaker resistance for the face can indeed be observed clearly in our calculated resistance profiles (Figure 3.2e) and is quantitatively indicated by lower values for all the functional indices (Figure 3.2f). The lower *proR* for the face reflects a less efficient formation of the barrier, possibly due to higher rates of proliferation [239], as in the case for infants. This also results in shifting the peak of the resistance towards the top of the SC (lower $X_{\max}$) with a lower $R_{\max}$. Comparison of the resistance profiles between protected and exposed arms reveals the effects of photo-ageing caused by chronic exposure to UV radiation, which damages the epidermis and impairs its differentiation processes [240, 241]. The exposed arm has a lower peak in resistance (lower $R_{\max}$) than the protected arm, achieved at a deeper point (larger $X_{\max}$), possibly due to impaired differentiation processes leading to lower availability of barrier component precursors, which limit the barrier formation.

Effects of topical application of oil evaluated using resistance profiles

We further use the resistance profiles to study and predict the effects of skin treatments on the permeability barrier. Pharmaceutical skin care products, such as oil-based moisturizers and emollients, aim to improve SC barrier function by partially occluding the skin, limiting the outflow of water and consequently trapping water in the SC to increase its hydration levels [229]. To quantitatively evaluate and compare the effects of topical application of different oils in increasing the resistance to water diffusion, we applied the SC compartment model to the previously published data on TEWL and water concentration profiles [242, 229] (Appendix A.1). It allowed us to derive the

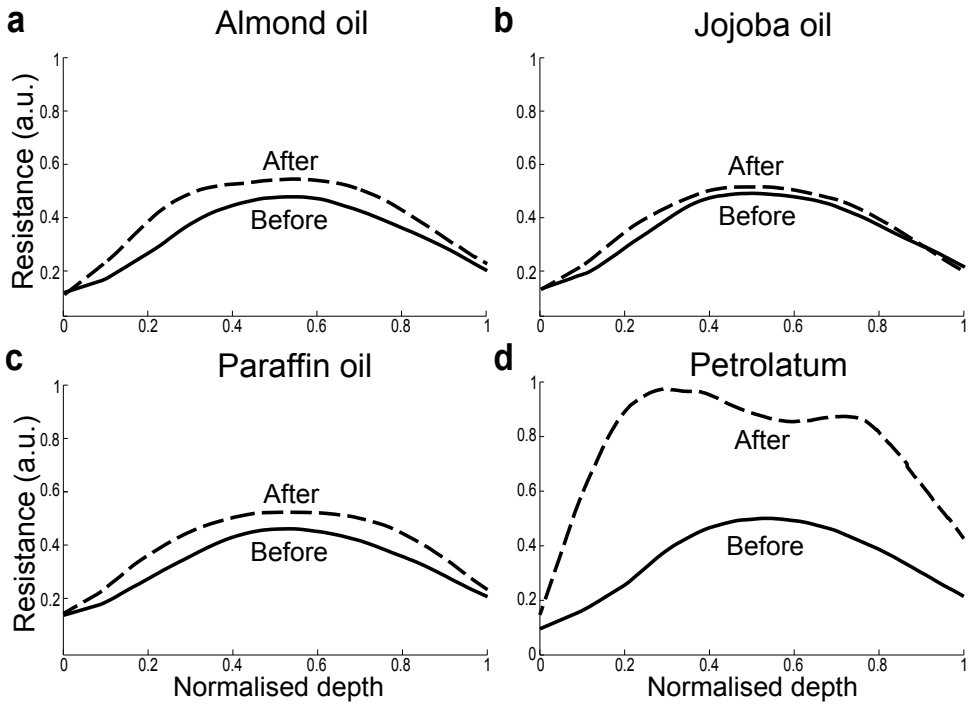


Figure 3.3: **Resistance profiles (means) before and 30 minutes after topical application of different oils:** (**a**) almond oil (n=92), (**b**) jojoba oil (n=98), (**c**) paraffin oil (n=99), and (**d**) petrolatum (n=86).

resistance profiles for the skin before and 30 minutes after topical application of four oils: almond, jojoba, paraffin, and petrolatum. The measurements at 30 minutes after application of the oils are considered to be at steady state [229].

Topical application of all oils increased the resistance over the entire depth of the SC, in a depth-dependent manner, with a higher increase observed in the middle to top than the bottom regions (Figure 3.3). This suggests that the permeability barrier is not only affected by oils through occlusion of the skin since the subsequent decrease in TEWL would simply scale up the resistance profiles in a depth-independent manner. The depth-dependent increase in resistance can be partly explained by local increase in hydration. The increase is highest in the middle region of the SC [243], where most of the NMFs reside and bind to water to prevent its diffusion, resulting in increased resistance against diffusion of water. This result is also consistent with the findings that the middle region is the main barrier against diffusion of metal-ions [32].

Application of petrolatum almost doubles the resistance on average over the entire SC,

while the maximum increase in the resistance by application of the other three oils is about 20% (Figure 3.3d). This strong increase in resistance by application of petrolatum could be due to a larger increase in hydration caused by a larger occlusive effect of petrolatum and a higher concentration of petrolatum reaching deeper in the skin than the other oils [229], to strengthen the intercellular lipid bilayers and increase the resistance across the SC. Interestingly, two peaks are observed in the resistant profile after the topical application of petrolatum. This could be caused by molecular fractionation due to variation in speed of lipid transfer within the SC, which resembles the processes of liquid chromatography [244].

In silico simulation reveals the effects of topical application of petrolatum on spatial-temporal dynamics of water diffusion

To analyze the effects of topical application of petrolatum on the spatial-temporal diffusion of water in more detail, we developed a mathematical model, which describes the dynamical water inflow and outflow of each compartment, using the resistance profiles obtained above.

The dynamical change in the water concentration W_i in the i-th compartment can be described by an ordinary differential equation (ODE),

$$\frac{dW_i(t)}{dt} = \frac{W_{i-1}(t) - W_i(t)}{R_i} + \frac{W_{i+1}(t) - W_i(t)}{R_{i+1}}, \tag{3.2}$$

where R_i and R_{i+1} are resistances limiting the diffusion of water to and from the i-th compartment. The set of ODEs (3.2) for $i = 1, \ldots, n-1$ is referred to as the SC compartment *dynamic* model, which describes the spatial-temporal dynamics of water diffusion. Using the SC compartment dynamic model, we carried out *in silico* simulations of SC water absorption and desorption (details in Methods). These simulations mimic the conditions used in previously published experiments [22], in which water is applied topically to the skin for 10 seconds before being wiped off.

Whereas the original experiments [22] involved measuring the total SC water content at different time points and derived the rates of absorption and desorption of water to quantify the barrier function, our *in silico* experiments further predicted the temporal

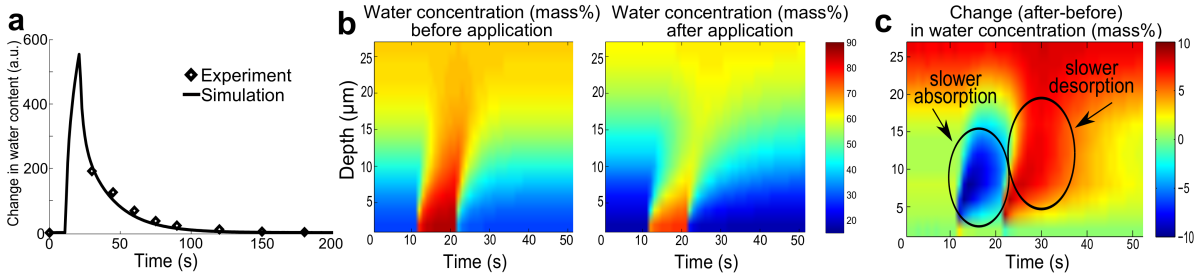


Figure 3.4: **Results of *in silico* absorption-desorption experiment with water applied topically for 10 seconds (time=10-20 s).** (**a**) Temporal dynamics of total water content (change from steady state) for adults; simulation results (solid line) and experimental data (diamonds) [22]. (**b**) Spatial-temporal dynamics of water concentration before and 30 minutes after topical application of petrolatum. (**c**) Spatial-temporal increase in water concentration after application of petrolatum. Negative values (time=10-20 s) and positive values (time=20-50 s) respectively indicate slower absorption and desorption after application of petrolatum.

dynamics of the spatial diffusion of water in the SC. Assuming that the total water content is obtained by summing up the water concentrations in all the compartments along the depth, we compared and confirmed the qualitative match between the total SC water content measured during the experiments for adults [22] and that obtained from our simulations for the skin of adults before topical application of petrolatum (Figure 3.4a).

Our simulation can visualize the effectiveness of topical application of petrolatum in improving the permeability barrier in terms of spatial-temporal water diffusion, which is difficult to observe through conventional experiments. Since petrolatum is generally applied to protect skin with a damaged barrier [245], e.g., for atopic dermatitis patients, detailed understanding of the dynamic effects of petrolatum and other emollients is clinically relevant. The simulation results clearly indicate that the area with high water concentration shrinks by topical application of petrolatum (Figure 3.4b). This is due to the change in kinetics, as the increased resistance by petrolatum prevents water from flowing in and out. It is exhibited by the spatial-temporal change in water concentration by petrolatum application (Figure 3.4c): a slower absorption

of water penetrating less deep for the first 10 seconds while water is applied, and a slower desorption at around 25-35 seconds leading to the increased water concentration to be sustained.

3.2.3 Conclusions

The critical function of the skin acting as a barrier to water diffusion and to tissue dehydration is typically assessed by measuring TEWL. The TEWL however is a single value that provides no information about the dynamic mechanisms (e.g. barrier formation or degradation) that are responsible for the depth-dependent characteristics of the permeability barrier. This paper proposed the SC compartment model, used it to combine existing static TEWL data and water concentration profiles, both of which can be measured non-invasively *in vivo*, and extracted information on depth-dependency of the permeability barrier. Our method used multiple compartments with depth-dependent diffusion coefficients in the proposed SC compartment model, combined with *in vivo* non-invasive measurements. This proposed method is a refinement of previously published one with single compartment SC models combined with tape stripping experiments [160, 195] (detailed comparison in Supporting Information S1). We used the derived resistance profiles to evaluate the permeability barrier of different skin types, and elucidated differences in the underlying mechanisms of barrier formation, maintenance and degradation.

The obtained resistance profiles revealed a depth-dependent water permeability barrier, which peaks at the middle region of the SC, indicating that the barrier is formed, maintained, and degraded from the bottom to the top of the SC. Quantitative characterization of the resistance profiles allowed us to compare the permeability barrier of different skin types (infants vs. adults, different skin sites, before and after application of oils) and lead to the following observations on the underlying mechanisms. Higher proliferation rates both in infants (compared to adults) and in the face (compared to arm sites) lead to a less efficient formation of the barrier, indicated by a slow formation of the barrier (low *proR*) with lower maximum resistance (low $R_{\max}$). Photo-ageing by UV radiation impairs differentiation processes and limits barrier formation, as ex-

hibited by a lower peak in resistance (low $R_{\max}$) achieved at a deeper point in the SC (high $X_{\max}$) on the exposed arms (compared to the protected arms). The increased resistance after topical application of petrolatum leads to less penetration of water and a prolonged increase in water concentration, as predicted by *in silico* experiments for spatial-temporal dynamic of water diffusion in the SC.

Our mathematical modelling approach provides a tool for the analysis of experimental data for a deeper understanding of the mechanisms underlying barrier function. It can be used to predict the effects of skin treatments on spatial-temporal dynamics of water penetration in the SC, through *in silico* experiments. This exemplifies the power of appropriate mathematical frameworks providing additional insights in underlying dynamical mechanisms, which cannot be obtained solely through experiments [36]. This approach can also be applied to obtain clinical insights, for example by quantifying the effects of skin treatments in improving barrier function, using resistance profiles for different skin types and sites with pathological skin barrier conditions (such as atopic dermatitis and psoriasis) or after topical application of various drugs and skin care products such as corticosteroids or moisturizers. Similar *in silico* simulations to those presented in this paper can be used to study the spatial-temporal dynamics of percutaneous penetration of drugs and absorption kinetics of allergenic substances and may provide insights into the key biological processes involved in disease states or in treatments and identify patient-specific SC barrier dysfunction and targeted treatments.

Non-invasive measurement techniques allow for accurate measurement of depth dependent concentrations of NMF, lipids, and proteins [28, 152], in addition to water concentration used in this paper. As such detailed quantitative measurements for SC components become increasingly available, appropriate mathematical frameworks for combining multiple sets of experimental data, such as the one proposed here, are needed to maximize the insights that can be gained from measurement data, and progress our understanding of the SC permeability barrier. While the current model serves as a first step for modelling permeability in the skin, its flexibility and simplicity will allow us to extend the model to incorporate other spatial-temporal processes,

such as water binding to NMFs, and to reveal further how various biological mechanisms contribute to barrier formation, maintenance, and degradation, for example by clarifying the relative contribution of both water binding to NMF (hydration) and the extracellular lipids to resistance to water diffusion.

3.2.4 Methods

Derivation of resistance profiles

The resistance profiles describing the depth-dependent resistance to water diffusion (Figures 3.2 and 3.3) are obtained in the following three steps, using MATLAB version 2012b (The MathWorks, Inc., MA, USA). First, resistances $R_i = \frac{W_i - W_{i-1}}{\mathrm{TEWL}}$ are calculated with the SC compartment model (3.1) using TEWL [$\mathrm{g\,m^{-2}\,h^{-1}}$] and water concentration [mass%] measured by Raman spectroscopy for each individual [22, 228, 229] (all the data used in our paper is summarised in Dataset S1[3]). The thickness of each compartment in the compartment model is set to be 2 µm, corresponding to the measurement of water concentration at every 2 µm in depth. The unit of resistance using this specific combination of measurements is displayed as arbitrary units (a.u.), since [mass%] is a relative unit (% mg water/mg protein). Second, the resistance profile for each individual is obtained by plotting the resistances against the normalized depth (depth divided by the SC thickness) and interpolating them. The SC thickness is calculated from the water concentration profiles by the method described in [148]. The Matlab code to derive the resistance profiles for each individual is available in the supporting information (Code S1[4]). Finally, all the resistance profiles are averaged over the group of individuals to obtain the mean resistance profile for the corresponding group. The functional and structural indices are also calculated for every individual resistance profile and averaged over the group (Figure 3.2).

[3]Dataset S1. This dataset contains the experimental data used in this chapter. It includes water concentration profile and TEWL data on infants and adults [22], different skin sites [228], and before and after application of four oils [229]. DOI: 10.1371/journal.pone.0117292.s001

[4]Code S1. Matlab code for reproducing the results in this chapter. DOI: 10.1371/journal.pone.0117292.s003

In silico experiments

The *in silico* absorption-desorption experiments (Figure 3.4) were performed using simulation of the SC compartment dynamic model (Equation (3.2)). The resistances $\{R_i\}$ are obtained from the resistance profiles, and the water profiles are obtained from the previously published measurement data [22, 229]. Topical application of water is simulated by increasing W_0 by $W_{\text{exp}} = 60$ [mass%] for 10 seconds. The value of W_{exp} was chosen arbitrarily to ensure that the pool of water applied on top of the skin diffuses from the top to deeper SC layers due to the difference in water concentration, with W_0 being around 90 [mass%] after the application of water, while a typical initial W_0 is 30 [mass%]. Numerical simulation were conducted using the *ode45* solver of MATLAB version 2012b (The MathWorks, Inc., MA, USA). The Matlab code can be found in Code S1.

Direct comparison between the experimental and model simulation results was carried out as follows. We first ran the simulation using the SC compartment dynamic model (3.2) to obtain the spatial-temporal dynamics of water concentration before the application of petrolatum. Summation of the water concentration in all the compartments along the depth provided the simulated time-course of total SC water content [mass%]. To directly compare it to the total SC water content [a.u.] experimentally measured by conductance, we obtained a scaling parameter for the unit conversion by minimizing the sum of squared errors between the simulation and experimental data at each time point using *fminunc* in Matlab. We confirmed that the results are robust against the choice of initial values for minimization.

Statistical analysis

The statistical significance of the difference between the means of indices was determined using a two-tailed Student's t-test for comparing the means of infants and adults and using one-way ANOVA for comparing the means of the three skin sites (MATLAB version 2012b, The MathWorks, Inc., MA, USA). The variance in the mean resistance profiles is not displayed (Figures 3.2b, e) for visual clarity. However, quanti-

tative indices were used to determine the statistical significance between the resistance profiles and their characteristics; thus, they include variance.

3.3 Discussion

In this section, the following points will be addressed: further discussion of the results and suggestions for further research; a detailed comparison of previously reported results on SC barrier depth-dependency in relation to the results presented here; and the different ways of applying and visualising the resistance profiles.

3.3.1 Discussion on results of application and future direction

The development of children's skin and its barrier function in particular has been studied in recent decades [246, 238, 22, 236]. Here, comparison between resistance profiles of children revealed a considerable difference, especially in barrier functioning, while the structural indices are similar. This indicates that even though structure (normalised for SC thickness) is comparable and sufficiently functional, the skin is still in development for the first months up to a year after birth. After birth, the barrier function as measured by TEWL seems to be similar to that of adults [237]. Several studies show that in the months after birth, up to one year, TEWL increases and is considerably higher than adults levels [247, 22, 248, 235, 249]. In future research, we could follow resistance profiles at different time points during the first year, to observe the structural and functional changes in developing skin.

One of the risks of infant skin is that while the barrier is not fully developed, the skin is more susceptible to skin diseases such as atopic dermatitis [250]. Several studies have shown that strengthening of the barrier by application of emollients from birth can prevent the development of AD [136, 135].

The application of oils or emollients aims at improving the barrier in two ways: occlusion and replenishing of extracellular lipids. The effect of occlusion by oils on the resistance profiles is taken into account through TEWL, which results in 'effective' re-

sistance profiles. Even though petrolatum has mainly occlusive properties, it has been shown to penetrate within the SC [229, 251] which could result in the interesting profile featuring two peaks after the application of petrolatum.

Besides lipids, NMF has an effect on the resistance profile through its role in the hydration of the SC. The exact contribution of NMF to hydration and barrier function is not well understood, hence it would be interesting to study the role of NMF in relation to the resistance profile in more detail.

In our model we assume that the partition coefficient is constant within the SC. Binding by NMF could influence the partition coefficient, but as the relative mobility of the water molecules does not change significantly along the depth [66], we assume that partitioning does not play a role in the depth-dependent differences in steady state water concentration and permeability.

NMF concentration has a peak in the middle of the SC, as shown by Raman spectroscopy [30]. This is supported by experiments which demonstrate a peak in the uptake of water in the same middle SC region after overhydrating the skin [145, 30]. The effect of this peak in NMF under normal hydration conditions in terms of barrier function is unknown. Water does not only permeate through the intercellular lipids as the main permeation pathway, but it also penetrates the corneocytes. There it can bind to NMF, and the corneocytes serve as storage for water [174].

For future research, the resistance profile framework could be used to model the effects of NMF. The SC compartment model could be extended to include parallel compartments, which represent corneocytes where water can bind to NMF (figure 3.5). Water can diffuse freely between compartments at different depths, and can be taken up by corneocytes and bound to NMF in the parallel compartments. Despite the stength of water binding to NMF being continuous, in the model it could be simplified to two states: free and bound water. Free water is assumed to diffuse passively, and the level of NMF determines the rates and availability of water binding, and possibly the maximum capacity of water uptake by corneocytes. Bound water inside the corneocytes cannot diffuse, only unbind to form free water. Modelling the role of NMF and fitting to experimental data could contribute to finding conditions and rates for water binding and unbinding, and understanding the role of NMF in constituting the resistance

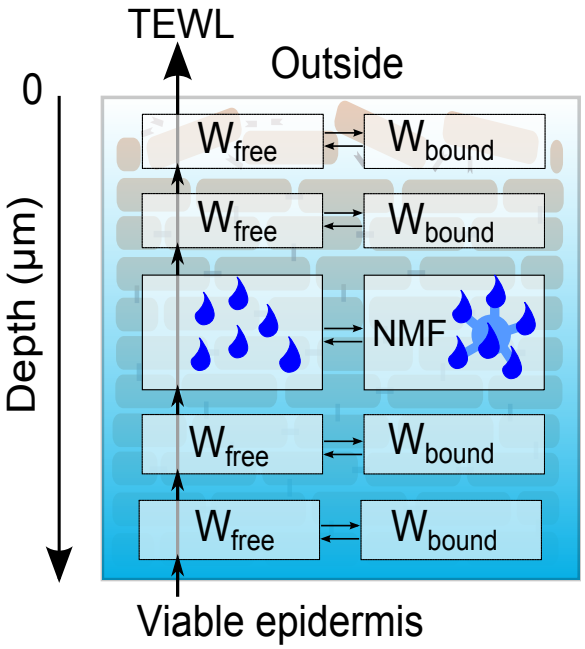


Figure 3.5: **Model for studying contribution of NMF to barrier function.** Compartments with bound water (corneocytes) exist in parallel with free water compartments, where the amount of NMF determines its binding capacity to water.

profile. For example, the change in water profiles after hydration could be simulated using the model described above (figure 3.5), where the water binding and unbinding rates are related to Raman NMF concentration profiles [30]. The simulation results could be compared or fitted to experimentally obtained water concentration profiles after hydration (wet bandage or towel wrapped around arm) for different durations [30, 149, 27]. The dynamic change in water concentration profiles could be due to the NMF profile, which has a peak at a similar location as the peaks in water concentration after hydration. Simulation of the model using the known NMF profile could confirm whether the peak in NMF explains the remarkable water profile after hydration.

The SC compartment dynamic model from section 3.2.2 is applied to describe the inflow and outflow of water only. For future research, it would be interesting to look at applicability of this model to drug transport, especially since drugs that do not penetrate easily or target the epidermis can benefit from a more detailed description of local diffusion differences within in the SC. Kubo *at al.* have already shown varying

permeability at different depths within the SC for small metal ions [32].
Like water concentration, the penetration of drugs can be measured by Raman at different depths [252, 155, 156, 151, 157, 158] (see section 2.2). Time course measurement of such penetration profiles have been obtained for (trans)retinol [252, 151], triphosphate [156] and 5-Fluorouracil [155]. A model similar to the SC compartment dynamic model, with compartments matching the Raman depths of penetration of substances, could be used to fit the diffusion coefficients or resistances, particularly if accurate time course data is available. When fitting the diffusion parameters of the resistance profile model, the resistance to diffusion between compartments should be constant in time, yet varying between compartments in depth to create a depth-dependent profiles. If all time course data were to be fitted at the same time, an accurate diffusion coefficient along the SC could be obtained, which would enable the prediction of drug absorption and for refinement of PK/PD models.

3.3.2 Results on depth-dependency of SC barrier in relation to existing literature

This section is adapted from Supporting Information S1 of Van Logtestijn *et al.* [223] (DOI: 10.1371/journal.pone.0117292.s002).

When applying the SC compartment model to a variety of experimental data, the resulting resistance profiles clearly show a depth-dependent resistance to water diffusion, without exception. In terms of Fick's laws of diffusion, this means that the diffusion coefficient is depth-dependent within the SC. However, previous research has shown that the diffusion coefficient can be approximated by a constant diffusion rate along the depth. By using tape stripping to measure the change of TEWL at different depths, and plotting the inverse of TEWL at each point in depth, a linearly decreasing line can be fitting to these points. This shows that the diffusion can be assumed to be a constant, as $\frac{1}{TEWL} = \frac{1}{D} - \frac{x}{D}$ [160, 195].

This section clarifies where the different conclusions on the depth-dependency of the SC permeability barrier (depth-dependent or homogeneous) come from. Using the SC

compartment model, and both the data presented above and from Kalia *et al*. [160], we can show that our findings are not contrasting the previously published results, in two ways: First, we can reproduce the homogeneity of the inverse TEWL plots using our own data, showing that our *depth-dependent* results can be interpreted as *homogeneous* if the assumptions of Kalia *et al*. are followed. Second, using our SC compartment model, we can show that *depth-dependent* resistance profiles can be obtained from the previously published tape stripping results.

We specifically demonstrate that:

1. Data showing a depth-dependent permeability barrier [22, 228] can reproduce the 'homogeneity' in the 1/TEWL plot;
2. Depth-dependent resistance profiles can be obtained from data that show a 'homogeneous' barrier [160, 195].

1. Data showing a depth-dependent permeability barrier can reproduce the 'homogeneity' in the 1/TEWL plot

To demonstrate that the data for depth-dependent SC barrier [22, 228] can reproduce the 'homogeneity' as in [160, 195], we conduct *in silico* tape stripping experiments using our SC compartment model. The 'homogeneity' is evaluated by calculating TEWL after tape stripping of each layer.

In our SC compartment model, TEWL is described by

$$\mathrm{TEWL} = \frac{\sum_{i=1}^{n} \Delta W_i}{\sum_{i=1}^{n} R_i} = \frac{W_n - W_0}{\sum_{i=1}^{n} R_i}. \tag{3.3}$$

It is obtained by summing up the resistance R_i of the i-th compartment $R_i = \frac{\Delta W_i}{\mathrm{TEWL}}$ (Equation (3.1)) for all the compartments ($i = 1, , n$) as $\sum_{i=1}^{n} R_i = \frac{\sum_{i=1}^{n} \Delta W_i}{\mathrm{TEWL}}$. This representation of TEWL suggests that the water flow is driven by the difference in water concentration between the viable epidermis W_n and environment W_0, since $W_n - W_0 = \sum_{i=1}^{n} \Delta W_i$. The TEWL after tape stripping of the top x compartments is calculated by

$$\mathrm{TEWL}_x = \frac{W_n - W_0}{\sum_{i=x+1}^{n} R_i}, \tag{3.4}$$

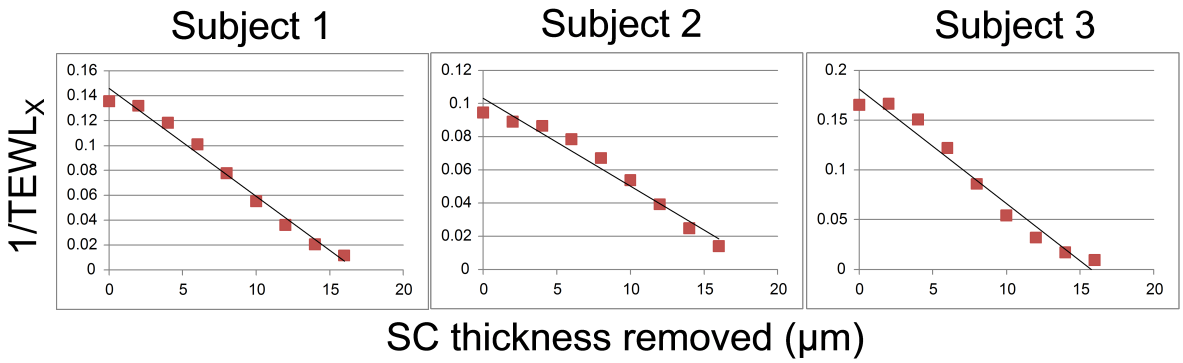


Figure 3.6: ***In silico* simulation of tape stripping experiments with depth-dependent permeability barrier.** The 1/TEWL plots were obtained by *in silico* experiments using data obtained from the arm of three randomly chosen adult subjects [228].

setting the resistance of all removed compartments to zero. The removed compartments do not contribute to the total resistance that water encounters when it flows from the viable epidermis to the outside environment. These *in silico* tape stripping experiments thus provide $TEWL_x$ for different depth x, or SC thickness removed, using the resistance profiles R_i and the water concentration at the top and bottom layers (W_0 and W_n).

Our paper demonstrated the depth-dependent resistance profiles for skin at different sites and for different ages using the TEWL and water profile data in [22, 228]. Using each of the depth-dependent resistance profiles, we derived TEWLx by *in silico* tape stripping experiments described above. The resulting 1/TEWL plots (e.g. figure 3.6) exhibit a similar linear decrease in 1/TEWLx against the SC thickness removed (x), as in 1/TEWL plots obtained from the actual tape stripping experiments (e.g. figure 7 in [160]). This agreement confirms the validity of the *in silico* tape stripping experiments, using the SC compartment model, to directly compare the results from in silico and actual tape stripping experiments.

Linear fitting of the 1/TEWL plots obtained by *in silico* tape stripping experiments using the data in [22, 228] (e.g. figure 3.6) results in high R^2 values, in the range of 0.94-0.995 (e.g. figure 3.7), which is in a similar range as those obtained by tape stripping experiments [160, 195]. These high R^2 values suggest that data for depth-dependent SC

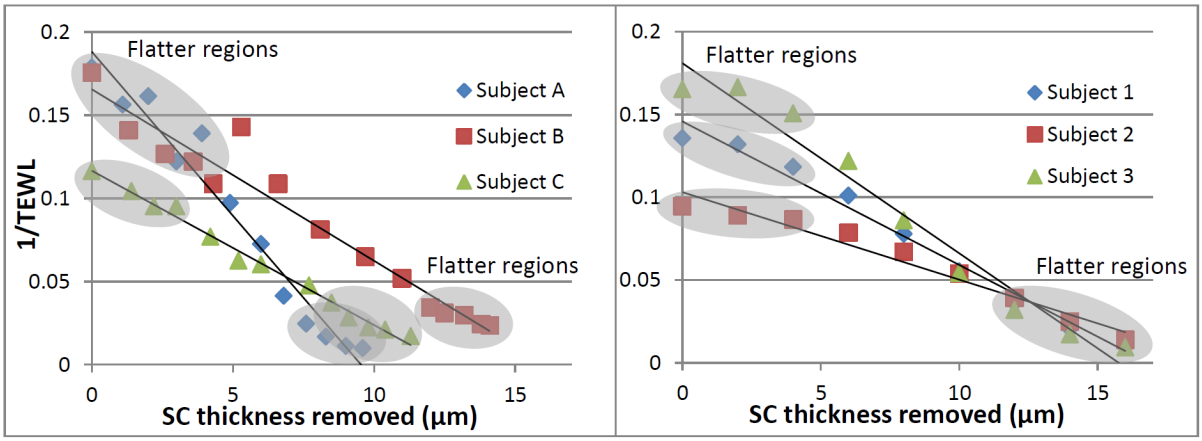


Figure 3.7: **Similarities between experimental and data and simulation of tape stripping using depth-dependent profiles.** Linear fitting of the 1/TEWL plots obtained by (a) actual experiments (data from table 1 in [160]) and (b) *in silico* experiments.

barrier (with depth-dependent resistance profiles as presented in this chapter) exhibit the 'homogeneity' as claimed previously in [160, 195], where homogeneity means that the corresponding 1/TEWL plot is linear. Therefore, the linearity of the 1/TEWL plot is not sufficient to claim that the permeability barrier is depth-independent.

This paradoxical conclusion of the homogeneity for a non-homogeneous barrier results from the implicit assumption made when the 1/TEWL plots are fitted to a linear line. Linear fitting of the 1/TEWL plots implicitly assumes the 'homogeneity' with respect to the SC thickness removed, by assuming that the SC is represented as a single compartment, with a unique and depth-independent diffusion coefficient D in Fick's first law of diffusion. The linear fitting, under the assumption of a single D, can therefore inevitably lead to the conclusion of the homogeneity even for a non-homogeneous barrier.

A closer look at the 1/TEWL plots in figure 3.7 clarifies that the linear slope actually flattens for a few microns at the top and bottom of the SC (shown as 'flatter regions' in figure 3.7), which is dismissed in a linear fit of the data under the assumption of a single compartment SC model. This flattening of the data at the bottom and top SC layers suggests the possible depth-dependent characteristics of the SC, as they are caused by an increase in the resistance at the bottom of the SC (*proR*) and a decrease in

resistance at the top (*degR*). Although the linear fit gives an initial approximation of the 1/TEWL plots, our SC compartment model makes the most of the depth-dependent, non-invasive *in vivo* measurement data (water concentration profile and depth) to study the depth-dependent characteristics of the SC resistance in more detail, as the model consists of multiple compartments with different diffusion coefficients.

2. Depth-dependent resistance profiles can be obtained from data that show a 'homogeneous' barrier

In silico tape stripping experiments described above derive 1/TEWL plots from resistance profiles. A similar method, in the reverse order, can derive resistance profiles from 1/TEWL plots obtained by tape stripping experiments. The resistance R_i for the i-th compartment is obtained by

$$R_i = (W_n - W_0)\left(\frac{1}{TEWL_{i-1}} - \frac{1}{TEWL_i}\right), \tag{3.5}$$

since $\sum_{i=x+1}^{n} R_i = \frac{W_n - W_0}{TEWL_x}$ from $TEWL_x = \frac{W_n - W_0}{\sum_{i=x+1}^{n} R_i}$.

We applied this method to the data (TEWL and corresponding depth) obtained by tape stripping experiments (Subject A in Kalia et al. [160], table 1). The derived resistance profile (figure 3.8) exhibits a good fit with a parabola (blue line in figure 3.8), a shape similar to a typical resistance profile. If the resistance is depth-independent (homogeneous), the resistance profiles would fit to a horizontal line. This result confirms that the SC compartment model allows us to derive resistance profiles, using the data from tape stripping experiments, to reveal the depth-dependency of SC permeability barrier.

To conclude, we have shown that both confocal Raman spectroscopy and tape stripping experiments can be equally used to study the depth-dependency of the SC water permeability barrier, using our proposed SC compartment model. Resistance profiles can be obtained using data from tape stripping experiments and allow us to conduct *in silico* tape stripping experiments.

These methods reveal the depth-dependency of the SC resistance to water diffusion,

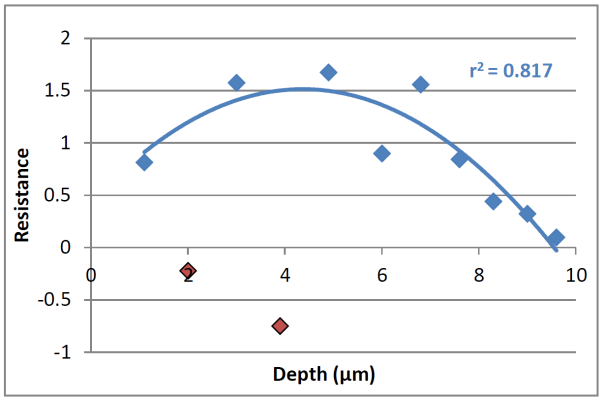


Figure 3.8: **Tape stripping data reveals a depth-dependent resistance profile.** The resistance profile derived from the data of tape stripping experiments (Subject A in Kalia et al. [160], table 1), with a parabolic fit (R^2=0.817). The two data points (shown in red) exhibiting a decrease in TEWL after tape stripping (negative resistance values) are not included in the fitting.

with the resistance decreasing at both the top and bottom ends of the SC. The key assumption in our SC compartment model is the multiple compartments with possibly different diffusion coefficients to represent the SC. A linear fitting to 1/TEWL plots obtained by tape stripping experiments assumes the SC to be one compartment with a fixed diffusion coefficient, and thus dismisses the depth-dependency. We demonstrated how interpretation of 1/TEWL plots obtained by tape stripping experiments, using the SC compartment model with multiple compartments, revealed a depth-dependent resistance profile.

Depth-dependent resistance of the SC is a natural consequence of the fact that the SC components, which constitute the resistance, are built and degraded in a depth-dependent manner, as opposed to a constant resistance of the barrier which is built and degraded abruptly. For example, the resistance of the SC top layer decreases due to the desquamation. It is in concordance with data obtained by tape stripping experiments, e.g. figure 5 in Kalia *et al.* [160] demonstrating that TEWL hardly increases after removal of the first 4 µm.

3.3.3 Application and visualisation of resistance profiles

The confocal Raman data are pivotal in deriving the resistance profiles using our proposed SC compartment model. The water concentration profiles are measured every 2 microns. While we utilize this in the model by matching the compartment size to the measurement depths, it also means that the accuracy of depth measurements is limited by the measurement interval of two microns. This could lead to inaccuracies in the determination of thickness, and the averaging and comparison of normalised profiles would be affected. However, the error margin in thickness would be limited to around ±10% (2 µm on a mean SC thickness of 21.3 µm for adults).

When visualising the resistance profiles, we use linear interpolation between the measurement points with intervals of two microns. There are two reasons for this interpolation. When normalising to SC thickness, all individual profiles have to be normalised to their respective thickness, before averaged to find the mean profile of the group of individuals. However, the data points now have different normalised depths. Therefore, interpolation is necessary in order to calculate the average of all individual profiles. The second reason for using normalisation is visualisation. The interval of two microns is sufficiently small such that we do not expect significant differences within the interpolated area between two measurement points.

There are three ways of presenting the resistance profiles in terms of their spatial alignment. In this chapter, we use both resistance profiles aligned at the top and profiles normalised to SC thickness. While the water concentration profiles are traditionally top-aligned, the decision on how to plot the depth of the resistance profile is based on the utilisation. If we are interested in visualising the change in thickness, as in chapter 4, the alignment should at the top as well. However, if thickness is a factor that needs to be eliminated in order to compare profiles with different thickness, we use normalised profiles. In all cases, the mean is taken of all individually aligned profiles. A third possible way is to align the resistance profiles at the bottom of the SC, where the obtained SC thickness is used to align the profile instead. For instance, when one is visualising hydration differences which include swelling and changing of thickness, the profiles could be aligned at the bottom of the SC. This would ensure the (non-

normalised) profiles with different thickness caused by swelling could be compared. If we want to study how the barrier is produced from the SG/SC interface upwards, as in chapter 5, the resistance profiles could be aligned at the bottom of the SC.

In conclusion, we propose a compartment model to characterise the resistance to water diffusion in the SC, using non-invasive *in vivo* experimental data. This profile shows a depth-dependent barrier function, with three regions for barrier formation, maintenance and degradation respectively. The resistance profiles obtained from different skin sites, ages, and after the application of oils can be used to compare the depth-dependency of barrier structure and function of the SC.
In the next chapter, we will apply the resistance profiles to additional experimental data from AD patients, and compare their barrier state to healthy skin after barrier damage. We will also further analyse the relationships between SC thickness, TEWL and water concentration defined by the resistance profiles, as well as the components that contribute to the resistance.

Chapter 4

Resistance profiles: application and analysis

The resistance profiles show the depth-dependency of the SC permeability barrier. In the previous chapter, a compartmental diffusion model of the SC to obtain the resistance profiles was presented, which was devised to be applicable to experimentally or clinically obtained TEWL and Raman water profile data. The model integrates the data such that the SC permeability barrier function along its depth can be visualised and used to study differences between skin sites, ages, before and after treatment, and analyse spatio-temporal dynamics of water diffusion.

To achieve a better understanding of the depth-dependency of the SC permeability barrier, it is necessary to study the resistance profiles in different static cases, such as diseased skin, and dynamic cases, such as recovery after insult. In order to then investigate the underlying causes of the observed differences, the relationship between the resistance profiles and the barrier components should be known.

Here, we apply the resistance profiles framework to study various sets of experimental data sets in more detail. The application to different sets of data, both static and time series as well as in combination with profiles of barrier components, use the resulting resistance profile for *further analysis*. We show that the resistance profiles are easily applied to (available and published) experimental data, and that further analysis of this data can reveal new insights, especially if multiple sets or types of data are combined

or compared. Besides visualisation and comparison of resistance profiles for different skin as in presented in chapter 3, the resistance profiles can also be applied to analyse how the SC barrier is formed, maintained and degraded, and specifically linked to depth-dependent barrier components and processes.

First, we focus on barrier deficiencies in non-lesional skin of AD patients. Even clinically unaffected skin of AD patients is not the same as healthy skin, with reported differences including increased TEWL, decreased hydration and altered lipids synthesis [253, 254]. We aim to quantify and visualise this subclinical damage in AD non-lesional skin using the resistance profiles.
Furthermore, we compare the barrier deficiencies in non-lesional AD skin to barrier deficiencies incurred by both mechanical and chemical insults on healthy skin. This allows us to relate AD barrier damage to common and well-studied insults. Both abrasion and exposure to a 1% sodium lauryl sulfate (SLS) solution are common experimental ways to perturb the SC that are not too invasive or destructive to the skin, which we hypothesised could lead to similar barrier disruption as non-lesional skin in AD. SLS, an ingredient in many soaps and cosmetic products, is a model irritant which induces irritation and damage to the SC barrier, when applied to the skin (usually for 24 hours using a patch with 0.01-10% SLS) [255, 256, 257, 258, 259]. Experimentally, it is commonly used to weaken the barrier before application of emollients, moisturisers or other skin treatment, in order to monitor their effect on recovery or irritation [260, 261, 262, 263, 264, 265]. Mechanical abrasion damages the barrier by disrupting the structure of the corneocytes [264]. Even though tape stripping is more commonly used in experimental dermatology to induce barrier damage, the barrier damage is relatively severe compared to everyday insults, as it strips off entire layers of corneocytes. No dramatic removal of cell layers occurs with abrasion, which is therefore preferable.
As Raman water profiles and TEWL values were collected at multiple time points, the recovery after insult can be visualised by following the changes in resistance profiles. Non-normalised profiles are used here, such that visualisation of the recovery includes the change in SC thickness.

Second, the resistance profiles obtained from data in [228] are used to investigate how the three resistance profile variables, TEWL, water concentration and thickness, are correlated. Their relation through the resistance profile is predicted by the SC compartment model in equation (3.1), which is further elaborated here. The correlations between TEWL, water concentration and thickness are then tested in experimental data from three skin sites of 40 volunteers. Previous research has found a negative correlation between SC thickness and TEWL [148].
Furthermore, based on the SC compartment model, we hypothesise that the surface water concentration negatively correlates to thickness, and positively to TEWL [148].

Third, we investigate if SC thickness and profiles of measurable barrier components, NMF and lipids, contribute to the resistance. Using least squares regression, we test to what extent the components can account for the variability in resistance among individuals, and at what depth. We hypothesise that the contribution of NMF and lipid content to the barrier differs along the depth, and can only partially explain or predict the resistance.

4.1 Water resistance profile as a marker of skin barrier damage in atopic dermatitis patients

This section is reproduced from the paper *'Water resistance profile as a marker of skin barrier damage in atopic dermatitis patients'* by Van Logtestijn *et al.*[1] published in the *Journal of Dermatological Science*[2] [266], with permission of the copyright holder Elsevier (ap-

[1]Mark D. A. van Logtestijn[a], Peter J. Caspers[b,c], Sanja Kezic[d], Douglas R. Hoffman[e], David W. Koenig[e], Masahiro Ono[f], Georgios N. Stamatas[g], and Reiko J. Tanaka[a]. [a] Department of Bioengineering, Imperial College London, London, UK. [b] Department of Dermatology, Center for Optical Diagnostics and Therapy, Erasmus MC, Rotterdam, The Netherlands. [c] RiverD International B.V., Rotterdam, The Netherlands. [d] Coronel Institute of Occupational Health, Academic Medical Center, Amsterdam, The Netherlands. [e] Kimberly-Clark Corporation, Neenah, WI, USA. [f] Department of Life Sciences, Imperial College London, London, UK. [g] Johnson & Johnson Sant Beaut France, Issy-les-Moulineaux, France.

[2]*Journal of Dermatological Science*, pages 126-128, volume 81, issue 2, February 2016. DOI: 10.1016/j.jdermsci.2015.10.017

pendix B).

The stratum corneum (SC) is the main barrier of the skin, offering a first line of defence against external pathogens and insults. The SC of patients with atopic dermatitis (AD) has underlying barrier deficiencies, even in non-lesional sites [254]. A defective SC barrier is more vulnerable to environmental insults that trigger immune reactions, further deteriorating the barrier [267].

Transepidermal water loss (TEWL) is a commonly used measurement to assess SC barrier function, but does not provide information about the depth-dependent characteristics. In this study, we attempted to establish a method to visualise the depth-dependent barrier profiles and evaluate barrier deficiency by applying a recently proposed mathematical method [223] to clinical datasets from AD and healthy skin. The method calculates the resistance of SC to water diffusion along the SC depth, and thereby quantifies and visualises the depth-dependent barrier function, through integration of data of TEWL and water concentration profiles measured by confocal Raman microspectroscopy [28]. In order to evaluate the efficiency of the proposed method, we addressed the hypotheses that the subclinical damage in AD non-lesional skin can be quantified and visualised by a depth-dependent barrier resistance profile, and that the degree of the barrier deficiency in AD non-lesional skin is similar to that in mechanically or chemically insulted healthy skin by abrasion or exposure to Sodium Lauryl Sulphate (SLS).

We first calculated the depth-dependent resistance from data collected in our previous studies in which Raman spectra and TEWL (Appendix A.1) were measured in AD patients [266] and healthy controls[3] [268] (Figure 1a). We also calculated the SC thickness from the water concentration profiles by the method described previously [148]. The AD individuals were divided into three groups with high (> 20.8), mid (16.8-20.8) and low (< 16.8) TEWL values [$\mathrm{g\,m^{-2}\,h^{-1}}$] to reflect interpersonal differences in severity of AD barrier deficiency. All three groups show a significantly lower resistance and

[3] Supplementary information: Experimental data on water concentration and TEWL and thickness from Sanja Kezic. DOI: 10.1016/j.jdermsci.2015.10.017

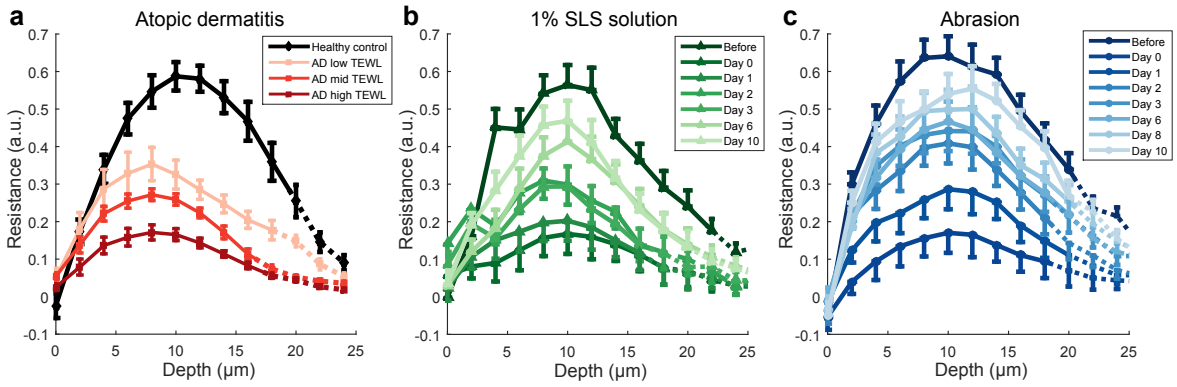


Figure 4.1: **Resistance profiles for non-lesional skin from AD patients and for healthy skin following insults.** Mean resistance profiles for (a) AD non-lesional skin (n = 37) with high (>20.8), mid (16.8-20.8) and low (<16.8) TEWL [$\mathrm{g\,m^{-2}\,h^{-1}}$] and healthy controls (n=13), and for healthy skin before and after (b) SLS exposure (n = 20) and (c) abrasion (n = 18). Resistances within and outside of the SC thickness are shown by solid and dotted lines, respectively. Error bars indicate the standard error of the mean. In (b) and (c), error bars are shown either above or below the mean.

a lower SC thickness compared to the healthy control, which has a TEWL value of $7.8\mathrm{g\,m^{-2}\,h^{-1}}$. The differences in the peak resistance value (R_{max}) between the control and each of the AD groups are significant (Students t-test, $p < 0.0001$), indicating the effectiveness of the proposed method in characterising the disease status of the SC.

Next, we evaluated the effects of skin insults by SLS exposure and abrasion on healthy skin. Resistance profiles were calculated from TEWL values and water concentration profiles measured after application of a patch with 1% SLS solution to the forearm for 24 hours [31] and after abrasion [269] (Appendix A.1). Abrasion was accomplished by passing 320J emery paper (3M Company, Maplewood, MN, USA) over forearm skin ten times until TEWL increased by ≥ 20 units [269]. The obtained resistance profiles clearly demonstrate the spatio-temporal effects of the damage and recovery incurred by different insults on the depth-dependent SC barrier function (Figure 4.1b,c). The resistance profile immediately after the SLS insult (Day 0) demonstrates an overall decrease throughout the SC, with a shift of the peak towards the SC surface due to thinning of the SC (Figures 4.1b, 4.2a), followed by gradual increase in both the resis-

tance values and SC thickness during the recovery phase (Days 1-10). A similar overall reduction in the resistance profile throughout the SC is observed after abrasion.

The SLS exposure showed a slower recovery of water resistance profile than abrasion, with time constants c = 9.5 vs 5.5, calculated by fitting the recovery curves of $R_{\max}$ to a negative exponential function $(1 - ae^{-t/c})$ (Figure 2b). SLS structurally damages the main constituent barrier components, including alteration of SC lipid organisation [270] and a significant reduction of natural moisturizing factor (NMF) components [31] throughout the SC. Repair of the damaged barrier requires replenishment of its components, for example by increased expression of involucrin, transglutaminase 1, and profilaggrin [255]. Recovery of water resistances from SLS damage therefore takes longer than the recovery from the removal of only the top layers of the SC by abrasion, via increased cornification. Finally, resistance profiles of AD skin were compared to those of healthy individuals following insults. The conformity between the different data sets was confirmed by the correspondence of the resistance profiles for the healthy control (Figure 1a) and pre-insult (Figure 4.1b,c).

The resistance profiles were compared quantitatively by three indices; the peak resistance values ($R_{\max}$, Figure 4.2b), the rate of production of the resistance from the bottom of the SC (*proR*, Figure 4.2c), and that of degradation towards the top (*degR*, Figure 4.2d) [223]. There is a striking resemblance in the resistance profiles for the AD high TEWL group and those for the healthy individuals immediately after SLS exposure and after abrasion (Figure 4.1), demonstrated by similar values for all the calculated indices (Figure 4.2b-d). Agreement between all three indices suggests that the physical property of the barrier of AD patients non-lesional skin is similar to that of healthy skin affected by SLS or abrasion, despite differences in the underlying mechanisms of barrier deficiency. For example, mechanisms of barrier formation might be altered by a feedback regulation that is activated upon barrier damage in skin following SLS exposure or abrasion, while the mechanisms of barrier formation are known to be altered in AD patients, for example by an impaired lamellar body secretion or a filaggrin deficiency, limiting the formation of the lipid envelope and NMF [267]. The indices for the mid and low TEWL groups are similar to those in the recovery phase

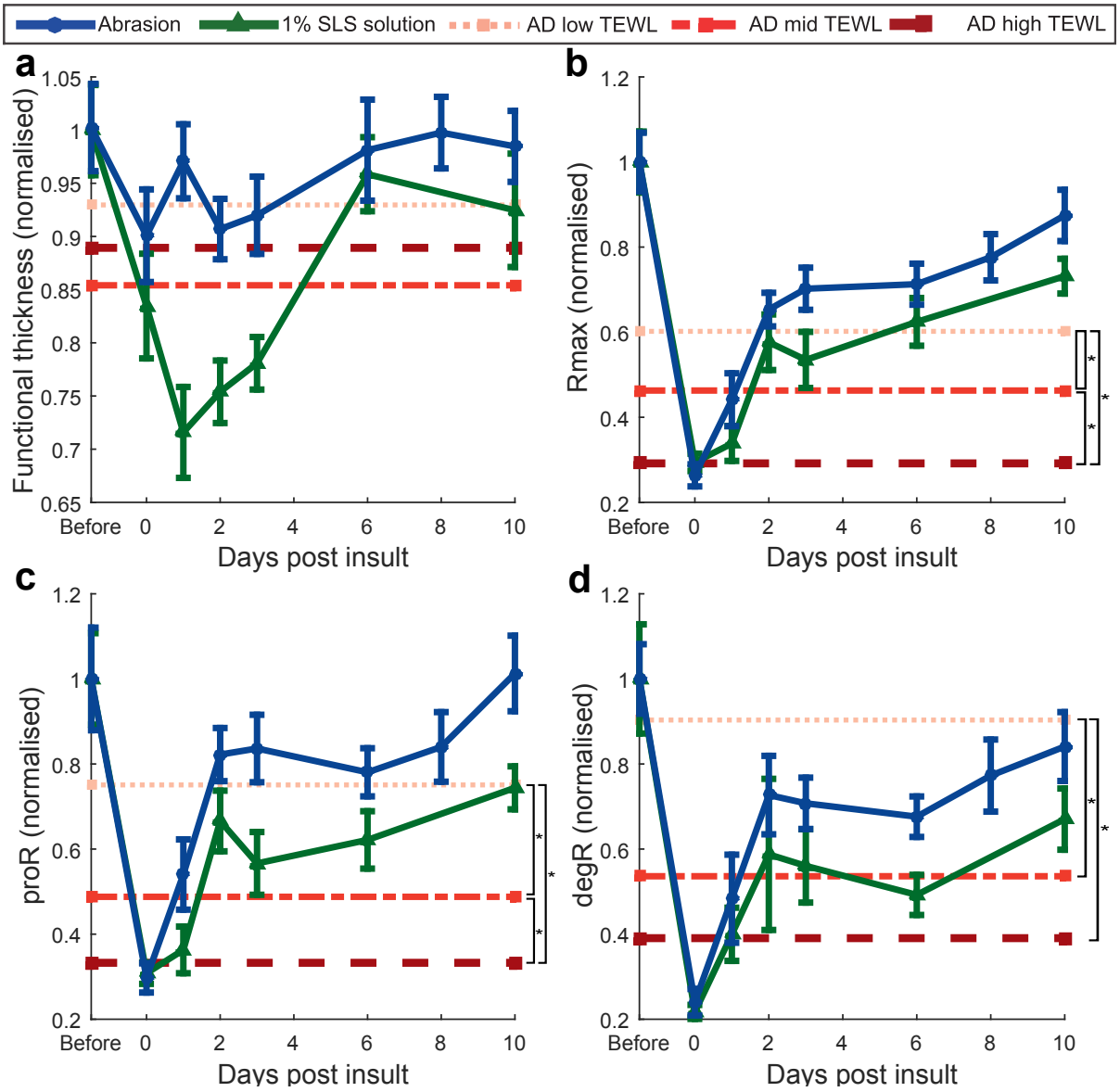


Figure 4.2: **Quantification of damage and recovery of barrier function from insults on healthy skin and its comparison to AD non-lesional skin.** Four indices are used to compare AD non-lesional skin (n = 37), healthy controls (n = 13), healthy skin before and after SLS exposure (n = 20) and abrasion (n=18): (a) the SC thickness, (b) the maximum resistance value ($R_{\max}$), (c) the spatial rate of resistance production ($proR$) and (d) the spatial rate of resistance degradation ($degR$). The indices are normalised to the values before the insults, or normalised to healthy controls for the AD groups. Significance between the AD group indices (student t-test, $p < 0.05$) is indicated by an asterix *. Error bars indicate the standard error of the mean.

from abrasion and SLS exposure, suggesting that the three AD groups have different abilities to repair and maintain the barrier, possibly due to variability in the magnitude of deficiency in filaggrin levels or lamellar body secretion.

In conclusion, we demonstrated that the resistance profiles successfully quantified and visualised the depth-dependent barrier deficiency using clinical datasets, confirming the efficiency of the proposed method. Interestingly, the resistance profiles of non-lesional skin of AD patients were similar to those of healthy individuals following chemical (SLS) or mechanical (abrasion) insults, suggesting that these different pathological conditions may have similar structural abnormalities, although the underlying mechanisms and the recovery kinetics are different.

4.2 Correlation between SC thickness, TEWL and water concentration

In chapter 3, the compartmental model of resistance against water diffusion in the SC describes the relation between water concentration, TEWL and thickness, based on Fick's laws of diffusion and using the resistance profiles. Here, the relation between the three variables is tested with experimental data.

To predict this relation through the resistance profiles, we reproduce equation (3.1)

$$\text{TEWL} = D_i K_i \frac{\Delta W_i}{\Delta x_i} = \frac{W_i - W_{i-1}}{R_i} = \frac{W_v - W_o}{R_{SC}} ,$$

where $R_{SC} \propto x_{SC}$, and we assume that the water concentration in the viable epidermis at the SG/SC interface W_v is constant. We can then rewrite the relation between SC thickness x_{SC}, surface water concentration W_o and TEWL as

$$\text{TEWL} \propto \frac{W_v - W_o}{x_{SC}} , \tag{4.1}$$

where W_v is a constant. Equation (4.1) shows us the expected relation between TEWL, SC thickness and surface water concentration, in a steady-state situation in the SC.

We use the surface water concentration as one of our correlation variables. As the water concentration in the viable epidermis is constant and much less variable between individuals [148], only the surface water concentration is needed to represent ΔW.

Boireau-Adamezyk *et al.* have collected TEWL measurements and water concentration profiles from CMS at three skin sites (cheek, protected and exposed arm) of 40 female individuals [228]. From the water concentration profile, the SC thickness can be calculated [148], and all measurements can be combined to obtain the resistance profile for each skin site of each individual.
The correlation coefficients between SC thickness, surface water concentration and TEWL are presented in table 4.1, together with their significance (significant if $p < 0.05$, probability that there is no correlation) and Pearson's Rho (R^2).

Table 4.1: **Correlation between TEWL, thickness, and surface water concentration for different skin sites.** * denotes a significant correlation of $p < 0.05$, with n=40.

Skin site	**Variable 1**	**Variable 2**	**Correlation coefficient**	***p*-value**	R^2
Face	TEWL	W_o	0.107	0.510	$1.15{\cdot}10^{-2}$
	TEWL	x_{SC}	-0.208	0.196	$4.33{\cdot}10^{-2}$
	W_o	x_{SC}	-0.448 *	$3.71{\cdot}10^{-3}$	0.201
Exposed arm	TEWL	W_o	0.448 *	$3.74{\cdot}10^{-3}$	0.201
	TEWL	x_{SC}	$7.99{\cdot}10^{-3}$	0.961	$6.38{\cdot}10^{-5}$
	W_o	x_{SC}	-0.374 *	$1.75{\cdot}10^{-2}$	0.140
Protected arm	TEWL	W_o	0.528 *	$4.57{\cdot}10^{-4}$	0.279
	TEWL	x_{SC}	-0.498 *	$1.07{\cdot}10^{-3}$	0.248
	W_o	x_{SC}	-0.613 *	$2.59{\cdot}10^{-5}$	0.376

From the correlation results in table 4.1, we can make the following observations. First, there is no significant correlation between TEWL and thickness for face and exposed arm, and a significant negative correlation for the protected arm. A small negative correlation has been reported earlier [148]. Apparently, a thicker skin does not automatically lead to a significantly lower TEWL, despite the elongated intercellular path-

way. In the instance where a healthy SC has a certain steady-state thickness, TEWL and water concentration, and another layer of cells would be added, thus increasing SC thickness, and reducing the surface water concentration. However, it would not necessarily increase TEWL if the added layer has a resistance such that the water concentration difference over the added thickness results in TEWL remaining the same. Let us use equation (3.3) to demonstrate this, with layers of skin represented by n number of compartments i, with equal heights x_i

$$\sum_{i=1}^{n} R_i = \frac{\sum_{i=1}^{n} \Delta W_i}{\text{TEWL}} , \tag{4.2}$$
$$x_{SC} = \sum_{i=1}^{n} x_i .$$

if a new layer n+1 is added to increase SC thickness, with equal compartment thickness $x_{n+1} = x_i$ and

$$R_{n+1} = \frac{W_{n+1} - W_n}{\text{TEWL}} , \tag{4.3}$$

then TEWL stays the same with added thickness

$$\sum_{i=1}^{n+1} R_i = \frac{\sum_{i=1}^{n+1} \Delta W_i}{\text{TEWL}} , \tag{4.4}$$
$$x_{SC} = \sum_{i=1}^{n+1} x_i .$$

However, if the resistance in the added layer $n + 1$ is larger, or the resulting change in water concentration is smaller than in (4.4), such that

$$R_{n+1} > \frac{W_{n+1} - W_n}{\text{TEWL}} , \tag{4.5}$$

then TEWL will have to decrease.

Second, we observe a significant negative relation between surface water concentration and thickness for all skin sites. It follows directly from equations (4.2)-(4.5) that an increase in thickness leads to an increase in ΔW and a decrease in surface water concentration, if the extra layer adds any resistance. Possibly, for example in the case of a skin disease with increased KLK activity at the top of the SC causing a thickened

Table 4.2: **Correlation between TEWL, thickness, and surface water concentration for all three skin sites combined.** * denotes a significant correlation of $p < 0.05$, with n=120.

Skin sites	Variable 1	Variable 2	Correlation	p-value	R^2
	TEWL	W_o	0.430 *	$9.38 \cdot 10^{-7}$	0.185
All	TEWL	x_{SC}	-0.529 *	$5.46 \cdot 10^{-10}$	0.279
	W_o	x_{SC}	-0.555 *	$4.75 \cdot 10^{-11}$	0.308

epidermis with scaled detached layers, extra layers do not provide additional resistance, and the increased thickness does not decrease surface water concentration (or TEWL).

Third, there is a positive relation between TEWL and surface water concentration, significant for both arm sites, insignificant for the face. If resistance is high, it is likely that both the TEWL and the surface water concentration are low, and vice versa.
The R^2 values are low, between 0.14 and 0.38 for the significant correlations. This indicates that there is a lot of (interpersonal) variability in the studied variables, and particularly in the resistance profile which relates the three variables to each other. This variability in resistance is likely to be caused by underlying differences in barrier components. These differences in resistance profiles will result in varying relations between TEWL, thickness and water concentration between individuals, and between skin sites, as seen in chapter 3. Similar correlations reported earlier include TEWL versus SC thickness ($R^2 = -0.35$, for n=14, exposed arm), and TEWL versus ΔW ($R^2 = -0.50$) [148]. Part of the explanation for the lower R^2 values presented here could be the higher number of individuals.

It is important to distinguish between correlations at the same skin sites for different individuals, and correlations at different skin sites (for the same individual). Above, we investigated the former case by looking if these correlations can explain interpersonal differences in the SC barrier and resistance profiles. In the latter case, besides interpersonal differences, the correlations describe differences between inherent skin structure and function of skin sites. A clearer and more significant correlation is ex-

pected, as there are larger differences between skin site in terms of TEWL, thickness and hydration.

Table 4.2 shows the correlations if all skin sites are grouped into one dataset (all data from table 4.1 combined, n=120). Indeed, there is a significant positive correlation between TEWL and surface water concentration, as well as significant negative correlations for TEWL versus thickness and for surface water concentration versus thickness. The main difference with correlations in table 4.1 is the significant negative correlation between TEWL and SC thickness, which was not observed for face and exposed arm. It is well documented that the facial skin is thinner and has higher TEWL than arm sites [20, 271, 272, 228, 273].

4.3 Depth profiles of lipids and NMF partially explain the resistance profiles

The relation between TEWL, water concentration and thickness is determined by the resistance profile. However, there are many processes and components that constitute the resistance, and play a role in regulating the resistance along the depth of the SC. One of the aims of this thesis is to understand how barrier components constitute the barrier and its resistance. From the CMS spectra used in section 4.2 (from cheek, protected and exposed arm of 40 female individuals [228]), not only can water concentration profiles be obtained, but the spectra also contain the bandwidths that contain the bands for various barrier components; both the high wavenumber range (2600-3800 cm^{-1}) and the fingerprint region (400-1800 cm^{-1}) were collected. From the Raman spectra, depth profiles of water, NMF components, lipids components and lipid/protein ratios can be obtained [228]. Even though we are limited in available CRS measurements of barrier components to lipids and NMF, these are the two main components that limit extracellular diffusion and hold water by binding to it, respectively. As discussed in chapter 2, extracellular lipids and NMF are known to be important barrier components, and defects in lipid and filaggrin processing or availability can lead to reduced skin barrier function [54, 274]. Also, the lipid/protein ratio as obtained by

CRS has been shown to be a good determinant for skin barrier function, as it strongly correlates with the inverse of TEWL, and a negative correlation with AD severity (as measured by SCORAD) [144].

The availability of depth profiles of NMF and lipids content (lipid/protein ratio) obtained *in vivo* and non-invasively from CRS allows us to analyse the extent of the contribution of these components to the resistance along the depth of the SC. Using these profiles, together with the resistance profiles and skin thickness of the same individuals and skin sites (see section 4.2), linear squares regression (LSR) will be applied to each point in depth to see if the components (and thickness) can explain the variability in resistance between individuals.

First, it shows the contribution of NMF, lipids and SC thickness (as measured by CRS) to resistance, both in terms of the extent of their contribution, and changes along the depth. The depth profiles of the contribution of the components can suggest their role in different parts of the SC, for example NMF with higher contributions in the middle and top, and lower at the bottom where filaggrin still has to be degraded. Second, it will show how much of the variance in NMF and lipid accounts for the variance in resistance. As this analysis can be performed at every point in depth, we can visualise how the explained variance in resistance changes along the depth. If the variability in resistance can be explained by the variability in the components, this indicates that the components strongly influence the resistance. For instance, if a person with a higher lipid content than average is more likely to have an above average resistance to water diffusion, this indicates there is a large contribution of lipids to barrier function.

4.3.1 Least squares regression

Linear least squares regression is applied to the Raman data, in order to analyse the contribution of the components to the resistance along the depth of the SC. For the least squares regression, we denote the resistance profiles $R \in \mathbb{R}^{n \times i}$ and the SC components $X \in \mathbb{R}^{m \times n \times i}$, with individuals n, indices m and depths i. Resistance values $\mathbf{r_i} \in \mathbb{R}^n$ denote the resistance at a certain depth from a resistance profile, $\mathbf{r_i} \subset R_n$. For $n = 40$

individuals, and depths $i = 0, 2, 4, \ldots, x_{SC}$ µm, we define the system of linear equations for depth i

$$X_i \mathbf{c_i} = \mathbf{r_i} \,, \tag{4.6}$$

with

$$X_i = \begin{bmatrix} 1 & \text{lipids}_{1,i} & \text{NMF}_{1,i} & \text{thickness}_{1,i} \\ \vdots & \vdots & \vdots & \vdots \\ 1 & \text{lipids}_{n,i} & \text{NMF}_{n,i} & \text{thickness}_{n,i} \end{bmatrix}, \tag{4.7}$$

$$\mathbf{c_i} = \begin{bmatrix} c_{1,i} & c_{2,i} & c_{3,i} & c_{4,i} \end{bmatrix}^\top \,, \tag{4.8}$$

$$\mathbf{r_i} = \begin{bmatrix} r_{1,i} & \ldots & r_{n,i} \end{bmatrix}^\top \,. \tag{4.9}$$

Solving for least square coefficients $\hat{\mathbf{c}}$, we get

$$\hat{\mathbf{c}}_\mathbf{i} = (X_i^\top X_i)^{-1} X_i^\top \mathbf{r_i} \,. \tag{4.10}$$

Therefore, we can express the relationship between the components and resistance by

$$\mathbf{r_i} = \hat{c}_{1,i} + \hat{c}_{2,i}\text{lipids}_i + \hat{c}_{3,i}\text{NMF}_i + \hat{c}_{4,i}\text{thickness}_i \,. \tag{4.11}$$

The resulting $\hat{c}_i$ are the coefficients for depth i, which describe the contribution of the components to the resistance at depth i. The above is repeated for all depths $i = 0, 2, 4, \ldots, x_{SC}$ µm to obtain a depth profile of $\hat{c}_i$.

The thickness can be included explicitly as a component in the LSR, as demonstrated above. However, as the thickness is not a profile like the other two components NMF and lipids, it is the same value at all dephts i. Alternatively, thickness could be included by normalising the depths of all profiles to the SC thickness. All profiles (resistance, NMF, lipids) are normalised and interpolated such that a profile with values for normalised depths $i = 0, 0.01, 0.02 \ldots, 1$. We define the system of linear equations for normalised depths i using equations (4.6)-(4.11), but instead of X_i we use

$$\bar{X}_i = \begin{bmatrix} 1 & \text{lipids}_{1,i} & \text{NMF}_{1,i} \\ \vdots & \vdots & \vdots \\ 1 & \text{lipids}_{n,i} & \text{NMF}_{n,i} \end{bmatrix}, \tag{4.12}$$

For the normalised profile, the LSR uses the components $\bar{(X)}_i$ and resistance $\bar{r}_i$ to obtain least square coefficients $\bar{c}_i$ for the normalised depths i

$$\bar{\mathbf{r}}_\mathbf{i} = \bar{c}_{1,i} + \bar{c}_{2,i}\text{lipids}_i + \bar{c}_{3,i}\text{NMF}_i \, . \tag{4.13}$$

The lipid/protein ratio and NMF are in arbitrary units. To make the LSR coefficients comparable, both R_i and X_i are standardised such that every column (component) has zero mean and unit standard deviation (i.e., transformed into z-scores).

4.3.2 Depth profiles of the contribution of SC components to resistance

Least squares regression is performed as previously described in the section 4.3.1. Figure 4.3 shows the resulting profiles of $\hat{c}$ using equations (4.6)-(4.11), which includes thickness. Profiles of $\bar{c}$ with normalised thickness, using equations (4.12)-(4.13), are shown in figure 4.4. Due to standardisation of the data for all components, the profiles of coefficients and their relative contribution to resistance are directly comparable between the components.

Lipids contribute positively to resistance throughout the SC, with some differences between the three skin sites. When comparing the three sites, lipids contribute most in the bottom half for the face, and most in the middle and top regions for the two arm sites. NMF does not contribute as much, especially within the lower half of the SC. Their contribution increases towards the top across all skin sites, as expected. More filaggrin proteins are degraded into NMF components towards the top, so more NMF is available, while the water concentration decreases so limited water is available to bind to NMF. The exception is a peak in NMF at the bottom of the SC for the protected arm site.

Lipids have a higher contribution to resistance than NMF through most of the SC, as they form the main resistance to diffusion in the intercellular pathway. However, towards the top, the coefficient for NMF is higher, specifically for the face and protected arm. This shows that NMF and lipids contribute differently at certain depths of the

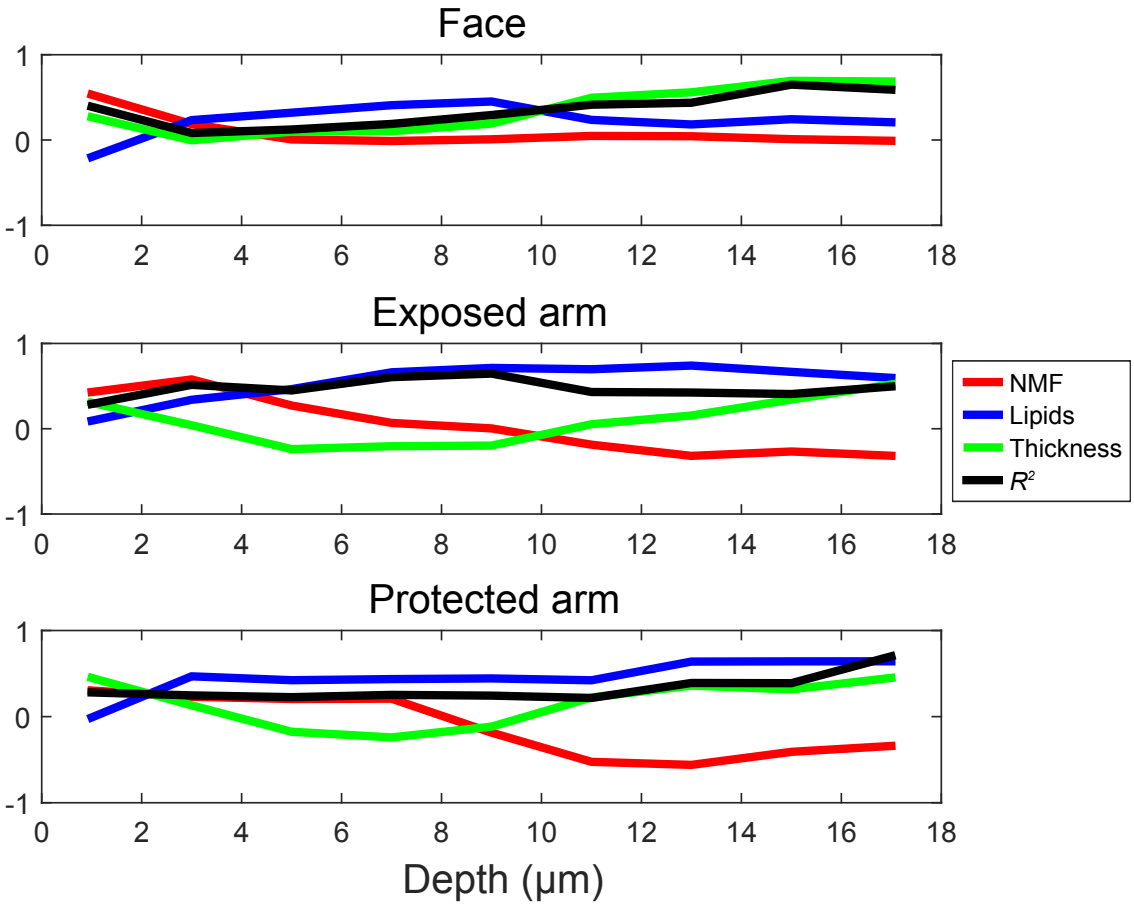


Figure 4.3: **Least squares regression results show contribution of barrier components to resistance along depth.** Plotted are $\hat{c}_i$ weights corresponding to NMF, lipid and thickness profiles (interpolated), for three skin sites (cheek, exposed and protected arm). SC thickness is included as a constant along the depth.

SC. As their respective profiles are depth-dependent due to processing and regulation, so are their effects on the resistance.

However, the contribution of lipids and NMF only explains part of the resistance. The R^2 value (figures 4.3 and 4.4) is the percentage of variance in resistance that can be explained by the variance in the components measured. Their variance only explains up to 70% of the variance in resistance, with most under 40%, especially for the normalised profiles. There are several reasons why these two components cannot explain most of the variance in the resistance. The rest is likely to be explained by other

factors that contribute to resistance, such as quality/strength of corneocytes, cornified envelope and corneodesmosomes, optimal pH, and well-regulated desquamation processes. Another explanation could be that lipid/protein profiles are suboptimal at describing the barrier qualities of lipids, and that lipid organisation and ratios rather than exact amount would give more accurate results [54, 275]. In addition, the NMF components measured here to obtain one score for NMF could be an inaccurate representation of *all* hygroscopic components that make up 'NMF'.

The contribution of thickness (figure 4.3) can be interpreted as the effect the total thickness of the SC has on the resistance at a certain depth. For instance, a higher $\hat{c}$ coefficient at depth i means that a thicker skin would lead to a higher resistance at this depth. For all skin sites the thickness has a high and positive coefficient at the bottom half, and a negative at the top half. Intuitively, this indicates that with a thicker SC, the deeper resistance values are higher, as the profiles here are not normalised for SC thickness. The face has one data point at the top of the SC which has a high positive contribution of thickness, but this could be due to CRS measurement inaccuracies at 'depth 0' of the SC.
To compare the diffence between thickness as 'component' and by including as normalisation, both are plotted here. When thickness is used for normalisation of profiles (figure 4.4), the R^2 values are lower. However, this is achieved with less variables, while adding dependent variables will generally increase the percentage explained of the variance in the response variable.

Our linear LSR analysis only tests linear combinations of the variables. Other combinations such as multiplications, exponentials and higher powers have been tested as well. However, these did not significantly improve R^2 to warrant the added complexity and 'overfitting' by using a larger number of parameters or coefficients.

4.4 Discussion

This chapter shows three separate applications of the resistance profile, where further analysis leads to insight into either studied skin, or in underlying mechanisms of the

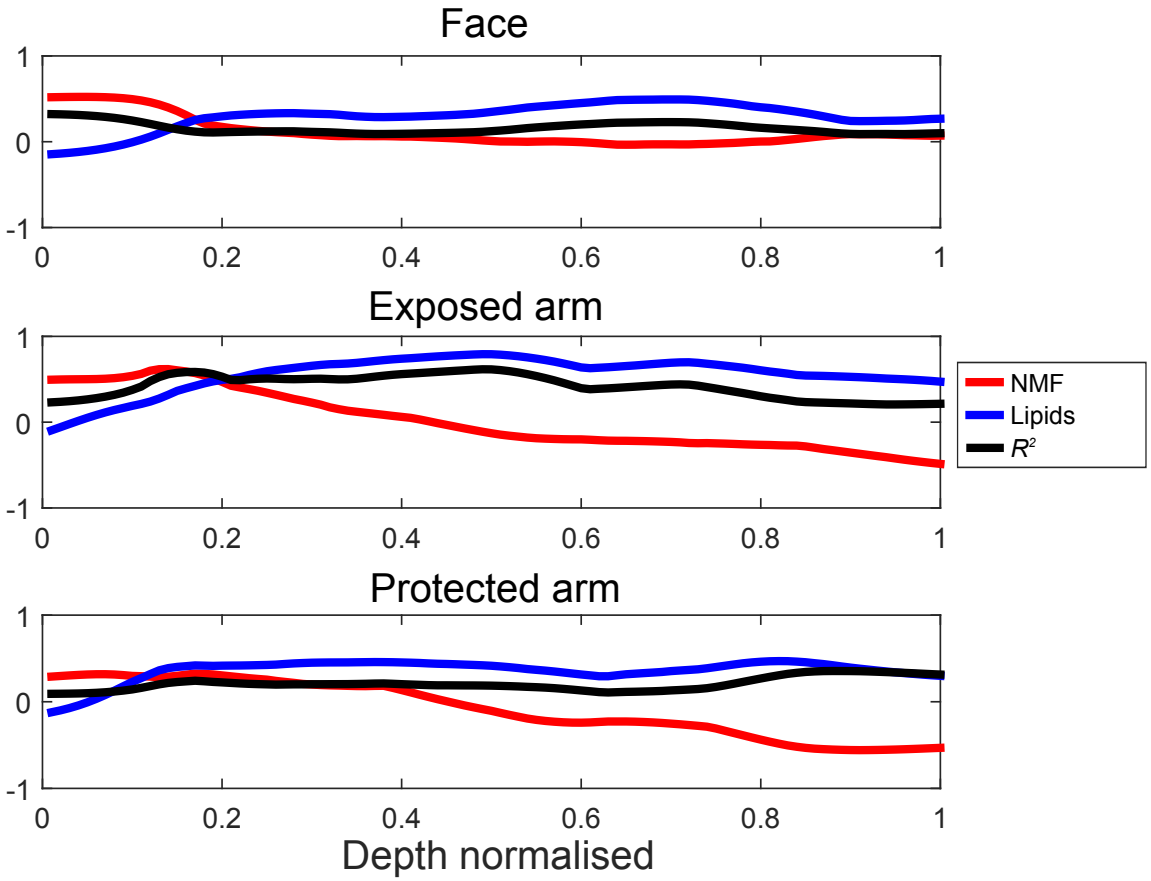


Figure 4.4: **Least squares regression results for normalised depth.** Plotted are $\bar{c}_i$ weights corresponding to NMF and lipid profiles for three skin sites (cheek, exposed and protected arm). All profiles are normalised to SC thickness and linearly interpolated.

resistance profiles themselves. Resistance profiles are applicable to a variety of data, to analyse and compare, with simple visualisation that incorporates the main information on SC barrier state: TEWL, hydration and thickness.

Comparison of resistance profiles for AD patients to healthy people clearly showed a weakened skin barrier function in non-lesional sites, with a reduction in resistance, and SC thickness. The barrier damage in AD was similar to common barrier disruptions as abrasion and exposure to SLS. Furthermore, the resistance profiles and derived indices were suitable for following and comparing barrier recovery.

It would be interesting to collect additional data from AD patients besides water con-

centration and TEWL, such that the resistance profiles and derived indices could be associated to known deficiencies in AD. For instance, filaggrin mutations are the main risk factor for the development of AD and lead to reduced NMF. If NMF profiles and the type of filaggrin mutation would be obtained parallel to the resistance profiles, one could investigate if a correlation exists. Potentially, resistance profile abnormalities or the indices could be markers for filaggrin and NMF deficiencies. Future research should focus on relating the obtained resistance profiles to processes of barrier formation, maintenance and degradation. When more data is available, analysis could include correlation of the resistance profile indices to (markers of) cornification and desquamation rates during recovery, which may provide further insight into the repair processes that lead recovery.

This chapter explored the relationships between resistance, and barrier parameters and components; the resistance profiles describe the correlation between SC thickness, TEWL and SC thickness. The question of how barrier components contribute to resistance was only answered partly through the regression of resistance with a linear combination of lipids, NMF and thickness. The LSR analysis in section 4.3.1 would benefit from the inclusion of additional data. Specifically, depth profiles of other barrier components in the skin could be added to the analysis (possibly by using partial least squares if enough extra variables are added). Confocal Raman spectroscopy can measure profiles of lipid organisation/compactness, individual lipids such as cholesterol and ceramides, and individual NMF components. Other possible depth-dependent profiles of skin components that influence barrier function, such as KLK activity, could be obtained by tape stripping despite its invasive nature.
With the available data in section 4.3.1, we were able to explain part of the contribution of NMF, lipids and SC thickness to resistance, and yet the majority of the contribution to resistance still remains unclear from this data. In the next chapter, we will therefore take a modelling approach to investigate how a resistance profile composed by its constituent barrier components, and how these are regulated.

Chapter 5

Depth-dependent regulation of stratum corneum homeostasis

5.1 Introduction

In the previous chapters we showed that the SC barrier to water diffusion is depth-dependent. However, it is unclear how this barrier is established by its components along the depth of the SC, and how it is regulated. Knowing which components contribute most to the barrier, and how they change along the SC depth, is essential to understanding how their combination and interplay make up the SC barrier, and how their regulation ensures tissue homeostasis. Homeostasis is defined here as maintaining a healthy permeability barrier (through structure and thickness), as providing an adequate permeability barrier is the main function of the SC. SC homeostasis will be quantified by TEWL, the main experimental measure of tissue homeostasis, to allow for comparison of simulation results to experimental data.

This chapter aims to show how the previously described resistance profile is both produced and regulated by depth-dependent concentrations and barrier components in the skin, as well as how they are affected by the environment and how changes in components can establish or lead to skin disease. In the SC the corneocytes lose their nucleus and cellular production machinery, so there can be no gene expression or any

active regulation. Therefore, all the regulatory processes must come from changes in the cellular environment, as all the components themselves are present or secreted at the SG/SC interface. This provides an opportunity to study the regulation of a dynamic and continuously renewing tissue based on changes in extracellular environment and concentrations along the depth.

We will take a modelling approach to create a framework, based on the resistance profiles, that incorporates known depth-dependent effects of SC barrier and regulatory components, and combining those to study homeostatic mechanisms. First, we will develop small and simple models for the main skin components that play a role in its barrier function and regulation. Besides describing the depth-dependency of the components, we model the components' contribution to barrier function, in a simple mechanistic way. The models will be based on available experimental data and, where possible, will be fit to the data. Furthermore, mimicking various experimental conditions by model perturbations will be used to test model behaviour and to compare to experimental results. These simple models have two functions: they will help us gain a general mechanistic understanding of the depth-dependency of the components in relation to the barrier function, and the submodels can be combined to create a model framework to study skin barrier homeostasis (figure 5.1). Incorporation of several simple submodels and their interaction into one system will allow us to analyse and test proposed regulation mechanisms and interplay between components, replicate experiments, and make predictions using *in silico* simulation.

Currently, to the best of my knowledge, no mathematical models exist that attempts to study the SC barrier homeostasis, incorporating barrier components and their interplay and regulation. Interplay between components and general homeostatic mechanisms have been described and proposed, but not tested as integrated systems, neither experimentally nor through modelling approaches (see section 2.3). Conventional experimental methods are inappropriate for studying *in vivo*. Modelling can be a suitable first step in examining if previously proposed regulatory mechanisms indeed behave as expected when considered in an integrated system representing the SC and its components. Initially, the model will only describe qualitative behaviour and prediction.

As more experimental data becomes available and our understanding improves, the model can be refined to produce quantitative information.

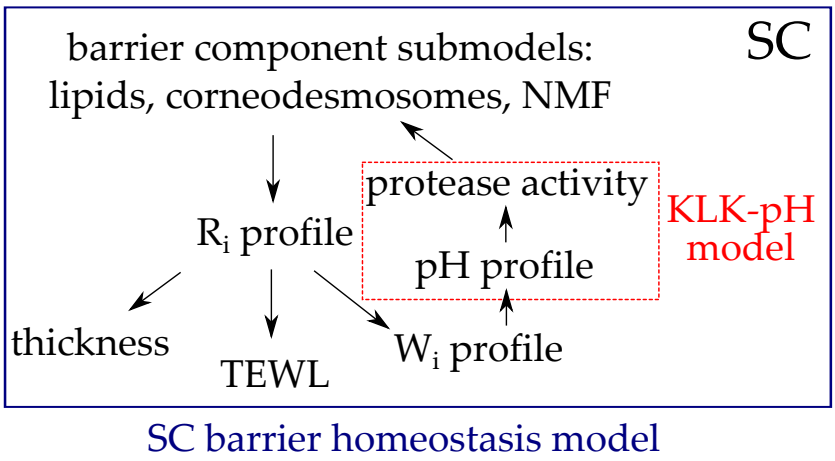


Figure 5.1: **Overview of relation between submodels developed in this chapter.**

This chapter first describes the depth-dependency of SC components that constitute the SC barrier function, and how we can model each of them. The components considered are NMF and its production from filaggrin, corneodesmosomes, lipids and desquamatory proteases. Also, water is considered explicitly in relation to the environment by looking at the influence of relative humidity. All those components are known to directly affect SC barrier function and/or play an important role in its regulation, as discussed in chapter 2. The resistance profile is a function of the two main barrier components (lipids and corneodesmosomes), and the degradation of these components by pH-activated KLKs. Their (simple) depth-dependent functions should result in a resistance profile comparable to experimentally observed ones. Given the typical depth-dependent resistance profile with an increase in resistance at the bottom of the SC and a decrease of resistance towards the top, maintaining high resistance in between, it is likely that respectively cornification and desquamation processes are responsible for the changes in resistance. Therefore, when discussing depth-dependency of components, we mainly look at cornification and desquamation. Desquamation is a process that affects the barrier through multiple components at the same time; when corneodesmosomes are degraded, the valuable tight structure is lost. Not only are the corneodesmosomes broken down and cell membrane structures weakened, the or-

ganisation of lipid bilayers, which need the tight cellular structure for scaffolding of their permeability limiting pathway, is affected as well. In this chapter, we specifically address desquamation and its regulation.

5.2 Modelling depth-dependency of components

In this chapter, we consider the height x of the stratum corneum instead of depth as in previous chapters. The height goes from $x = 0$ at the bottom of the SC to height $x = x_{\max}$ at the surface. The reason is that all models presented here (simple linear function, ODEs, PDEs) explicitly consider the upward movement of cells and barrier components, from the SG/SC to the outside. Here, we are interested in how the barrier components develop, degrade, and contribute to the barrier function as they move up higher through the SC, rather than looking inwards with increasing depth. For consistency, the orientation of the figures stays the same, i.e. the left of the figure is the skin surface (0 depth) and the right side is the SC/SG interface.

5.2.1 Natural moisturising factor

We first consider natural moisturising factor (NMF). It plays an important role in SC hydration and plasticity, as well as barrier homeostasis processes [63, 276, 224]. The term NMF encompasses a large group of small hygroscopic molecules, including amino acids, pyrrolidone carboxylic acid (PCA), urea, lactate and various ions, which are products of filaggrin degradation. Those components are mostly formed from filaggrin proteolysis. Pro-filaggrin is released at the SG/SC interface, and after dephosphorylation and proteolysis, filaggrin is formed at the bottom of the SC, where its task is to aggregate keratin filements (figure 5.2) [63]. Scott and Harding showed that filaggrin is only broken down with decreased water activity [277], suggesting that the water concentration profile regulates the depth at which filaggrin is degraded.

Published experimental data shows that there is a peak in NMF in the (higher) middle region of the SC [30, 22]. Filaggrin is mainly found in the lower layers of the SC [277].

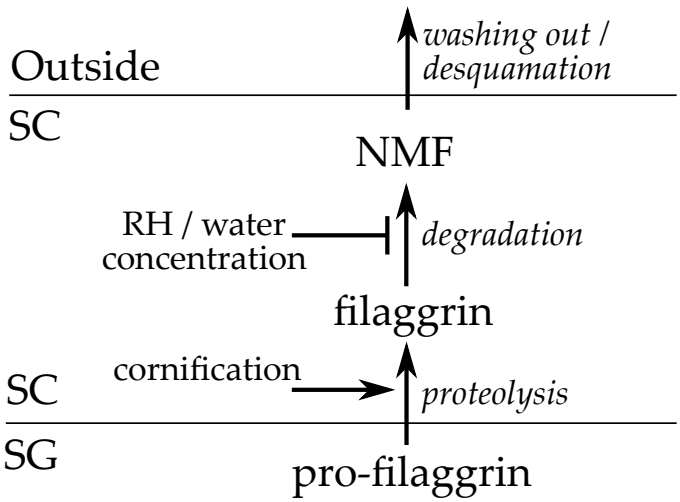


Figure 5.2: **Filaggin processing forms NMF along the depth of the SC.**

Interestingly, both in babies and in people with a filaggrin mutation a decrease in NMF is observed. The profiles are quantitatively similar, but qualitatively lower by approximately 50% [22, 268]. The NMF profiles obtained by Raman spectroscopy show a linear increase from a basal level at the SC/SG, until a couple of layers under top SC where it starts to decrease.

Atopic dermatitis patients often possess a FLG loss-of-function mutation [57], even though FLG mutation does not necessarily lead to a manifestation of AD. Both the filagrin phenotype and the severity of AD determine the levels of NMF [278, 279, 153], and patients with a FLG mutation, with consequently lower NMF, generally have a more severe form of AD [153].

Model

Using a simple model of the known process of filaggrin degradation into the smaller NMF compounds, we aim to show how the depth profile of NMF establishes.

A set of two coupled PDEs represent the hydrolysis of FLG F to NMF N with time t, along the depth of the SC, which is described by increasing height x (equals decreasing depth)

$$\frac{\partial F(x,t)}{\partial t} = d_F \frac{\partial^2 F(x,t)}{\partial x^2} - a_F \frac{\partial F(x,t)}{\partial x} - sF \ , \tag{5.1}$$

$$\frac{\partial N(x,t)}{\partial t} = d_N \frac{\partial^2 N(x,t)}{\partial x^2} - a_N \frac{\partial N(x,t)}{\partial x} + sF \ . \tag{5.2}$$

Advection is the movement of cells, and the majority of NMF is inside the cells. A number of NMF molecules, like ions, also reside in the extracellular space, where diffusion would dominate. The initial values of FLG and NMF can be set, as well as the rates of proteolysis, diffusion and advection.

The initial conditions ($t_0 = 0$) are

$$F(x, t_0) = 0 \ , \tag{5.3}$$

$$N(x, t_0) = 0 \ , \tag{5.4}$$

with boundary conditions

$$F(0, t) = \theta_F \ , \tag{5.5}$$

$$F(1, t) = 0 \ , \tag{5.6}$$

$$N(0, t) = \theta_N \ , \tag{5.7}$$

$$\frac{\partial N}{\partial x}(1, t) = -\beta_N \ . \tag{5.8}$$

The Neumann boundary condition for N at $x = 1$ conserves a constant outflow of NMF at the top of the SC by desquamation. The FLG Dirichlet boundary condition at $x = 1$ ensures all FLG is degraded and no FLG is left at the top of the SC, and the NMF and FLG Dirichlet boundary conditions at $x = 0$ describe the basal level of NMF present at the SG/SC interface.

Results

Figure 5.3 shows the simulation of the filaggrin and NMF profiles using equations (5.1)-(5.2) and initial and boundary conditions (5.3)-(5.8) with nominal parameters from table 5.1. The results are in good qualitative accordance with the literature, with

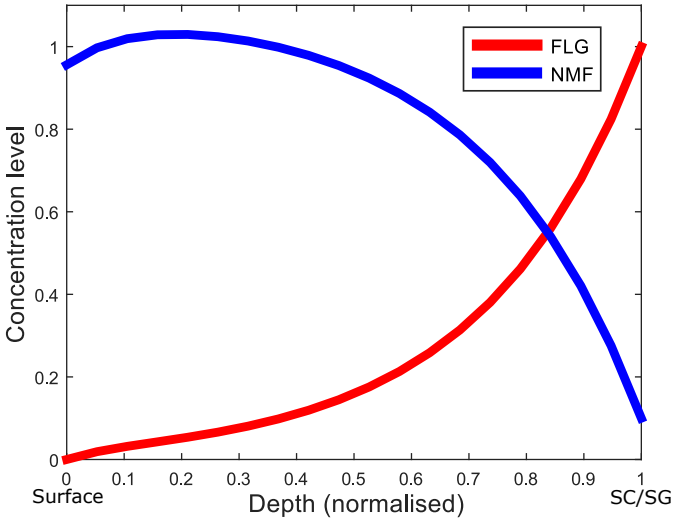


Figure 5.3: **Simulation of filaggrin and NMF depth profiles.**

NMF a peak in NMF in the middle to top region, and FLG mainly in the bottom SC [30, 22, 277].

The parameter which has most effect on the qualitative results is the rate of filaggrin degradation to NMF. This degradation rate s, relative to diffusion rates d_F and d_N, will change at which depth most of the FLG is degraded. We expect the FLG to be degraded in the lower layers of the SC, so the degradation rate should be larger than the diffusion rates. If the rate is too low, not enough FLG degradation will take place in the lower layers, and the level of NMF throughout the SC will be reduced significantly. Additionally, decreasing the advection rates a_F and a_N will move the peak in NMF closer to the SG/SC, while experimental data shows it should be in the middle/top region.

In order to compare these results to further experimental data, and validate the model and its ability to reproduce experimentally observed differences in both KLK and FLG levels, we perturb the model in two ways.

First, to simulate decreasing availability of FLG for people with a FLG mutation, we decrease parameter β_F. Decreasing β_F by 50% means there is constantly only half of the FLG supplied, and both profiles should be qualitatively similar but lower than the original ones as decreasing the FLG level at the SG/SC interface will decrease the

Table 5.1: **Nominal parameters used for simulation of NMF model.**

Description	Parameter	Nominal value
Filaggrin diffusion	d_F	0.1
NMF diffusion	d_N	0.1
Filaggrin advection	a_F	1
NMF advection	a_N	1
Fillagrin degradation to NMF	s	5
FLG concentration at bottom SC	θ_F	1
NMF outflow	β_N	0.2
Initial NMF concentration at bottom SC	θ_N	0.1

NMF profile. Setting β_F to 0 should see only a basal amount of NMF in the SC, constant along the depth.

Figure 5.4a shows the profiles for simulation with $\beta_{F,AD} = \frac{\beta_{F,\text{nom}}}{2}$. The results confirm our expectations by showing that a 50% reduction in FLG leads to a significant reduction of NMF. The NMF profiles for someone with a FLG mutation are qualitatively similar, but lower. These results are in close agreement with previously published results, which demonstrated a quantitatively similar reduction in NMF profiles from carriers of a FLG loss-of-function mutation [268].

Second, a change in water content should affect the activity of the proteolysis of FLG, such as for high hydration or for unborn babies [277]. Likewise, defects in proteolytic enzymes in disease could lower the rate of degradation of FLG into NMF. To simulate defective proteolysis of FLG, the rate of FLG degradation to NMF can be decreased. A lack of proteolysis causes FLG to appear throughout the SC at higher levels, and not in the basal layers only [277]. Figure 5.4b shows a simulation with reduced fillagrin degradation to NMF $s_{\text{red}} = \frac{s_{\text{nom}}}{5}$. As expected, a higher FLG concentration is maintained throughout the SC, and the level of NMF is reduced.

In this model, NMF is not broken down further into smaller components. We assume the NMF is 'washed out' at the top of the SC, which is implicitly included in the surface Neumann boundary condition. The decrease in NMF towards the top is a result

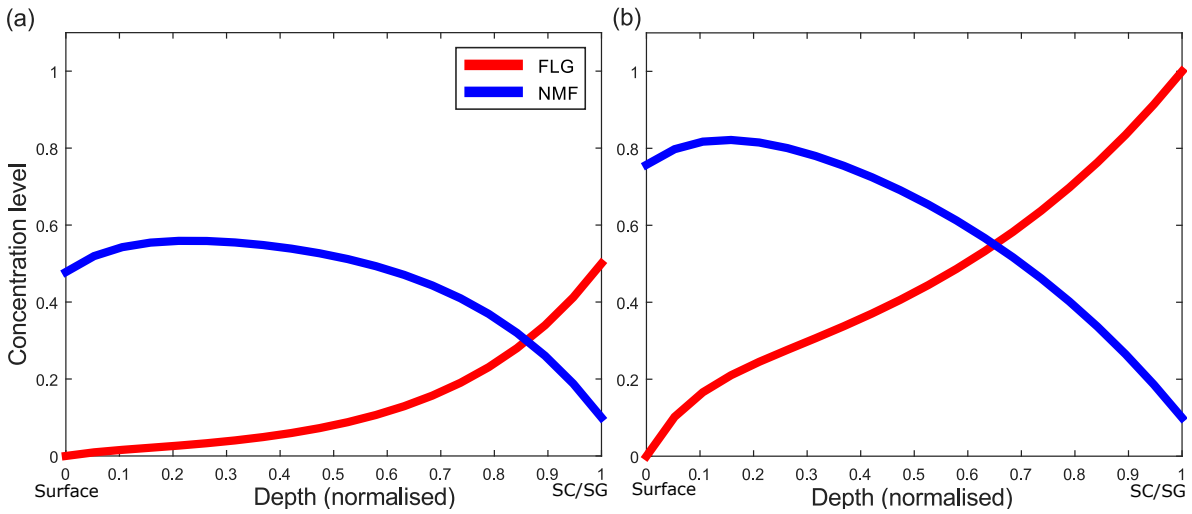


Figure 5.4: **Simulation of filaggrin and NMF profiles with reduced initial fillagrin and fillagrin degradation rate** (a) Simulation with reduced initial filaggrin levels at 50% of the nominal amount. (b) Simulation with reduced fillagrin degradation rate at 20% of the nominal rate.

of 'washing out', and we can assume that includes further breakdown of NMF. The breakdown products might also still be hygroscopic and considered part of NMF.

The direct contribution of NMF to the barrier function or resistance remains unclear. *In vivo* studies have shown that extraction of NMF components reduces SC hydration, and increases pH [280, 281, 282]. Direct influence on TEWL or thickness, however, have not been established, although the effect of NMF components on pH could be of significance, as altered pH has direct implication on desquamation (see chapter 2 and section 5.3).

Various experiments show how the water concentration profile changes after hyperhydration, typically by applying a water-soaked towel to the volar forearm [30, 149, 27, 283]. Hydration causes swelling of corneocytes, also documented using *in vitro* experiments [243], cause their thickness to increase to up to twice their normal thickness. The remarkable peak in hyperhydrated SC could be partially explained by the peak in NMF, which occurs at similar depth. Between the peak in hydration and the SG/SC interface there is a decrease in water content, which coincides with the location where most filaggrin resides, before it is turned into NMF. As NMF binds water in a

continuum rather than a discrete manner, the water in regions with more NMF will be more bound and less free to diffuse, causing a local peak at depths with high NMF levels. Even though these hyperhydration conditions are not representative of normal functioning, and are only temporary, they do suggest that there are depth-dependent differences in the ability to hold water, with NMF very likely to play a major role.

5.2.2 Water and relative humidity

The water concentration profiles, and the correlation between TEWL and thickness through the resistance profiles, have been discussed extensively in previous chapters (in particular chapter 3 and section 4.2). Here, we summarise the most important effects of relative humidity (RH) on the skin barrier, through changes in the water concentration profile.

The direct effect of a changing RH is a perturbation of the steady-state water concentration and flow, which can be useful for both experimentally and modelling approaches. Various experiments have studied the influence of varying RH on the condition of the skin, its barrier function and components. The varying short and long-term effects of changing RH can be utilised as a perturbation of our SC homeostasis model.
In a recent extensive review of the effects of RH on skin barrier function, Engebretsen *et al.* [284] conclude that the main effects of low RH are a decrease in water content, increased TEWL after short exposure, enhanced barrier (decreased TEWL) after long exposure, and increased thickness (in mice) [285]. In winter, which is characterised by drier air, SC lipids decrease (increase in unsaturated fatty acids), hydration decreases, pH increases, and lower levels of NMF are found. Upregulated barrier formation mechanisms are indicated by experiments where the barrier is disrupted by tape stripping or acetone treatment, showing accelerated recovery after prolonged exposure to a dry environment and delayed recovery after exposure to a humid environment [285]. FLG degradation to NMF only happens for normal and low RH, but not for very high RH, as FLG proteolysis is water dependent [277]. Lipid organisation improves until 60% RH, but decreases for higher RH (over 70%) [68]. Furthermore, patients with atopic dermatitis see an increase in incidence and flares with reduced RH [284].

Model

In our SC compartment model the RH is implemented through surface water concentration W_o, where $W_o \propto RH$

$$\sum_{i=1}^{n} R_i = \frac{\sum_{i=1}^{n} (W_{i+1} - W_i)}{\text{TEWL}} = \frac{W_v - W_o}{\text{TEWL}}\,, \tag{5.9}$$

with $W_v = W_{n+1}$ and $W_o = W_1$.

For the exact relation between RH and water concentration/activity at the top of the SC, see for example Li *et al.* [200]. If the RH is lowered, the outermost water concentration level W_o will decrease. This will lead to an increase in TEWL, if we assume $\sum R_i$ stays the same. The assumption that $\sum R_i$ stays the same implies that the components of the barrier are not affected by the change in RH initially, and only the water concentration directly re-establishes a new steady state through passive diffusion. If water content is the sum of the water concentration in all n layers (or only the top m layers, where $m<n$), the water content of the skin also drops when reducing RH. Our model therefore confirms the experimental findings that for lower RH water content decreases and TEWL increases.
The decrease in TEWL after prolonged exposure is possibly caused by a mechanism that induces a structural change in the SC structure or components. In equation (5.9), $\sum R_i$ should be increased to decrease TEWL again, despite a low RH.

5.2.3 Corneodesmosomes

Corneodesmosomes are vital for corneocyte cohesion and barrier function, and there is a clear relationship between the number of corneodesmosomes and the strength of corneocyte cohesion [286]. The number of CDs decrease towards the top of the SC [286, 287]. When corneocytes move up and desquamation processes including CDs degradation start, the non-peripheral CDs are lost first, a few layers below the surface. The edge CDs are degraded closer to the surface of the SC. The average number of CDs is about one per μm^2, which totals 400-600 corneodesmosomes per side of a corneocyte

[288]. According to Skerrow *et al*. [289], corneodesmosomes occupy approximately 30 % of the cell surface in the bottom half of the SC, but represent less than 7 % of the cell surface in the top half. Chapman and Walsh [286] found that this was 20.1% and 8.9% respectively on pig skin, decreasing even further to 5.7% at the top of the SC.

Model

After initial formation of the CD complexes, interlinked with the cornified envelopes, the amount of corneocytes remains constant, until desquamatory proteases starts to degrade the CDs. We can approximate this by a simple linearly increasing function of corneodesmosomes C in the bottom layers of the SC, until a maximum number of corneodesmosomes C_{max} is reached

$$C(x) = \begin{cases} \alpha_{\mathrm{C}} + \beta_{\mathrm{C}} x & \text{if } C < C_{max} \,, \\ C_{max} & \text{if } C \geq C_{max} \,, \end{cases} \tag{5.10}$$

with initial amount α_{C} at the bottom of the SC ($x = 0$) and rate of increase per unit depth β_{C}. Desquamation D will decrease the number of CDs towards the top of the SC

$$\bar{C}(x) = C(x)(1 - D(x)) \,. \tag{5.11}$$

We will address the exact desquamation function $D(x)$, including a fitting to the aforementioned data of number of CDs along depth, in section 5.3.

5.2.4 Lipids

From chapter 2, we know that the quantity and ratio of lipids affects the barrier function. However, these do not change with depth after their synthesis has been completed in the lower layers of the SC where the lipids are partly present in a hexagonal packing; it is the lateral lipid chain packing (organisation) that has been shown to vary with depth. Pilgram *et al.* [290] used electron diffraction to study the amount of orthorhombic and hexagonal packing after tape stripping. They observed predominantly orthorhombic packing in the SC, with decreased amount of orthorhombic and

increased amount of hexagonal packing in the outer layers of the SC. When compared to healthy skin, the lipid organisation of AD patients is aberrant as a result of changing amounts and ratio of lipids, leading to an increased amount of hexagonal packing [291]. A decade later, Damien & Boncheva [55] use attenuated total internal reflection Fourier-transform infrared spectroscopy to show the depth dependency of the lipid organisation *in vivo*. The extent of orthorhombic organisation increases slightly in the bottom half of the SC, and sharply decreases to mostly hexagonal near the surface. The percentage of total thickness with predominantly orthorhombic organisation inversely correlates with TEWL, showing its effect on barrier function.

Model

Modelling the depth-dependent changes in lipids, we start with the production of the barrier from the SC/SG interface. After release of lamellar bodies the lipid are first processed and organised (which happens in parallel with the cornification and formation of the cellular envelope and corneodesmosomes). We assume a linear increase in the contribution to resistance in the bottom few layers of the SC, up to a certain maximum resistance that is reached by a maximum 'capacity' of the lipids to provide resistance to water diffusion. This maximum contribution of lipids to the barrier is achieved if there are sufficient lipids, in the optimum ratio, organised in orthorhombic packing.

As an qualitative approximation, we group lipids amounts, ratio, and organisation in one lipid 'quality' variable L, which describes the resistance to water diffusion that the lipids provide along the depth. This can be modelled by a simple linearly increasing function with a maximum L_{max}

$$L(x) = \begin{cases} \alpha_{\mathrm{L}} + \beta_{\mathrm{L}} x & \text{if } L < L_{max} \,, \\ L_{max} & \text{if } L \geq L_{max} \,, \end{cases} \tag{5.12}$$

with initial amount α_{L} at the bottom of the SC ($x = 0$) and rate of increase per unit depth β_{L}.

With the degradation of corneodesmosomes, the cells are getting disjointed and sep-

arated, which could disrupt the organisation of the lipids in the intercellular layers. This seems to be supported by evidence that the lipids organisation becomes more hexagonal at towards the top of the SC, coinciding with desquamation, as discussed above. Modelling of lipids could use the CDs as indicator of the disorganisation of lipids towards the top of the SC, and could be qualitatively defined by the same function.

Towards the top, the lipid 'quality' will be degraded by a desquamation function D

$$\bar{L}(x) = L(x)(1 - D(x)) \,. \tag{5.13}$$

We will address the exact desquamation function $D(x)$ in the section 5.3, where equation (5.13) will be fitted to the lipid organisation data discussed above.

5.3 Desquamation: pH-dependent KLK activity model

An important depth-dependent process in the SC is desquamation, where serine proteases such as KLKs degrade corneodesmosomes towards the top of the SC, to decrease barrier integrity and cohesion which ultimately allows for the shedding of corneocytes. Naturally, this process must occur only towards the top of the SC, and the depth at which this process occurs must consequently be regulated tightly to maintain the thickness and barrier function of the SC. The importance of ordered desquamation becomes clear from its frequent misregulation in skin dysfunction and disease (see chapter 2).

A most interesting question is how desquamation is regulated spatially; which signalling, feedback and inhibitory mechanisms ensure gradual and controlled desquamation? As the corneocytes in the SC are anucleated, no active spatial regulation involving gene expression can take place, and depth-dependent changes in (extracellular) molecular concentrations are likely to activate desquamatory processes. The SC is the barrier and interface between the body and its environment, each with very different conditions. Therefore, gradients will form across the SC, most notably water concentration and pH gradients. The pH gradient is thought to be the main regulator of

desquamation, +by modulating the activation and inhibition of desquamatory serine proteases. However, this proposed regulation is not straightforward. The SC exhibits a pH gradient ranging from approximately pH 7 at the SG/SC junction, to pH 5 at the outermost layers [29]. Kallikreins (KLKs), a family of serine proteases, are known to play an important role in the degradation of corneodesmosomes. Specifically, KLKs 5, 7 and 14 have been shown to degrade corneodesmosomes, with pH-dependent activity [84]. KLK activity has a pH neutral to slight basic optimum, with decreasing activity when pH acidifies. Degradation takes place at the top layers of the SC, which have a more acidic pH, which means KLKs inhibited in the lower regions of the SC.
Lympho-epithelial Kazal-type-related inhibitor (LEKTI), is such an inhibitor of KLKs. LEKTI inhibits KLKs 5, 7 and 14 in a pH-dependent manner, increasing with pH [292, 293]. In a lower acidic pH environment, towards the surface of the SC, the inhibition of KLK by LEKTI could be reversed, allowing the active KLK to degrade corneodesmosomes. Despite this prosposed mechanism where pH-dependent inhibition regulates KLK activity, it has been reported that an increased in skin surface pH leads to higher KLK activites and increased desquamation [294, 295]. In AD, an increased surface pH induces KLK5-mediated barrier damage [296]. These findings seem counter-intuitive to the theories that lower pH towards the skin surface regulates desquamation by increasing KLK activity.

Here, we aim to find a simple mechanistic model which could explain the regulation, and reconcile both observations that the decreasing pH gradient induces desquamation and that increased surface pH increase KLK actvitiy. We take the KLK and its inhibitor LEKTI, and investigate if and how their pH dependency could explain the regulation of KLK activity and resulting desquamation. Recognising various other proteases and protease inhibitors, such as aspartate and cysteine proteases and cholesterol sulphate respectively [297] (see chapter 2), might play a role too, we are interested in the general mechanisms of regulation. Therefore, we take only KLK and LEKTI as an mechanistic example that could hold in general for corneodesmosome degradating proteases and their inhibitors. Each could have qualitatively different pH optima, association constants or inhibitors, yet share a common quantitative mechanisms.
As we propose a role of pH and depth-dependent regulation in the SC for KLK, this

part is essential in closing the loop of how components are regulated, specifically the desquamation of components and maintenance of a certain SC thickness. Therefore, we want to find a simplified mechanistic model that can explain both the increase in activity towards the top of the SC where pH decreases, as well as an increase in activity when pH is increased.

5.3.1 Model

Here we construct a model of depth-dependent KLK activity regulated by pH, which leads to the degradation of barrier components and desquamation. After constructing the model, it will be simulated and validated qualitatively, by comparing the KLK activity profiles to tape stripping data. Also, the degradation of components resulting from the KLK activity will be compared to experimental data, in order to verify both the effects of desquamation and KLK activity on the components and finalise the component profile models from section 5.2 by incorporating the effects of desquamation.

We use an adaptation of the model from Takana *et al*. [37] applied to the SC. While Tanaka *et al*. uses the ODE model to describe dynamics of KLK activation and inhibition in the SG/SC interface, and the effect of KLK activity on inflammation, we will apply the core of the model regarding the interaction between KLK and its inhibitor in a pH-dependent manner (first three ODEs in methods of Takana *et al*. [37]) to describe KLK activity inside the SC only. Our particular interest is how the KLK activity changes along the depth of the SC, and how the KLK activity results in degradation of corneodesmosomes and desquamation. Hence, we compute the the pH-mediated activation and inhibition of desquamatory proteases along the depth of the SC.
The main difference between our equations and those from the Tanaka *et al*. model are that we do not consider any newly produced pro-KLK, nor their activation from their inactive pro-from, as these processes occur at the SC/SG interface and the bottom of the SC. Instead, we consider the KLK moving up through the SC with the cells due to normal turnover. While moving up, the concentrations of KLK and LEKTI do not change. The KLK activity at a point in depth is instead determined by changing environmental conditions, which affect inhibition of KLK activity as well as degradation

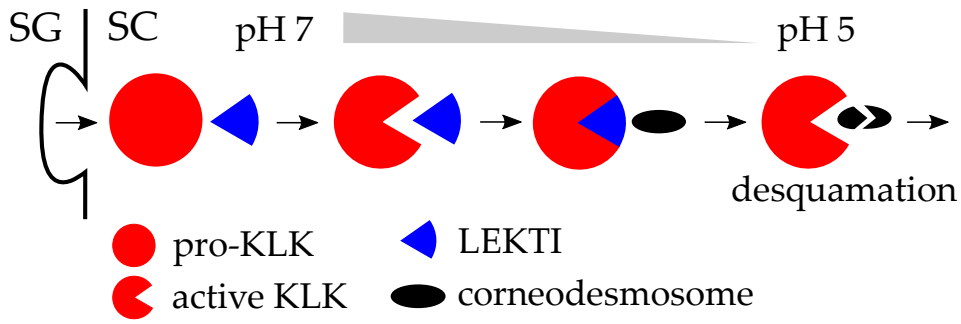


Figure 5.5: **KLK is activated and inhibited along depth of SC.** After pro-KLK is secreted from lamellar bodies at the SC/SG interface, it is converted to its active form. Regulated by a pH gradient, KLK is first inhibited by LEKTI in a high-pH environment. When pH decreases towards the top layers of the SC, this KLK-LEKTI complex dissociates, allowing the active form to degrade corneodesmosomes leading to desquamation.

of KLK and LEKTI. We assume KLK and LEKTI move up through the SC together with the corneocytes, and not by diffusing through the intercellular space. Although the model was originally developed for KLK5, our adaptation is a simplified model that aims at capturing the essential interaction between desquamatory proteases and their inhibitors in the SC. Therefore, we use KLK and LEKTI in our model to represent all desquamatory proteases and inhibitors, including but not limited to KLK5, KLK7, KLK14, and different types of LEKTI.

Profile of active KLK amount - binding of KLK to its inhibitor LEKTI

Even though we use KLKs and its inhibitor LEKTI, we aim to describe the general relationship between desquamatory proteases, their activity, and their inhibitors. As shown in figure 5.5, after being secreted from lamellar bodies and processed to its active form, KLK is inhibited by LEKTI. This inhibition is reversed when moving up towards the SC surface, and active KLK starts degradation of corneodesmosomes. The reversible inhibition of KLK by LEKTI happens by forming the inactive protease-inhibitor complex LEKTI-KLK, where the inhibition is governed by pH-dependent

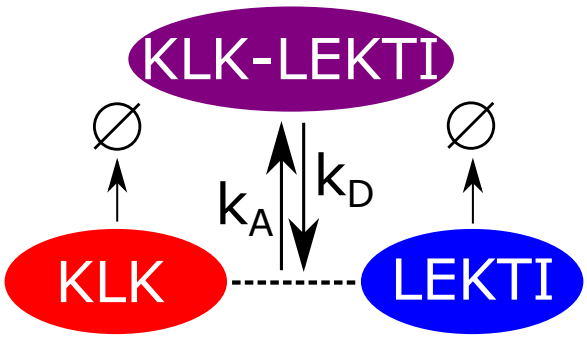


Figure 5.6: **Inhibition of KLK by LEKTI through pH-dependent association and dissociation.** LEKTI inhibits KLK activity by binding to its active site. Dissociation and association rates k_D and k_A are pH-dependent.

association rate k_a and dissociation rate k_d (figure 5.6)

$$[\text{KLK}] + [\text{LEKTI}] \rightleftarrows_{k_d}^{k_a} [\text{LEKTI-KLK}]\,. \tag{5.14}$$

We use the following ODEs to describe the process in equation (5.14) dynamically

$$\frac{\partial[\text{LEKTI-KLK}](x,t)}{\partial t} = k_a(pH)\cdot[\text{KLK}](x,t)\cdot[\text{LEKTI}](x,t) - k_d(pH)\cdot[\text{LEKTI-KLK}](x,t)\,, \tag{5.15}$$

$$\frac{\partial[\text{KLK}](x,t)}{\partial t} = -k_a(pH)\cdot[\text{KLK}](x,t)\cdot[\text{LEKTI}](x,t) + k_d(pH)\cdot[\text{LEKTI-KLK}](x,t)\,, \tag{5.16}$$

$$\frac{\partial[\text{LEKTI}](x,t)}{\partial t} = -k_a(pH)\cdot[\text{KLK}](x,t)\cdot[\text{LEKTI}](x,t) + k_d(pH)\cdot[\text{LEKTI-KLK}](x,t)\,, \tag{5.17}$$

with concentrations of KLK, LEKTI and LEKTI-KLK dependent on height x and time t. As with the SC compartment model, we can create depth-dependent profiles by solving these equations for different x. The steady-state solution of equations (5.15)-(5.17) will differ throughout the SC depending on the local pH concentration.
To find the steady-state concentration at t_{ss} at every point in height x, depending on initial conditions and association/dissociation rates, we solve the following equations

$$k_a(pH)\cdot[\text{KLK}](x,t_{ss})\cdot[\text{LEKTI}](x,t_{ss}) = k_d(pH)\cdot[\text{LEKTI-KLK}](x,t_{ss})\,, \tag{5.18}$$

$$[\text{KLK}](0,0) = [\text{LEKTI-KLK}](x,t_{ss}) + [\text{KLK}](x,t_{ss})\,, \tag{5.19}$$

$$[\text{LEKTI}](0,0) = [\text{LEKTI-KLK}](x,t_{ss}) + [\text{LEKTI}](x,t_{ss})\,, \tag{5.20}$$

Table 5.2: **Affinity constants for different pH levels.** Values are derived using equation (5.21) using k_a and k_d data from figure 6 in Deraison *et al.* [292].

pH level	**KLK5:** K_D **[M**$^{-1}$**]**	**KLK7:** K_D **[M**$^{-1}$**]**
4.5	$8.1 \cdot 10^{-8}$	$1.7 \cdot 10^{-4}$
5.5	$1.1 \cdot 10^{-9}$	$4.5 \cdot 10^{-7}$
6.5	$5.3 \cdot 10^{-11}$	$6.0 \cdot 10^{-9}$
7.5	$1.5 \cdot 10^{-12}$	$4.7 \cdot 10^{-9}$

with [LEKTI](0, 0) and [KLK](0, 0) initial conditions at $t = 0$ and $x = 0$.

From equations (5.18)-(5.20) we see that besides the initial values of KLK and LEKTI, the affinity constant K_D is needed to solve this system of three equations

$$K_D(pH) = \frac{k_d(pH)}{k_a(pH)} = \frac{[\text{KLK}](x, t_{ss}) \cdot [\text{LEKTI}](x, t_{ss})}{[\text{LEKTI-KLK}](x, t_{ss})}. \tag{5.21}$$

The affinity constant is a function of the association and dissociation constants. Deraison *et al*. have measured association and dissociation rates for varying pH, for both KLK5 and KLK7 [292]. Using equation (5.21) and the data on k_a and k_d to obtain the values of K_D for different pH values (table 5.2), we can construct a pH-dependent function $K_D(pH)$ by interpolation.

If we assume a linear pH profile with pH 7.0 at height $x = 0$ and pH 5.0 at $x = \lambda$, we can now obtain a profile of the amount of active KLK, by solving equations (5.18)-(5.20) with $K_D(pH)$ and initial conditions for KLK and LEKTI.

pH-dependent activity of KLK

The *amount* of active KLK at a certain location in the SC is not the only factor that determines the actual degradation of corneodesmosomes; the *activity* of KLK also varies with pH. Deraison *et al.* measured KLK activity p_{act} for different values of pH, as a percentage of the maximum activity at pH 7.5 (table 5.3). Where equations (5.18)-(5.20) solely describe the binding of KLK with its inhibitors to find the availability of non-bound 'free' KLK, we also need to describe how the desquamation activity of KLKs

Table 5.3: **KLK activity for different pH levels.** KLK5+LEKTI is activity of KLK after inhibition by amount of LEKTI. The percentages are relative to the maximum activity at pH7 which is taken as 100% for KLK5 and KLK7 respectively. Data from supplementary information to Deraison *et al.* [292].

pH level	KLK5 [%]	KLK5+LEKTI [%]	KLK7 [%]	KLK7+LEKTI [%]
4.5	16	12	21	18
5.5	38	24	35	30
6.5	47	30	95	42
7.5	100	51	100	50

D^{KLK} depends on both the amount and activity of KLK

$$D^{KLK} = p_{act}(pH)[\text{KLK}(x,t)]\,. \tag{5.22}$$

Combining equations (5.18)-(5.22), data from tables 5.2 and 5.3 and initial amounts of KLK and LEKTI, we can obtain a profile of degradation by KLK D^{KLK} in the SC.

Necessity of including degradation of LEKTI and KLK

In order to allow an increase in pH to increase degradation activity by KLK, we need to include degradation of KLK and LEKTI in this model. If we consider equations (5.18)-(5.20) and (5.22), we notice that the degradation activity by KLK only changes with x because pH changes with x; an increase in surface pH is equal to decreasing x, as all processes are reversible. Only an irreversible depth-dependent process could provide an explanation for simultaneously increasing pH and KLK activity. Therefore, degradation is considered. Myaid *et al.* have found mesotrypsin to activate KLK and degrade LEKTI, even in the enzyme-inhibitor complex; when mesotrypsin is added to 100% inhibited KLK-LEKTI complexes, the KLK activity recovers [293]. To my knowledge, the natural degradation rate of KLK has not been studied in skin.
The degradation term $\frac{\lambda - c \cdot x}{\lambda}$ is added to equations (5.19) and (5.20), such that the following set of three equations define the KLK steady state activity at height x in the

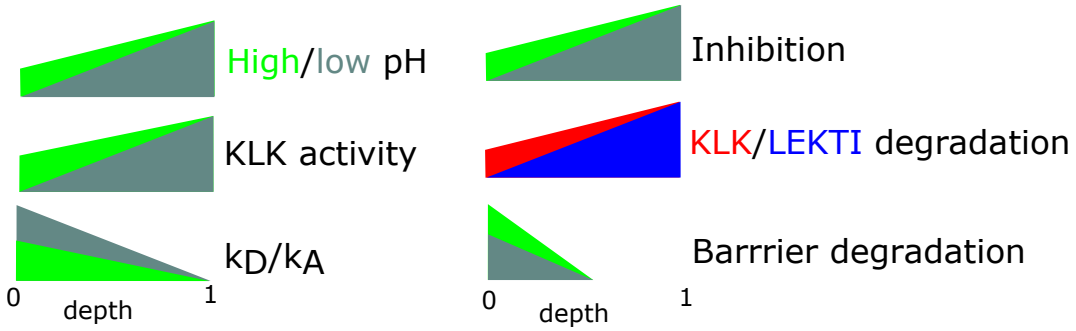


Figure 5.7: **Schematic overview of qualitative gradients of concentrations and rates.** Two different profiles shows the effect of decreased pH gradients, with green profile for high surface pH (increased) and grey for low surface pH (normal). Degradation of LEKTI (blue) is assumed to be faster than degradation of KLK (red). Depth 0 is skin surface, 1 is SC/SG interface.

SC

$$k_a(pH) \cdot [\text{KLK}](x, t_{ss}) \cdot [\text{LEKTI}](x, t_{ss}) = k_d(pH) \cdot [\text{LEKTI-KLK}](x, t_{ss}), \tag{5.23}$$

$$\frac{\lambda - c_K \cdot x}{\lambda} \cdot [\text{KLK}](0, 0) = [\text{LEKTI-KLK}](x, t_{ss}) + [\text{KLK}](x, t_{ss}), \tag{5.24}$$

$$\frac{\lambda - c_L \cdot x}{\lambda} \cdot [\text{LEKTI}](0, 0) = [\text{LEKTI-KLK}](x, t_{ss}) + [\text{LEKTI}](x, t_{ss}), \tag{5.25}$$

with x denoting SC height, and c_K and c_L degradation constants, and λ the SC thickness. The degradation term $\frac{\lambda - c \cdot x}{\lambda}$ is chosen such that there is no degradation at the bottom of the SC (at $x = 0$), and that while moving upwards, less of the initial KLK and LEKTI is available. With every increase in height x, more of the available KLK and LEKTI are degraded, assuming that degradation is linearly related to upward movement and time spend in the SC.

Desquamation

When combined, the pH gradient, inhibition of KLK to LEKTI, pH-dependent binding affinity and KLK activity, and degradation of LEKTI form the basic mechanism of depth-dependent regulation of desquamation. A simplified qualitative representation of those profiles, with the effects of an increase in surface pH, is summarised in figure 5.7.

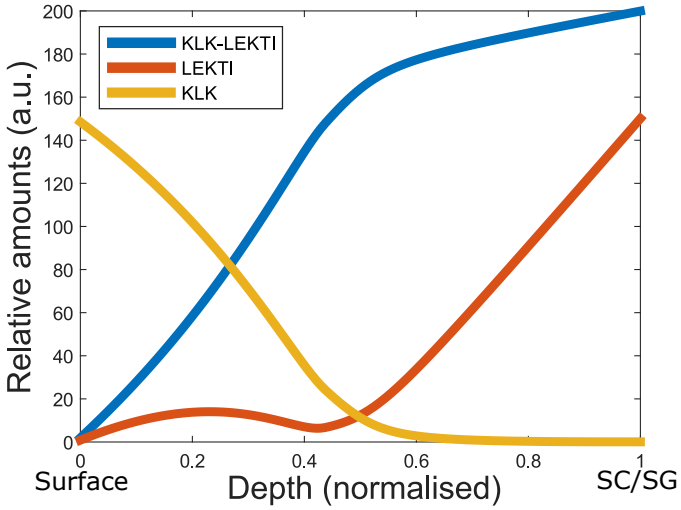


Figure 5.8: **LEKTI, KLK and the LEKTI-KLK complex profiles simulation over depth, with physiological pH gradient.** Values of KLK5 are used, KLK7 give qualitatively similar results.

We assume the degradation activity $D^{KLK}(pH)$ is linearly related to the level of degradation of the barrier components. Therefore, when describing the degradation of barrier components, the degradation will be a factor $1 - \gamma D^{KLK}(pH)$ multiplied by the barrier components, where 1 is a full barrier, and 0 is completely degraded. The profiles of corneodesmosomes and lipids in sections 5.2.3 and 5.2.4 will therefore be multiplied by $1 - \gamma D^{KLK}(pH)$ to include the effects of desquamation.
In the next section, the pH-dependent KLK model of desquamation and the barrier component models developed above will be combined to study SC barrier homeostasis.

5.3.2 Results and validation

When simulating the KLK activity, the qualitative behaviour we want to observe has two elements. First, there should be no degradation of corneodesmosomes in the bottom half of the SC, and therefore we expect a low KLK activity. Second, the degradation activity of the KLKs should increase towards the top, and the activity towards the top of the SC should be higher when surface pH increases. Figure 5.8 shows the

Table 5.4: **Nominal simulation parameters for the desquamation model.** Values of KLK and LEKTI in arbitrary units.

Parameter	Value	Description
$[KLK](0,0)$	200	Initial concentration of KLK (assumption)
$[LEKTI](0,0)$	350	Initial concentration of LEKTI (assumption)
c_K	0.25	Rate of KLK degradation (assumption)
c_L	1	Rate of LEKTI degradation (assumption)
$K_D(pH)$	table 5.2	Diffusion constants as function of pH [292]
$p_{act}(pH)$	table 5.3	Percentage of KLK activity as function of pH [292]

results of the simulation using equations (5.22)-(5.25). Steady-state equilibria of KLK, LEKTI, and the KLK-LEKTI complex were calculated at different heights to obtain the profiles, with a linear pH gradient of 7 (bottom) to 5 (top). Table 5.4 shows the nominal parameters used in the simulation. Whereas K_D and p_{act} are taken from literature, the other parameters are chosen to obtain a qualitative behaviour consisting of two specific elements to mimic experimentally observed behaviour.
The simulation results show that our model is able to show increasing degradation activity of KLK in the top layers of the SC (figure 5.8). When the surface pH is raised from pH 5 to pH 6 and pH 7, the activity and degradation are increased too (figure 5.9). Together, these results confirm that the model can produce the desired qualitative behaviour.

A parameter analysis was performed to ensure that the results are not limited by the choice of parameters, and to find the conditions for which the parameters qualitatively reproduce the desired results. The condition $[LEKTI](0,0) > [KLK](0,0)$ on the initial values of KLK and LEKTI is necessary to ensure that active KLK increases towards the surface of the SC. This means that initially, at the bottom of the SC, an abundance of LEKTI must be present to bind all KLK, which is later released due to a decrease in pH and a degradation of LEKTI. The parameter analysis demonstrated a further condition that the rates of degradation of LEKTI must be higher than that of KLK ($cL > cK$) to ensure the degradation activity increases up if surface pH becomes less acidic.

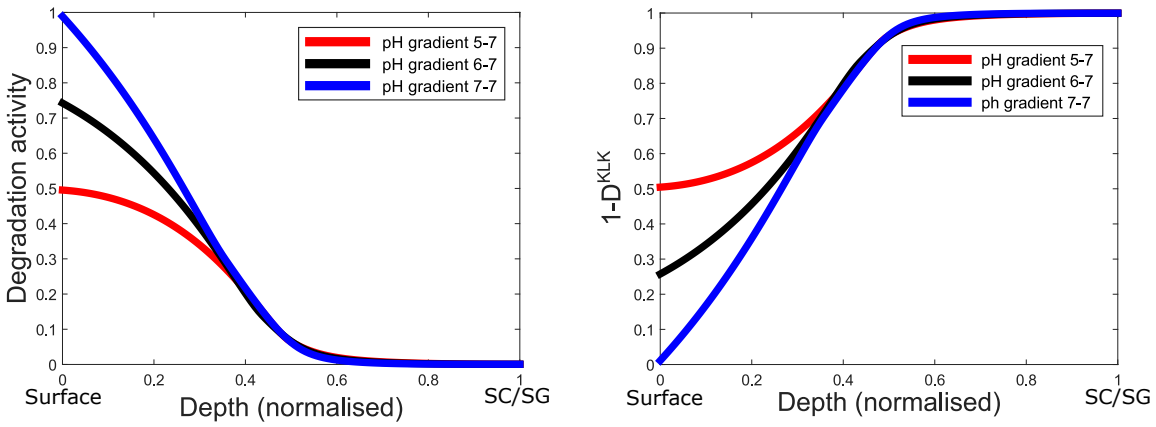


Figure 5.9: **Degradation activity $D^{KLK}(pH)$ for increasing pH at top of SC from 5 to 7.** Left panel shows degradation activity $D^{KLK}(pH)$, right panel shows the level of degradation of barrier components $1 - D^{KLK}(pH)$; 1 for no degradation and 0 for total degradation. pH gradient is linear from pH 7 at the bottom of the SC to surface pH 5 (red), 6 (black) and 7 (blue, constant pH).

To validate the degradation activity of KLK D^{KLK} and the resulting degradation of barrier components $1 - \gamma D^{KLK}$, we compare the profiles of D^{KLK} and $1 - \gamma D^{KLK}$ to multiple sets of experimental data.
In figure 5.10, a simulated profile of the degradation activity of KLK D^{KLK} is compared to the following experimental data sets:

(a) KLK5 and KLK7 activity after tape stripping, five depths, depth estimated from number of tape strips [163];

(b) KLK5 and KLK7 activity after tape stripping, three depths, depth estimated from number of tape strips [298].

The experimental values are normalised to the value at the deepest point around the basal layer of the SC, and shifted to zero. At this depth the KLK activity should be the lowest and there should not be any degradation of corneodesmosomes by KLK. The values are then qualitatively compared to a simulated profile of KLK, which is scaled to fit the experimental data.
Even though KLK activity can only be measured *ex vivo* after tape stripping, and consequently not quantitatively accurate, we can use the general qualitative shape of the

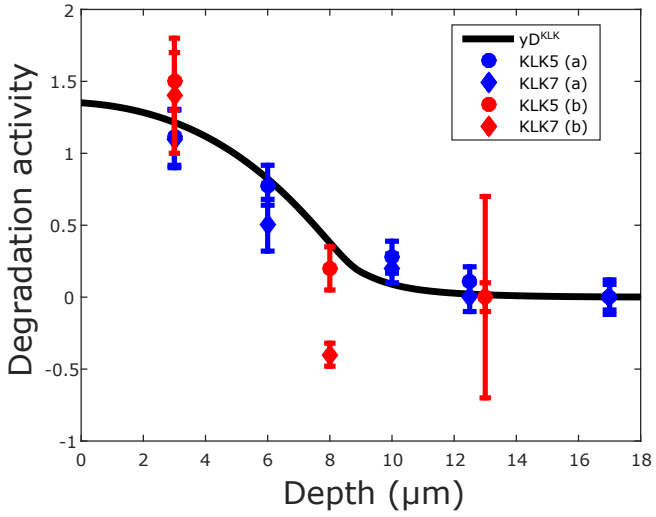


Figure 5.10: **Comparison of KLK activity to experimental data.** All experimental data points are normalised to their respective value measured at the deepest point and shifted to 0 degradation activity at the bottom of the SC.

data to compare with our simulated profile. Both data and simulation show a low, flat region at the bottom half of the SC, with a strong increase from roughly halfway the SC, confirming our simulated profiles of KLK activity qualitatively.

In figure 5.11, a simulated profile of $1 - \gamma D^{KLK}$ is compared to the following sets of experimental data which show the degradation of corneodesmosomes and lipid organisation towards the top of the SC:

(c) Counts of corneodesmosomes along depth [289];

(d) Counts of corneodesmosomes along depth [286];

(e) Lipid organisation along depth after tape stripping (ex vivo), in percentage orthorhombic [291].

The experimental data was normalised to their respective maximum values. Fitting of the simulation profile to the experimental data was achieved by adjusting γ, with γ_L for lipids and γ_C for corneodesmosomes. A different scaling was necessary for corneodesmosomes and lipids because degradation of corneodesmosomes has a quantitatively different effect on lipid organisation.

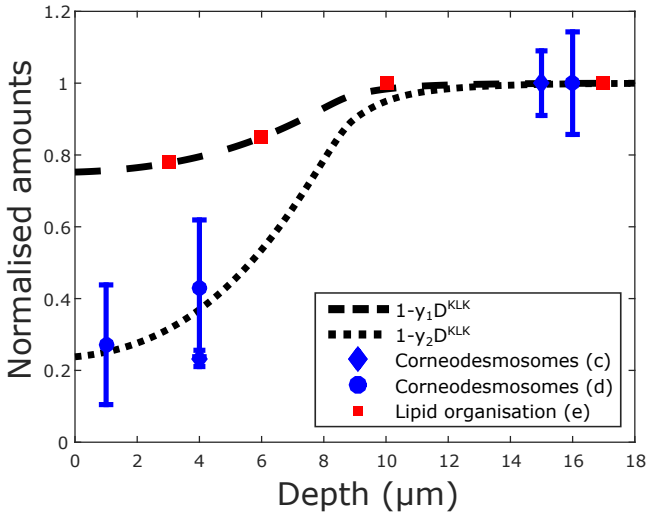


Figure 5.11: **Comparison of barrier component degradation to experimental data.** A different γ was used for corneodesmosomes and lipid organisation to fit the two profiles separately. All experimental data points are normalised to the maximum value.

The good qualitative fit to both corneodesmosome and lipid organisation data is obtained, using only one scaling parameter for fitting. This shows that the term $1-\gamma D^{KLK}$ is suitable for representing the degradation of components based on the KLK activity, which ultimately leads to desquamation.

5.4 Integration into SC barrier homeostasis model

In the final section of this chapter we combine the submodels developed earlier into a framework for studying depth-dependent SC barrier and its regulation – the *SC barrier homeostasis model*. In this model, SC homeostasis is quantified as the maintenance of physiological TEWL. Besides the barrier components and the pH-dependent KLK activity model, equations for water concentration, pH, and thickness will be combined through the resistance profile. The combined model is used for simulation and testing of proposed barrier homeostatic mechanisms. This is achieved by replicating experiments *in silico* and predicting the reaction of the SC to perturbations.

5.4.1 Model

We use a PDE to describe the water concentration profile W, using the resistance profile R. If we want to allow for variable thickness over time, we need to introduce a dimensionless variable $x_n = \frac{x}{\lambda(t)}$ to describe the normalised height, with $\lambda(t)$ the time-dependent thickness of the stratum corneum.

$$\frac{\partial W(x_n,t)}{\partial t} = \frac{1}{\lambda(t)^2}\frac{\partial}{\partial x_n}\left(\frac{1}{R(x_n)}\frac{\partial W(x_n,t)}{\partial x_n}\right), \tag{5.26}$$

with initial and boundary conditions

$$W(x_n,t_0) = 0 \tag{5.27}$$

$$W(0,t) = W_{bottom} \tag{5.28}$$

$$W(\lambda(t),t) = W_{top}\,, \tag{5.29}$$

where W_{bottom} and W_{top} are the water concentration at the top and bottom of the SC respectively.

A second PDE is used for the pH gradient

$$\frac{\partial pH(x_n,t)}{\partial t} = \frac{D_{pH}}{\lambda(t)^2}\frac{\partial^2 pH(x_n,t)}{\partial x_n^2}\,, \tag{5.30}$$

with boundary conditions:

$$pH(0,t) = pH_{\text{bottom}}\,, \tag{5.31}$$

$$pH(1,t) = pH_{\text{top}}(1 + W_{\text{top}} - W_s)\,, \tag{5.32}$$

with a nominal linear pH gradient from $pH_{\text{bottom}} = 7$ to $pH_{\text{top}} = 5$, and a nominal surface water concentration $W_s = 25\%$ at $pH = 5$. Here, the pH is influenced by W_{top} only, after which a linear gradient forms. However, this could be changed to include levels of NMF or other factors that could affect pH or desquamation.

The thickness is determined by the resistance profile. If the resistance at the top of the SC is lower than the resistance in nominal conditions, the thickness will decrease, and vice versa.

$$\frac{\partial \lambda(t)}{\partial t} = \rho(R_{top} - R_n)\,, \tag{5.33}$$

with R_n the nominal resistance at the top of the SC, and c_λ a constant determining the adjustment rate. If the resistance is lower than threshold R_n, we assume that the cells will shed off and the thickness will decrease. If the resistance is higher than R_n, the cells will not be shed, and the skin thickness increases due to newly produced corneocytes from the SG. As we use normalised height $x_n = x/\lambda$, the changed thickness is automatically incorporated in all other depth-dependent equations. This mechanisms maintains a certain thickness for a given resistance profile.

For the depth-dependent profile of the barrier components B, we assume that the main components that form the barrier are corneodesmosomes C and lipids L (sections 5.2.3 and 5.2.4).

$$L(x_n) = \begin{cases} \alpha_L x_n + \beta_L & \text{if } L < L_{max}\,, \\ L_{max} & \text{if } L \geq L_{max}\,, \end{cases} \tag{5.34}$$

$$C(x_n) = \begin{cases} \alpha_C x_n + \beta_C & \text{if } C < C_{max}\,, \\ C_{max} & \text{if } C \geq C_{max}\,. \end{cases} \tag{5.35}$$

Both lipid and corneodesmosomes make up barrier strength B. As we do not know their exact interaction or relative contribution to barrier function, we assume a simple additive function

$$B(x_n) = L + C\,. \tag{5.36}$$

The degradation of the barrier function by KLKs leading to desquamation, as discussed previously in section 5.3, completes the resistance profile by describing the decrease in resistance towards the top of the SC

$$R(x_n) = B(1 - \gamma D^{KLK})\,. \tag{5.37}$$

These equations describe the SC barrier homeostasis model with depth-dependent profiles. The values in the equations above can be calculated for all normalised height x_n between zero and one to obtain those profiles.

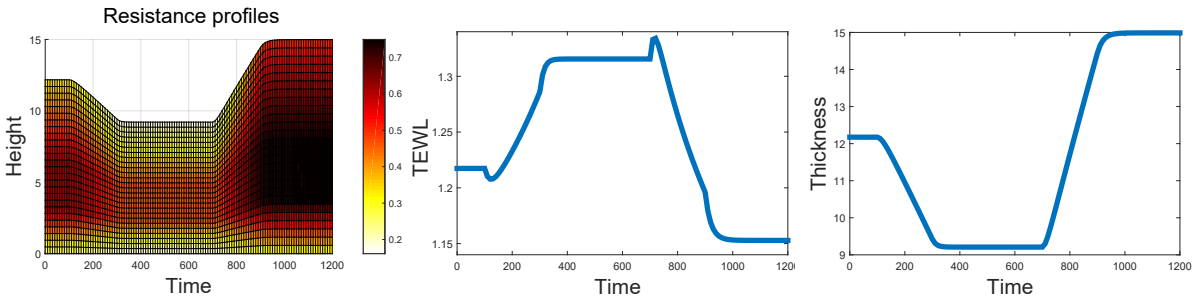


Figure 5.12: **Simulation of changes in relative humidity.** Relative humidity is increased at $t = 100$ to simulate a humid environment, and decreased to a dry condition at $t = 700$.

5.4.2 Results

In this section, we perform simulations of the SC barrier homeostasis model to study the interactions between the barrier components and regulation mechanism that were modelled in this chapter. First, equations (5.26)-(5.37) are simulated using nominal parameters. These parameters reach a steady-state homeostasis after an initial transient phase (depending on the chosen initial conditions). All further simulations start from the steady state. The tables in appendix A.2 present the simulated model variables (table A.3) and the nominal parameters (table A.4).

Two different scenarios are simulated: a change in environmental relative humidity and a change in skin surface pH. These *in silico* simulations *qualitatively* replicate *in vivo* experiments to test if the model behaves as expected, and if the proposed interactions lead to experimentally observed system behaviour.

Change in relative humidity. A change from high humidity to low humidity is simulated. First, the humidity is increased at $t = 100$. After a new steady state is reached, the RH is decreased to a dry condition at $t = 700$. This dry condition has a lower RH than the initial steady state. The changes in RH are implemented through adjusting the surface water concentration W_o, which leads to a new steady state by changing the water concentration profiles, pH and resistance profiles.

From experiments, we know that the barrier function is enhanced in dry condi-

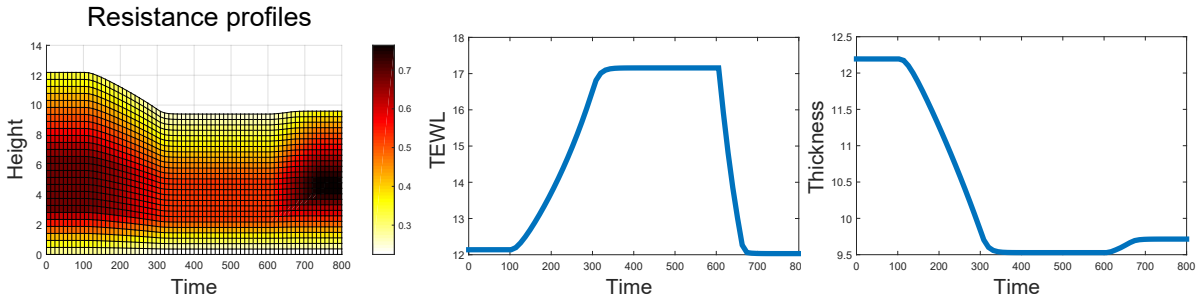


Figure 5.13: **Simulation of the effect of increased surface pH.** Skin surface pH is increased at $t = 100$. At $t = 600$, the maximum contribution of barrier components B_{max} was increased to replicate the effects of strengthening the SC barrier by treatment.

tions [285]. TEWL increases temporarily when moved to low humidity after a period in high humidity, and pH increases [299]. After the initial increase, TEWL decreases.

Figure 5.12 shows the simulation time course resistance profiles, TEWL and SC thickness. In agreement with the experimental data, TEWL increased and thickness decreased in high humidity. When changing from high to low RH, the barrier function is indeed enhanced. The remarkable temporary peak in TEWL is observed when moving from a humid to dry environment, which has been reported before [299].

Increase in pH. As seen from the pH-KLK model presented above, the pH concentration in the SC is vital for the regulation of desquamation [294]. NMF contains many acids and contributes to the decrease in pH, and if removed by soaking the pH increases [280, 282, 300].

In the simulation of this scenario, reduced FLG levels are introduced at $t = 100$. This leads to a reduction in NMF to roughly half of the nominal level (see section 5.2.1), which we assume linearly increases pH from pH 5 to pH 6. Such a state with increased pH is similar to the state of an AD patient, where a high pH increases KLK activity and dysegulated desquamation. At $t = 600$, while maintaining an increased surface pH, a 'treatment' is applied: the maximum contribution of barrier components B_{max} was increased to replicate the effects of strengthening the SC barrier by treatment. The type of treatment represented by

the consequent increase in resistance could be occlusion or replenishing of the barrier components, which leads to increased hydration or artificially improved barrier function.

The simulation results in figure 5.13 demonstrate a decrease in resistance profiles and thickness and an increase in TEWL after elevated surface pH. When the treatment strengthens the barrier components and increases the resistance, this leads to a strong decrease in TEWL to nominal levels. However, thickness only increase slightly and remains below the nominal levels, due to the unchanged defective desquamation. This shows that artificially increasing resistance profile through occlusion or addition of barrier components can reinstate a functional barrier, but will not improve the altered desquamation induced by elevated pH.

5.5 Discussion

In this chapter, we developed models of barrier component profiles and regulation. Using the resistance profiles as a framework, these models were integrated to simulate regulation of skin homeostasis.

Desquamation has to take place at the right depth, only near the top of the SC, to maintain SC thickness and barrier function. By distinguishing between *amounts* of available active KLK and the *activity* of KLK, and adding degradation terms, we are able to qualitatively explain how the pH gradient in the SC regulates desquamation. While a decrease in pH towards the top of the SC leads to the dissociation of the KLK-LEKTI inhibition complex and consequently the degradation of corneodesmosomes by KLK, an increase in surface pH. This counter-intuitive behaviour could be replicated if the degradation of KLK and LEKTI were considered. These results were obtained using only the main components and essential regulatory mechanisms that determine qualitative behaviour.

All models presented in this chapter were combined and linked into the SC barrier homeostasis model. By simulation of different scenarios, we can study how interaction between the individual components and their regulation leads to barrier homeostasis.

The simulation demonstrated that the proposed model leads to a physiological steady state, and the simulated scenarios qualitatively replicated experimental observations. To my knowledge, this is the first model that attempts to model SC barrier homeostasis through the interaction between barrier components and their regulation. It provides a framework for studying the interactions proposed by experimentalists, and allows for the testing of system behaviour resulting from a change in one component.
The current model has a number of limitations, including its qualitative nature. While a qualitative model can general interactions and the main regulatory mechanisms in barrier homeostasis, a quantitative model could be used for more in-depth study and prediction of the effects of specific treatments. For future research, the model could be improved and refined to exhibit quantitative behaviour. In particular, if more accurate time course data of the components and barrier state would be available, model parameters could be fitted.

The interaction with layers below the SC, including cornification processes, were not considered. The incorporation of cornification could be an extension for future research. Cornification rates are currently assumed constant, but could depend on TEWL through calcium and affect the building of the barrier by the rate of release of barrier components.

Chapter 6

Extension into the stratum granulosum: tight junction barrier homeostasis

6.1 Introduction

The epidermal permeability barrier function resides in the two uppermost layers: the stratum corneum and the stratum granulosum. In the stratum granulosum, tight junctions between keratinocytes form a barrier which provides selectively paracellular permeability, regulating the movement of water, ions and various larger molecules [96, 97, 91]. The tight junction barrier separates the basal and apical domains of the epidermis (viable epidermis and SC, respectively), allowing for essential distinct extracellular milieus in the SG and SC [102] (for a more detailed overview of TJ composition and function research see chapter 2). So far, this thesis has mainly focused on the depth-dependent permeability barrier in the stratum corneum. However, the TJ barrier in the SG emerges as a key second epidermal barrier, where depth-dependent processes play an important role too, and it directly affects and regulates the SC barrier as well as general epidermal homeostasis. Therefore, this chapter will extend our scope to the SG and its TJ barrier, and in particular how depth-dependent processes and spatial mechanisms maintain TJ barrier homeostasis. In addition, its role in epidermal homeostasis will be discussed.

The TJs are located in the second SG layer (SG2), and form a honeycomb-like mesh covering all the intercellular spaces [3, 105, 301]. The structure and location of the tight junctions, sealing off the paracellular pathway, strongly incidate its barrier function, which is confirmed for a variety of ions, solutes and water [302, 101, 303, 97]. The separation of the basal and apical epidermal compartments by the TJ barrier directly affects the terminal differentiation, through the regulation of local ion concentrations in both compartments. The location of the TJ barrier in relation to the SC, just below the SG/SC interface, means that it is the last moment in their upward movement through the SC during which they are in a viable tissue, just before losing their nucleus and undergoing cornification. Hence, the TJ barrier is important for organisation and preparation before transition to SC, predisposing SC barrier quality [9, 8]. It is therefore not surprising that TJ barrier impairment due to claudin-1 deficiency in mice leads to a reduced SC barrier function and increased TEWL [9]. As expected, an aberrant TJ barrier disrupts the process of SC barrier formation, specifically by altering lipid composition and profillagrin processing [8, 9]. One of the consequences of altered fillagrin processing is an increase in SC pH [8] (see chapter 5). In turn, a defective SC barrier affects the TJs; it causes a change in local concentrations in the SG/SC and below, most notably in the calcium gradient, which leads to changes in expression of claudins and TJ barrier function over time [10]. Furthermore, the TJ barrier is known to be compromised in skin diseases as psoriasis [112] and atopic dermatitis [109], where impairment of TJs by reduced expression of claudin-1 and claudin-23 leads to a reduced barrier function as measured by TER and further immune dysregulation. Its role in epidermal (permeability) barrier defects and disease suggests it could be a future target for treatment, despite our limited understanding of TJs and its proteins and functions [102].

Similar to the stratum corneum, the stratum granulosum's TJ barrier continuously maintains its selective permeability function. Even during continuous turnover, keratinocytes have to transition from the basal to the apical side of the TJ barrier. The continuous turnover of the epidermis raises the question of how keratinocytes moving upwards towards the SC can translocate across a TJ barrier, while this barrier is maintained across intercellular spaces in a single layer of cells. The transition requires

tight spatial and temporal regulation. Until recently, this transition has only be described for simple layer epithelium [304].

In November 2016, we[1] published a paper on 'Epidermal cell turnover across tight junctions based on Kelvins tetrakaidecahedron cell shape' [305]. It addresses the question of how a single layer TJ barrier across a tissue can be maintained while cells continuously transition through that barrier.

Based on time-course *in vivo* imaging of bicellular and tricellular TJs during transition, and using the approximation of cell shape by Kelvin's tetrakaidecahedron (TKD), we discovered the mechanism that allows cells to transition the TJ barrier in stratified epithelia without compromising barrier integrity [305]. This mechanism consists of the orderly formation and degradation of new tricellular and bicellular TJs at specific edges of the cells (figure 6.1). The SG consists of three layers: SG1, SG2 and SG3 (from outside to inside). The TJs are found between cells in the SG2 layer only, on apical edges shared between two SG2 cells. When a SG2 cell moves upwards to the top SG layer (SG1), where it cornifies and forms the SC, its TJs have to be replaced, from the SG2 cell transitioning to the SG1, to the SG3 cell transitioning into the SG2. Staining for TJ proteins (see [305]), the top view of a f-TKD shows a polygon of bTJs that encircles a cell, closing the extracellular spaces to its neighbours. During the barrier transition, tricellular junctions appear, and a smaller hexagon appears beneath the exterior bTJ polygon. The old bTJ polygon is then replace by the inner tTJ polygon, which turns into a new polygon of bTJs between the cell entering the SG2 and its neighbours. Thus, where a double polygon is visible, a cell translocates to the apical side of the TJ barrier (figure 6.1). This process is the basis for maintaining single layer TJ barrier homeostasis in a continually renewing epidermis.

In the previous chapters we have seen that the barrier function of the SC follows from the shape of the corneocytes (flattened and elongated, creating a long intercellular permeation pathway) and structure of the SC, with overlapping corneocytes with intercellular lipis structures, and kept tightly together by corneodesmosomes. Similarly, the

[1] M. Yokouchi, T. Atsugi, **M.D.A. van Logtestijn**, R.J. Tanaka, M. Kajimura, M. Suematsu, M. Furuse, M. Amagai, A. Kubo.

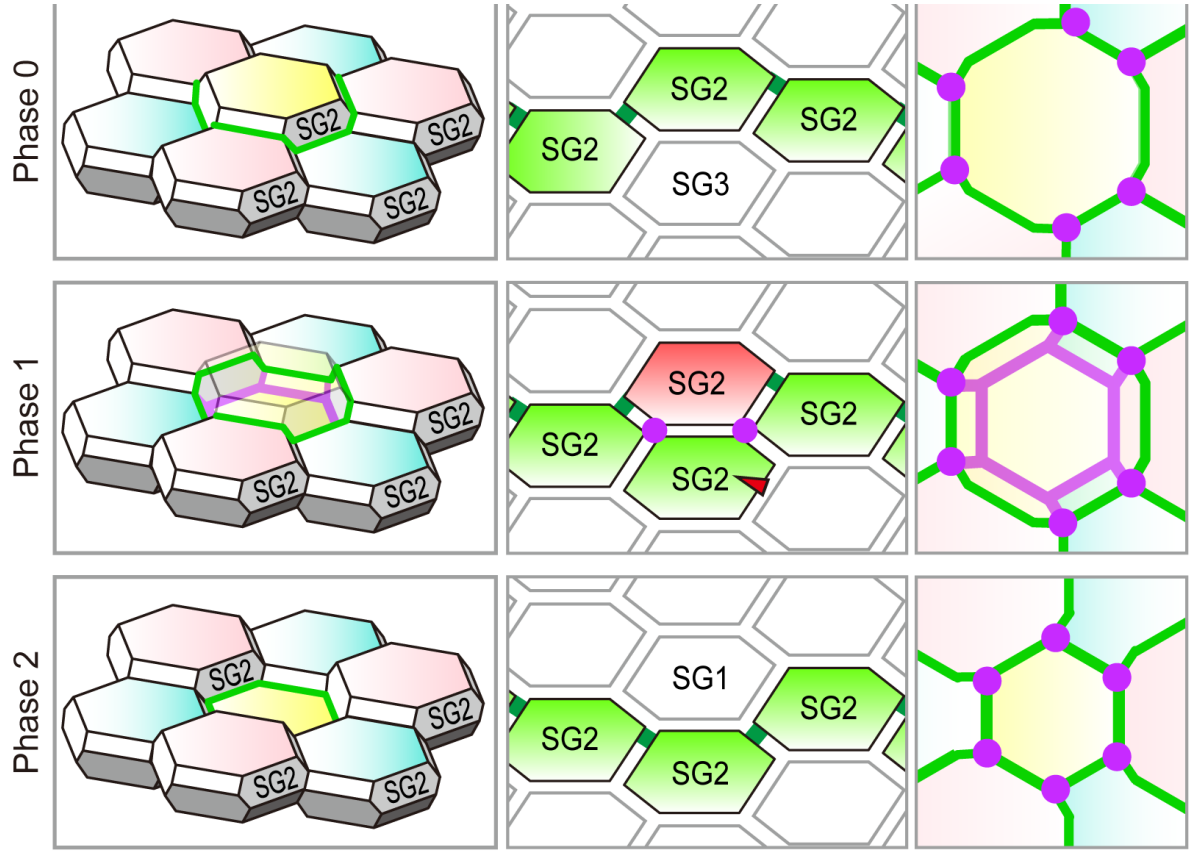


Figure 6.1: **Overview of transition phases and tight junction location.** Bicellular tight junctions in green and tricellular junctions in blue. Reproduced from figure 4b in [305].

shape of the keratinocytes seems to be important in how the TJ barrier and its turnover functions. Originally proposed by Lord Kelvin in 1887 as the optimal solution to his problem of finding the shape of cells with equal volume and minimal surface area that would partition a space [306], Kelvin's tetrakaidecahedron has been proposed more recently to closely represent the shape of a corneocyte [307, 308]. Using 2D and 3D live imagining techniques (figures 1-3 in [305]), we prove that corneocytes can indeed be represented as f-TKDs and that this particular shape is essential to the transition mechanism.

Our recent publication has shown the mechanism that allows this transition without breaking the TJ barrier. However, it is yet unknown how the transition is coordinated and regulated. For the barrier to be maintained during transition, the TJ proteins need to be transcribed and translocated to arrive at the correct site when the cell is ready to

start the transition and form the tight junctions. Temporal coordination is important because the transition needs to be tightly regulated, both in terms of the cells position in relation to the other cells and the barrier, and in terms of the timing of the start of the transition. When the transition of a cell starts too early or too late, the barrier might be compromised by a break in the tight junction cover. The formation and degradation of the tricellular tight junctions have to appear in different places at different times, depending of the location (height) of the cell in relation to the TJ barrier. Also, temporal coordination is important in balancing transition rates and turnover times with the rest of the epidermis. Turnover cycle times[2] that are too short or too long will disrupt tissue homeostasis, including tissue composition and thickness.

As the barrier maintenance during transition is vital for the skin's barrier function, it is a regulatory target. Currently, the spatial mechanism of barrier transition, including the formation and degradation of the tTJs and bTJs, has been observed. However, the timing of the steps and their regulation ('temporal coordination') is still unknown. This timing can tell us something about the underlying processes and signalling, and hints at (and excludes) possible functions of the various identified steps. The increased cornification as an initial reaction to skin barrier damage further suggests that it is important for the TJ barrier to be flexible and be able to upregulate transition rates while still maintaining a functioning barrier. In order to increase our understanding of the TJ barrier transition and its role in tissue homeostasis, a first step would be to study the timing and coordination of the transition process.

In this chapter, we construct a 3D geometric model of the keratinocyte and the entire SG tissue. Using this model, we simulate TJ barrier homeostasis by including a proposed algorithm governing TJ barrier transition. There have been previous examples of modelling and simulation of epidermal cells as TKDs. Honda *et al.* simulated the upward migration in the epidermis of keratinocytes with a TKD shape, which self-organised into stacked columns [309]. More recently, TKDs have served as 3D geometrical models of corneocytes to study stratum corneum permeability and (drug)

[2]In this chapter, the notion of cycle time refers to the SG2 turnover cycle time, which is the time it takes for a cell to cycle through the SG2, or equally the time for the SG2 to completely renew itself, and should not be confused to cell cycle time.

diffusion [183, 310, 184, 185, 311]. Complementing the experimental results presented above [305], modelling will help us to better understand and interpret experimental results, and to use those results to propose and test temporal coordination mechanisms. Through simulation of various scenarios and parameter sets, we can both predict timings, suggest possible mechanisms, and inform future experiments. Available experimental data is compared with simulation results, and model parameters that describe the proposed temporal coordination are obtained by fitting. We investigate the biological relevance of this temporal coordination which can be used to describe the transition dynamics, and suggest possible functions for the regulation of the TJ barrier and its role in epidermal homeostasis.

The following methods section first describes the development of the 3D geometry model of the f-TKD and the SG, and the derivation of geometrical parameters for the f-TKD from experimental 2D images. It then details the transition rules and algorithm used for simulation, based on the transition mechanism proposed in Yokouchi *et al.* [305], after which the simulation results are presented and discussed.

The experimental results referred to in this chapter are published under a Creative Commons Attribution (CC BY) license in the following paper [305]:

- M. Yokouchi, T. Atsugi, **M.D.A. van Logtestijn**, R.J. Tanaka, M. Kajimura, M. Suematsu, M. Furuse, M. Amagai, A. Kubo. Epidermal cell turnover across tight junctions based on Kelvins tetrakaidecahedron cell shape. *eLife* 2016;5:e19593. DOI: 10.7554/eLife.19593.

Two figures in this chapter are reproduced from the paper. Also, part of the computational simulation code we developed for the paper is used in this chapter. Any material from the paper used here is cited accordingly.

6.2 Methods

6.2.1 3D f-TKD cell model and geometry

Statum granulosum keratinocytes are modelled as flattened tetrakaidecahedrons (f-TKD). Their 3D geometry is derived here, as well as expressions for top view surface area that can be compared to experimental images to obtain 3D cell geometry from 2D images.

A flattened tetrakeidecahedron (f-TKD) with a hexagonal basis is used as a 3D model for the keratinocyte cells. Three parameters uniquely characterise the f-TKD 3D geometry [183] (Figure 6.2a):

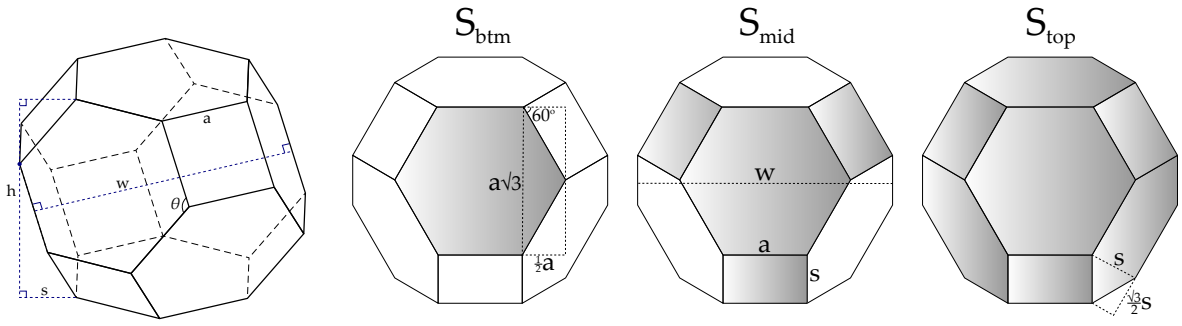


Figure 6.2: **f-TKD geometry** (a) 3D view adapted from Feuchter *et al*. 2006 [183] (b) f-TKD surfaces, as seen from a 2D top view.

- a: edge length of basic hexagonal (µm),
- w: width - distance between the two parallel sides (µm),
- h: height of the TKD (µm).

There is one condition on w and a that needs to be satisfied:

$$w > 2a.$$

An extra parameter s, the distance between the inner and outer hexagon (in 2D), as

shown in the top view of the TKD (figure 6.2), is defined as a function of w and a

$$w = 2a + 2\frac{\sqrt{3}}{2}s\,,$$
$$s = \frac{w - 2a}{\sqrt{3}}\text{‘}.$$

The volume of the f-TKD V_{TKD} can be determined as a function of h, w and a.

Top view surface areas Using the 3D geometry of the f-TKD, we can define the surface areas for the three basic shapes of the SG2 cells that can be observed from a top view as by a microscope (figure 6.2b).

$$S_{btm} = \frac{3}{2}\sqrt{3}a^2, \tag{6.1}$$
$$S_{mid} = \frac{3}{2}\sqrt{3}a^2 + 3s \cdot a = \frac{3}{2}\sqrt{3}a^2 + \sqrt{3} \cdot a(w - 2a), \tag{6.2}$$
$$S_{top} = \frac{3}{2}\sqrt{3}a^2 + 3s \cdot a + 3(s \cdot a + \frac{s^2\sqrt{3}}{2}) = \frac{3}{2}\sqrt{3}a^2 + 2\sqrt{3} \cdot a(w - 2a) + \frac{\sqrt{3}\,(2a - w)^2}{2}. \tag{6.3}$$

F-TKD volume To obtain the total f-TKD volume V_{TKD}, we first decompose the TKD structure into three layers, see figure 6.3, each with height $h/3$, and calculate their volumes:

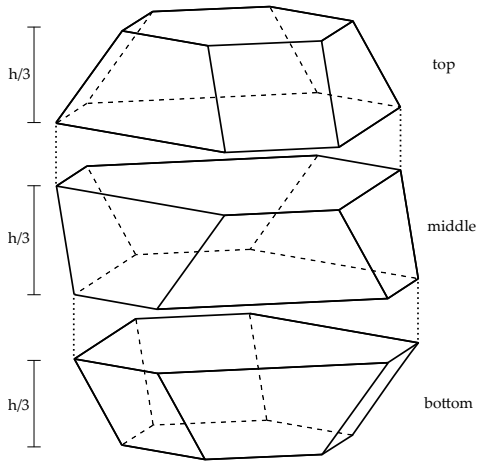


Figure 6.3: **TKD decomposition in three layers**

$$V_{TKD} = V_{top} + V_{bottom} + V_{bottom} \tag{6.4}$$

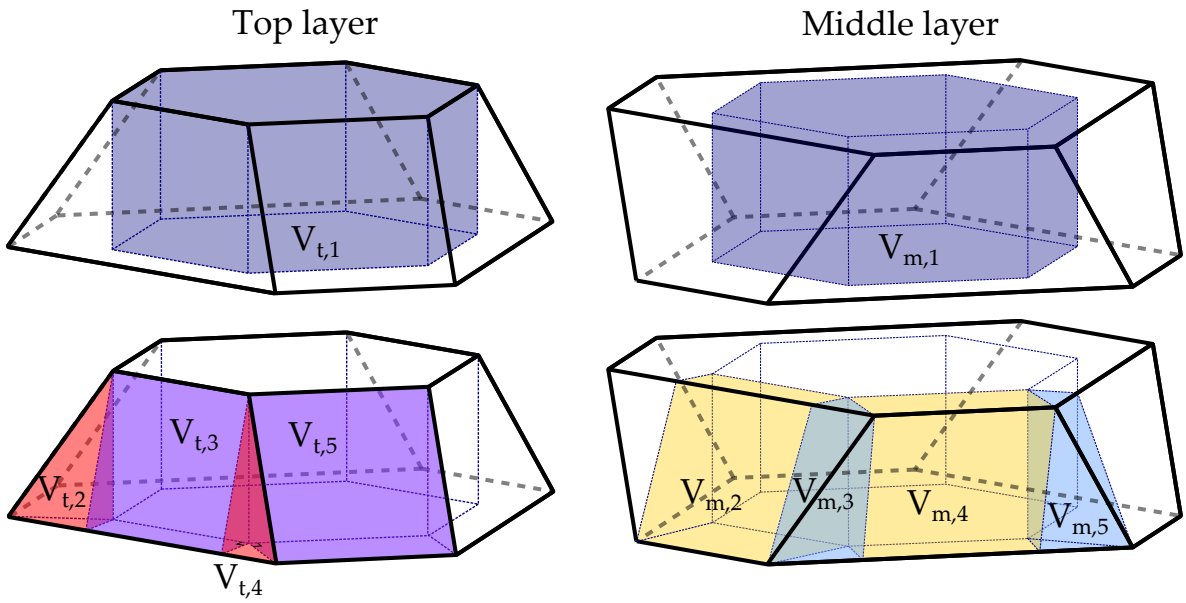


Figure 6.4: **Decomposition of f-TKD.** Decomposition into top layer (left) and middle layer (right), top view. Both layers have height $h/3$.

Top and bottom layer volume The top and bottom layers are the same, so the volume obtained for the top layer is the same as for the bottom layer $V_{top} = V_{bottom}$.

We first decompose the layer in 3 separate forms, denoted $V_{t,1}$ to $V_{t,3}$. See figure 6.4 (left) for top view of decomposition.

$$
\begin{aligned}
V_{t,1} &= \frac{S_{bmt} \cdot h}{3} \\
V_{t,2} &= \frac{\sqrt{3} \cdot h \cdot s^2}{72} \\
V_{t,3} &= \frac{s \cdot h \cdot a}{12} \\
V_{t,4} &= V_{t,2} \\
V_{t,5} &= \frac{s \cdot h \cdot a}{6} \\
V_{top} &= V_{t,1} + 3 \cdot V_{t,2} + 3 \cdot V_{t,3} + 3 \cdot V_{t,4} + 3 \cdot V_{t,5}
\end{aligned}
$$

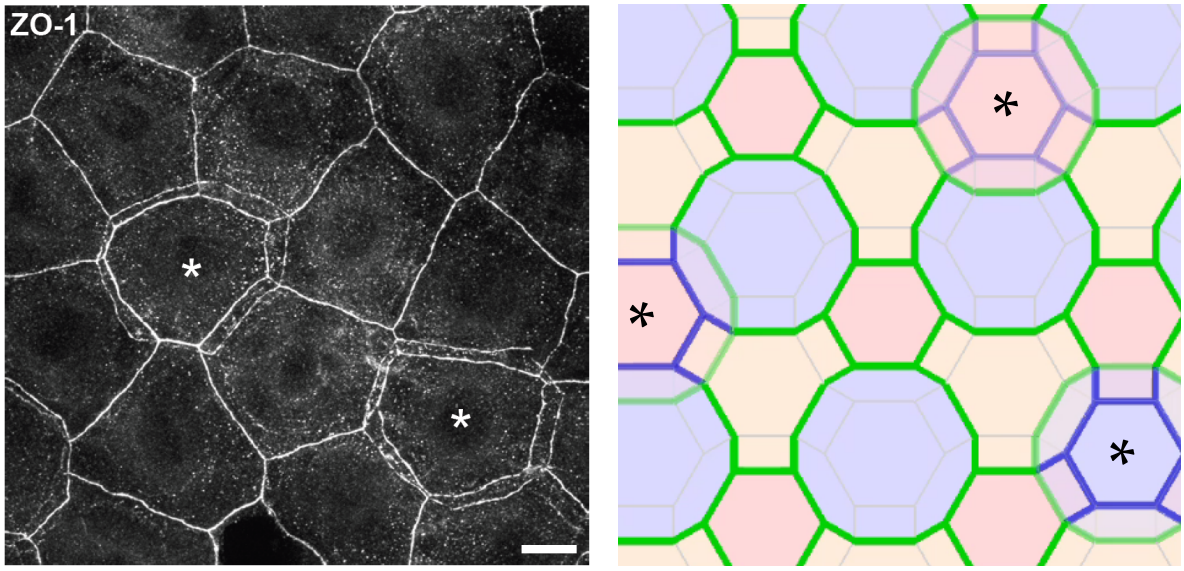


Figure 6.5: Experimental image (left) and simulation (right). A star * denotes a cell in transition

Middle layer volume We first decompose the layer in 5 separate forms, denoted $V_{m,1}$ to $V_{m,5}$. See figure 6.4 (right) for top view of decomposition.

$$
\begin{aligned}
V_{m,1} &= V_{t,1} \\
V_{m,2} &= a \cdot \frac{s}{2} \cdot \frac{h}{3} + a \cdot \frac{s}{4} \cdot \frac{h}{3} = \frac{a \cdot h \cdot s}{4} \\
V_{m,3} &= \frac{\sqrt{3} \cdot s^2 \cdot h}{24} + \frac{\sqrt{3} \cdot s^2 \cdot h}{72} = \frac{\sqrt{3} \cdot s^2 \cdot h}{18} \\
V_{m,4} &= V_{m,2} \\
V_{m,5} &= V_{m,3} \\
V_{mid} &= V_{m,1} + 3 \cdot V_{m,2} + 3 \cdot V_{m,3} + 3 \cdot V_{m,4} + 3 \cdot V_{m,5}
\end{aligned}
$$

The total volume of the TKD is

$$V_{TKD} = \frac{\sqrt{3} \cdot h \cdot (a + w)^2}{6}. \tag{6.5}$$

6.2.2 Obtaining geometrical parameters from experimental data

The cell geometry of the SG2 cells, as described by the f-TKD model in section 6.2.1, can be approximated using experimental data.

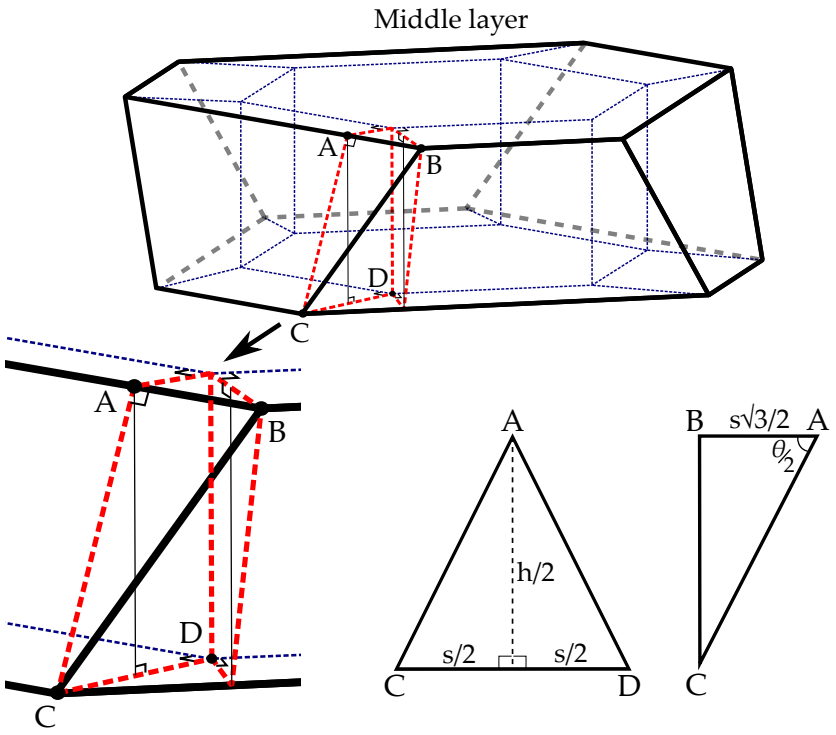


Figure 6.6: **Derivation of angle** θ

From the 2D top view images obtained by our computational model (Figure 6.2), we observe three distinct shapes, outlined by stained bicellular tight junctions in the (non-transitioning) SG2. We call these shapes top, mid and bottom surfaces, according to the different depths within the SG2 layer they are observed. The double hexagons experimentally observed for SG2 cells transitioning into the SG1 layer consist of the top shape for the outer hexagon and the bottom shape for the inner hexagon. The surface areas of each of these shapes, S_{top} and S_{btm} respectively, are determined by w and a. The experimental S_{top} and S_{btm} values were obtained by measuring the surface areas of the outer and inner hexagons from images such as the left plane of figure 6.5 [305].

Based on experimental measurements of 23 pairs of inner and outer polygon surfaces, representing 23 transitioning f-TKDs, a and w were calculated using equations (6.1) and (6.3) for each of the cells (table 6.1).

The angle of a side hexagon (arrow in figure 6.2) we call θ. To determine the height h, the angle θ is fixed. When assuming $\theta = 120^o$, h is dependent on a and w only. The

Table 6.1: **TKD geometry obtained from experimental data and geometric equations.**

Variable	Mean	St. dev.	Obtained by
S_{top} [µm^2]	1044.3	98.7	Experiments [305]
S_{btm} [µm^2]	814.7	75.4	Experiment [305]
a [µm]	17.7	0.8	Eq. (6.1), S_{top}
w [µm]	38.9	1.9	Eq. (6.3), S_{btm}, a
θ [degrees]	120	-	Assumption
h [µm]	8.7	1.5	a, w, θ
V [µm^3]	8131.2	1733.8	Eq. (6.5), a, w, h

triangle-based pyramid as part of $V_{t,2}$ can be used to determine h as a function of the angle θ given that a and w are known. The distance CD between point C and D is $\sqrt{\frac{s^2}{4}+\frac{h^2}{9}}$, from figure 6.6b. From 6.6c,

$$\begin{aligned}
\tan\frac{\theta}{2} &= \frac{\sqrt{\frac{s^2}{4}+\frac{h^2}{9}}}{\frac{s\sqrt{3}}{2}},\\
\frac{s^2}{4}+\frac{h^2}{9} &= \frac{3}{4}s^2\left(\tan\frac{\theta}{2}\right)^2,\\
h^2 &= 9\frac{s^2}{4}\left(3\left(\tan\frac{\theta}{2}\right)^2-1\right),\\
\therefore h &= \frac{3}{2}s\sqrt{3\left(\tan\frac{\theta}{2}\right)^2-1} = \frac{\sqrt{3}}{2}(w-2a)\sqrt{3\left(\tan\frac{\theta}{2}\right)^2-1}.
\end{aligned}$$

If $\theta = 120°$, then $\varphi = 120°$, and $\tan\frac{\theta}{2} = \sqrt{3}$. Accordingly,

$$h = \frac{\sqrt{3}}{2}(w-2a)\sqrt{8} = \sqrt{6}(w-2a). \tag{6.6}$$

Using $h = \sqrt{6}(w-2a)$, we can completely define the geometry of the f-TKD from experimental data (table 6.1).

6.2.3 3D model of the stratum granulosum

The 3D TJ model of the SG2 and underlying layers is comprised of stacked layers of optimally packed SG cells modelled by flattened TKDs (f-TKD), similar to the geome-

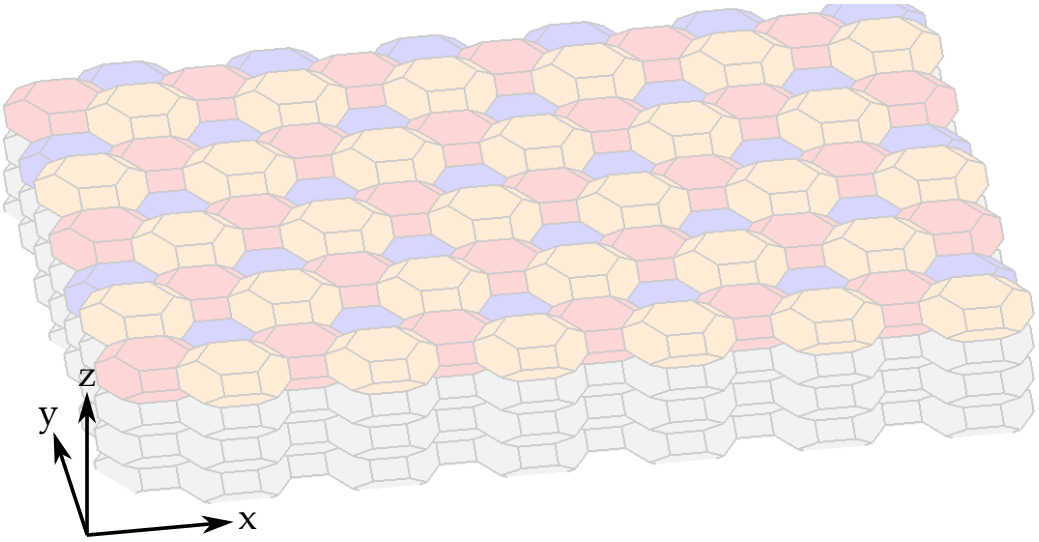


Figure 6.7: **3D model of SG2 and underlying layers.** The highest SG2 sublayer SG2-A in yellow, the middle sublayer SG2-B in pink, the lowest sublayer SG2-C in blue, and the underlying layers in grey.

try model for a corneocyte plasma membrane [183]. For modelling the f-TKD and its geometry see section 6.2.1. The number of cells per layer is L_w (x direction) by L_l (y direction). The SG2 layer has three sublayers (A, B, C) which have cells at the same height (z coordinate), but with space in between them in the x and y directions to allow for optimal packing (layer SG2-A). The next two layers below (SG2-B and SG2-C) will be the same number of cells, but shifted in all dimensions, such that the three layers are packed together without leaving any open space (coloured cells in Figure 6.7).
In the simulation figures and movies, TKD cell parameters $a = 2$, $w = 6$ and $h = 2$ are used for reasons of visibility and clarity.
This configuration of three sublayers of cells is then repeated several times, shifted in the z direction only, such that the top of a layer matches with the bottom of the layer that is three sublayers above. The number of cells in the SG2 C_{SG2} is equal to the number of cells in the three sublayers, so $C_{SG2} = 3L_wL_l$. The height h_{3l} of the SG2 layer is $h_{3l} = \frac{5}{3}h_c$.

All cells are comprised out of 14 faces and 24 vertices, and every vertex has a three-dimensional Cartesian coordinate (x, y, z). All edges of a cell and the edge coordinates can be obtained from the faces and vertices.

6.2.4 Simulation

Proposed rules for transition The following rules are proposed, based on experimental findings in Yokouchi *et al.* [305]. Three basic rules are applied to determine the appearance of bicellular and tricellular tight junctions.

1. Bicellular tight junctions (green) can appear on edges that are shared between two cells in the SG2, given that both cells transitioning into and out of the SG2 are considered part of the SG2.
2. Tricellular TJs (blue) can appear during transition on edges that are shared between 3 cells in the SG2
3. The tight junctions only appear on edges that are at the top of the SG2 (so in contact with SG1 cells).

Two basic rules are applied to determine when a cell transitions from SG2 to SG1 and from SG3 to SG2.

1. An SG2 cell located higher than its six adjacent SG2 cells differentiates to become an SG1 cell, after a waiting period.
2. The differentiation of cells from SG3 to SG2 and SG2 to SG1 are synchronized in each cell column. The actual SG2-to-SG1 transition is assumed to occur in a certain transition time t_t, during which the SG2 cell gradually becomes an SG1 cell (transparent).

Visualisation of tight junctions and cell transition Only the SG2 cells are differentiated by colour, with one per column, where all cells at the same height z have the same colour (Figure 6.7).

Bicellular TJs are coloured green, tTJs are coloured blue (Figure 6.8). During transition, the cell transitioning from SG2-SG1 gradually becomes transparent, which allows us to see the tTJs (starred cells in Figure 6.5). The cell making the SG3-SG2 transition has the same colour as the cell above, as it is now considered part of the SG2 in the

sense that it can form tTJs. The tTJs increase in transparency first, and when they reach halfway the transition and are fully opaque, they start losing their transparency. During the last 30% of the transition, the green bTJ that will replace the tTJ will become increasingly visible through the blue tTJ which becomes increasingly transparent.

The transition process of SG2-SG1 translocation comprises a transition where the blue tTJs appear and disappear. This is simulated by gradually linearly decreasing and increasing the transparency of the blue tTJs. In the current simulations, the first half of the transition time t_t the transparency is increasing and the second half of t_t the transparency is decreasing.

Simulation algorithm After initialising the 3D TKD model, the simulation algorithm based on the proposed rules is:

1. Initialise simulation. Every cell j is assigned a waiting time t_w^j, randomly chosen from the waiting time distribution.
2. For cells in transition or in waiting, update time spent in transition/waiting.
3. If the time spent waiting exceeds t_w^j, the cell starts transition.
4. If the time spent in transition exceeds t_w^j, the cell moves to SG1.
5. If a cell enters transition, the cell below it in the same column starts to transition into the SG2. The edges of its top hexagon are now considered part of the SG2.
6. If a cell enters SG2-SG1 transition, all its 6 neighbours check if they are higher (z direction) than their respective neighbours. If that is the case, that neighbour cell begins its period of waiting time t_w^j.
7. Calculate the TJs according to the rules (section 6.2.4).
8. Output a plot of the SG2 cells, the cells of the SG1 and below, and the TJs.
9. Update the time by δ_t and increase the z coordinate of all vertices by δ_z (upward movement of cells).
10. Repeat steps 2-9.

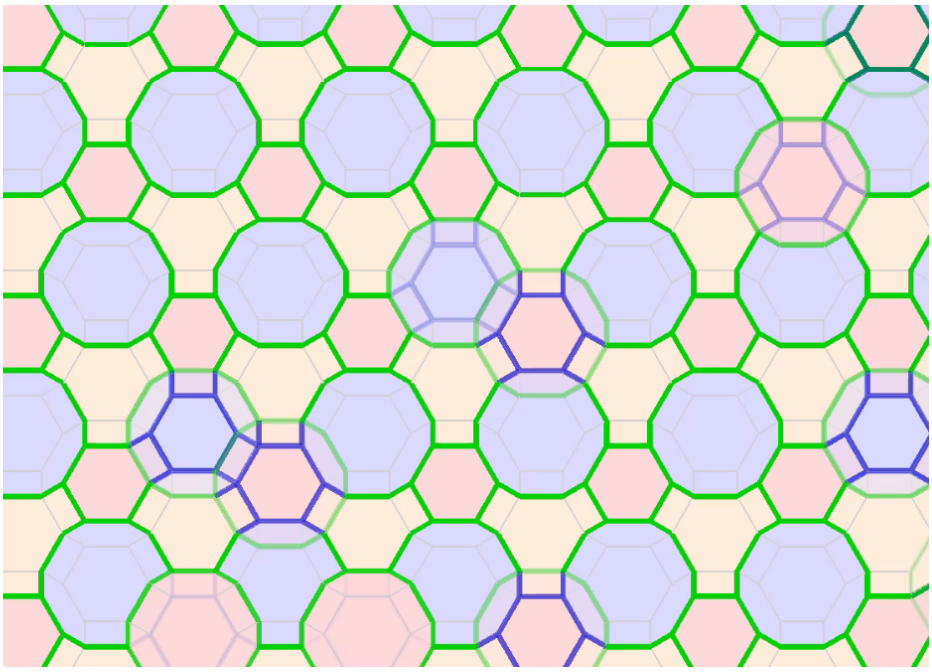


Figure 6.8: **Example simulation result.** 2D top view, with $C_{\mathrm{nb}} = 2$, $C_{\mathrm{trans}} = 10$, and $r_{\mathrm{nb}} = 25\%$. Green lines are bicellular TJs, tricellular TJs in blue.

Implementation The simulations were implemented and run in MATLAB R2015b, which was also used to produce the simulation videos and further analysis and optimisation.

6.2.5 Calculation of TJ barrier turnover indices

Three indices of dynamic TJ barrier turnover are obtained experimentally and from simulations: the percentage of total cells in transition r_{trans}, the percentage of cells in transition that have a lower neighbour transitioning at the same time per total cells in transition r_{nb}, and the cycle time t_{cycle}, which is the time a cell spends in the SG2 layer

$$r_{\mathrm{trans}} = 100 \cdot \frac{C_{\mathrm{trans}}}{C_{\mathrm{SG2}}}\,, \tag{6.7}$$

$$r_{\mathrm{nb}} = 100 \cdot \frac{C_{\mathrm{nb}}}{C_{\mathrm{trans}} - C_{\mathrm{nb}}}\,, \tag{6.8}$$

$$t_{\mathrm{cycle}} = t_{i+1} - t_i\,. \tag{6.9}$$

The equations to calculate r_{trans} and r_{nb} from simulation results are based on the number of cells in transition C_{trans}, the total number of cells in the SG2 C_{SG2}, and the number of sets of two neighbours transitioning at the same time C_{nb}. The times t_i and t_{i+1} denote the times the cell i enters and leaves the SG2, respectively. Figure 6.8 shows an example simulation results including calculated indices.

6.2.6 Experimental data

The experimental TJ images that are used to determine f-TKD geometry (table 6.1) and dynamic turnover indices (table 6.3) were obtained by Yokouchi *et al.* [305]. The source data is available from DOI: 10.7554/eLife.19593.

6.3 Results

6.3.1 Temporal coordination of SG2 cell transition maintains TJ barrier homeostasis

Simulation of the TJ barrier transition requires both a model of the stratum granulosum and an transition algorithm that incorporates the turnover mechanisms, including their timing. A 3D model that approximates the form of the keratinocytes is a flattened tetrakeidecahedron. Its full geometry is uniquely defined by three parameters: height h, basic hexagonal edge length a and width w (section 6.2.1). Optimally packing layers of f-TKD cells creates a 3D model of the SG, in which the TJ barrier resides in the second layer. The geometry can be obtained by comparing experimental images (figure 6.5) to 2D projections of the 3D f-TKD model (figure 6.2), resulting in the values in table 6.1.

The algorithm that allows dynamic simulation of this static model is based on the transition mechanism discovered in Yokouchi *et al*. and a proposed temporal coordination of the transition events (see methods section 6.2.4). The temporal coordination of the SG2 cell turnover cycle is proposed based on translating the transition mechanisms into a simulation algorithm, and consists of a timeline including the timing and order of transition events (figure 6.10). When a cell j enters the SG2, for a period t_{low}, it waits until all its six neighbouring cells have transitioned into SG1. From the moment a cell is higher than its 6 SG2 neighbours, it takes a certain waiting time t_w until it starts the transition from SG2 to SG1. After the transition time t_t, the cell has fully translocated to the apical side of the TJ barrier and enters the SG1.
Simultaneously, as cell j enters the SG2 at time t_{i+1}^{j}, the cell below $j+1$ enters the SG2 at time t_i^{j+1}, therefore $t_{i+1}^{j} = t_i^{j+1}$.

$$t_{\text{cycle}} = t_{i+1} - t_i = t_{\text{low}} + t_w + t_t \tag{6.10}$$

Time-course simulation of the TJ barrier transition leads to two types of results: 2D and 3D movies[3] which visualise the TJ barrier (including localisation, formation and

[3]Movies from [305] – 2D movie DOI:10.7554/eLife.19593.029, 3D movie DOI:10.7554/eLife.19593.030

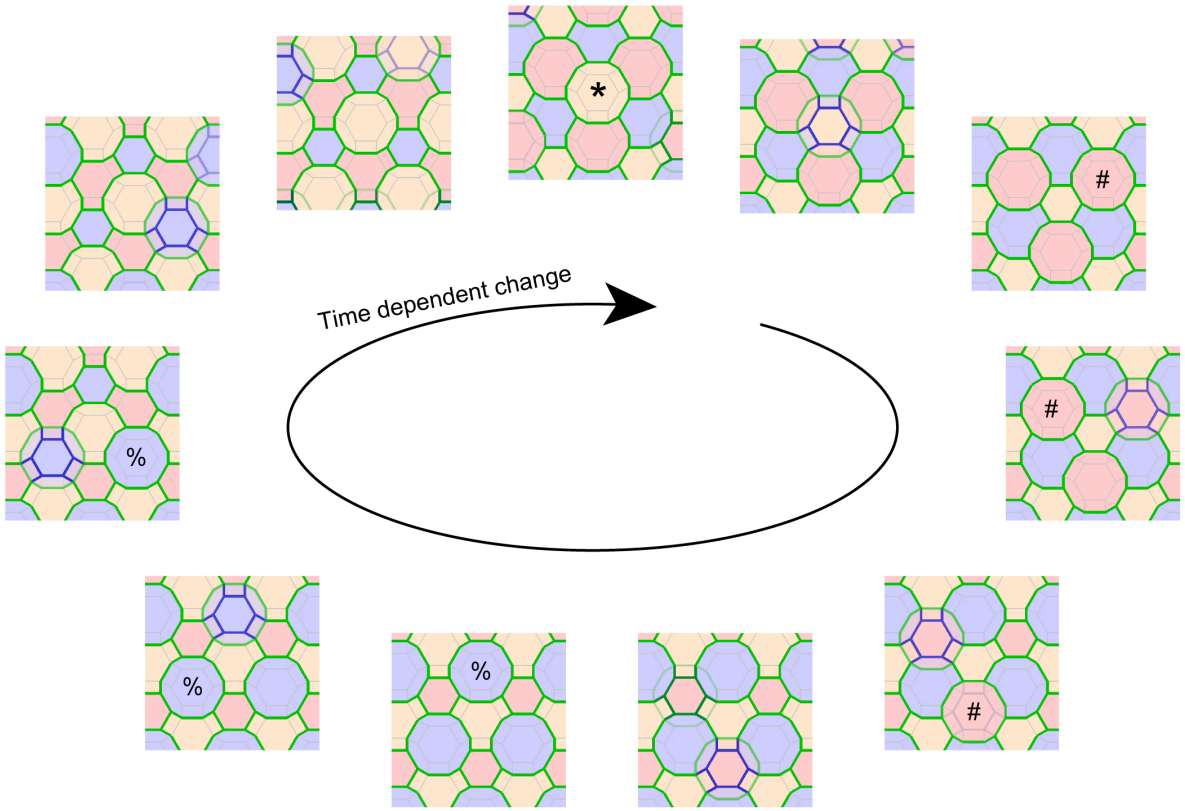


Figure 6.9: **Movie shows simulation of TJ barrier transition over time.** *, # and % denote cells from three different layers that are higher than their neighbours and about to start transition. Reproduced from [305].

degradation of bTJs and tTJs) and the transition of cells from the basal to apical side of the TJ barrier, and indices describing tissue and cellular dynamics of the TJ barrier turnover (see methods section 6.2.5).

From the simulation results we conclude that the proposed mechanisms and temporal coordination maintains TJ barrier homeostasis during turnover. An orderly barrier turnover is observed, no junctionless gaps appear between in between cells during transition and the complete continuous intracellular cover of tight junctions is never broken (figure 6.9). A stable position (z direction in figure 6.7 and movies) of the TJ barrier relative to the tissue is maintained, which also confirms tissue homeostasis, as regulating the location of the barrier is important for its local function of maintaining ion levels and providing two separate milieus.

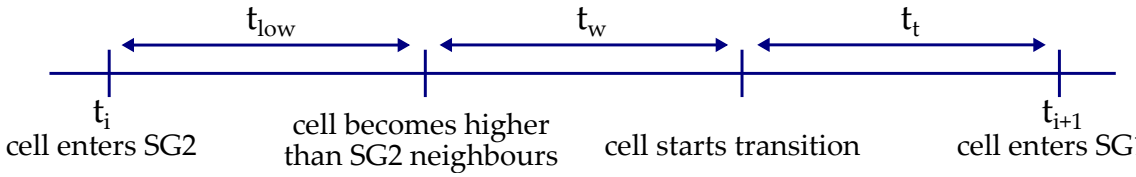


Figure 6.10: **Proposed temporal coordination of the SG2 cell turnover cycle.** After a cell enters the SG2, it waits for a period t_{low} until all its neighbouring cells have transitioned into SG1 and it becomes higher than its neighbours. It then takes a period of waiting t_w until it starts the transition from SG2 to SG1. After the transition time t_t, the cell has fully translocated to the apical side of the TJ barrier and enters the SG1.

The nominal parameters used in the simulation (table 6.2) can either be derived directly from experimental data, or identified by comparing simulation results to experimental observations.

6.3.2 Identifying the parameters of the temporal coordination of barrier transition

In order to predict the timing of temporal coordination, the simulation results are fitted to experimental data. Additionally, a good fit of our simulation results to experimental data can confirm the feasibility of the proposed mechanisms and temporal coordination.

From the experimental images, three different indices describing dynamic tissue characteristics of the barrier turnover can be obtained: the cycle time t_{cycle}, the percentage of total cells in transition at a time r_{trans}, and the percentage of transitioning cells that have a neighbour in transition r_{nb} (for calculation see methods section 6.2.1). These three indices can easily be obtained from experimental images of TJ barrier, as well as from the simulation, at every time point per run, for different simulation parameters.

First, the experimentally obtained indices (table 6.3) are used to identify the three simulation parameters transition time t_t, upward movement speed v_z, and waiting time t_w. These simulation parameters are essential in determining the proposed temporal

Table 6.2: **Nominal parameters used in simulation**

Parameter	Description	Value
t_w	Waiting time	$f(t_w; \mu, \sigma)$
$t_w^{\max}$	Maximum waiting time	12.0 h
μ	t_w distribution mean	4.94 h
σ	t_w distribution standard deviation	3.13 h
t_t	Transition time	2.4 h
C_{SG2}	Number of total SG2 cells	147
h_c	Cell height	8.7 µm
h_{3l}	SG2 layer height	14.5µm
v_z	Upward movement speed	0.363 µm/h
δ_t	Simulation time step	7.8 mins
δ_z	Upward movement per time step	0.0526 µm/δ_t

coordination that lead to homeostasis, and simulation with these parameters should have turnover dynamics with indices comparable with the experimentally obtained indices.

The time a cell spends in transition t_t is the time it takes for a cell to make the transition from the SG2 to the SG1 layer, observed by the formation and degradation of tTJs. If at any time on average r_{trans}% of the cells are in transition, it follows that the cells are in transition r_{trans}% of the cycle time t_{cycle}, and therefore $t_t = t_{\text{cycle}} \cdot r_{\text{trans}} = 2.4\text{h}$.

Despite its continuous turnover, the SG2 stays in place relative to the base of the epithelium. Using the assumption that the spatial location of the TJ barrier and the SG2 in the tissue does not move on average, the velocity of the upwards movement in the z direction v_z (in µm/h) can be estimated. The cells move upwards, and translocate from inside to outside the TJ barrier and eventually out of the SG to the SC, but the TJ barrier and the SG layer itself stay in the same position. Therefore, during the cycle time of one cell turnover, all cells needs to move up with the height of one cell on average

$$v_z = \frac{h_c}{t_{\text{cycle}}} = \frac{8.7}{24} = 0.363\,\mu\text{m/h}. \tag{6.11}$$

The waiting time t_w is assumed to be random and different per cell, and has a normal distribution. The waiting time of a single cell t_w^j is randomly sampled from a normal distribution with probability density function

$$f(t_w;\mu,\sigma) = \begin{cases} \frac{1}{\sigma\sqrt{2\pi}} e^{-\frac{(t_w-\mu)^2}{2\sigma^2}} & \text{for } t_w \in [0,\ t_w^{\max}]\ , \\ 0 & \text{for } t_w < 0,\ t_w^{\max} > 0\ , \end{cases} \tag{6.12}$$

where a maximum waiting time $t_w^{\max}$ is used to prevent excessively long maximum waiting times.

The reason for assuming a normal distribution is twofold. First, in order to obtain $\bar{r}_{\text{nb}} \approx 11.11\%$ (table 6.3), more than 11.11% of the waiting time distribution has to be smaller than the transition time t_t, as only those smaller values will result in transitioning neighbours. Also, it has to be considerably more than 11.11% since not all the neighbour cells can immediately enter the waiting time; some the neighbouring cells also have to wait for t_w until they become the highest cell. A long waiting time is required for some cells to ensure a sufficiently long mean cycle time t_{cycle}. This will not be achieved with a constant t_w; only when a distribution has a sufficient amount of both long and short waiting times the mean cycle time will be sufficiently long (appendix A.3). Second, while there are other distributions that can satisfy the conditions above, a normal distribution can be parameterised such that it approximates various other likely distributions in the waiting time region of interest, e.g. a uniform or exponential distribution (appendix A.3).

In order to identify the t_w parameters of temporal coordination, the simulation results are fitted to experimental data by optimising the waiting time distribution. The waiting time probability density function $f(t_w;\mu,\sigma)$ is optimised such that our simulation results in obtaining the same $\bar{t}_{\text{cycle}}$, $\bar{r}_{\text{trans}}$ and $\bar{r}_{\text{nb}}$ (we denote the simulation mean of any variable x by $\bar{x}$) as the experimentally observed t_{cycle}, t_{cycle} and r_{nb} (table 6.3).

For optimisation of $f(t_w;\mu,\sigma)$ (equation (6.12)) we define a cost function Φ as an equally weighted sum of the squared error of the three normalised indices

$$\Phi(\mu,\sigma) = w_1\left(\frac{\bar{t}_{\text{cycle}}}{t_{\text{cycle}}} - 1\right)^2 + w_2\left(\frac{\bar{r}_{\text{trans}}}{r_{\text{trans}}} - 1\right)^2 + w_3\left(\frac{\bar{r}_{\text{nb}}}{r_{\text{nb}}} - 1\right)^2 . \tag{6.13}$$

Table 6.3: **Experimentally obtained parameters for transition dynamics.**

Parameter	Mean	Obtained
t_{cycle} (h)	24	Observed, estimated [312, 305]
r_{trans} (%)	9.6	Counted in experimental images [305]
r_{nb} (%)	11.11	Counted in experimental images [305]

First, for a set of distributions with varying waiting time mean and standard deviation (appendix A.4), we run 10 simulations of 150 hours, and take the means of the three indices over time and runs. Then, we minimise Φ for arguments μ and standard deviation σ by finding the set of three indices that is closest to the experimental data and the corresponding optimal waiting time distribution

$$\left(\mu^{\text{opt}}, \sigma^{\text{opt}}\right) = \underset{\mu,\sigma}{\text{argmin}}\, \Phi(\mu, \sigma) = (4.93, 3.0)\,. \tag{6.14}$$

The optimal waiting time distribution therefore has an optimal mean $\mu^{\text{opt}} = 4.93$h and a standard deviation $\sigma^{\text{opt}} = 3.0$h. The maximum waiting time is arbitrarily set at $t_w^{\max} = 12$h to prevent the exponential distribution from sampling very large values.

Simulation using our proposed mechanisms and temporal coordination match the experimental results and identifies the optimal waiting time distribution, which intersects the plane of possible results from a range of waiting time distributions (figure 6.12). By finding that a parameters set exists for which our simulation sufficiently approximates the experimentally observed turnover dynamics, we show that our proposed model and mechanisms can indeed predict the dynamics of the TJ barrier turnover and explain the experimental observations. As expected, a normal distribution with a relatively high standard deviation is needed to satisfy all three indices. For the optimal waiting time distribution, the normalised errors of all three indices are within 5%. The cost function is robust to the chosen weights of the different indices: if the cost function weights are changed (for example if there is uncertainty in one of the measurements and it should have been weighted less), the optimal distribution stay within a small range (figure A.7 in appendix A.5).

6.3.3 Minimal experimental data required to predict temporal coordination parameters and transition dynamics

The TJ barrier transition dynamics depend on the temporal coordination parameters: waiting time distribution and transition times. The three indices t_{cycle}, r_{trans} and r_{nb}, which can be measured experimentally and simulated by our model, are markers of the transition dynamics. Therefore, we can use the experimentally obtained indices to infer the temporal coordination parameters, by comparison to simulation results with varying waiting time distribution and transition times. Here, we investigate the relation between cycle time, percentage of cells in transition and neighbours in transition, and show the minimal experimental data that is required to predict the temporal coordination parameters and transition dynamics.

We use linear least squares regression to fit a linear plane to the sets of indices resulting from simulation with varying waiting time distributions (see section 6.3.2 and appendix A.4). For n sets of the three indices, we define the system of linear equations

$$X\mathbf{c} = \mathbf{t_{cycle}} \,,$$

with

$$\begin{aligned} X &= \begin{bmatrix} 1 & r_{\text{trans},1} & r_{\text{nb},1} \\ \vdots & \vdots & \vdots \\ 1 & r_{\text{trans},n} & r_{\text{nb},n} \end{bmatrix} , \\ \mathbf{c} &= \begin{bmatrix} c_1 & c_2 & c_3 \end{bmatrix}^\top , \\ \mathbf{t_{cycle}} &= \begin{bmatrix} t_{\text{cycle},1} & \dots & t_{\text{cycle},n} \end{bmatrix}^\top . \end{aligned}$$

Solving for least square coefficients $\hat{\mathbf{c}}$ gives

$$\begin{aligned} \hat{\mathbf{c}} &= (X^\top X)^{-1} X^\top \mathbf{t_{cycle}} \,, \\ \hat{\mathbf{c}} &= \begin{bmatrix} 47.42 & -2.25 & -0.08 \end{bmatrix}^\top . \end{aligned}$$

Therefore, we can express the plane and the relationship between the indices by

$$\begin{aligned} t_{\text{cycle}} &= \hat{c}_1 + \hat{c}_2 r_{\text{trans}} + \hat{c}_3 r_{\text{nb}} \,, \\ t_{\text{cycle}} &= 47.42 - 2.25 r_{\text{trans}} - 0.08 r_{\text{nb}} \,. \end{aligned}$$

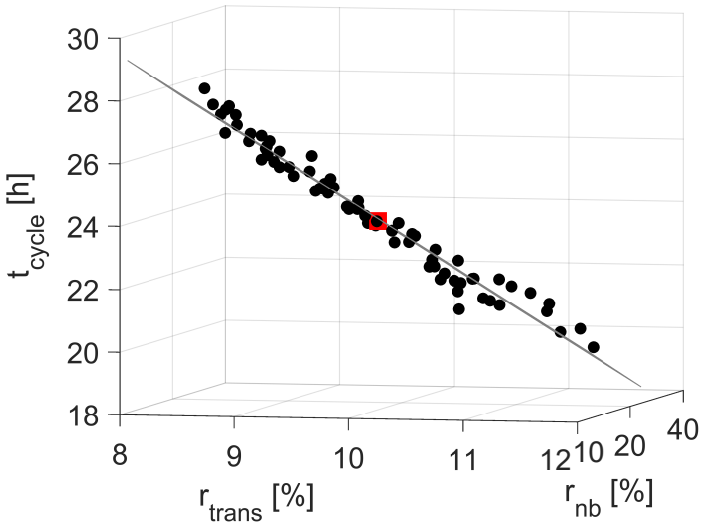
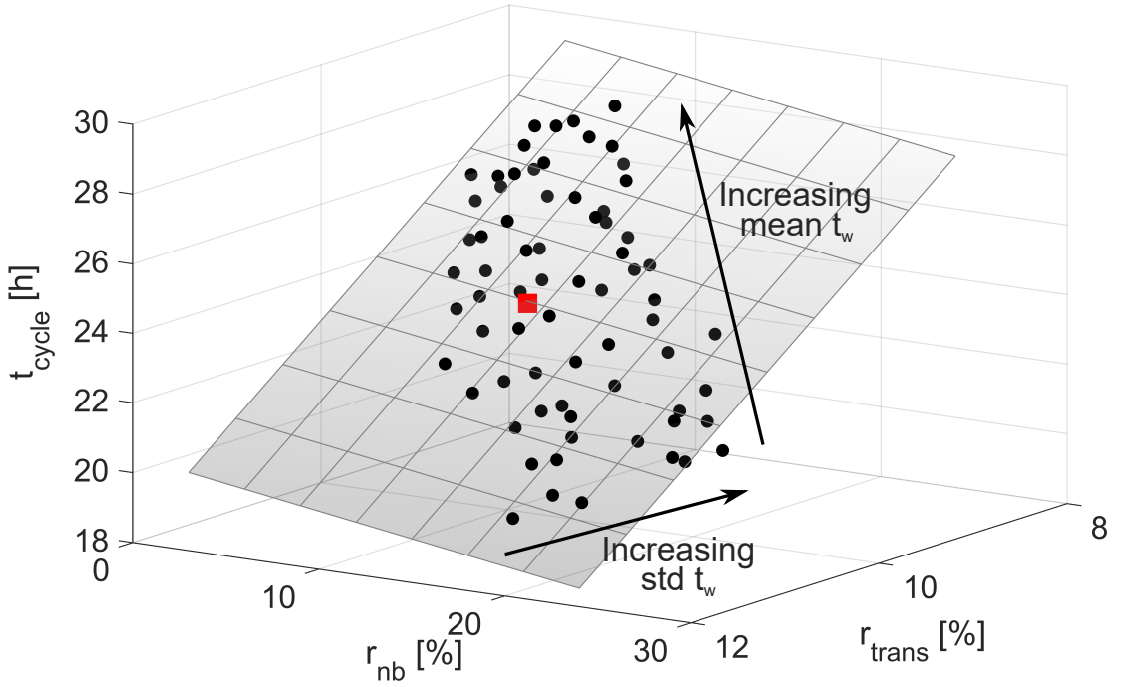


Figure 6.11: **Side view of fitted linear plane and data points shows good fit of simuation results to experimental data.** Circles denote obtained simulation indices resulting from different waiting time distributions with varying mean and standard deviations. The red square represents the experimental data means.

The mean simulation indices for varying waiting time distributions lie on a linear plane (figure 6.12). All points are close to the plane, with small deviations from the plane likely to be due to effects of stochasticity. This good fit to a linear plane shows that there is a linear dependency between the three indices. As a results of our proposed mechanisms and timings, only combinations of the three indices that lie on the plane can be reached. The plane intersects with the means of the experimental data, which confirms that our model can explain the experimental data.
The obtained plane and expression for the relation between the indices is a result of the proposed mechanisms and temporal coordination, regardless of experimental data, with the sole assumption that the transition time is constant. Different transition times would change the plane for the same set of waiting time distributions.

The linear dependency implies that knowing two out of three indices is sufficient to predict the temporal coordination mechanisms (figure 6.13). While r_{trans} and r_{nb} can be obtained accurately and easily from a still experimental image taken at any time point, t_{cycle} requires time course data of a single cell for around 24 hours. Accurate measurements of t_{cycle} is dependent on long time course and short time interval measurements

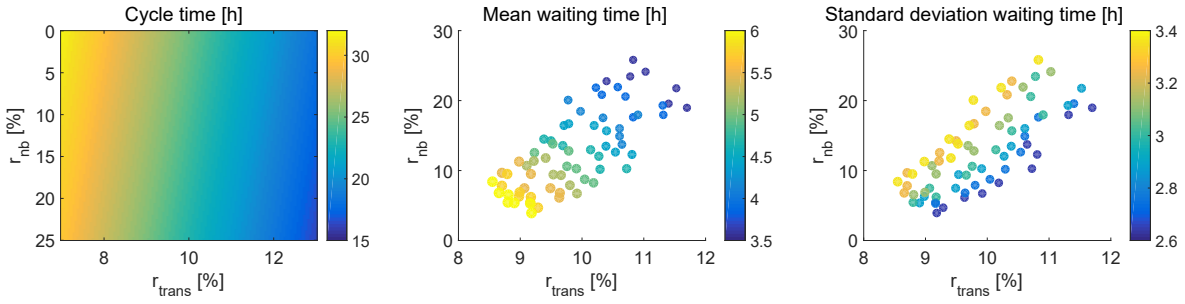


(a)

Figure 6.12: **Interdependence of simulation indices.** Circles represent obtained simulation indices resulting from different waiting time distributions with varying mean (from 3.6-6h) and standard deviations (from 2.4-3.6h), indicated by the arrows. The red square denotes the mean of the experimental data. The circles lie on a linear plane which includes the experimental data point, suggesting interdependence of the indices.

of experimental images, as well as tracking of individual cells, which makes it both time-consuming and potentially inaccurate. Instead, by only measuring the indices r_{trans} and r_{nb}, the cycle time can be predicted alongside the waiting time distribution.

If a higher percentage of cells in transition r_{trans} is observed in experiments, this corresponds to a shorter cycle time, and shorter mean waiting times and standard deviation. When r_{nb} is found to be larger, this leads to a decrease in mean waiting time, but an increase in the standard deviation, thus increasing the waiting time variability between cells. These predictions could be valuable to experimentalists for interpreting different genetic, external or environmental perturbation conditions, and their effect



(a) (b) (c)

Figure 6.13: **Cycle time and waiting time distribution can be predicted from static experimental measurements of r_{trans} and r_{nb}.** (a) Cycle time t_{cycle} as function of r_{trans} and r_{nb} (described by fitted plane) (b) waiting time distribution mean as function of r_{trans} and r_{nb} (c) waiting time distribution standard deviation as function of r_{trans} and r_{nb}

on temporal coordination. This could indicate what regulates barrier transition rates and turnover speeds. For instance, if the r_{trans} decreases after tape stripping the SC and thereby damaging the skin's barrier, this would indicate a shorter cycle time and increased signalling of barrier transition to repair the SC. It would be interesting to obtain time course measurements of the increased transition rates following barrier disruption, especially if they could be linked to barrier function measurements such as TER or TEWL. Quantitatively, the exact values of the indices and transition dynamics might not be generalisable across tissue location and subjects, which may, for example, be due to different epidermal thickness and basal proliferation rates. Qualitatively, however, the results presented in this chapter can be generalised since they are a result of the transition mechanisms.

6.3.4 Biological significance of the waiting time

The tight junction barrier is positioned right below the SC in the second SG layer. It creates two distinct environments, which play a role in the differentiation and cornification processes. This means that the location of the barrier should be tightly regulated by timing the expression, translation and translocation of the barrier proteins, as well as the timely construction and degradation of the TJs. If the timing of any of these pro-

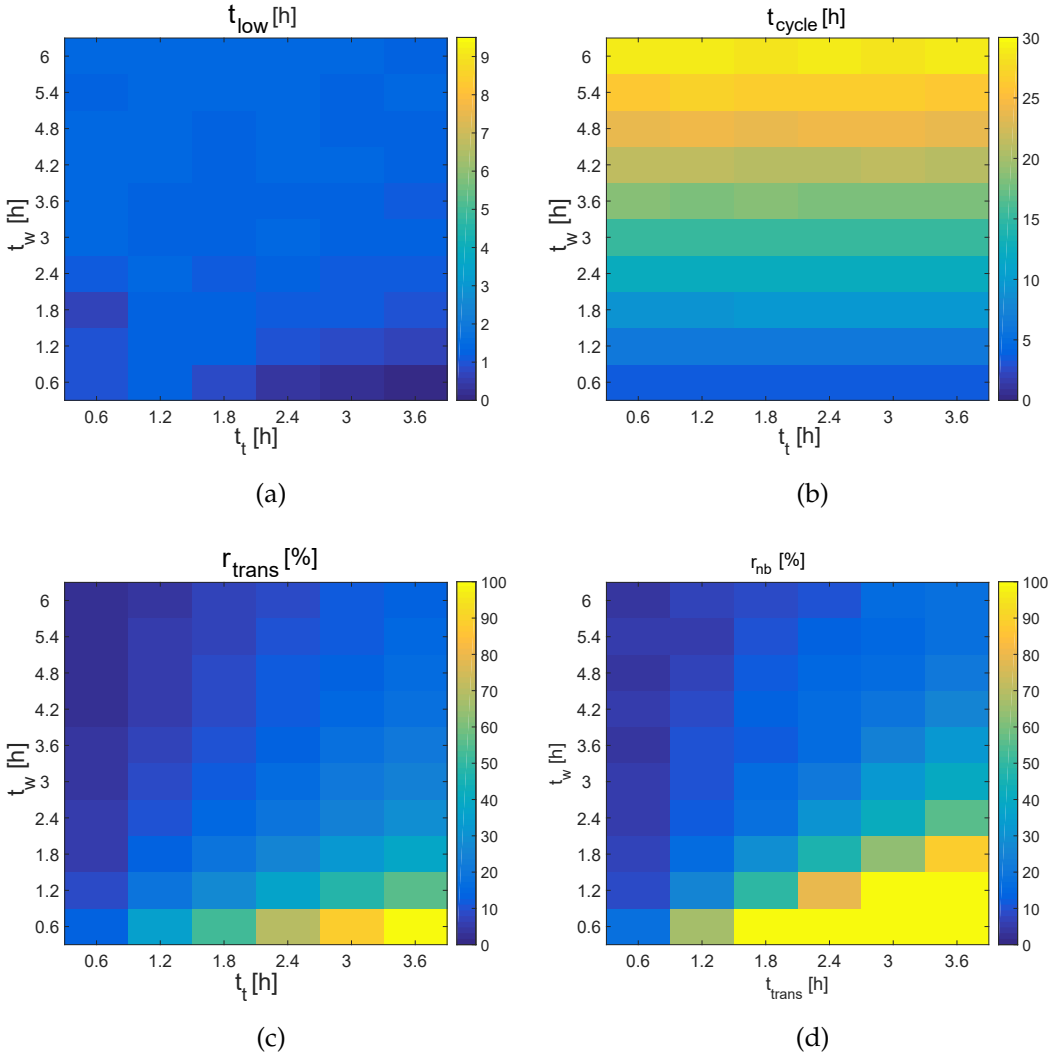


Figure 6.14: **Waiting time affects cycle time and could function as a buffer to maintain the tight junction barrier function during increased proliferation.** The panels show the effects of transition time versus cycle time on (a) t_{low}, (b) t_{cycle}, (c) r_t and (d) r_{nb}. A decrease in transition time decreases cycle time and t_{low}, whereas a decrease in waiting time does not decrease cycle time and t_{low}. This suggests the waiting time serves as a buffer and is a mechanism to increase turnover and maintain tissue homeostasis during increased proliferation.

cesses is altered, the barrier will be affected. Therefore, it is clear that both the timing of TJ-related processes, as well as the ability to adapt to changes in differentiation and to regulate differentiation are important. Studying the barrier transition could help the mechanical understanding of those processes and their effect on differentiation.

In various skin diseases, such as psoriasis or atopic dermatitis, the expression and localisation of the TJ proteins is altered which affects their functioning as a barrier [97, 109]. Also, it has been shown that the TJ barrier influences differentiation, and vice versa [313]. Although hyperproliferation severely disrupt skin structure and composition in diseases like psoriasis [314], an increase in proliferation and differentiation is observed during skin repair as well [315]. Increases in proliferation and differentiation significantly reduces turnover cycle times. This could be beneficial, for example to speed up barrier repair and provide a quick recovery of basic barrier functions in case of a loss of protection against external pathogens and loss of water. While reducing the cycle time, it is necessary to allow a sufficient amount time for the transition process as required to maintain a functional TJ barrier [316, 317].
To reduce the cycle time t_{cycle} of the barrier transition, either t_w or t_{trans} could be lowered, or both. The time it takes for cells to reach the top of the SG2 layer t_{low} is dependent on both t_w and t_{trans}. To reduce the cycle time significantly, a decrease in t_w or t_{trans} should lead to a large decrease in t_{low} too, as in normal conditions t_{low} is longer than t_w and t_{trans}. Simulation with decreased t_w or t_{trans} shows that reducing t_w leads to a decrease in t_{low} and t_{cycle}, whereas t_{trans} does not (figure 6.14).

The large decrease in t_{low} for decreasing waiting time suggests that this could be a mechanism for decreasing the cycle time in case of increased proliferation, while keeping t_{trans} constant. A constant transition time follows from the assumption that the transition needs a minimal period to successfully go through all the stages of bTJ and tTJ formation and degradation. The decrease in t_w could, however, be achieved by increasing signalling, transcription and translocation of TJ proteins to the TJ site. Therefore the waiting time could function as a buffer to adjust its cycle time. Thereby it would respond faster to damage or changes in SC barrier (e.g. re-establishing the calcium gradient or reducing increased TEWL) while maintaining TJ barrier homeostasis

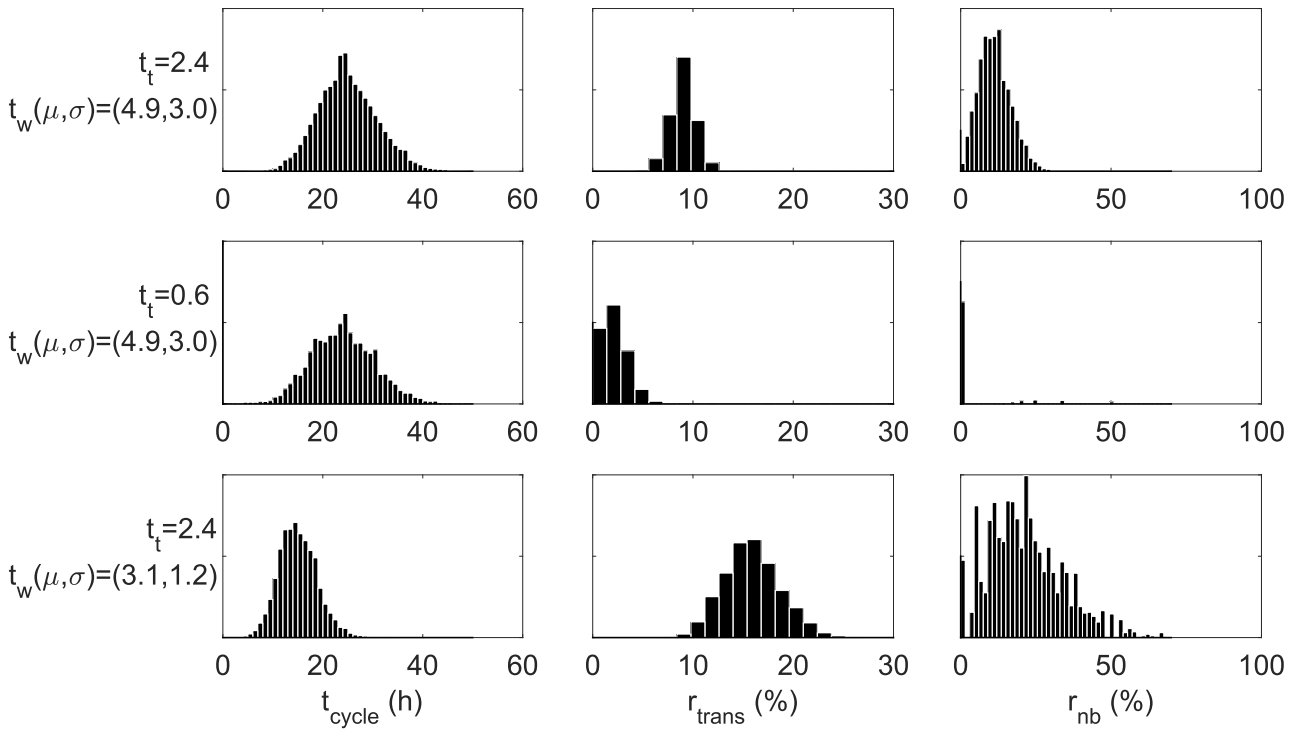


Figure 6.15: **Changes in waiting and transition time distinctly alter experimentally measurable indices.** t_{cycle} is per cell, r_{trans} and r_{nb} are taken at 30-minute intervals for 15 runs with set t_{trans} and t_w.

and preventing to break the continuous TJ barrier, without the need to compromise or speed up the transition processes. Rompolas *et al*. further show that the SG turnover time (average lifetime of a cell in the granular layer) seems to be consistent with a memoryless process, and consequently suggest that the exit of the SG is stochastic, providing a buffer function. This supports the system proposed in this chapter where we found that a waiting time distribution, as opposed to fixed waiting times, is necessary to fit the experimental data.

Reducing either t_{trans} or t_w has distinct effects on all three indices t_{cycle}, r_{trans} and r_{nb} (figure 6.15). Therefore if experimentally measuring the indices for epidermis with increased proliferation results in a decrease in r_{trans} and r_{nb}, a decrease in t_{trans} is indicated; whereas an increase in r_{trans} and r_{nb} confirms our hypothesis that t_w is decreased and t_{trans} kept constant. Reducing t_{trans} decreases the two indices r_{trans} and r_{nb}.
We invite experimentalists to verify the proposed mechanism of barrier transition and the obtained parameters of temporal coordination. Furthermore, for future experiments it would be interesting to investigate the signalling pathway or mechanisms that regulates the timing of the start of the transition. This could be achieve by measuring the transcription and translocation of TJ proteins. The timing of these processes may provide indications of the signalling mechanisms and trigger of the transition, both temporal and spatial.

6.4 Discussion

In this chapter we developed a 3D computational model of the TJ barrier in the SG, with keratinocytes represented by f-TKDs. Simulation of TJ barrier translocation while cells transition upwards towards the SC provides an insight into the exact workings of the transition mechanism. By developing the model and algorithms, and comparing simulation results to experimental observations, we discovered the necessary temporal coordination and transition algorithm. The combination of modelling and experiments that lead to these results shows the importance and additional value of modelling in complementing experimental approaches.

Based on the results in Yokouchi et al. [305], we have modelled the exact shape of the SG keratinocyte as a f-TKD. Naturally, this is an approximation; although accurate, the shape will not always be exactly a f-TKD, and might be more complex or variable depending on spatial configuration and forces exerted on a cell by its neighbours. Also, there are differences in spatial conformation between humans and mice, and between skin sites in both mice and humans, specifically in terms of the columnar organisation and stacking of the cells (examples of early work from the 1970s and early 1980s include [51, 52, 318, 319, 320, 321, 322, 307, 312]). However, even though the discovered mechanisms are based on the shape of the f-TKD, the fundamental mechanism of translocation of a single layered barrier in a renewing tissue could be generalisable to all stratified epithelia, irrespective of exact shape.

The results in the chapter provided indications to the role of TJ barrier transition in maintaining and regulating epidermal homeostasis. In addition, we are interested in how the TJ barrier can be incorporated into a modelling approach to study the interplay between the SC and TJ barriers. These topics will be covered in the next discussion sections.

6.4.1 Epidermal homeostasis

Here, the arrival of the cells to the SG has not been addressed explicitly. In the simulation, we assume that cells entering the SG2 are readily present in the SG1 when a cell leaves the SG2, positioned right below in a vertical column of cells. The SG1 cell then becomes an SG2 cell as soon as the previous SG2 transitions to the SG1. Likewise, the cell entering the SG1 does so in a synchronised way. Obviously, the cells below are already in place positionally; there is no 'gap' below, nor is there physical movement of a cell relative to others. The tight junctions relocate to a lower position while all cells move upwards, as visualised in the 3D simulation videos. Therefore, the transition that is referred to is functional and continuous, and cannot be defined as a discrete event. Both in homeostatic state, as well as in recovery after wounding or disease, it is relevant to look at how the dynamics and regulation of the TJ transition relate to the proliferation of cells in the basal layer, as these must be balanced to

maintain epidermal homeostasis.

The regulation of basal cell proliferation and differentiation, as well as the subsequent dynamics of upward vertical cellular movement in the differentiation column or unit, have been the subject of considerable interest since the late 1960s. Recent research has focused on two questions, using a number of imaging techniques and lineage tracking. The first question concerns proliferation dynamics, and there are two prevailing yet partially contradicting theories. Based on early works [323, 320, 307] the Epidermal Proliferation Unit (EPU) was proposed, where slow cycling stem cells produces transit amplifying cells which can divide a limited number of times until they differentiate. Several transit amplifying cells then maintain and control epidermal homeostasis through terminal differentiation into columns of stacked cells moving upwards. This way, one stem cell can maintain a vertical unit of cells (the EPU). The second theory was first proposed by [324, 325, 214]: A single population of committed progenitor cells (PC) undergo stochastic asymmetric division, where the cycling PCs can divide in three ways – creating two cycling daugter cells, two differentiating cells, or one cycling and one differentiating cell daughter cell. If the probabilities of the first and second option are equal across the population, this will maintain a steady population of PCs while producing the differentiating cells needed to supply the rest of the epidermis. Stem cells do not play a role in physiological steady state, but there may be a quiescent population which can upregulate production of PCs in growth or regeneration after damage to the epidermis. Finally, the Blanpain lab concludes that a slow cycling stem cell, going through a cell cycle every four weeks, maintains a population of progenitor cells, where both populations of stem cells and PCs divide asymmetrically [326, 327]. This seems to reconcile both existing theories.

The second questions is how the cells are organised spatially in the epidermis. In mouse ear epidermis, clear vertical stacks of cells can be observed in the epidermis, inspiring the EPU hypothesis [323]. Other sites in mice and human might not always have such strictly organised columns of differentiated and cornified cells, but the mechanisms are likely to be similar. The current consensus is that the differentiating cells organise in pre-exiting vertical spatial columns or unit, but not necessarily directly supplied by the underlying basal cells beneath it as in the EPU model [325, 328].

Rompolas *et al*. [328] coin the more appropriate term Epidermal Differentiation Unit (EDU) to specify the differentiation units, spatially separating the differentiation unit from the directly underlying basal proliferating cells as they do not necessarily feed into the EDU above them. Computational models also show that cells with TKD shape and random packing spontaneously self-organise into stacked columns, utilising only a local rule that each cell tries to occupy less crowded spaces in the tissue [309]. Therefore, a lack of active control in organising the tissue into columns is likely which corresponds to the EDU findings where the regular structure is formed independently from the supply of cells from the basal layer [328].

Our current way of modelling assumes that the upward movement and transition of cells through the epidermis is synchronised in a vertical column; the SG2-SG1 transition triggers the transition of underlying cells in a 'pulling' fashion, where the top cell of the column dictates the transition of the cell directly below, cascading downwards. This fits the EDU hypothesis. The differentiation unit determines the upwards movement of cells in a similar fashion, drawing cells form the underlying pool provided by the PCs, rather than stem cells pushing up the cells in a fixed column. Furthermore, the results presented here, in Yokouchi *et al*. [305] and in Rompolas *et al*. [328] suggest that the exit of cells from the SG2 is controlled. This means that the TJ barrier is one of the main locations in the viable epidermis which can regulate skin homeostasis. For epidermal homeostasis, the basal proliferation, differentiation at SG2 leading to cornification, and desquamation at the top of the SC have to be balanced. Disruptions to this balance will, for example, lead to changes in thickness, and will also affect differentiation rates which can have a negative effect on the quality of both barriers. The TJ barrier transition mechanism could contribute to balancing these rates by acting as a buffer (see section 6.3.4).

Skin repair processes that after wounding or skin (barrier) damage utilise these different mechanisms at different depths in the epidermis, which often react at different time scales. For example, after SC barrier damage, cornification rates are increased, quickly providing extra lamellar bodies and cells to the SC after damage, before upregulating differentiation to increase the rates of lamellar body and cell production [72, 78].

Even though the exact signalling and mechanisms that balance proliferation and the exit of cells from the SG2 are unknown, there are two general possibilities. A signal can be propagated in a pulling way, with cells leaving the SG at a faster rate propagating faster differentiation and upward movement of cells below – for example, through a form of contact inhibition or signalling. Eventually, the stems cells or PCs will be reached, which can shorten their cycle times and increase proliferation rates. Alternatively, a different signalling mechanism directly increases proliferation, pushing up differentiating cells into their respective columns, and forcing an increase in TJ barrier transition rate, for instance by decreasing the waiting time.

As shown in sections 6.3.3 and 6.3.4, the indices that can be obtained experimentally predict the transition dynamics (turnover time). In steady state, the transition rate corresponding to the turnover time would be balanced with the proliferation rate, or adjusted in case of skin barrier damage or disease. Therefore, further experiments are encouraged to test our hypothesis that the indices predict the transition dynamics, and to confirm the predicted distributions of the indices in section 6.3.4. If confirmed, further experiments could be conducted to obtain indices for different skin sites with other proliferation and turnover rates, in diseased skin, and after induced barrier damages. Using these results, we may be able to prove the predictions made here and show under which conditions (disease or altered transition dynamics) the TJ junction barrier cannot be maintained. Also, the effects of SC barrier damage on the TJ barrier, for example through changing calcium concentrations in the SG, will be useful in examining the interplay between the TJ and SC barriers, which will be discussed next.

6.4.2 Interplay between TJ and SC barriers

The two main barriers of the skin, the stratum corneum and the tight junction barrier in the stratum granulosum, work together to maintain the skin permeability barrier, and thereby play a vital role contributing to tissue homeostasis of the entire epidermis. While the SC barrier provides protection against external pathogens and prevents dehydration, the TJ barrier selectively blocks water, ions and solutes from passing through the paracellular pathway. In recent years, several studies have demonstrated

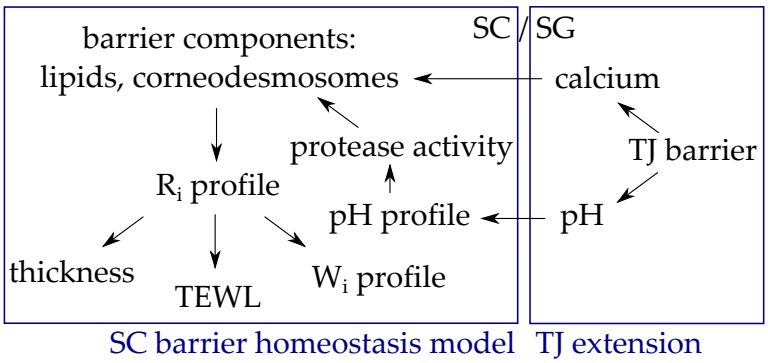


Figure 6.16: **Schematic overview of stratum corneum homeostasis model and proposed tight junction barrier extension.**

an interplay between the TJ and SC barriers, where impairment of the SC barrier effects the TJ barrier, and vice versa [10, 9, 8, 11]. If we consider the effect of the tight junction barrier on the SC barrier using our SC barrier homeostasis model from chapter 5, the tight junction barrier would form an extension from the SC towards the SG, where the tight junctions regulate calcium and pH, which affects the barrier components and the pH gradient in the SC (figure 6.16) [329, 220].
Previous research shows calcium is likely to be the main signal regulating the interplay between the SC and TJ barriers. The role of calcium in regulation of both the SC [77, 80, 79, 74, 330, 331] and TJ barriers [329, 219, 117] is well documented, and Behne *et al.* demonstrate that a major calcium translocation takes place after barrier insult [332]. The most extensive effort to mathematically model the epidermal calcium gradient and its formation and regulation has been carried out by Adams *et al.* [219, 220, 221], who also show the contribution of the SC and TJs to maintaining the calcium gradient, by incorporating them as resistance to diffusion of extracellular calcium.

The exact mechanisms and signalling responsible for the interplay between the SC and TJ barriers to maintain the skin barrier, mediated through calcium, are yet to be elucidated. It is not trivial to simultaneously study both barriers experimentally, mainly due to a current lack of tools to evaluate the TJ barrier function *in vivo*. Even though there are various ways to investigate the SC permeability barrier non-invasively or minimally invasively, for example by TEWL, the TJ barrier is less accessible (only by removing the SC) and conventionally measured by TER and permeation assays. Fur-

thermore, *in vitro* studies will lack the essential epidermal calcium gradient.

Therefore, we propose a mathematical model of three coupled ODEs to study the regulatory mechanisms responsible for the healthy interplay between the TJ and SC barriers and to identify how their malfunction may lead to skin diseases such as atopic dermatitis and psoriasis. This model will test a hypothesis that TJ barrier dysfunction causes SC barrier defects through modulating intercellular Ca^{2+} concentrations and pH at the SG/SC interface, both of which are known to affect cornification of keratinocytes and production of SC components such as lipids and filaggrin (figure 6.17) [8]. The three variables, calcium ion concentration at the SG/SC interface Ca^{2+}, TJ barrier function, and SC barrier function, are regulated through feedback f_{C-T}, f_{T-C}, f_{S-C} and f_{C-S}. The interaction through these feedback constants or functions describe the interaction between the two barriers through calcium: Ca^{2+} induces TJ formation (f_{C-T}); the TJ barrier maintains a peak in Ca^{2+} concentration at the SG/SC interface (f_{T-C}); the SC barrier also help maintain a Ca^{2+} concentration peak at the SG/SC interface (f_{S-C}); and Ca^{2+} regulates cornification and SC barrier formation (f_{C-S}).
Time-course simulation of the developed model for both healthy and disease conditions will examine how the impaired TJ barrier causes SC barrier defects, via perturbed regulation of Ca^{2+} concentrations in the SC/SG interface. The simulation results can be compared qualitatively and calibrated with the experimental data on SC barrier damage. System behaviour can be studied by exploring the parameter space, for example using bifurcation analysis, firstly to determine for which parameter ranges or feedback functions the system is stable and maintains homeostasis, and secondly to explore for which conditions instability occurs, leading to barrier dysfunction and possibly disease.

This modelling approach may provide a useful tool for informing further experimental research on the interplay between the TJ and SC barrier, which potentially plays an important role in both homeostasis of the skin barrier and various skin diseases. In the future, we hope to be able to couple the SC homeostasis model and the extension to the TJ, and link the depth-dependent processes in TJ barrier transition to the depth-dependent processes that form and maintain the SC barrier.

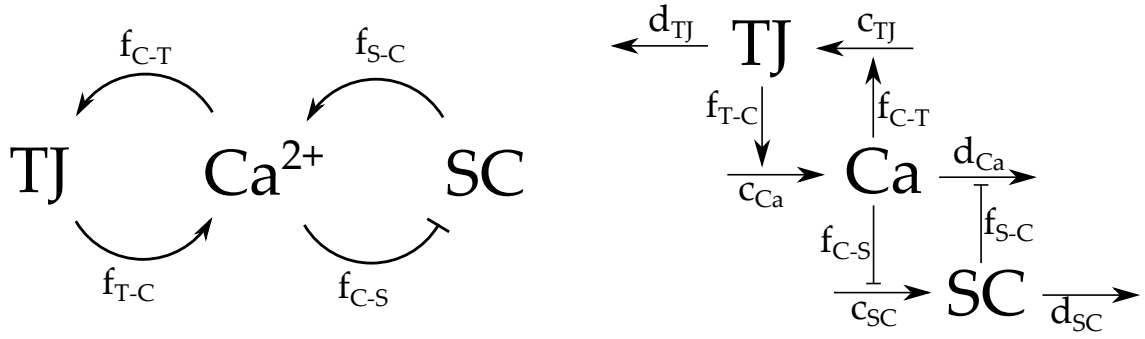


Figure 6.17: **Proposed model for interplay between stratum corneum and tight junction barriers through calcium** Left

To conclude, the f-TKD model of the tight junction barrier demonstrates how, using the form of the cells, terminal differentiation and barrier transition can be controlled. *In silico* simulation identifies the temporal coordination and dynamics of the transition, and suggests the role of barrier translocation in epidermal homeostasis. Next steps include more experimental research to verify our hypothesis and temporal coordination predictions, and investigation of TJ and SC barrier interplay in order to link the results in this chapter to our SC barrier models.

Chapter 7

Concluding remarks

The skin permeability function is of vital importance for the protection of our body against external pathogens and dehydration. Two barriers residing in the upper layers of the epidermis provide this function: the stratum corneum barrier and the tight junction barrier in the stratum granulosum. These two barriers have to maintain a constant functioning, while the cells that are an integral part of the barrier move up through the epidermis due to continuous tissue renewal. Depth-dependent processes are crucial in developing, maintaining and degrading the SC barrier at the right depths, and for the transition of keratinocytes across the TJ barrier. Therefore, in this thesis we specifically focused on depth-dependent processes and their role in the permeability barrier of the skin.

In chapter 3, a compartmental model was developed to characterise and visualise the resistance to water diffusion along the depth of the SC. Resistance profiles were obtained by applying the model to published water concentration profiles and transepidermal water loss data, and demonstrated a depth-dependent permeability barrier in the stratum corneum. The resistance profiles can be applied to study differences between barrier structure and function across various group: skin sites, adults versus infants, before and after skin treatment, and diseased versus healthy or damaged skin. They can also be used to monitor the recovery after common chemical or mechanical insults. Application to new data is encouraged, particularly if other skin parameters are measured simultaneously such that they could be related to the resistance pro-

file indices. The depth-dependent resistance profiles and the quantification by indices provide insight into the development, maintenance and degradation of the barrier along the depth of the SC, and could therefore be related to markers of cornification or desquamation rates. A more detailed understanding of permeability within the SC could also be useful for refinement of drug permeation models.

In chapter 4, we were able to partially explain interpersonal variability in resistance by the depth profiles of lipids and NMF, and SC thickness. With increased availability of Raman data, and the ability to measure a variety of different components in the SC, future analysis might reveal more clearly the contribution of barrier components to resistance in the SC.

The SC barrier homeostasis model presented in chapter 5 is an integration of several models that were developed to simulate depth profiles of components in the SC. A major factor in barrier homeostasis is the regulation of desquamation, which should only take place in the top layers to maintain SC thickness and a functional barrier. A model of the pH-mediated KLK activity and inhibition by LEKTI demonstrated that the pH gradient is sufficient to regulate desquamation, and that a higher surface pH leads to an increase in desquamation.
The SC barrier homeostasis model qualitatively simulates and predicts the regulation of barrier homeostasis through the interplay between barrier components and the regulation of desquamation. In the future, the model can be further refined, adjusted and extended to generate more accurate quantitative predictions.
Disrupted barrier homeostasis can lead to the onset of diseases. For instance in AD, dysregulation of desquamation by disruption of normal pH levels plays a role the barrier destruction [296], and inherited or acquired barrier abnormalities result in sustained inflammation and immune system activation, further deteriorating the barrier [125, 126]. The modelling of multiple components and their interactions in a systematic way will benefit our comprehension of barrier misregulation in AD. In the future, such models could be used to devise more effective and personalised treatment by predicting and studying barrier homeostasis and the effects of treatment.

To study the maintenance of the TJ barrier, a geometric 3D model of the SG was con-

structed in chapter 6. The proposed transition mechanism is based on the tetrakaidecahedron form of the keratinocytes and the consequent optimal stacking [305]. We simulated the transition of keratinocytes from the basal to the apical side of the TJ barrier following a proposed mechanism, and demonstrated that the TJ barrier is maintained at all times. The temporal coordination for the replacement of TJs and the transition dynamics can be inferred from comparing simulation results to experimental data. Future research should aim to experimentally validate our proposed hypotheses, including its role in epidermal homeostasis: by controlling the transition across the TJ barrier, it could function as a buffer. A buffer could balance the transition rate in tissue homeostasis, and increase the transition rate in case of barrier repair and increased proliferation.

Research into TJ barrier homeostasis is still in its early stage; our understanding of SC barrier homeostasis is more advanced. The model and results presented in this thesis contribute to a more mechanistic understanding of the processes and coordination of the barrier transition, through modelling and comparison to experimental data. Additional research is needed to uncover the signalling mechanism that underlie our proposed temporal coordination, for instance the signal indicating that a cell is higher than its neighbours and starts the transition process. Even though the transition mechanism was proposed for the epidermis, using the TKD shape for keratinocytes, the mechanism may be applicable to other epithelial tissue with single-layered TJs including simple epithelia.

Furthermore, it would be interesting to study the relative contribution of SC and TJ barriers to the outside-in permeability barrier as well as the interaction between the two barriers. A clear interplay has been found in experiments [10, 9, 8, 11] and, as set out in the previous chapter, a modelling approach could help discover how the SC and TJ barriers are regulated through calcium.

The field of dermatology is well-placed to include more modelling, specifically in systems biology; a large amount of experimental and clinical data, an accessible tissue and experimental techniques to obtain more *in vivo* data. Here we took a such a modelling approach, and showed how modelling can complement experiments through analysis, integration and replication of data.

This thesis contributes to understanding the role of depth-dependent processes in the regulation of both barriers in a continuously self-renewing tissue. Hopefully, future studies keep considering the depth-dependency of the epidermis and continue to apply modelling to the field of dermatology.

Appendix A

Supplementary information

A.1 Overview of TEWL and water concentration profile data

Table A.1: **TEWL data used for the calculation of resistance profiles for infants, adults and skin sites.** Data from Nikolovski *et al.* [22] and Boireau-Adamezyk *et al.* [228].

	Adults	**Infants**	**Exposed arm**	**Protected arm**	**Face**
Mean TEWL	5	25	8.37	7.54	12.94
Std TEWL	1.7	9.6	2.43	2.12	3.24

Table A.2: **TEWL data used for the calculation of resistance profiles before and after the application of four different oils.** Data from Patzelt *et al.* [242].

	Almond oil		**Jojoba oil**		**Paraffin oil**		**Petrolatum**	
	Before	**After**	**Before**	**After**	**Before**	**After**	**Before**	**After**
Mean TEWL	11.82	11.82	11.95	10.70	11.82	10.67	10.95	5.08
Std TEWL	2.18	2.68	1.54	1.78	1.35	1.54	2.1	1.78

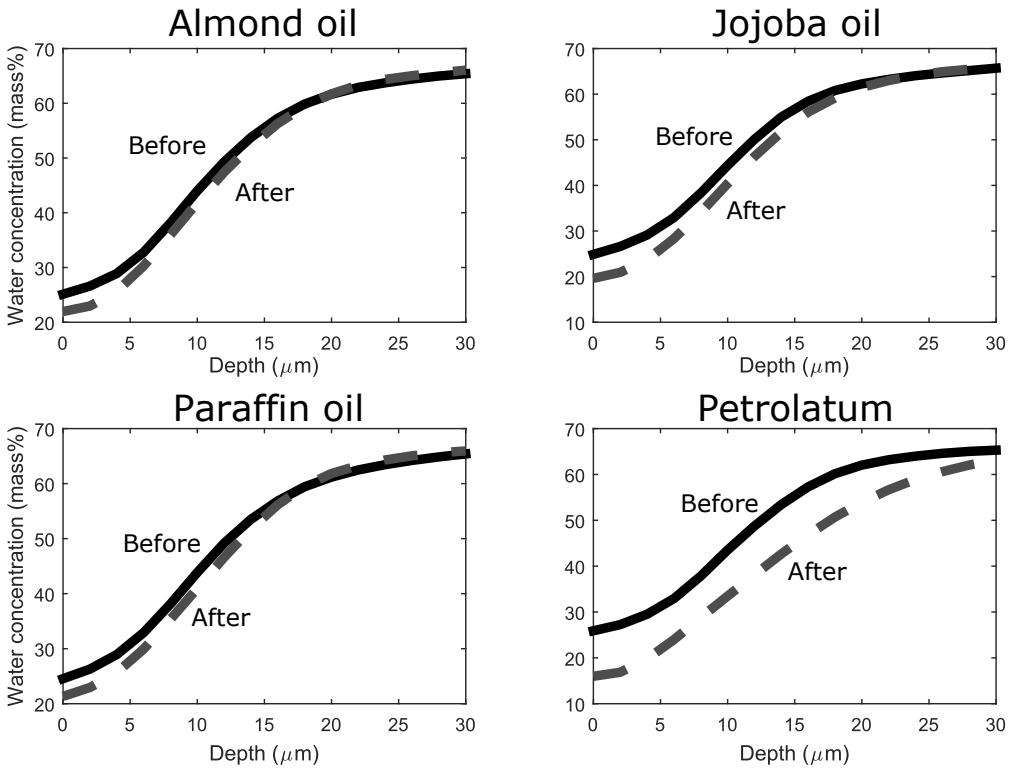


Figure A.1: **Water concentration profiles used for the calculation of resistance profiles before and after application of four different oils.** Data from Stamatas *et al.* [229].

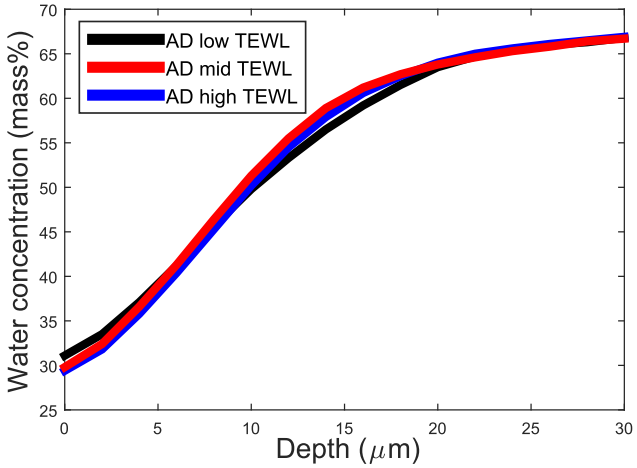


Figure A.2: **Water concentration profiles used for the calculation of resistance profiles for AD patients.** Data from Kezic *et al.* [268].

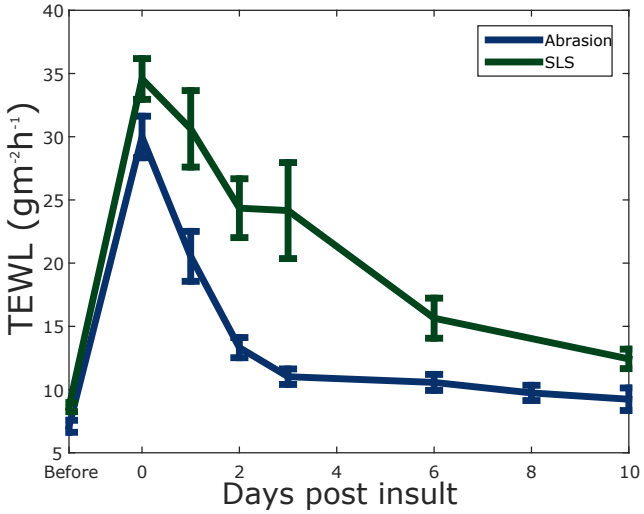


Figure A.3: **TEWL data used for the calculation of resistance profiles before and after abrasion and the application of SLS.** Data from Hoffman *et al.* [31, 269].

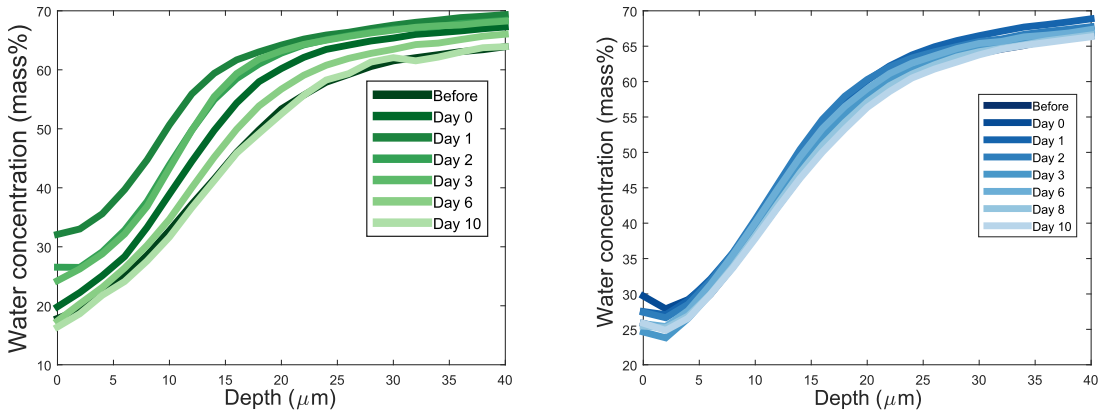


Figure A.4: **Water concentration profiles used for the calculation of resistance profiles before and after abrasion and the application of SLS.** Data from Hoffman *et al.* [31, 269].

A.2 Overview of SC barrier homeostasis model variables and nominal parameter set

Table A.3: **Variables in the SC barrier homeostasis model.**

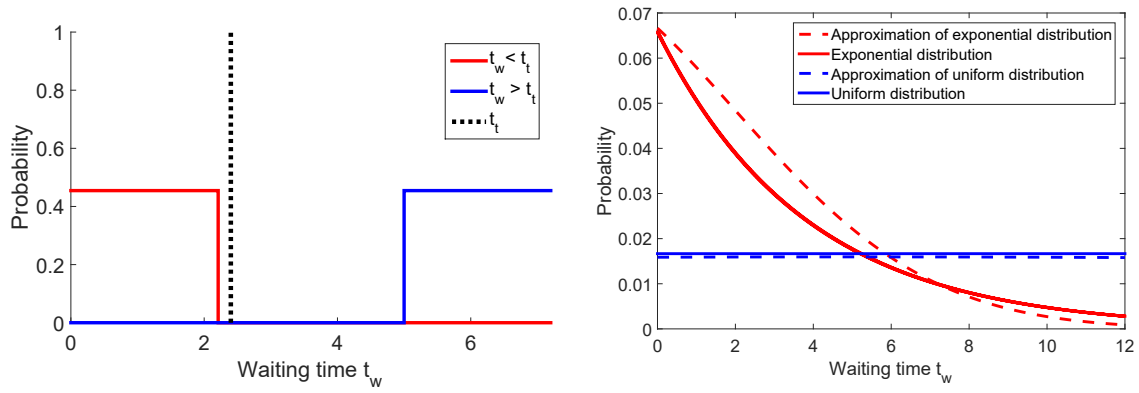
Variables	Description
t	Time [a.u.]
x	Height [µm] (opposite of depth, bottom SC is 0), $x \in [0, \lambda]$
x_n	Normalised height, $x_n \in [0, 1]$
λ	SC thickness [µm]
W	Water concentration [mass%]
R	Resistance to water diffusion [a.u.]
L	Lipid 'quality' [a.u.]
C	Amount of corneodesmosomes
pH	pH
KLK	Protease activity [a.u.]
D^{KLK}	Degradation activity [%]
B	Barrier components at height x and time t [a.u.]

Table A.4: **Nominal simulation parameter values for the SC barrier homeostasis model.**

Parameters	Value	Description	Obtained
W_{top}	25	Water concentration at the SC/air interface $W(\lambda, t)$	Raman water concentration profiles (chapter 3)
W_{bottom}	70	Water concentration at the SC/SG interface $W(0, t)$	Raman water concentration profiles (chapter 3)
pH_{top}	7	pH at the SC/air interface $W(\lambda, t)$	[29]
pH_{bottom}	5	pH at the SC/SG interface $W(0, t)$	[29]
W_s	25	Water concentration at $pH = 5$	W_{top}
B_{max}	0.7	Maximum barrier contribution of components	Maximum resistance observed in data (chapter 3)
α_C	0.05	Initial amount of corneodesmosomes	Assumption: B_{max} reached in first few layers
β_C	0.1	Rate of increase of corneodesmosomes per unit depth	Assumption: B_{max} reached in first few layers
C_{max}	0.7	Maximum barrier contribution of corneodesmosomes	Maximum resistance observed in data (chapter 3)
α_L	0.05	Initial lipid 'quality'	Assumption: B_{max} reached in first few layers
β_L	0.1	Rate of increase of lipid 'quality' per unit depth	Assumption: B_{max} reached in first few layers
L_{max}	0.7	Maximum barrier contribution of lipids	Maximum resistance observed in data (chapter 3)

A.3 Choice of waiting time distribution

Here, we elaborate the choice of the type of waiting time distribution. Extreme cases with only $t_w < t_t$ or $t_w > t_t$ will not replicate experimental data with a sufficiently long cycle time as well as neighbouring cells in transition. The two necessary conditions require *both* short enough and long enough waiting times to achieve simultaneous transition of neighbour cells and a sufficiently long cycle time, respectively (figure A.5a). Three types of distributions can match the necessary conditions and replicate experimental data: normal, uniform and exponential. The normal distribution is the most likely candidate, from a biological perspective as well as for its versatility. As we consider a cut-off at 0 and $t_{max} = 12h$, both the uniform and exponential distributions can be approximated by a normal distribution, with low mean or high standard deviation respectively (figure A.5b). On top of that, a normal distribution with a much smaller standard deviation than its mean can approximate a constant waiting time. Therefore, if a constant or a uniform or exponential distribution would be a better fit to the data, this could be observed during optimisation; the normal distribution would approximate one of the other distributions. Considering all the above, choosing a normal distribution to optimise as the waiting time distribution is justified.



(a) (b)

Figure A.5: **The normal distribution can match experimental data, and can approximate other distributions.** (a) The waiting time distribution requires shorter waiting times than transition times $t_w < t_t$ (red) as well as longer waiting times than transition times $t_w > t_t$ (blue). The transition time is denoted by the black dotted line. (b) A normal distribution can approximate uniform and exponential distributions, given a cut-off at 0 and $t_{max} = 12h$.

A.4 Optimisation

The optimisation of the waiting time distribution to fit the experimental data is performed *after* simulation of a range of different distributions, due to the time required per simulation run and the stochastic nature of the model. We selected 100 distributions with varying combinations of ten different means and ten standard deviations (figure A.6), and performed ten simulations of 150 hours. This was then repeated with a refinement in the grid around the optimal point (figure A.6, standard deviation from 2.5–3.5 hours) to obtain a more accurate fit.

Per distribution, the indices were obtained and averaged over the ten runs of 150 hours. A cost function was used to find the optimum waiting time distribution to fit the experimentally obtained indices, as described in section 6.3.2.

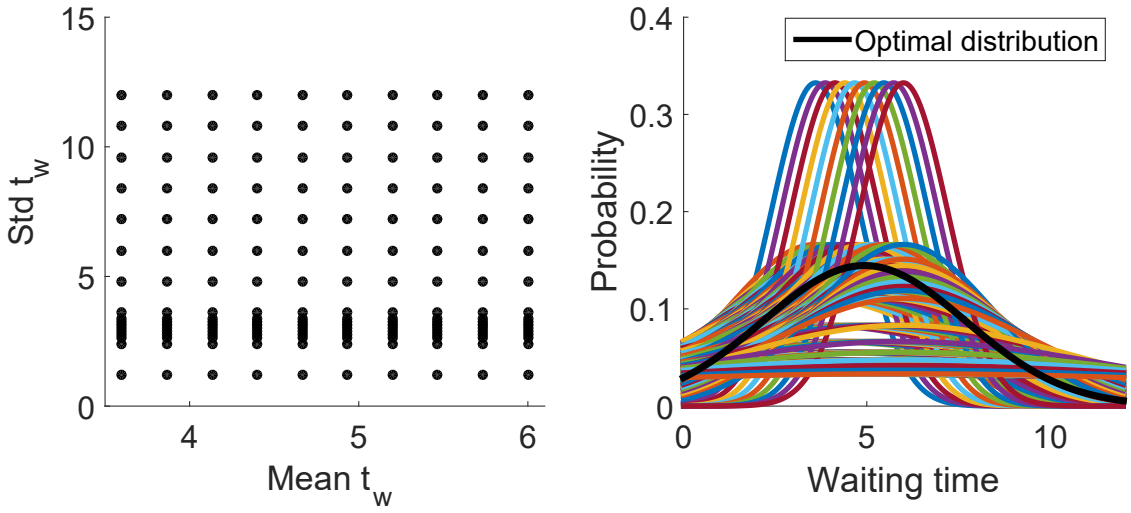


Figure A.6: **Optimisation using a priori simulation results for different normal waiting time distributions with a range of mean and standard deviation values.** Simulated sets of mean and standard deviations (left) with corresponding distributions (right). The black line denotes the optimal waiting time distribution.

A.5 Robustness of optimal waiting time distribution to cost function weights

Equal weights were used for all three indices in the cost function (6.13) in section 6.3.2, which optimises the error between simulation and experimental indices to find the optimum waiting time distribution. We test the robustness of the optimal waiting time distribution by individually changing all weights w_1, w_2, w_3 in the cost function Φ from 0.01 to 1. The band that contains all the optimal distributions for a hundredfold change in every weight is shown in figure A.7. These results indicate that the weights in the cost function only have a small effect on the optimal waiting time distribution.

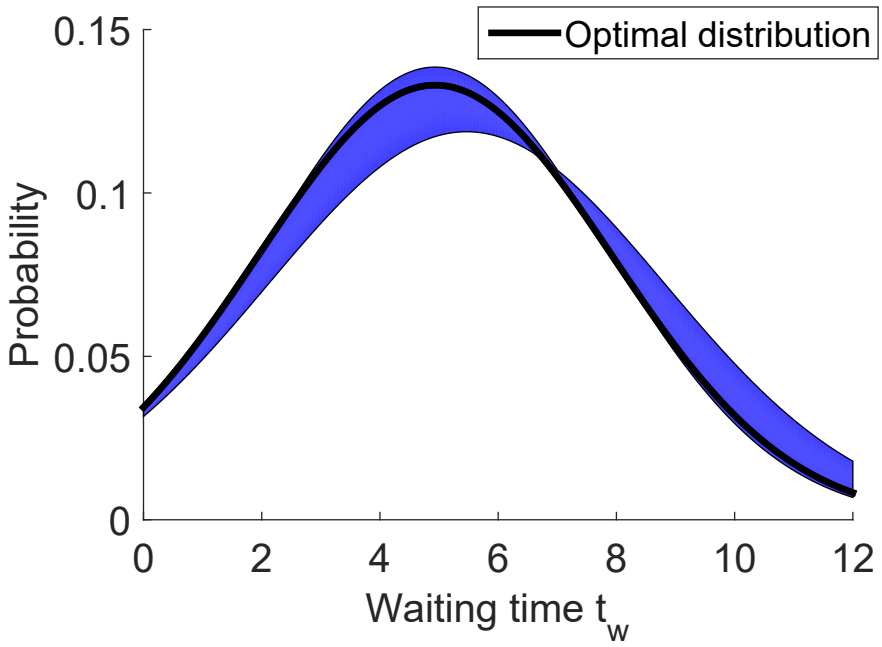


Figure A.7: **Robustness of optimal waiting time distribution to cost function weights.** The band contains all optimal distributions after individually changing all weights w_1, w_2, w_3 in the cost function Φ from 0.01 to 1. The black line denotes the optimal waiting time distribution for equal weights.

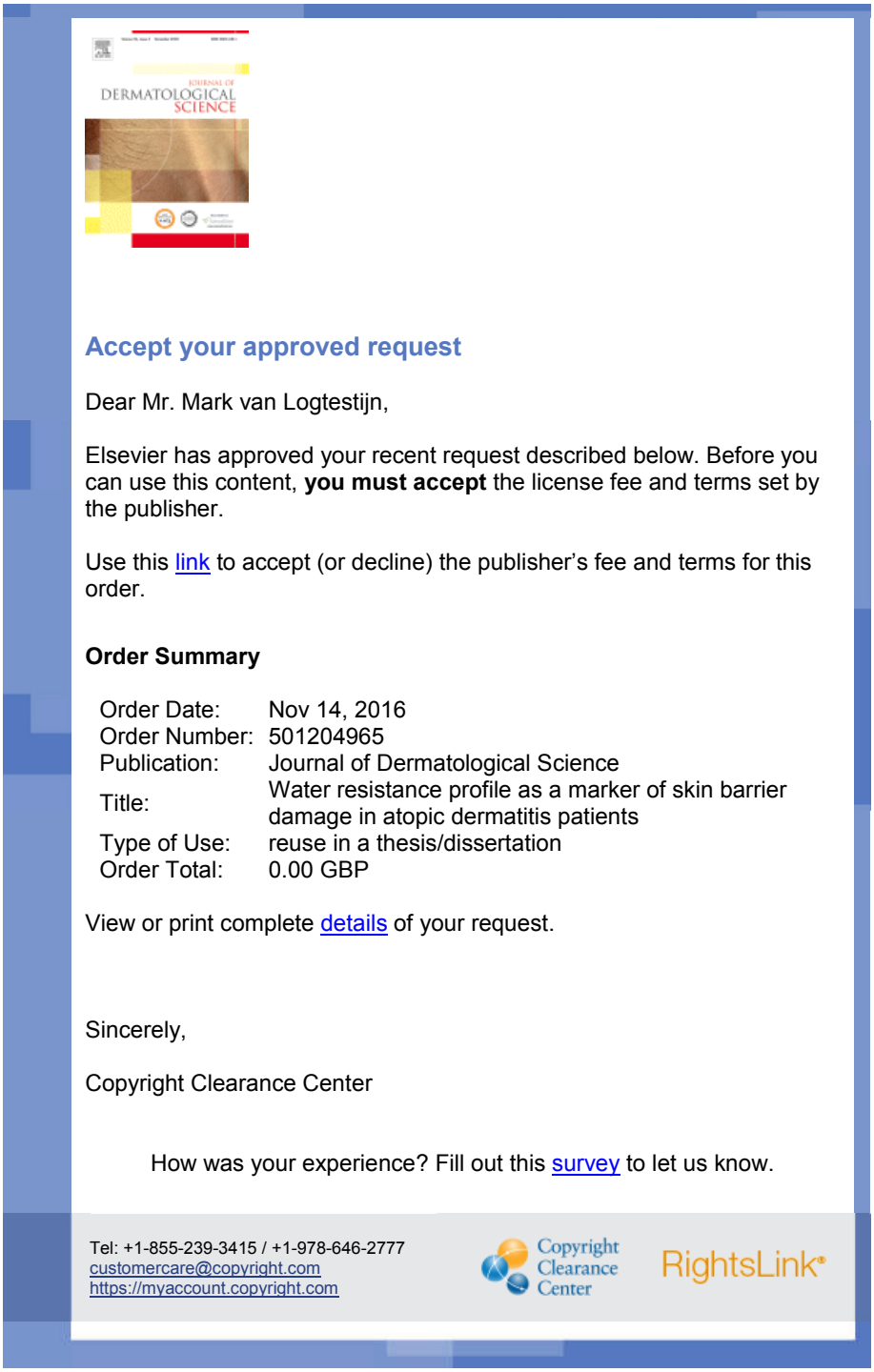
Appendix B

Copyright permission

Table B.1: Permission to republish third party copyrighted work

Page No.:	55
Type of work:	Journal article
Name of work:	Water resistance profile as a marker of skin barrier damage in atopic dermatitis patients
Source of work:	Journal of Dermatological Science, pages 126-128, volume 81, issue 2, February 2016.
Copyright holder:	©2015 Elsevier Ireland Ltd. Published by Elsevier Inc. All rights reserved.
Permission requested on:	14.11.16
I have permission:	Yes
Permission note:	Written permission, confirmation email attached below as figure B.1.

From: no-reply@copyright.com
Sent: 17 November 2016 09:25
To: van Logtestijn, Mark
Subject: RESPONSE REQUIRED for your request to Elsevier



JOURNAL OF DERMATOLOGICAL SCIENCE

Accept your approved request

Dear Mr. Mark van Logtestijn,

Elsevier has approved your recent request described below. Before you can use this content, **you must accept** the license fee and terms set by the publisher.

Use this link to accept (or decline) the publisher's fee and terms for this order.

Order Summary

Order Date:	Nov 14, 2016
Order Number:	501204965
Publication:	Journal of Dermatological Science
Title:	Water resistance profile as a marker of skin barrier damage in atopic dermatitis patients
Type of Use:	reuse in a thesis/dissertation
Order Total:	0.00 GBP

View or print complete details of your request.

Sincerely,

Copyright Clearance Center

How was your experience? Fill out this survey to let us know.

Tel: +1-855-239-3415 / +1-978-646-2777
customercare@copyright.com
https://myaccount.copyright.com

Copyright Clearance Center RightsLink®

Figure B.1: Elsevier copyright permission confirmation

Bibliography

[1] G. LA, "My organ is bigger than your organ," *Archives of Dermatology*, vol. 126, no. 3, pp. 301–302, 1990.

[2] R. D. Sontheimer, "Skin is not the largest organ," *The Journal of investigative dermatology*, vol. 134, pp. 581–2, mar 2014.

[3] M. Furuse, M. Hata, K. Furuse, Y. Yoshida, A. Haratake, Y. Sugitani, T. Noda, A. Kubo, and S. Tsukita, "Claudin-based tight junctions are crucial for the mammalian epidermal barrier: A lesson from claudin-1-deficient mice," *Journal of Cell Biology*, vol. 156, no. 6, pp. 1099–1111, 2002.

[4] K. Turksen and T. C. Troy, "Permeability barrier dysfunction in transgenic mice overexpressing claudin 6," *Development*, vol. 129, no. 7, pp. 1775–1784, 2002.

[5] M. Matsuki, F. Yamashita, A. Ishida-Yamamoto, K. Yamada, C. Kinoshita, S. Fushiki, E. Ueda, Y. Morishima, K. Tabata, H. Yasuno, M. Hashida, H. Iizuka, M. Ikawa, M. Okabe, G. Kondoh, T. Kinoshita, J. Takeda, and K. Yamanishi, "Defective stratum corneum and early neonatal death in mice lacking the gene for transglutaminase 1 (keratinocyte transglutaminase)," *Proceedings of the National Academy of Sciences of the United States of America*, vol. 95, no. 3, pp. 1044–9, 1998.

[6] P. M. Elias, "Stratum corneum defensive functions: an integrated view," *The Journal of investigative dermatology*, vol. 125, pp. 183–200, aug 2005.

[7] C. R. Harding, A. Watkinson, and A. V. Rawlings, "Dry skin, moisturization and corneodesmolysis," *International journal of cosmetic science*, vol. 22, pp. 21–51, 2000.

[8] T. Yuki, A. Komiya, A. Kusaka, T. Kuze, Y. Sugiyama, and S. Inoue, "Impaired tight junctions obstruct stratum corneum formation by altering polar lipid and profilaggrin processing," *Journal of Dermatological Science*, vol. 69, no. 2, pp. 148–158, 2013.

[9] T. Sugawara, N. Iwamoto, M. Akashi, T. Kojima, J. Hisatsune, M. Sugai, and M. Furuse, "Tight junction dysfunction in the stratum granulosum leads to aberrant stratum corneum barrier function in claudin-1-deficient mice," *Journal of Dermatological Science*, vol. 70, no. 1, pp. 12–18, 2013.

[10] J. H. Baek, S. E. H. Lee, K. J. Choi, and E. H. Choi, "Acute modulations in stratum corneum permeability barrier function affect claudin expression and epidermal tight junction function via changes of epidermal calcium gradient," *Yonsei Med J*, vol. 54, no. 2, pp. 523–528, 2013.

[11] A. Celli, Y. Zhai, Y. J. Jiang, D. Crumrine, P. M. Elias, K. R. Feingold, and T. M. Mauro, "Tight junction properties change during epidermis development," *Experimental Dermatology*, vol. 21, no. 10, pp. 798–801, 2012.

[12] M. Merad, F. Ginhoux, and M. Collin, "Origin, homeostasis and function of Langerhans cells and other langerin-expressing dendritic cells," *Nature reviews. Immunology*, vol. 8, no. 12, pp. 935–47, 2008.

[13] M. A. Lowes, A. M. Bowcock, and J. G. Krueger, "Pathogenesis and therapy of psoriasis.," *Nature*, vol. 445, no. 7130, pp. 866–73, 2007.

[14] M. Boguniewicz and D. Leung, "Atopic Dermatitis: A Disease of Altered Skin Barrier and Imune Dysregulation," *Imunnological Reviews*, vol. 242, no. 1, pp. 233–246, 2011.

[15] P. M. Elias, Y. Hatano, and M. L. Williams, "Basis for the barrier abnormality in atopic dermatitis: Outside- inside-outside pathogenic mechanisms," *Journal of Allergy and Clinical Immunology*, vol. 100, no. 2, pp. 130–134, 2012.

[16] H. Williams, A. Stewart, E. von Mutius, W. Cookson, and H. R. Anderson, "Is eczema really on the increase worldwide?," *Journal of Allergy and Clinical Immunology*, vol. 121, no. 4, 2008.

[17] J. A. Odhiambo, H. C. Williams, T. O. Clayton, C. F. Robertson, and M. I. Asher, "Global variations in prevalence of eczema symptoms in children from ISAAC Phase Three," *Journal of Allergy and Clinical Immunology*, vol. 124, no. 6, pp. 1251–1258.e23, 2009.

[18] S. C. Dharmage, A. J. Lowe, M. C. Matheson, J. A. Burgess, K. J. Allen, and M. J. Abramson, "Atopic dermatitis and the atopic march revisited," *Allergy: European Journal of Allergy and Clinical Immunology*, vol. 69, no. 1, pp. 17–27, 2014.

[19] T. Zheng, J. Yu, M. H. Oh, and Z. Zhu, "The atopic march: Progression from atopic dermatitis to allergic rhinitis and asthma," *Allergy, Asthma and Immunology Research*, vol. 3, no. 2, pp. 67–73, 2011.

[20] M. Machado, J. Hadgraft, and M. E. Lane, "Assessment of the variation of skin barrier function with anatomic site, age, gender and ethnicity," *International journal of cosmetic science*, pp. 397–409, jun 2010.

[21] L. S. Telofski, A. P. Morello, M. C. Mack, and G. N. Stamatas, "The infant skin barrier: can we preserve, protect, and enhance the barrier?," *Dermatology research and practice*, jan 2012.

[22] J. Nikolovski, G. N. Stamatas, N. Kollias, and B. C. Wiegand, "Barrier function and water-holding and transport properties of infant stratum corneum are different from adult and continue to develop through the first year of life.," *The Journal of Investigative Dermatology*, vol. 128, pp. 1728–36, jul 2008.

[23] D. Mohammed, P. J. Matts, J. Hadgraft, and M. E. Lane, "Variation of stratum corneum biophysical and molecular properties with anatomic site," *The AAPS journal*, vol. 14, pp. 806–12, dec 2012.

[24] M. Machado, T. M. Salgado, J. Hadgraft, and M. E. Lane, "The relationship between transepidermal water loss and skin permeability," *International journal of pharmaceutics*, vol. 384, pp. 73–7, jan 2010.

[25] J. W. Fluhr, H. Dickel, O. Kuss, I. Weyher, T. L. Diepgen, and E. Berardesca, "Impact of anatomical location on barrier recovery, surface pH and stratum corneum hydration after acute barrier disruption," *British Journal Of Dermatology*, vol. 146, pp. 770–776, 2002.

[26] E. Candi, R. Schmidt, and G. Melino, "The cornified envelope: a model of cell death in the skin.," *Nature reviews. Molecular cell biology*, vol. 6, pp. 328–40, apr 2005.

[27] P. J. Caspers, G. W. Lucassen, H. A. Bruining, and G. J. Puppels, "Automated depth-scanning confocal Raman microspectrometer for rapid in vivo determination of water concentration profiles in human skin.," *Journal of Raman Spectroscopy*, vol. 31, pp. 813–18, 2000.

[28] P. J. Caspers, G. W. Lucassen, E. A. Carter, H. A. Bruining, and G. J. Puppels, "In vivo confocal Raman microspectroscopy of the skin: noninvasive determination of molecular concentration profiles.," *The Journal of investigative dermatology*, vol. 116, pp. 434–42, mar 2001.

[29] H. Ohman and A. Vahlquist, "In vivo studies concerning a pH gradient in human stratum corneum and upper epidermis.," *Acta dermato-venereologica*, vol. 74, pp. 375–379, 1994.

[30] J. M. Crowther and P. J. Matts, "Molecular Concentration Profiling in Skin Using Confocal Raman Spectroscopy," in *Textbook of Aging Skin* (M. A. Farage, K. W. Miller, and H. I. Maibach, eds.), pp. 735–747, Berlin, Heidelberg: Springer Berlin Heidelberg, 2010.

[31] D. R. Hoffman, L. M. Kroll, A. Basehoar, B. Reece, C. T. Cunningham, and D. W. Koenig, "Immediate and extended effects of sodium lauryl sulphate exposure on stratum corneum natural moisturizing factor," *International journal of cosmetic science*, vol. 36, pp. 93–101, oct 2014.

[32] A. Kubo, I. Ishizaki, A. Kubo, H. Kawasaki, K. Nagao, Y. Ohashi, and M. Amagai, "The stratum corneum comprises three layers with distinct metal-ion barrier properties," *Scientific reports*, vol. 3, p. 1731, apr 2013.

[33] J. M. Brandner, M. Haftek, and C. M. Niessen, "Adherens Junctions, Desmosomes and Tight Junctions in Epidermal Barrier Function," *The Open Dermatology Journal*, vol. 4, no. October 2015, pp. 14–20, 2010.

[34] J. M. Brandner, M. Zorn-Kruppa, T. Yoshida, I. Moll, L. Beck, and A. De Benedetto, "Epidermal tight junctions in health and disease," *Tissue Barriers*, vol. 3, no. 1-2, p. e974451, 2014.

[35] N. J. Reynolds, "One hundred and twenty-five years and counting: into an era of systems dermatology.," *The British journal of dermatology*, vol. 171, pp. 1279–81, dec 2014.

[36] R. J. Tanaka and M. Ono, "Skin Disease Modeling from a Mathematical Perspective," *Journal of Investigative Dermatology*, vol. 133, pp. 1472–8, jun 2013.

[37] R. J. Tanaka, M. Ono, and H. A. Harrington, "Skin Barrier Homeostasis in Atopic Dermatitis: Feedback Regulation of Kallikrein Activity," *PLoS ONE*, vol. 6, no. 5, p. e19895, 2011.

[38] E. Domínguez-Hüttinger, M. Ono, M. Barahona, and R. J. Tanaka, "Risk-factor dependent dynamics of atopic dermatitis : Modelling multi-scale regulation of epithelium homeostasis," *Interface focus*, vol. 3, p. 20120090, 2013.

[39] E. Domínguez-Hüttinger, P. Christodoulides, K. Miyauchi, A. D. Irvine, M. Okada-Hatakeyama, M. Kubo, and R. J. Tanaka, "Mathematical Modeling of Atopic Dermatitis Reveals Double switch Mechanisms Underlying Four Common Disease Phenotypes," *Journal of Allergy and Clinical Immunology*, 2017.

[40] Y. G. Anissimov, O. G. Jepps, Y. Dancik, and M. S. Roberts, "Mathematical and pharmacokinetic modelling of epidermal and dermal transport processes," *Advanced drug delivery reviews*, vol. 65, pp. 169–90, feb 2013.

[41] S. Mitragotri, Y. G. Anissimov, A. L. Bunge, H. F. Frasch, R. H. Guy, J. Hadgraft, G. B. Kasting, M. E. Lane, and M. S. Roberts, "Mathematical models of skin permeability: an overview.," *International journal of pharmaceutics*, vol. 418, pp. 115–29, oct 2011.

[42] O. G. Jepps, Y. Dancik, Y. G. Anissimov, and M. S. Roberts, "Modeling the human skin barrier - Towards a better understanding of dermal absorption.," *Advanced drug delivery reviews*, vol. 65, pp. 152–68, feb 2013.

[43] P. J. Caspers, G. W. Lucassen, R. Wolthuis, H. A. Bruining, and G. J. Puppels, "In vitro and in vivo Raman spectroscopy of human skin.," *Biospectroscopy*, vol. 4, pp. s31–s39, jan 1998.

[44] P. R. Bergstresser and J. R. Taylor, "Epidermal 'turnover time'–a new examination.," *The British journal of dermatology*, vol. 96, no. 5, pp. 503–509, 1977.

[45] G. D. Weinstein, J. L. McCullough, and P. Ross, "Cell proliferation in normal epidermis.," *The Journal of investigative dermatology*, vol. 82, no. 6, pp. 623–628, 1984.

[46] K. M. Halprin, "Epidermal "turnover time"–a re-examination.," *The British journal of dermatology*, vol. 86, pp. 14–9, jan 1972.

[47] A. Y. Finlay, R. J. Marschall, and R. Marks, "A fluorescence photographic photometric technique to assess stratum corneum turnover rate and barrier function in vivo," *British Journal of Dermatology*, vol. 107, no. 1, pp. 35–42, 1982.

[48] D. Roberts and R. Marks, "The determination of regional and age variations in the rate of desquamation: a comparison of four techniques," *The Journal of investigative dermatology*, vol. 74, no. 1, pp. 13–16, 1980.

[49] C. Blair, "Morphology and thickness of the human stratum corneum.," *The British journal of dermatology*, vol. 80, pp. 430–436, jul 1968.

[50] P. M. Elias, "Epidermal lipids, barrier function, and desquamation.," *Journal of Inverstigative Dermatology*, vol. 80(Suppl), no. 6, pp. 44s–9s, 1983.

[51] I. C. Mackenzie, "Ordered structure of the epidermis.," *The Journal of investigative dermatology*, vol. 65, no. 1, pp. 45–51, 1975.

[52] I. C. Mackenzie, K. Zimmerman, and L. Peterson, "The pattern of cellular organization of human epidermis.," *The Journal of investigative dermatology*, vol. 76, no. 6, pp. 459–461, 1981.

[53] J. A. Bouwstra and M. Ponec, "The skin barrier in healthy and diseased state.," *Biochimica et biophysica acta*, vol. 1758, pp. 2080–95, dec 2006.

[54] J. van Smeden, M. Janssens, G. S. Gooris, and J. a. Bouwstra, "The important role of stratum corneum lipids for the cutaneous barrier function," *Biochimica et biophysica acta*, vol. 1841, pp. 295–313, mar 2014.

[55] F. Damien and M. Boncheva, "The extent of orthorhombic lipid phases in the stratum corneum determines the barrier efficiency of human skin in vivo.," *The Journal of investigative dermatology*, vol. 130, pp. 611–4, feb 2010.

[56] L. Norlén and A. Al-Amoudi, "Stratum corneum keratin structure, function, and formation: The cubic rod-packing and membrane templating model," *Journal of Investigative Dermatology*, vol. 123, no. 4, pp. 715–732, 2004.

[57] A. Sandilands, C. Sutherland, A. D. Irvine, and W. H. I. McLean, "Filaggrin in the frontline: role in skin barrier function and disease.," *Journal of cell science*, vol. 122, pp. 1285–1294, 2009.

[58] A. E. Kalinin, A. V. Kajava, and P. M. Steinert, "Epithelial barrier function: assembly and structural features of the cornified cell envelope.," *BioEssays : news and reviews in molecular, cellular and developmental biology*, vol. 24, pp. 789–800, oct 2002.

[59] A. Ishida-Yamamoto, S. Igawa, and M. Kishibe, "Order and disorder in corneocyte adhesion," *The Journal of dermatology*, vol. 38, pp. 645–54, jul 2011.

[60] A. V. Rawlings and P. J. Matts, "Stratum Corneum moisturization at the molecular level: an update in relation to the dry skin cycle," *Journal of Investigative Dermatology*, no. 124, pp. 1099–1110, 2005.

[61] S. Verdier-Sévrain and F. Bonté, "Skin hydration: a review on its molecular mechanisms.," *Journal of cosmetic dermatology*, vol. 6, pp. 75–82, jun 2007.

[62] A. V. Rawlings, I. R. Scott, C. R. Harding, and P. A. Bowser, "Stratum corneum moisturization at the molecular level," *Journal of Investigative Dermatology*, vol. 103, no. 5, pp. 731–740, 1994.

[63] C. R. Harding, J. Bartolone, and A. Rawlings, "Effects of natural moisturizing factor and lactic acid isomers on skin function.," *Dry Skin and Moisturizers: Chemistry and Function*, pp. 229–241, 2000.

[64] S. J. Brown and W. H. I. McLean, "One remarkable molecule: filaggrin.," *The Journal of investigative dermatology*, vol. 132, pp. 751–62, mar 2012.

[65] E. Hoste, P. Kemperman, M. Devos, G. Denecker, S. Kezic, N. Yau, B. Gilbert, S. Lippens, P. De Groote, R. Roelandt, P. Van Damme, K. Gevaert, R. B. Presland, H. Takahara, G. Puppels, P. Caspers, P. Vandenabeele, and W. Declercq, "Caspase-14 is required for filaggrin degradation to natural moisturizing factors in the skin.," *The Journal of investigative dermatology*, vol. 131, pp. 2233–41, nov 2011.

[66] E. Boireau-Adamezyk, A. Baillet-Guffroy, and G. N. Stamatas, "Mobility of water molecules in the stratum corneum: effects of age and chronic exposure to the environment.," *The Journal of investigative dermatology*, vol. 134, pp. 2046–9, jul 2014.

[67] C. Choe, J. Lademann, and M. E. Darvin, "Depth profiles of hydrogen bound water molecule types and their relation to lipid and protein interaction in the human stratum corneum in vivo," *The Analyst*, vol. 141, no. 22, pp. 6329–6337, 2016.

[68] R. Vyumvuhore, A. Tfayli, H. Duplan, A. Delalleau, M. Manfait, and A. Baillet-Guffroy, "Effects of atmospheric relative humidity on Stratum Corneum structure at the molecular level: ex vivo Raman spectroscopy analysis.," *The Analyst*, vol. 138, pp. 4103–4111, may 2013.

[69] T. Matsui, K. Miyamoto, A. Kubo, H. Kawasaki, T. Ebihara, K. Hata, S. Tanahashi, S. Ichinose, I. Imoto, J. Inazawa, J. Kudoh, and M. Amagai, "SASPase regulates stratum corneum hydration through profilaggrin-to-filaggrin processing.," *EMBO molecular medicine*, vol. 3, pp. 320–33, jun 2011.

[70] L. Eckhart, S. Lippens, E. Tschachler, and W. Declercq, "Cell death by cornification," *Biochimica et Biophysica Acta - Molecular Cell Research*, vol. 1833, pp. 3471–3480, 2013.

[71] M. Demerjian, J.-P. Hachem, E. Tschachler, G. Denecker, W. Declercq, P. Vandenabeele, T. Mauro, M. Hupe, D. Crumrine, T. Roelandt, E. Houben, P. M. Elias, and K. R. Feingold, "Acute modulations in permeability barrier function regulate epidermal cornification: role of caspase-14 and the protease-activated receptor type 2," *The American journal of pathology*, vol. 172, pp. 86–97, jan 2008.

[72] G. Menon, K. Feingold, and P. Elias, "Lamellar body secretory response to barrier disruption.," *Journal of Investigative Dermatology*, vol. 98, pp. 279–89, 1992.

[73] M. Denda, L. C. Wood, S. Emami, C. Calhoun, B. E. Brown, P. M. Elias, and K. R. Feingold, "The epidermal hyperplasia associated with repeated barrier disruption by acetone treatment or tape stripping cannot be attributed to increased water loss," *Archives of dermatological research*, vol. 288, pp. 230–8, may 1996.

[74] P. Elias, S. Ahn, B. Brown, D. Crumrine, and K. R. Feingold, "Origin of the epidermal calcium gradient: regulation by barrier status and role of active vs passive mechanisms," *The Journal of investigative dermatology*, vol. 119, pp. 1269–74, dec 2002.

[75] G. K. Menon, K. R. Feingold, A. H. Moser, B. E. Brown, and P. M. Elias, "De novo sterologenesis in the skin. II. Regulation by cutaneous barrier requirements," *Journal of lipid research*, vol. 26, no. 5, pp. 418–427, 1985.

[76] G. Grubauer, P. M. Elias, and K. R. Feingold, "Transepidermal water loss: the signal for recovery of barrier structure and function.," *Journal of lipid research*, vol. 30, pp. 323–33, mar 1989.

[77] G. K. Menon, P. M. Elias, and K. R. Feingold, "Integrity of the permeability barrier is crucial for maintenance of the epidermal calcium gradient," *The British journal of dermatology*, vol. 130, pp. 139–47, feb 1994.

[78] P. M. Elias, S. K. Ahn, M. Denda, B. E. Brown, D. Crumrine, L. K. Kimutai, L. Kömüves, S. H. Lee, and K. R. Feingold, "Modulations in epidermal calcium regulate the expression of differentiation-specific markers," *The Journal of investigative dermatology*, vol. 119, pp. 1128–36, nov 2002.

[79] T. Mauro, G. Bench, E. Sidderas-Haddad, K. Feingold, P. Elias, and C. Cullander, "Acute barrier perturbation abolishes the Ca2+ and K+ gradients in murine epidermis: Quantitative measurement using PIXE," *Journal of Investigative Dermatology*, vol. 111, pp. 1198–1201, 1998.

[80] G. K. Menon, L. F. Price, B. Bommannan, P. M. Elias, and K. R. Feingold, "Selective Obliteration of the Epidermal Calcium Gradient Leads to Enhanced Lamellar Body Secretion," *Journal of Investigative Dermatology*, vol. 102, no. 5, pp. 789–795, 1994.

[81] C. Caubet, N. Jonca, M. Brattsand, M. Guerrin, D. Bernard, R. Schmidt, T. Egelrud, M. Simon, and G. Serre, "Degradation of corneodesmosome proteins by two serine proteases of the kallikrein family, SCTE/KLK5/hK5 and SCCE/KLK7/hK7," *The Journal of investigative dermatology*, vol. 122, pp. 1235–44, may 2004.

[82] C. Borgoño, I. P. Michael, N. Komatsu, A. Jayakumar, R. Kapadia, G. L. Clayman, G. Sotiropoulou, and E. P. Diamandis, "A potential role for multiple tissue kallikrein serine proteases in epidermal desquamation.," *The Journal of biological chemistry*, vol. 282, pp. 3640–52, feb 2007.

[83] G. Pampalakis and G. Sotiropoulou, "Tissue kallikrein proteolytic cascade pathways in normal physiology and cancer," *Biochimica et Biophysica Acta - Reviews on Cancer*, vol. 1776, no. 1, pp. 22–31, 2007.

[84] M. Brattsand, K. Stefansson, C. Lundh, Y. Haasum, and T. Egelrud, "A proteolytic cascade of kallikreins in the stratum corneum.," *The Journal of investigative dermatology*, vol. 124, pp. 198–203, jan 2005.

[85] A. Eissa and E. P. Diamandis, "Human tissue kallikreins as promiscuous modulators of homeostatic skin barrier functions," *Biological Chemistry*, vol. 389, no. 6, pp. 669–680, 2008.

[86] T. Roelandt, B. Thys, C. Heughebaert, A. De Vroede, K. De Paepe, D. Roseeuw, B. Rombaut, and J.-P. Hachem, "LEKTI-1 in sickness and in health," *International journal of cosmetic science*, vol. 31, pp. 247–54, aug 2009.

[87] A. Hovnanian, "Netherton syndrome : skin inflammation and allergy by loss of protease inhibition," *Cell tissue Research*, vol. 351, pp. 289–300, 2013.

[88] P. Fortugno, A. Bresciani, C. Paolini, C. Pazzagli, M. El Hachem, M. D'Alessio, and G. Zambruno, "Proteolytic activation cascade of the Netherton syndrome-defective protein, LEKTI, in the epidermis: implications for skin homeostasis," *The Journal of investigative dermatology*, vol. 131, pp. 2223–32, nov 2011.

[89] T. Yuki, A. Haratake, H. Koishikawa, K. Morita, Y. Miyachi, and S. Inoue, "Tight junction proteins in keratinocytes: Localization and contribution to barrier function," *Experimental Dermatology*, vol. 16, no. 4, pp. 324–330, 2007.

[90] C. M. Van Itallie and J. M. Anderson, "Architecture of tight junctions and principles of molecular composition," *Seminars in Cell and Developmental Biology*, vol. 36, pp. 157–165, 2014.

[91] S. M. Krug, J. D. Schulzke, and M. Fromm, "Tight junction, selective permeability, and related diseases," *Seminars in Cell and Developmental Biology*, vol. 36, pp. 166–176, 2014.

[92] J. M. Brandner, "Tight junctions and tight junction proteins in mammalian epidermis," *European Journal of Pharmaceutics and Biopharmaceutics*, vol. 72, no. 2, pp. 289–294, 2009.

[93] K. Morita and Y. Miyachi, "Tight junctions in the skin," *Journal of Dermatological Science*, vol. 31, no. 2, pp. 81–89, 2003.

[94] J. M. Brandner, S. Kief, C. Grund, M. Rendl, P. Houdek, C. Kuhn, E. Tschachler, W. W. Franke, and I. Moll, "Organization and formation of the tight junction system in human epidermis and cultured keratinocytes.," *European journal of cell biology*, vol. 81, no. 5, pp. 253–263, 2002.

[95] M. Furuse, Y. Izumi, Y. Oda, T. Higashi, and N. Iwamoto, "Molecular organization of tricellular tight junctions," *Tissue Barriers*, vol. 2, no. 1, p. e28960, 2014.

[96] N. Kirschner, R. Rosenthal, M. Furuse, I. Moll, M. Fromm, and J. M. Brandner, "Contribution of Tight Junction Proteins to Ion, Macromolecule, and Water Barrier in Keratinocytes.," *The Journal of investigative dermatology*, vol. 133, no. 5, pp. 1161–9, 2013.

[97] N. Kirschner, P. Houdek, M. Fromm, I. Moll, and J. M. Brandner, "Tight junctions form a barrier in human epidermis.," *European journal of cell biology*, vol. 89, no. 11, pp. 839–42, 2010.

[98] P. Claude and D. A. Goodenough, "Fracture faces of zonulae occludentes from 'tight' and 'leaky' epithelia," *Journal of Cell Biology*, vol. 58, no. 2, pp. 390–400, 1973.

[99] P. Claude, "Morphological factors influencing transepithelial permeability: a model for the resistance of the zonula occludens.," *The Journal of membrane biology*, vol. 39, no. 2-3, pp. 219–232, 1978.

[100] H. Schlüter, R. Wepf, I. Moll, and W. W. Franke, "Sealing the live part of the skin: the integrated meshwork of desmosomes, tight junctions and curvilinear ridge structures in the cells of the uppermost granular layer of the human epidermis.," *European journal of cell biology*, vol. 83, no. 11-12, pp. 655–665, 2004.

[101] J. L. Madara, "Regulation of the movement of solutes across tight junctions," *Annual review of physiology*, vol. 60, pp. 143–159, 1998.

[102] N. Kirschner, C. Bohner, S. Rachow, and J. M. Brandner, "Tight junctions: Is there a role in dermatology?," *Archives of Dermatological Research*, vol. 302, no. 7, pp. 483–493, 2010.

[103] T. Matsui and M. Amagai, "Dissecting the formation, structure and barrier function of the stratum corneum," *International Immunology*, vol. 27, no. 6, pp. 269–280, 2015.

[104] A. Kubo, K. Nagao, and M. Amagai, *3D Visualization of Epidermal Langerhans Cells*, pp. 119–127. Totowa, NJ: Humana Press, 2013.

[105] A. Kubo, K. Nagao, M. Yokouchi, H. Sasaki, and M. Amagai, "External antigen uptake by Langerhans cells with reorganization of epidermal tight junction barriers," *The Journal of experimental medicine*, vol. 206, no. 13, pp. 2937–2946, 2009.

[106] S. V. Walsh, a. M. Hopkins, and a. Nusrat, "Modulation of tight junction structure and function by cytokines.," *Advanced drug delivery reviews*, vol. 41, no. 3, pp. 303–13, 2000.

[107] N. S. Harhaj and D. A. Antonetti, "Regulation of tight junctions and loss of barrier function in pathophysiology," *The International Journal of Biochemistry & Cell Biology*, vol. 36, no. 7, pp. 1206–1237, 2004.

[108] A. Kubo, K. Nagao, and M. Amagai, "Epidermal barrier dysfunction and cutaneous sensitization in atopic diseases," *The Journal of clinical investigation*, vol. 122, no. 2, pp. 440–7, 2012.

[109] A. De Benedetto, N. M. Rafaels, L. Y. McGirt, A. I. Ivanov, S. N. Georas, C. Cheadle, A. E. Berger, K. Zhang, S. Vidyasagar, T. Yoshida, M. Boguniewicz, T. Hata, L. C. Schneider, J. M. Hanifin, R. L. Gallo, N. Novak, S. Weidinger, T. H. Beaty, D. Y. M. Leung, K. C. Barnes, and L. A. Beck, "Tight junction defects in patients with atopic dermatitis," *Journal of Allergy and Clinical Immunology*, vol. 127, no. 3, pp. 773–786, 2011.

[110] A. D. Benedetto, A. Kubo, and L. A. Beck, "Skin Barrier Disruption : A Requirement for Allergen Sensitization ?," *Journal of Investigative Dermatology*, vol. 132, no. 3, pp. 949–963, 2012.

[111] M. Yokouchi, A. Kubo, H. Kawasaki, K. Yoshida, K. Ishii, M. Furuse, and M. Amagai, "Epidermal tight junction barrier function is altered by skin inflammation, but not by filaggrin-deficient stratum corneum," *Journal of Dermatological Science*, vol. 77, no. 1, pp. 28–36, 2015.

[112] N. Kirschner, C. Poetzl, P. von den Driesch, E. Wladykowski, I. Moll, M. J. Behne, and J. M. Brandner, "Alteration of Tight Junction Proteins Is an Early Event in Psoriasis," *The American Journal of Pathology*, vol. 175, no. 3, pp. 1095–1106, 2009.

[113] M. Svoboda, Z. Bílková, and T. Muthný, "Could tight junctions regulate the barrier function of the aged skin?," *Journal of Dermatological Science*, vol. 81, no. 3, pp. 147–152, 2016.

[114] L. Gonzalez-Mariscal, S. Lechuga, and E. Garay, "Role of tight junctions in cell proliferation and cancer," *Progress in Histochemistry and Cytochemistry*, vol. 42, no. 1, pp. 1–57, 2007.

[115] T. a. Martin and W. G. Jiang, "Loss of tight junction barrier function and its role in cancer metastasis.," *Biochimica et biophysica acta*, vol. 1788, no. 4, pp. 872–91, 2009.

[116] E. A. Runkle and D. Mu, "Tight junction proteins: From barrier to tumorigenesis," *Cancer Letters*, vol. 337, no. 1, pp. 41–48, 2013.

[117] S. Rachow, M. Zorn-Kruppa, U. Ohnemus, N. Kirschner, S. Vidal-y Sy, P. von den Driesch, C. Börnchen, J. Eberle, M. Mildner, E. Vettorazzi, R. Rosenthal, I. Moll, and J. M. Brandner, "Occludin Is Involved in Adhesion, Apoptosis, Differentiation and Ca2+-Homeostasis of Human Keratinocytes: Implications for Tumorigenesis," *PLoS ONE*, vol. 8, no. 2, 2013.

[118] S. S. Oliveira and J. A. Morgado-Díaz, "Claudins: multifunctional players in epithelial tight junctions and their role in cancer," *Cellular and Molecular Life Sciences*, vol. 64, no. 1, pp. 17–28, 2007.

[119] K. Turksen and T. C. Troy, "Junctions gone bad: Claudins and loss of the barrier in cancer," *Biochimica et Biophysica Acta - Reviews on Cancer*, vol. 1816, no. 1, pp. 73–79, 2011.

[120] T. A. Martin, M. D. Mason, and W. G. Jiang, "Tight junctions in cancer metastasis," *Frontiers in bioscience (Landmark edition)*, vol. 16, pp. 898–936, 2011.

[121] D. Y. M. Leung and T. Bieber, "Atopic dermatitis," *Lancet*, vol. 361, no. 9352, pp. 151–160, 2003.

[122] T. Bieber, "Atopic dermatitis," *Annals of Dermatology*, vol. 22, no. 2, pp. 125–137, 2010.

[123] E. Proksch, R. Fölster-Holst, and J.-M. Jensen, "Skin barrier function, epidermal proliferation and differentiation in eczema.," *Journal of dermatological science*, vol. 43, pp. 159–69, sep 2006.

[124] D. Benedetto, "Tight Junction Defects in Atopic Dermatitis," vol. 127, no. 3, pp. 773–786, 2012.

[125] P. M. Elias and M. Steinhoff, ""Outside-to-inside" (and now back to "outside") pathogenic mechanisms in atopic dermatitis.," *The Journal of investigative dermatology*, vol. 128, pp. 1067–70, may 2008.

[126] P. M. Elias, Y. Hatano, and M. L. Williams, "Basis for the barrier abnormality in atopic dermatitis: outside-inside-outside pathogenic mechanisms.," *The Journal of allergy and clinical immunology*, vol. 121, pp. 1337–43, jun 2008.

[127] P. M. Elias and M. Schmuth, "Abnormal skin barrier in the etiopathogenesis of atopic dermatitis.," *Current opinion in allergy and clinical immunology*, vol. 9, pp. 437–46, oct 2009.

[128] D. Leung, M. Boguniewicz, M. Howell, I. Nomura, and Q. Hamid, "New insights into atopic dermatitis," *The Journal of Clinical Investigation*, vol. 113, pp. 651–657, 2004.

[129] E. Rodríguez, H. Baurecht, E. Herberich, S. Wagenpfeil, S. J. Brown, H. J. Cordell, A. D. Irvine, and S. Weidinger, "Meta-analysis of filaggrin polymorphisms in eczema and asthma: Robust risk factors in atopic disease," *Journal of Allergy and Clinical Immunology*, vol. 123, no. 6, 2009.

[130] A. D. Irvine, "Fleshing out filaggrin phenotypes.," *The Journal of investigative dermatology*, vol. 127, no. 3, pp. 504–507, 2007.

[131] G. M. O'Regan, A. Sandilands, W. H. I. McLean, and A. D. Irvine, "Filaggrin in atopic dermatitis.," *The Journal of allergy and clinical immunology*, vol. 124, pp. R2–6, sep 2009.

[132] D. Y. M. Leung and E. Guttman-Yassky, "Deciphering the complexities of atopic dermatitis: Shifting paradigms in treatment approaches," *Journal of Allergy and Clinical Immunology*, vol. 134, no. 4, pp. 769–779, 2014.

[133] S. C. Dharmage, A. J. Lowe, M. C. Matheson, J. A. Burgess, K. J. Allen, and M. J. Abramson, "Atopic dermatitis and the atopic march revisited," *Allergy: European Journal of Allergy and Clinical Immunology*, vol. 69, no. 1, pp. 17–27, 2014.

[134] T. Bieber, M. Cork, and S. Reitamo, "Atopic dermatitis: a candidate for disease-modifying strategy.," *Allergy*, vol. 67, pp. 969–75, aug 2012.

[135] K. Horimukai, K. Morita, M. Narita, M. Kondo, H. Kitazawa, M. Nozaki, Y. Shigematsu, K. Yoshida, H. Niizeki, K. I. Motomura, H. Sago, T. Takimoto, E. Inoue, N. Kamemura, H. Kido, J. Hisatsune, M. Sugai, H. Murota, I. Katayama, T. Sasaki, M. Amagai, H. Morita, A. Matsuda, K. Matsumoto, H. Saito, and Y. Ohya, "Application of moisturizer to neonates prevents development of atopic dermatitis," *Journal of Allergy and Clinical Immunology*, vol. 134, no. 4, pp. 824–830.e6, 2014.

[136] E. L. Simpson, J. R. Chalmers, J. M. Hanifin, K. S. Thomas, M. J. Cork, W. H. I. McLean, S. J. Brown, Z. Chen, Y. Chen, and H. C. Williams, "Emollient enhancement of the skin barrier from birth offers effective atopic dermatitis prevention," *Journal of Allergy and Clinical Immunology*, vol. 134, no. 4, pp. 818–823, 2014.

[137] H.-J. Lee, N. Y. Yoon, N. R. Lee, M. Jung, D. H. Kim, and E. H. Choi, "Topical acidic cream prevents the development of atopic dermatitis- and asthma-like lesions in murine model.," *Experimental dermatology*, vol. 23, pp. 736–41, oct 2014.

[138] R. E. Imhof, M. E. P. De Jesus, P. Xiao, L. I. Ciortea, and E. P. Berg, "Closed-chamber transepidermal water loss measurement: Microclimate, calibration and performance," *International Journal of Cosmetic Science*, vol. 31, no. 2, pp. 97–118, 2009.

[139] A. Rougier, C. Lotte, P. Corcuff, and H. I. Maibach, "Relationship between skin permeability and corneocyte size according to anatomic site, age, and sex in man.," *Journal of the Society of Cosmetic Chemistry*, vol. 39, no. Januray/February, pp. 15–26, 1988.

[140] R. P. Chilcott, C. H. Dalton, A. J. Emmanuel, C. E. Allen, and S. T. Bradley, "Transepidermal water loss does not correlate with skin barrier function in vitro.," *The Journal of investigative dermatology*, vol. 118, pp. 871–5, may 2002.

[141] N. Lu, P. Chandar, D. Tempesta, C. Vincent, J. Bajor, and H. McGuiness, "Characteristic differences in barrier and hygroscopic properties between normal and cosmetic dry skin. I. Enhanced barrier analysis with sequential tape-stripping.," *International journal of cosmetic science*, vol. 36, pp. 167–74, apr 2014.

[142] A. P. Teixeira, J. L. Rangel, L. J. Raniero, M. G. Tosato, P. P. Fávero, and A. A. Martin, "Confocal raman spectroscopy: Determination of natural moisturizing factor profile related to skin hydration," *Revista Brasileira de Engenharia Biomedica*, vol. 30, no. 1, pp. 11–16, 2014.

[143] S. Koppes, P. Kemperman, I. van Tilburg, F. Calkoen-Kwa, K. Engebretsen, G. Puppels, P. Caspers, and S. Kezic, "Determination of natural moisturizing factors in the skin: Raman microspectroscopy versus HPLC," *Biomarkers*, vol. 0, no. 0, pp. 1–12, 2016.

[144] M. Janssens, J. van Smeden, G. J. Puppels, a. P. M. Lavrijsen, P. J. Caspers, and J. a. Bouwstra, "Lipid to protein ratio plays an important role in the skin barrier function in patients with atopic eczema.," *The British journal of dermatology*, vol. 170, pp. 1248–55, jun 2014.

[145] M. Egawa and H. Tagami, "Comparison of the depth profiles of water and water-binding substances in the stratum corneum determined in vivo by Raman spectroscopy between the cheek and volar forearm skin: Effects of age, seasonal changes and artificial forced hydration," *British Journal of Dermatology*, vol. 158, pp. 251–260, 2008.

[146] T. M. Hancewicz, "A Consensus Modeling Approach for the Determination of Stratum Corneum Thickness Using In-Vivo Confocal Raman Spectroscopy," *Journal of Cosmetics, Dermatological Sciences and Applications*, vol. 02, no. 04, pp. 241–251, 2012.

[147] A. Böhling, S. Bielfeldt, A. Himmelmann, M. Keskin, and K.-P. Wilhelm, "Comparison of the stratum corneum thickness measured in vivo with confocal Raman spectroscopy and confocal reflectance microscopy.," *Skin research and technology*, vol. 20, pp. 1–8, jun 2013.

[148] S. Bielfeldt, V. Schoder, U. Ely, A. V. D. Pol, J. D. Sterke, and K.-p. Wilhelm, "Assessment of human stratum corneum thickness and its barrier properties by in-vivo confocal Raman spectroscopy.," *IFSCC Magazine*, vol. 12, pp. 9–15, 2009.

[149] M. Egawa, T. Hirao, and M. Takahashi, "In vivo estimation of stratum corneum thickness from water concentration profiles obtained with Raman spectroscopy.," *Acta dermato-venereologica*, vol. 87, pp. 4–8, jan 2007.

[150] J. M. Crowther, A. Sieg, P. Blenkiron, C. Marcott, P. J. Matts, J. R. Kaczvinsky, and A. V. Rawlings, "Measuring the effects of topical moisturizers on changes in stratum corneum thickness, water gradients and hydration in vivo.," *The British journal of dermatology*, vol. 159, pp. 567–77, sep 2008.

[151] P. D. a. Pudney, M. Mélot, P. J. Caspers, A. Van Der Pol, and G. J. Puppels, "An in vivo confocal Raman study of the delivery of trans retinol to the skin.," *Applied spectroscopy*, vol. 61, pp. 804–11, aug 2007.

[152] G. M. O'Regan, P. M. J. H. Kemperman, A. Sandilands, H. Chen, L. E. Campbell, K. Kroboth, R. Watson, M. Rowland, G. J. Puppels, W. H. I. McLean, P. J. Caspers, and A. D. Irvine, "Raman profiles of the stratum corneum define 3 filaggrin genotype-determined atopic dermatitis endophenotypes.," *The Journal of allergy and clinical immunology*, vol. 126, pp. 574–80, sep 2010.

[153] V. Mlitz, J. Latreille, S. Gardinier, R. Jdid, Y. Drouault, P. Hufnagl, L. Eckhart, C. Guinot, and E. Tschachler, "Impact of filaggrin mutations on Raman spectra and biophysical properties of the stratum corneum in mild to moderate atopic dermatitis," *Journal of the European Academy of Dermatology and Venereology*, vol. 26, no. 8, pp. 983–990, 2012.

[154] F. J. González, J. Alda, B. Moreno-Cruz, M. Martínez-Escanamé, M. G. Ramírez-Elías, B. Torres-Álvarez, and B. Moncada, "Use of Raman spectroscopy for the early detection of filaggrin-related atopic dermatitis," *Skin Research and Technology*, vol. 17, pp. 45–50, feb 2011.

[155] G. Zhang, D. J. Moore, K. B. Sloan, C. R. Flach, and R. Mendelsohn, "Imaging the prodrug-to-drug transformation of a 5-fluorouracil derivative in skin by confocal Raman microscopy.," *The Journal of investigative dermatology*, vol. 127, no. October 2006, pp. 1205–1209, 2007.

[156] G. Zhang, C. R. Flach, and R. Mendelsohn, "Tracking the dephosphorylation of resveratrol triphosphate in skin by confocal Raman microscopy," *Journal of Controlled Release*, vol. 123, pp. 141–147, 2007.

[157] F. R. Carol, C. Xiao, R. Mendelsohn, and D. J. Moore, "Tracking phospholipid vesicle permeation into skin using infrared microspectroscopic imaging and confocal Raman spectroscopy," *Journal of Investigative Dermatology*, vol. 124, no. 2002, pp. A64–A64, 2005.

[158] M. Mélot, P. D. a. Pudney, A.-M. Williamson, P. J. Caspers, A. Van Der Pol, and G. J. Puppels, "Studying the effectiveness of penetration enhancers to deliver retinol through the stratum cornum by in vivo confocal Raman spectroscopy," *Journal of controlled release*, vol. 138, pp. 32–9, aug 2009.

[159] M. Gorcea, J. Hadgraft, D. J. Moore, and M. E. Lane, "In vivo barrier challenge and initial recovery in human facial skin.," *Skin research and technology*, vol. 19, pp. e375–82, feb 2013.

[160] Y. N. Kalia, F. Pirot, and R. H. Guy, "Homogeneous transport in a heterogeneous membrane: water diffusion across human stratum corneum in vivo.," *Biophysical journal*, vol. 71, pp. 2692–700, nov 1996.

[161] Y. Gao, X. Wang, S. Chen, S. Li, and X. Liu, "Acute skin barrier disruption with repeated tape stripping: an in vivo model for damage skin barrier," *Skin Research and Technology*, vol. 0, pp. 1–7, may 2012.

[162] R. Voegeli, S. Doppler, P. Joller, M. Breternitz, J. W. Fluhr, and a. V. Rawlings, "Increased mass levels of certain serine proteases in the stratum corneum in acute eczematous atopic skin," *International journal of cosmetic science*, vol. 33, pp. 560–5, dec 2011.

[163] D. Mohammed, P. J. Matts, J. Hadgraft, and M. E. Lane, "Depth profiling of stratum corneum biophysical and molecular properties," *The British journal of dermatology*, vol. 164, pp. 957–65, may 2011.

[164] D. Mohammed, K. Hirata, J. Hadgraft, and M. E. Lane, "Influence of skin penetration enhancers on skin barrier function and skin protease activity.," *European journal of pharmaceutical sciences : official journal of the European Federation for Pharmaceutical Sciences*, vol. 51, pp. 118–22, jan 2014.

[165] M. Breternitz, M. Flach, J. Prässler, P. Elsner, and J. W. Fluhr, "Acute barrier disruption by adhesive tapes is influenced by pressure, time and anatomical location: integrity and cohesion assessed by sequential tape stripping. A randomized, controlled study.," *The British journal of dermatology*, vol. 156, pp. 231–40, feb 2007.

[166] H. Löffler, F. Dreher, and H. I. Maibach, "Stratum corneum adhesive tape stripping: influence of anatomical site, application pressure, duration and removal.," *The British journal of dermatology*, vol. 151, pp. 746–52, oct 2004.

[167] M. Förster and M. Bolzinger, "Confocal Raman microspectroscopy for evaluating the stratum corneum removal by 3 standard methods," *Skin Pharmacology and . . .*, vol. 24, pp. 103–112, 2010.

[168] J. Lademann, U. Jacobi, C. Surber, H.-J. Weigmann, and J. W. Fluhr, "The tape stripping procedure–evaluation of some critical parameters," *European journal of pharmaceutics and biopharmaceutics*, vol. 72, pp. 317–23, jun 2009.

[169] R. Voegeli, J. Heiland, S. Doppler, a. V. Rawlings, and T. Schreier, "Efficient and simple quantification of stratum corneum proteins on tape strippings by infrared densitometry," *Skin research and technology : official journal of International Society for Bioengineering and the Skin (ISBS) [and] International Society for Digital Imaging of Skin (ISDIS) [and] International Society for Skin Imaging (ISSI)*, vol. 13, pp. 242–51, aug 2007.

[170] D. Mohammed, Q. Yang, R. H. Guy, P. J. Matts, J. Hadgraft, and M. E. Lane, "Comparison of gravimetric and spectroscopic approaches to quantify stratum corneum removed by tape-stripping.," *European journal of pharmaceutics and biopharmaceutics*, vol. 82, pp. 171–4, sep 2012.

[171] A. Fick, "Ueber Diffusion," *Annalen der Physik*, vol. 170, no. 1, pp. 59–86, 1855.

[172] A. Lee, J. King, and D. Barrett, "Percutaneous absorption: a multiple pathway model," *Journal of controlled release*, vol. 45, pp. 141–151, 1997.

[173] M. E. Johnson, D. Blankschtein, and R. Langer, "Evaluation of solute permeation through the stratum corneum: lateral bilayer diffusion as the primary transport mechanism.," *Journal of pharmaceutical sciences*, vol. 86, pp. 1162–72, oct 1997.

[174] L. Chen, G. Lian, and L. Han, "Use of "bricks and mortar" model to predict transdermal permeation: Model development and initial validation," *Industrial and Engineering Chemistry Research*, vol. 47, no. 17, pp. 6465–6472, 2008.

[175] A. N. A. M. Barbero, H. F. Frasch, and W. Virginia, "Transcellular Route of Diffusion through Stratum Corneum : Results from Finite Element Models," *Journal of pharmaceutical sciences*, vol. 95, no. 10, pp. 2186–2194, 2006.

[176] A. M. Barbero and H. F. Frasch, "Modeling of diffusion with partitioning in stratum corneum using a finite element model.," *Annals of biomedical engineering*, vol. 33, pp. 1281–92, sep 2005.

[177] H. F. Frasch and A. M. Barbero, "Steady-state flux and lag time in the stratum corneum lipid pathway: results from finite element models.," *Journal of pharmaceutical sciences*, vol. 92, pp. 2196–207, nov 2003.

[178] P. Xiao and R. E. Imhof, "Two dimensional finite element modelling for dynamic water diffusion through stratum corneum," *International Journal of Pharmaceutics*, vol. 435, no. 1, pp. 88–92, 2012.

[179] S. Hansen, A. Henning, A. Naegel, M. Heisig, G. Wittum, D. Neumann, K.-H. Kostka, J. Zbytovska, C.-M. Lehr, and U. F. Schaefer, "In-silico model of skin penetration based on experimentally determined input parameters. Part I: experimental determination of partition and diffusion coefficients," *European journal of pharmaceutics and biopharmaceutics : official journal of Arbeitsgemeinschaft für Pharmazeutische Verfahrenstechnik e.V*, vol. 68, pp. 352–67, feb 2008.

[180] T. Wang, G. Kasting, and J. Nitsche, "A multiphase microscopic diffusion model for stratum corneum permeability. I. Formulation, solution, and illustrative results for representative compounds," *Journal of Pharmaceutical Sciences*, vol. 95, no. 3, pp. 620–648, 2006.

[181] T. Wang, G. Kasting, and J. Nitsche, "A multiphase microscopic diffusion model for stratum corneum permeability. II. Estimation of physicochemical parameters, and application to a large permeability," *Journal of pharmaceutical ...*, vol. 96, no. 11, pp. 3024–3051, 2007.

[182] A. Naegel, S. Hansen, D. Neumann, C.-M. Lehr, U. F. Schaefer, G. Wittum, and M. Heisig, "In-silico model of skin penetration based on experimentally determined input parameters. Part II: mathematical modelling of in-vitro diffusion experiments. Identification of critical input parameters.," *European journal of pharmaceutics and biopharmaceutics : official journal of Arbeitsgemeinschaft für Pharmazeutische Verfahrenstechnik e.V*, vol. 68, pp. 368–79, feb 2008.

[183] D. Feuchter, M. Heisig, and G. Wittum, "A Geometry Model for the Simulation of Drug Diffusion through the Stratum Corneum," *Computing and Visualization in Science*, vol. 9, no. 2, pp. 117–130, 2006.

[184] A. Naegel, M. Heisig, and G. Wittum, "Computational Modeling of the Skin Barrier," in *Kursad Turksen (ed.), Permeability Barrier: Methods and Protocols, Methods in Molecular Biology, vol. 763*, vol. 763, pp. 1–32 (Chapter 1).

[185] A. Naegel, M. Heisig, and G. Wittum, "A comparison of two- and three-dimensional models for the simulation of the permeability of human stratum corneum," *European Journal of Pharmaceutics and Biopharmaceutics*, vol. 72, pp. 332–338, jun 2009.

[186] A. Naegel, M. Heisig, and G. Wittum, "Detailed modeling of skin penetration-An overview," *Advanced Drug Delivery Reviews*, vol. 65, no. 2, pp. 191–207, 2013.

[187] K. McCarley and A. Bunge, "Physiologically relevant twocompartment pharmacokinetic models for skin," *Journal of pharmaceutical sciences*, vol. 89, no. 9, pp. 1212–1235, 2000.

[188] K. D. McCarley and A. L. Bunge, "Pharmacokinetic models of dermal absorption.," *Journal of pharmaceutical sciences*, vol. 90, pp. 1699–719, nov 2001.

[189] S. Hansen, A. Naegel, M. Heisig, G. Wittum, D. Neumann, K. H. Kostka, P. Meiers, C. M. Lehr, and U. F. Schaefer, "The role of corneocytes in skin transport revised-a combined computational and experimental approach," *Pharmaceutical Research*, vol. 26, no. 6, pp. 1379–1397, 2009.

[190] Y. G. Anissimov and M. S. Roberts, "Diffusion modeling of percutaneous absorption kinetics: 3. Variable diffusion and partition coefficients, consequences for stratum corneum depth profiles and desorption kinetics.," *Journal of pharmaceutical sciences*, vol. 93, pp. 470–87, feb 2004.

[191] M. S. Roberts, Y. G. Anissimov, and R. A. Gonsalvez, "Mathematical models in percutaneous absorption," in *Percutaneous absorption: Drugs - Cosmetics - Mechanisms - Methodology* (R. L. Bronaugh and H. I. Maibach, eds.), pp. 1–44, New York: Marcel Dekker Inc., 4th ed., 2005.

[192] G. Lian, L. Chen, and L. Han, "An Evaluation of Mathematical Models for Predicting Skin Permeability," *Journal of pharmaceutical sciences*, vol. 97, no. 1, pp. 584–598, 2008.

[193] R. Potts and R. Guy, "Predicting skin permeability," *Pharmaceutical research*, vol. 9, no. 5, pp. 663–669, 1992.

[194] J. Hadgraft and M. E. Lane, "Transepidermal water loss and skin site: a hypothesis.," *International journal of pharmaceutics*, vol. 373, pp. 1–3, may 2009.

[195] D. A. Schwindt, K. P. Wilhelm, and H. I. Maibach, "Water diffusion characteristics of human stratum corneum at different anatomical sites in vivo.," *The Journal of investigative dermatology*, vol. 111, pp. 385–9, sep 1998.

[196] C. Rosado, P. Pinto, and L. M. Rodrigues, "Modeling TEWL-desorption curves: a new practical approach for the quantitative in vivo assessment of skin barrier.," *Experimental Dermatology*, vol. 14, pp. 386–90, may 2005.

[197] P. C. Pinto and L. M. Rodrigues, "Influence of the time of occlusion on the quantitative parameters obtained by modelling trans-epidermal water loss curves to describe the human cutaneous barrier function in vivo," *Medical and Biological Engineering and Computing*, vol. 43, pp. 771–775, 2005.

[198] C. Barba, A. Baratto, M. Martí, A. Semenzato, G. Baratto, A. M. Manich, J. L. Parra, and L. Coderch, "Water sorption evaluation of stratum corneum," *Thermochimica Acta*, vol. 583, no. 0, pp. 43–48, 2014.

[199] G. B. Kasting and N. D. Barai, "Equilibrium water sorption in human stratum corneum," *Journal of pharmaceutical sciences*, vol. 92, pp. 1624–31, aug 2003.

[200] X. Li, R. Johnson, B. Weinstein, E. Wilder, E. Smith, and G. B. Kasting, "Dynamics of water transport and swelling in human stratum corneum," *Chemical Engineering Science*, vol. 138, pp. 164–172, 2015.

[201] X. Li, R. Johnson, and G. B. Kasting, "On the Variation of Water Diffusion Coefficient in Stratum Corneum With Water Content," *Journal of Pharmaceutical Sciences*, vol. 3549, pp. 1–7, 2016.

[202] N. Grabe, T. Pommerencke, D. Müller, S. Huber, K. Neuber, and H. Dickhaus, "Modelling epidermal homeostasis as an approach for clinical bioinformatics.," *Studies in health technology and informatics*, vol. 124, pp. 105–10, jan 2006.

[203] G. Schaller and M. Meyer-Hermann, "A modelling approach towards epidermal homoeostasis control," *Journal of theoretical biology*, pp. 1–23, 2007.

[204] T. Süterlin, S. Huber, H. Dickhaus, N. Grabe, T. Sütterlin, S. Huber, H. Dickhaus, and N. Grabe, "Modeling multi-cellular behavior in epidermal tissue homeostasis via finite state machines in multi-agent systems.," *Bioinformatics (Oxford, England)*, vol. 25, pp. 2057–63, aug 2009.

[205] T. Sütterlin and N. Grabe, "Efficient Modeling of the Spatial Dynamics of Tissues by Automated Transformation of Graphical Cell Behavioral Models into Multi-Agent Based Simulationsitle," *Proceedings of the 6th Workshop on Computation of Biochemical Pathways and Genetic Networks, BioQuant Heidelberg, Sept. 2010*, pp. 1–12, 2010.

[206] S. Hu and F. Cucinotta, "Epidermal homeostasis and radiation responses in a multiscale tissue modeling framework.," *Integrative biology : quantitative biosciences from nano to macro*, vol. 6, pp. 76–89, dec 2013.

[207] S. Adra, T. Sun, S. MacNeil, M. Holcombe, and R. Smallwood, "Development of a three dimensional multiscale computational model of the human epidermis.," *PloS one*, vol. 5, p. e8511, jan 2010.

[208] N. Grabe and K. Neuber, "Simulating psoriasis by altering transit amplifying cells.," *Bioinformatics (Oxford, England)*, vol. 23, pp. 1309–12, jun 2007.

[209] H. Zhang, W. Hou, L. Henrot, S. Schnebert, M. Dumas, C. Heus, and J. Yang, "Modeling Epidermis Homeostasis and Psoriasis Pathogenesis," *Journal of The Royal Society Interface*, vol. 12, no. 103, pp. 1–21, 2014.

[210] X. Li, A. K. Upadhyay, A. J. Bullock, T. Dicolandrea, J. Xu, R. L. Binder, M. K. Robinson, D. R. Finlay, K. J. Mills, C. C. Bascom, C. K. Kelling, R. J. Isfort, J. W. Haycock, S. Macneil, and R. H. Smallwood, "Skin Stem Cell Hypotheses and Long Term Clone Survival - Explored Using Agent-based Modelling," *Scientific reports*, vol. 3, p. 1904, 2013.

[211] T. Sun, P. McMinn, M. Holcombe, R. Smallwood, and S. MacNeil, "Agent based modelling helps in understanding the rules by which fibroblasts support keratinocyte colony formation.," *PloS one*, vol. 3, p. e2129, jan 2008.

[212] C. Park, R. Smallwood, S. Sheffield, and S. A. Billings, "Development of spatiotemporal validation methods of an agent-based model of epithelial cells: analysis of a colony of keratinocytes César Pichardo-Almarza *," *International Journal of Informatics and Personalised Medicine*, vol. 1, no. 4, pp. 335–354, 2008.

[213] N. Grabe and K. Neuber, "A multicellular systems biology model predicts epidermal morphology, kinetics and Ca2+ flow," *Bioinformatics (Oxford, England)*, vol. 21, pp. 3541–7, sep 2005.

[214] D. P. Doupe, M. P. Alcolea, A. Roshan, G. Zhang, A. M. Klein, B. D. Simons, and P. H. Jones, "A Single Progenitor Population Switches Behavior to Maintain and Repair Esophageal Epithelium," *Science*, vol. 337, no. 6098, pp. 1091–1093, 2012.

[215] A. M. Klein, V. Nikolaidou-Neokosmidou, D. P. Doupe, P. H. Jones, and B. D. Simons, "Patterning as a signature of human epidermal stem cell regulation," *Journal of The Royal Society Interface*, vol. 8, no. 65, pp. 1815–1824, 2011.

[216] P. B. Warren, "Cells, cancer, and rare events: Homeostatic metastability in stochastic nonlinear dynamical models of skin cell proliferation," *Physical Review E - Statistical, Nonlinear, and Soft Matter Physics*, vol. 80, pp. 3–6, 2009.

[217] V. Zhdanov and N.-J. Cho, "Kinetics of the maintenance of the epidermis," *Central European Journal of Physics*, vol. 11, no. 8, pp. 1016–1023, 2013.

[218] N. V. Valeyev, C. Hundhausen, Y. Umezawa, N. V. Kotov, G. Williams, A. Clop, C. Ainali, C. Ouzounis, S. Tsoka, and F. O. Nestle, "A systems model for immune cell interactions unravels the mechanism of inflammation in human skin.," *PLoS computational biology*, vol. 6, p. e1001024, jan 2010.

[219] M. P. Adams, D. G. Mallet, and G. J. Pettet, "Active regulation of the epidermal calcium profile.," *Journal of theoretical biology*, vol. 301, pp. 112–21, may 2012.

[220] M. P. Adams, *Mathematical models of calcium and tight junctions in Normal and Reconstructed Epidermis*. PhD thesis, 2015.

[221] M. P. Adams, D. G. Mallet, and G. J. Pettet, "Towards a quantitative theory of epidermal calcium profile formation in unwounded skin," *PLoS ONE*, vol. 10, no. 1, 2015.

[222] K. C. Madison, "Barrier function of the skin: "la raison d'etre" of the epidermis.," *Journal of Investigative Dermatology*, vol. 121, no. 2, pp. 231–241, 2003.

[223] M. D. A. van Logtestijn, E. Domínguez-Hüttinger, G. N. Stamatas, and R. J. Tanaka, "Resistance to water diffusion in the stratum corneum is depth-dependent," *PloS one*, vol. 10, p. e0117292, jan 2015.

[224] A. V. Rawlings and C. R. Harding, "Moisturization and skin barrier function.," *Dermatologic Therapy*, vol. 17 Suppl 1, no. 1, pp. 43–48, 2004.

[225] P. M. Elias, "Epidermal barrier function: intercellular lamellar lipid structures, origin, composition and metabolism.," *Journal of Controlled Release*, vol. 15, pp. 199–208, jun 1991.

[226] J. L. Zatz, "Simulation studies of skin permeation," *Journal of the Society of Cosmetic Chemists*, vol. 43, no. January/February, pp. 37–48, 1992.

[227] Y. G. Anissimov, "Mathematical Models for Different Exposure Conditions," in *Dermal absorption and toxicity assessment* (M. S. Roberts and K. A. Walters, eds.), ch. 14, pp. 271–86, Informa Healthcare, New York; London, 2nd ed., 2008.

[228] E. Boireau-Adamezyk, A. Baillet-Guffroy, and G. N. Stamatas, "Age-dependent changes in stratum corneum barrier function.," *Skin research and technology*, p. advanced online publication (DOI:10.1111/srt.12132, 2014.

[229] G. N. Stamatas, J. de Sterke, M. Hauser, O. von Stetten, and A. van der Pol, "Lipid uptake and skin occlusion following topical application of oils on adult and infant skin.," *Journal of dermatological science*, vol. 50, pp. 135–42, may 2008.

[230] R. Scheuplein, "Permeability of the skin.," *Comprehensive Physiology*, vol. 51, no. 4, pp. 702–47, 1971.

[231] V. Rogiers, "EEMCO guidance for the assessment of transepidermal water loss in cosmetic sciences.," *Skin Pharmacology and Physiology*, vol. 14, pp. 117–28, 2001.

[232] P. Elias and K. Feingold, "Coordinate regulation of epidermal differentiation and barrier homeostasis.," *Skin Pharmacology and Physiology*, vol. 14, no. suppl 1, pp. 28–34, 2004.

[233] P. M. Elias, R. Gruber, D. Crumrine, G. Menon, M. L. Williams, J. S. Wakefield, W. M. Holleran, and Y. Uchida, "Formation and functions of the corneocyte lipid envelope (CLE).," *Biochimica et biophysica acta*, pp. 9–13, sep 2013.

[234] A. V. Rawlings and R. Voegeli, "Stratum corneum proteases and dry skin conditions," *Cell and tissue research*, vol. 351, pp. 217–35, feb 2013.

[235] K. Kikuchi, H. Kobayashi, K. O'goshi, and H. Tagami, "Impairment of skin barrier function is not inherent in atopic dermatitis patients: a prospective study conducted in newborns.," *Pediatric dermatology*, vol. 23, no. 2, pp. 109–13, 2006.

[236] G. N. Stamatas, J. Nikolovski, M. C. Mack, and N. Kollias, "Infant skin physiology and development during the first years of life: a review of recent findings based on in vivo studies.," *International journal of cosmetic science*, vol. 33, pp. 17–24, feb 2011.

[237] Y. N. Kalia, L. B. Nonato, C. H. Lund, and R. H. Guy, "Development of skin barrier function in premature infants.," *The Journal of investigative dermatology*, vol. 111, pp. 320–6, aug 1998.

[238] G. N. Stamatas, J. Nikolovski, M. A. Luedtke, N. Kollias, and B. C. Wiegand, "Infant skin microstructure assessed in vivo differs from adult skin in organization and at the cellular level.," *Pediatric dermatology*, vol. 27, no. 2, pp. 125–31, 2010.

[239] G. N. Stamatas, R. B. Estanislao, M. Suero, Z. S. Rivera, J. Li, a. Khaiat, and N. Kollias, "Facial skin fluorescence as a marker of the skin's response to chronic environmental insults and its dependence on age.," *The British journal of dermatology*, vol. 154, pp. 125–32, jan 2006.

[240] M. Yaar and B. A. Gilchrest, "Photoageing: mechanism, prevention and therapy.," *The British journal of dermatology*, vol. 157, pp. 874–87, nov 2007.

[241] E. M. T. Wurm, C. Longo, C. Curchin, H. P. Soyer, T. W. Prow, and G. Pellacani, "In vivo assessment of chronological ageing and photoageing in forearm skin using reflectance confocal microscopy.," *The British journal of dermatology*, vol. 167, pp. 270–9, aug 2012.

[242] A. Patzelt, J. Lademann, H. Richter, M. E. Darvin, S. Schanzer, G. Thiede, W. Sterry, T. Vergou, and M. Hauser, "In vivo investigations on the penetration of various oils and their influence on the skin barrier.," *Skin research and technology*, vol. 18, pp. 364–9, aug 2012.

[243] J. A. Bouwstra, A. de Graaff, G. S. Gooris, J. Nijsse, J. W. Wiechers, and A. C. van Aelst, "Water distribution and related morphology in human stratum corneum at different hydration levels.," *The Journal of investigative dermatology*, vol. 120, pp. 750–8, may 2003.

[244] A. Fauland, H. Köfeler, M. Trötzmüller, A. Knopf, J. Hartler, A. Eberl, C. Chitraju, E. Lankmayr, and F. Spener, "A comprehensive method for lipid profiling by liquid chromatography-ion cyclotron resonance mass spectrometry.," *Journal of lipid research*, vol. 52, pp. 2314–22, dec 2011.

[245] M. Lodén, "Role of topical emollients and moisturizers in the treatment of dry skin barrier disorders.," *American journal of clinical dermatology*, vol. 4, no. 11, pp. 771–88, 2003.

[246] F. Giusti, A. Martella, L. Bertoni, and S. Seidenari, "Skin Barrier, Hydration, and pH of the Skin of Infants Under 2 Years of Age," *Pediatric dermatology*, vol. 18, no. 2, pp. 93–96, 2001.

[247] J. Chittock, A. Cooke, T. Lavender, K. Brown, A. Wigley, S. Victor, M. Cork, and S. Danby, "Development of stratum corneum chymotrypsin-like protease activity and natural moisturising factors from birth to 4 weeks of age compared to adults," *British Journal of Dermatology*, pp. n/a–n/a, 2016.

[248] G. Yosipovitch, A. Maayan-metzger, P. Merlob, and L. Sirota, "Skin Barrier Properties in Different Body Areas in Neonates," *Pediatrics*, 2000.

[249] C. H. Lund, L. B. Nonato, J. M. Kuller, L. S. Franck, C. Cullander, and D. J. Durand, "Disruption of barrier function in neonatal skin associated with adhesive removal.," *The Journal of pediatrics*, vol. 131, pp. 367–372, 1997.

[250] M. Kelleher, A. Dunn-Galvin, J. O. Hourihane, D. Murray, L. E. Campbell, W. Irwin McLean, and A. D. Irvine, "Skin barrier dysfunction measured by transepidermal water loss at 2 days and 2 months predates and predicts atopic dermatitis at 1 year," *Journal of Allergy and Clinical Immunology*, vol. 135, no. 4, pp. 930–935.e1, 2015.

[251] C. Choe, J. Lademann, and M. E. Darvin, "Confocal Raman microscopy for investigating the penetration of various oils into the human skin in vivo," *Journal of Dermatological Science*, vol. 79, pp. 176–178, 2015.

[252] G. Lian, L. Chen, P. D. A. Pudney, M. Melot, and L. Han, "Modeling Transdermal Permeation. Part 2. Predicting the Dermatopharmacokinetics of Percutaneous Solute," *AIChE Journal*, vol. 56, no. 10, pp. 2551–2560, 2010.

[253] A. Di Nardo, P. Wertz, A. Giannetti, and S. Seidenari, "Ceramide and cholesterol composition of the skin of patients with atopic dermatitis," *Acta Dermato-Venereologica*, vol. 78, no. 1, pp. 27–30, 1998.

[254] M. Suárez-Fariñas, S. J. Tintle, A. Shemer, A. Chiricozzi, K. Nograles, I. Cardinale, S. Duan, A. M. Bowcock, J. G. Krueger, and E. Guttman-Yassky, "Nonlesional atopic dermatitis skin is characterized by broad terminal differentiation defects and variable immune abnormalities.," *The Journal of allergy and clinical immunology*, vol. 127, pp. 954–64.e1–4, apr 2011.

[255] H. Törmä, M. Lindberg, and B. Berne, "Skin barrier disruption by sodium lauryl sulfate-exposure alters the expressions of involucrin, transglutaminase 1, profilaggrin, and kallikreins during the repair phase in human skin in vivo.," *The Journal of investigative dermatology*, vol. 128, pp. 1212–9, may 2008.

[256] H. Törmä and B. Berne, "Sodium lauryl sulphate alters the mRNA expression of lipid-metabolizing enzymes and PPAR signalling in normal human skin in vivo," *Experimental Dermatology*, vol. 18, no. 5, pp. 1010–1015, 2009.

[257] C. M. De Jongh, M. M. Verberk, C. E. T. Withagen, J. J. L. Jacobs, T. Rustemeyer, and S. Kezic, "Stratum corneum cytokines and skin irritation response to sodium lauryl sulfate," *Contact Dermatitis*, vol. 54, pp. 325–333, 2006.

[258] R. R. Warner, Y. L. Boissy, N. a. Lilly, M. J. Spears, K. McKillop, J. L. Marshall, and K. J. Stone, "Water disrupts stratum corneum lipid lamellae: damage is similar to surfactants.," *The Journal of investigative dermatology*, vol. 113, pp. 960–6, dec 1999.

[259] D. G. Koopman, S. Kežić, and M. M. Verberk, "Skin reaction and recovery: A repeated sodium lauryl sulphate patch test vs. a 24-h patch test and tape stripping," *British Journal of Dermatology*, vol. 150, pp. 493–499, 2004.

[260] K. P. Wilhelm, C. Surber, and H. I. Maibach, "Effect of sodium lauryl sulfate-induced skin irritation on in vivo percutaneous penetration of four drugs.," *The Journal of investigative dermatology*, vol. 97, pp. 927–932, 1991.

[261] E. Berardesca and F. Distante, "The modulation of skin irritation," *Contact Dermatitis*, vol. 31, pp. 281–287, 1994.

[262] M. Lodén and a. C. Andersson, "Effect of topically applied lipids on surfactant-irritated skin.," *The British journal of dermatology*, vol. 134, pp. 215–220, 1996.

[263] E. Held, H. Lund, and T. Agner, "Effect of different moisturizers on SLS-irritated human skin.," *Contact dermatitis*, vol. 44, pp. 229–234, 2001.

[264] J. W. Fluhr, a. Akengin, a. Bornkessel, S. Fuchs, J. Praessler, J. Norgauer, R. Grieshaber, P. Kleesz, and P. Elsner, "Additive impairment of the barrier function by mechanical irritation, occlusion and sodium lauryl sulphate in vivo," *British Journal of Dermatology*, vol. 153, pp. 125–131, 2005.

[265] M. Tsang and R. H. Guy, "Effect of Aqueous Cream BP on human stratum corneum invivo," *British Journal of Dermatology*, vol. 163, pp. 954–958, 2010.

[266] M. D. A. van Logtestijn, P. J. Caspers, S. Kezic, D. R. Hoffman, D. W. Koenig, M. Ono, G. N. Stamatas, and R. J. Tanaka, "Water resistance profile as a marker of skin barrier damage in atopic dermatitis patients," *Journal of Dermatological Science*, vol. 81, no. 2, pp. 126–128, 2016.

[267] M. J. Cork, S. G. Danby, Y. Vasilopoulos, J. Hadgraft, M. E. Lane, M. Moustafa, R. H. Guy, A. L. Macgowan, R. Tazi-Ahnini, and S. J. Ward, "Epidermal barrier dysfunction in atopic dermatitis," *The Journal of investigative dermatology*, vol. 129, pp. 1892–908, aug 2009.

[268] S. Kezic, P. M. J. H. Kemperman, E. S. Koster, C. M. de Jongh, H. B. Thio, L. E. Campbell, A. D. Irvine, I. W. H. McLean, G. J. Puppels, and P. J. Caspers, "Loss-of-function mutations in the filaggrin gene lead to reduced level of natural moisturizing factor in the stratum corneum.," *The Journal of investigative dermatology*, vol. 128, pp. 2117–9, aug 2008.

[269] D. R. Hoffman, L. M. Kroll, A. Basehoar, B. Reece, C. T. Cunningham, and D. W. Koenig, "Immediate and extended effects of abrasion on stratum corneum natural moisturizing factor," *Skin Research and Technology*, vol. 21, pp. 1–7, jan 2015.

[270] P. Saad, C. R. Flach, R. M. Walters, and R. Mendelsohn, "Infrared spectroscopic studies of sodium dodecyl sulphate permeation and interaction with stratum corneum lipids in skin," *International Journal of Cosmetic Science*, vol. 34, no. 1, pp. 36–43, 2012.

[271] H. Tagami, "Location-related differences in structure and function of the stratum corneum with special emphasis on those of the facial skin.," *International journal of cosmetic science*, vol. 30, pp. 413–34, dec 2008.

[272] S. Luebberding, N. Krueger, and M. Kerscher, "Age-related changes in male skin: Quantitative evaluation of one hundred and fifty male subjects," *Skin Pharmacology and Physiology*, vol. 27, no. 1, pp. 9–17, 2013.

[273] R. Darlenski and J. W. Fluhr, "Influence of skin type, race, sex, and anatomic location on epidermal barrier function," *Clinics in Dermatology*, vol. 30, no. 3, pp. 269–273, 2012.

[274] T. C. Scharschmidt, M.-Q. Man, Y. Hatano, D. Crumrine, R. Gunathilake, J. P. Sundberg, K. a. Silva, T. M. Mauro, M. Hupe, S. Cho, Y. Wu, A. Celli, M. Schmuth, K. R. Feingold, and P. M. Elias, "Filaggrin deficiency confers a paracellular barrier abnormality that reduces inflammatory thresholds to irritants and haptens.," *The Journal of allergy and clinical immunology*, vol. 124, pp. 496–506, 506.e1–6, sep 2009.

[275] J. van Smeden, M. Janssens, E. C. J. Kaye, P. J. Caspers, A. P. Lavrijsen, R. J. Vreeken, and J. a. Bouwstra, "The importance of free fatty acid chain length for the skin barrier function in atopic eczema patients.," *Experimental dermatology*, vol. 23, pp. 45–52, jan 2014.

[276] J. Fowler, "Understanding the role of natural moisturizing factor in skin hydration," *Pract Dermatol*, no. July, pp. 36–40, 2012.

[277] I. Scott and C. Harding, "Filaggrin breakdown to water binding compounds during development of the rat stratum corneum is controlled by the water activity of the environment," *Developmental biology*, vol. 115, pp. 84–92, 1986.

[278] S. Kezic, A. Kammeyer, F. Calkoen, J. W. Fluhr, and J. D. Bos, "Natural moisturizing factor components in the stratum corneum as biomarkers of filaggrin genotype: Evaluation of minimally invasive methods," *British Journal of Dermatology*, vol. 161, no. 5, pp. 1098–1104, 2009.

[279] S. Kezic, G. M. O'Regan, N. Yau, a. Sandilands, H. Chen, L. E. Campbell, K. Kroboth, R. Watson, M. Rowland, W. H. I. McLean, and a. D. Irvine, "Levels of filaggrin degradation products are influenced by both filaggrin genotype and atopic dermatitis severity.," *Allergy*, vol. 66, pp. 934–40, jul 2011.

[280] N. Nakagawa, S. Sakai, M. Matsumoto, K. Yamada, M. Nagano, T. Yuki, Y. Sumida, and H. Uchiwa, "Relationship between NMF (lactate and potassium) content and the physical properties of the stratum corneum in healthy subjects.," *The Journal of investigative dermatology*, vol. 122, pp. 755–63, mar 2004.

[281] M. Robinson, M. Visscher, A. Laruffa, and R. Wickett, "Natural moisturizing factors (NMF) in the stratum corneum (SC). I. Effects of lipid extraction and soaking," *Journal of Cosmetic Science*, vol. 61, no. February, pp. 13–22, 2010.

[282] M. Robinson, M. Visscher, A. Laruffa, and R. Wickett, "Natural moisturizing factors (NMF) in the stratum corneum (SC). II. Regeneration of NMF over time after soaking," *Journal of Cosmetic Science*, vol. 61, no. February, pp. 13–22, 2010.

[283] A. K. Dąbrowska, C. Adlhart, F. Spano, G.-m. Rotaru, S. Derler, L. Zhai, N. D. Spencer, R. M. Rossi, L. Zhai, and N. D. Spencer, "In vivo confirmation of hydration-induced changes in human-skin thickness, roughness and interaction with the environment," *Biointerphases*, vol. 031015, 2016.

[284] K. A. Engebretsen, J. D. Johansen, S. Kezic, A. Linneberg, and J. P. Thyssen, "The effect of environmental humidity and temperature on skin barrier function and dermatitis," *Journal of the European Academy of Dermatology and Venereology*, vol. 30, no. 2, pp. 223–249, 2016.

[285] M. Denda, J. Sato, Y. Masuda, T. Tsuchiya, J. Koyama, M. Kuramoto, P. M. Elias, and K. R. Feingold, "Exposure to a dry environment enhances epidermal permeability barrier function.," *The Journal of investigative dermatology*, vol. 111, pp. 858–63, nov 1998.

[286] S. J. Chapman and A. Walsh, "Desmosomes, corneosomes and desquamation. An ultrastructural study of adult pig epidermis," *Archives of Dermatological Research*, vol. 282, no. 5, pp. 304–310, 1990.

[287] M. Fartasch, "Epidermal barrier in disorders of the skin," *Microscopy research and technique*, vol. 38, pp. 361–72, aug 1997.

[288] V. R. H. H. Neubert, R. Wepf, and R. H. H. Neubert, "Das Stratum Corneum: Struktur und Morphologie einer hoch effizienten Barriere," *Medicos*, vol. 4, pp. 21–28, 2008.

[289] C. J. Skerrow, D. G. Clelland, and D. Skerrow, "Changes to desmosomal antigens and lectin-binding sites during differentiation in normal human epidermis: a quantitative ultrastructural study," *Journal of cell science*, vol. 92 (Pt 4), pp. 667–677, 1989.

[290] G. S. Pilgram, A. M. Engelsma-van Pelt, J. A. Bouwstra, and H. K. Koerten, "Electron diffraction provides new information on human stratum corneum lipid organization studied in relation to depth and temperature," *The Journal of investigative dermatology*, vol. 113, pp. 403–9, sep 1999.

[291] G. S. Pilgram, D. C. Vissers, H. van der Meulen, S. Pavel, S. P. Lavrijsen, J. A. Bouwstra, and H. K. Koerten, "Aberrant lipid organization in stratum corneum of patients with atopic dermatitis and lamellar ichthyosis," *The Journal of investigative dermatology*, vol. 117, pp. 710–7, sep 2001.

[292] C. Deraison, C. Bonnart, F. Lopez, C. Besson, and A. Hovnanian, "LEKTI fragments specifically inhibit KLK5, KLK7, and KLK14 and control desquamation through a pH-dependent interaction," *Molecular biology of the cell*, vol. 18, pp. 3607–3619, 2007.

[293] M. Miyai, Y. Matsumoto, H. Yamanishi, M. Yamamoto-Tanaka, R. Tsuboi, and T. Hibino, "Keratinocyte-specific mesotrypsin contributes to the desquamation process via kallikrein activation and LEKTI degradation," *The Journal of investigative dermatology*, vol. 134, pp. 1665–74, jul 2014.

[294] J.-P. P. Hachem, D. Crumrine, J. Fluhr, B. E. Brown, K. R. Feingold, and P. M. Elias, "pH directly regulates epidermal permeability barrier homeostasis, and stratum corneum integrity/cohesion," *The Journal of investigative dermatology*, vol. 121, pp. 345–53, aug 2003.

[295] J.-P. Hachem, M.-Q. Man, D. Crumrine, Y. Uchida, B. E. Brown, V. Rogiers, D. Roseeuw, K. R. Feingold, and P. M. Elias, "Sustained serine proteases activity by prolonged increase in pH leads to degradation of lipid processing enzymes and profound alterations of barrier function and stratum corneum integrity," *The Journal of investigative dermatology*, vol. 125, pp. 510–20, oct 2005.

[296] H. Jang, A. Matsuda, K. Jung, K. Karasawa, K. Matsuda, K. Oida, S. Ishizaka, G. Ahn, Y. Amagai, C. Moon, S.-h. Kim, P. D. Arkwright, K. Takamori, H. Matsuda, and A. Tanaka, "Skin pH is the Master Switch of Kallikrein 5-Mediated Skin Barrier Destruction in a Murine Atopic Dermatitis Model," *Journal of Investigative Dermatology*, vol. 136, no. August, pp. 1–32, 2015.

[297] Y. Kitajima, "Implications of normal and disordered remodeling dynamics of corneodesmosomes in stratum corneum," *Dermatologica Sinica*, vol. 33, no. 2, pp. 58–63, 2015.

[298] R. Voegeli, A. V. Rawlings, M. Breternitz, S. Doppler, T. Schreier, and J. W. Fluhr, "Increased stratum corneum serine protease activity in acute eczematous atopic skin," *The British journal of dermatology*, vol. 161, pp. 70–7, jul 2009.

[299] J. Sato, M. Denda, S. Chang, P. M. Elias, and K. R. Feingold, "Abrupt decreases in environmental humidity induce abnormalities in permeability barrier homeostasis," *The Journal of investigative dermatology*, vol. 119, pp. 900–4, oct 2002.

[300] P. M. Elias, "Stratum corneum acidification: how and why?," *Experimental dermatology*, vol. 24, pp. 179–80, mar 2015.

[301] K. Yoshida, M. Yokouchi, K. Nagao, K. Ishii, M. Amagai, and A. Kubo, "Functional tight junction barrier localizes in the second layer of the stratum granulosum of human epidermis," *Journal of Dermatological Science*, vol. 71, no. 2, pp. 89–99, 2013.

[302] J. Anderson and C. M. Van Itallie, "Physiology and Function of the Tight Junction," *Cold Spring Harb Perspect Biol*, no. 1:a002584, pp. 1–16, 2009.

[303] A. Tamura and S. Tsukita, "Paracellular barrier and channel functions of TJ claudins in organizing biological systems: Advances in the field of barriology revealed in knockout mice," *Seminars in Cell and Developmental Biology*, vol. 36, pp. 177–185, 2014.

[304] B. E. Smith and R. E. Braun, "Germ Cell Migration Across Sertoli Cell Tight Junctions," *Science*, vol. 338, pp. 798–802, 2012.

[305] M. Yokouchi, T. Atsugi, M. V. Logtestijn, R. J. Tanaka, K. M, M. Suematsu, M. Furuse, M. Amagai, and A. Kubo, "Epidermal cell turnover across tight junctions based on Kelvin's tetrakaidecahedron cell shape," *eLife*, no. 5:e19593, pp. 1–20, 2016.

[306] W. Sir Thomson, "On the division of space with minimum partitional area," *Acta Mathematica*, vol. 11, pp. 121–134, 1887.

[307] T. D. Allen and C. S. Potten, "Significance of cell shape in tissue architecture," *Nature*, vol. 264, no. 5586, pp. 545–547, 1976.

[308] D. N. Menton, "A minimum-surface mechanism to account for the organization of cells into columns in the mammalian epidermis.," *The American journal of anatomy*, vol. 145, no. 1, pp. 1–22, 1976.

[309] H. Honda, M. Tanemura, and S. Imayama, "Spontaneous architectural organization of mammalian epidermis from random cell packing," *The Journal of investigative dermatology*, vol. 106, pp. 312–315, 1996.

[310] D. Feuchter, *Geometrie- und Gittererzeugung für anisotrope Schichtengebiete*. PhD thesis, Ruprecht-Karls-Universität Heidelberg, 2008.

[311] I. Muha, A. Naegel, S. Stichel, and A. Grillo, "Effective diffusivity in membranes with tetrakaidekahedral cells and implications for the permeability of human stratum corneum," *Journal of Membrane Science*, vol. 368, pp. 18–25, 2011.

[312] C. S. Potten, "Epidermal cell production rates," *The Journal of investigative dermatology*, vol. 65, pp. 488–500, 1975.

[313] N. Kirschner, R. Rosenthal, D. Günzel, I. Moll, and J. M. Brandner, "Tight junctions and differentiation - a chicken or the egg question?," *Experimental Dermatology*, vol. 21, no. 3, pp. 171–175, 2012.

[314] F. O. Nestle, D. Kaplan, and J. Barker, "Psoriasis," *The New England Journal of Medicine*, vol. 361, no. 5, pp. 496–509, 2009.

[315] J. Li, J. Chen, and R. Kirsner, "Pathophysiology of acute wound healing," *Clinics in Dermatology*, vol. 25, no. 1, pp. 9–18, 2007.

[316] H. Iizuka, "Epidermal architecture that depends on turnover time," *Journal of Dermatological Science*, vol. 10, no. 3, pp. 220–223, 1995.

[317] H. Iizuka, A. Ishida-Yamamoto, and H. Honda, "Epidermal remodelling in psoriasis," *The British journal of dermatology*, vol. 135, no. 3, pp. 433–8, 1996.

[318] D. N. Menton and A. Z. Eisen, "Structural organization of the stratum corneum in certain scaling disorders of the skin," *Journal of Investigative Dermatology*, vol. 57, no. 5, 1971.

[319] I. C. Mackenzie, "The Cellular Architecture of the Stratum Corneum," in *Stratum Corneum* (R. Marks and G. Plewig, eds.), pp. 146–152, Berlin, Heidelberg: Springer Berlin Heidelberg, 1983.

[320] I. Mackenzie, "Relationship between mitosis and the ordered structure of the stratum corneum in mouse epidermis," *Nature*, vol. 226, no. 5246, pp. 653–655, 1970.

[321] I. Mackenzie and J. Linder, "An Examination of Cellular Organization Within the Stratum Corneum by A Silver Staining Method," *Journal of Investigative Dermatology*, vol. 61, no. 4, pp. 245–250, 1973.

[322] E. Christophers, "Cellular Architecture of the Stratum Corneum," *Journal of Investigative Dermatology*, vol. 56, no. 3, pp. 165–169, 1983.

[323] J. C. Mackenzie, "Ordered structure of the stratum corneum of mammalian skin," *Nature*, vol. 222, pp. 881–882, 1969.

[324] E. Clayton, D. P. Doupé, A. M. Klein, D. J. Winton, B. D. Simons, and P. H. Jones, "A single type of progenitor cell maintains normal epidermis," *Nature*, vol. 446, no. 7132, pp. 185–189, 2007.

[325] D. P. Doupe, A. M. Klein, B. D. Simons, and P. H. Jones, "The Ordered Architecture of Murine Ear Epidermis Is Maintained by Progenitor Cells with Random Fate," *Developmental Cell*, vol. 18, no. 2, pp. 317–323, 2010.

[326] G. Mascre, S. Dekoninck, B. Drogat, K. K. Youssef, S. Brohee, P. A. Sotiropoulou, B. D. Simons, and C. Blanpain, "Distinct contribution of stem and progenitor cells to epidermal maintenance," *Nature*, vol. 489, no. 7415, pp. 257–262, 2012.

[327] C. Blanpain and B. D. Simons, "Unravelling stem cell dynamics by lineage tracing," *Nature Reviews Molecular Cell Biology*, vol. 14, no. 8, pp. 489–502, 2013.

[328] P. Rompolas, K. R. Mesa, K. Kawaguchi, S. Park, S. Brown, J. Boucher, A. M. Klein, V. Greco, D. Gonzalez, J. Boucher, A. M. Klein, and V. Greco, "Spatiotemporal coordination of stem cell commitment during epidermal homeostasis," *Science*, vol. 7012, no. May, pp. 1–9, 2016.

[329] M. Kurasawa, T. Maeda, A. Oba, T. Yamamoto, and H. Sasaki, "Tight junction regulates epidermal calcium ion gradient and differentiation," *Biochemical and Biophysical Research Communications*, vol. 406, no. 4, pp. 506–511, 2011.

[330] M. Savignac, A. Edir, M. Simon, and A. Hovnanian, "Darier disease : a disease model of impaired calcium homeostasis in the skin," *Biochimica et biophysica acta*, vol. 1813, pp. 1111–7, may 2011.

[331] M. Denda, S. Denda, M. Tsutsumi, M. Goto, J. Kumamoto, M. Nakatani, K. Takei, H. Kitahata, S. Nakata, Y. Sawabu, Y. Kobayashi, and M. Nagayama, "Frontiers in epidermal barrier homeostasis–an approach to mathematical modelling of epidermal calcium dynamics," *Experimental dermatology*, vol. 23, pp. 79–82, feb 2014.

[332] M. J. Behne, S. Sanchez, N. P. Barry, N. Kirschner, W. Meyer, T. M. Mauro, I. Moll, and E. Gratton, "Major translocation of calcium upon epidermal barrier insult: Imaging and quantification via FLIM/Fourier vector analysis," *Archives of Dermatological Research*, vol. 303, no. 2, pp. 103–115, 2011.